Title
Enhancing the Therapeutic Capacity of the MSC Secretome Using Engineered Biomaterials

Author
Gionet-Gonzales, Marissa

Publication Date
2021

Peer reviewed|Thesis/dissertation

Enhancing the Therapeutic Capacity of the MSC Secretome Using Engineered Biomaterials

By

MARISSA ANN GIONET-GONZALES

DISSERTATION

Submitted in partial satisfaction of the requirements for the degree of

DOCTOR OF PHILOSOPHY

in

Biomedical Engineering

in the

OFFICE OF GRADUATE STUDIES

of the

UNIVERSITY OF CALIFORNIA

DAVIS

Approved:

_____

J. Kent Leach, Chair

_____

Alyssa Panitch

_____

Eduardo A. Silva

_____

Lucas R. Smith

Committee in Charge

2021

ACKNOWLEDGMENTS

I would first like to thank Dr. Kent Leach, who has served as a phenomenal advisor to me during my PhD. I am continually amazed at how much time and effort he puts into prioritizing mentorship of his students. I have grown so much as a scientist thanks to his guidance and am incredibly thankful to have had the opportunity to work in his lab. I would also like to acknowledge my dissertation committee, Dr. Alyssa Panitch, Dr. Eduardo Silva, and Dr. Lucas Smith, for all their insights and contributions to my project. I would like to especially thank Dr. Smith, whose help and resources with muscle biology made it possible for our lab to delve into the muscle regeneration field.

This work would have been impossible if it were not for all the help and support that I received from my colleagues. I would like to thank the entire Leach lab, past and present, for fostering such a collaborative and welcoming lab environment: Dr. Debika Mitra, Dr. Steve Ho, Dr. Jenna Harvestine, Dr. Ben Hung, Dr. Jacklyn Woods, Dr. Charlotte Vorwald, Dr. Augustine Saiz, Dr. Tomas Gonzalez-Fernandez, Laney Casella, B.S., Takeyah Campbell, M.S., Vicky Thai, B.S., Jeremy Lowen, B.S., Katie Griffin, B.S., Bobby Gresham, B.S., Nicholas Johnson, M.S., Shierly Fok, M.S., and Sabrina Mierswa, B.S. I have learned so much from all of you and am honored to call you all, not only my colleagues, but also my friends. Thank you for making lab a fun and exciting place to do science! Additionally, I would like to thank my undergraduate research mentor Dr. Wenwan Zhong, and the California Alliance for Minority Participation in STEM (CAMP) program at UC Riverside for inspiring me and providing me the resources to apply for graduate school. Thank you Dr. Zhong for giving me the chance to work in your lab and for being a strong mentor and role model for me. I am forever in debt to all the support and guidance I received at my undergraduate institution.

Finally, I would like to thank my family and friends who continually supported and inspired me throughout my degree. Thank you to Dr. Anita Rajamani and Miranda Bustamante M.S. for being amazing friends to me when I first got to Davis and making me believe that I did belong

here. I would also like to thank my sister Julia Gionet-Gonzales B.S., who herself is an accomplished engineer, I am so grateful to have you as a sister. I am also incredibly lucky to have my grandparents, Joe and Francis Gionet, in my life, who have happily attended all the graduations and presentations and have always been there when I needed them. Thank you to my incredibly supportive significant other, Dr. Jordan Kujala, who has never hesitated to help and encourage me throughout my degree. Lastly, thank you to my parents Denise and Anthony Gionet-Gonzales, who have nurtured my passion for science from a young age, worked so hard for me to be able to pursue my education, stood by me for every ambitious goal I ever had, and continue to show me unconditional love and support. I love you all, and I would never have been able to make it where I am today without you.

ABSTRACT

Mesenchymal stromal cells (MSCs) are under broad investigation to catalyze tissue regeneration and treat numerous diseases, and cell-based approaches are a promising alternative to high concentrations of recombinant growth factors. Despite robust lineage-specific differentiation potential *in vitro*, MSC function *in vivo* is largely attributed to their potent secretome composed of a complex mixture of reparative growth factors (GFs). GF secretion is markedly increased when MSCs are formed into spheroids. However, MSC spheroids alone are insufficient to induce robust bone regeneration compared to BMP-2 delivery, often delivered in supraphysiological concentrations. **We hypothesize that the regenerative potential of MSC spheroids could be enhanced through 1) synergistic coupling with a complementary cell secretome and 2) engineering GF-sequestering materials for entrapment.** Considering the established synergistic relationship between muscle and bone, we first hypothesized that the MSC secretome could enhance the bioactivity of myokines secreted by myoblasts by increasing the concentration and diversity of endogenous GFs present for bone regeneration. We found that the osteogenic potential and GF concentration of conditioned media increased when exposed to myoblasts. When delivered into a rat critical-sized femoral defect using an alginate hydrogel, we observed increased bone formation in defects treated with conditioned media compared to the delivery of MSCs alone. As expected and in agreement with other studies, the majority of GF in our platform eluted within 24 hours, limiting the therapeutic effect of the scaffolds and motivating the critical need for engineered scaffolds that retain bioactive components from the system. We next modified alginate hydrogels with sulfate groups to sequester heparin-binding GFs

secreted from MSCs to enhance the potency and availability of the MSC secretome. We confirmed that sulfated alginate hydrogels sequestered a mixture of endogenous biomolecules secreted by entrapped MSCs, thereby prolonging the therapeutic effect of MSC spheroids for tissue regeneration. We further confirmed these growth factors remain bioactive, both indirectly by stimulating limited endothelial cell tubulogenesis from conditioned media and directly by measuring enhanced myoblast infiltration. We further investigated this platform *in vivo* by implanting it in a rat muscle crush injury. We found the combination of spheroids and sulfated alginate limited early fibrotic response and stimulated neuromuscular junction formation. This platform has the potential to significantly enhance current cellular tissue engineering approaches as well as become a model for investigating growth factor sequestration for other applications.

Contents

CHAPTER 1: INTRODUCTION

1.1 PROBLEM STATEMENT

Although the body possesses several intricate biological mechanisms for repair of tissues and organs, it can often fall short of complete and functional regeneration. This can occur due to a multitude of reasons including advanced age or disease, as well as instances in which critically sized or compound wounds arise. Examples of poor regeneration requiring biomedical intervention throughout the body include non-union fracture, fibrotic muscle and a variety of other injuries represented in **Fig. 1.1**. In these cases, the body is unable to fully regenerate a tissue, leading to significant or in some cases total loss of function in the respective organs. These examples highlight the need for increased research toward techniques and technologies that augment the natural repair mechanisms in the body.

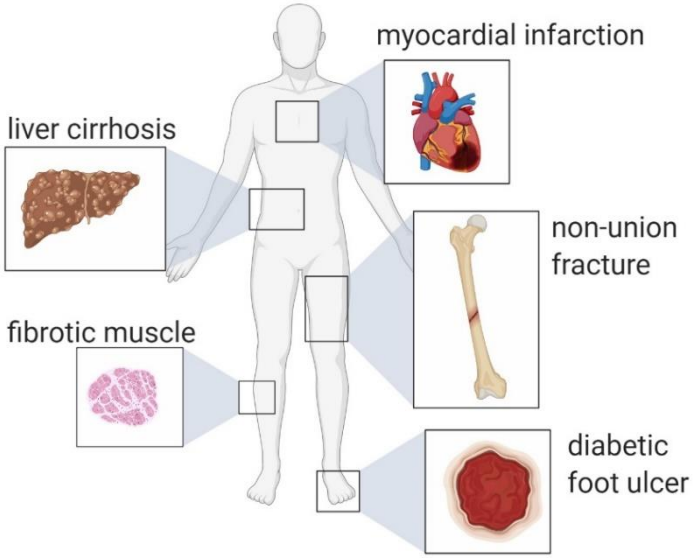

Figure 1.1. Poor regeneration can occur in several parts of the body, leading to lower quality of life. Tissue engineering seeks to enhance these repair mechanisms to increase tissue function.

Tissue engineering seeks to take on these challenges and has investigated many promising tools to aid the body in properly healing during these instances. Mesenchymal stromal cells (MSCs) have garnered increasing attention in this space, as they possess several well characterized regenerative capabilities. MSCs themselves are known to differentiate down chondrogenic, adipogenic and osteogenic linages that have the potential to integrate into their corresponding tissues.[1, 2] However, these functions of MSCs are often not the dominant regenerative effect in cell based therapies, considering the number of viable MSCs available for

direct incorporation into the tissue is extremely low.[4] MSCs possess indirect therapeutic potential due to their secretome, which contains a wide array of growth factors (GF), cytokines, and extracellular vesicles.[5, 6] These bioactive molecules can dictate resident cell function toward tissue repair and therefore represent a promising avenue for the use of MSCs within the tissue engineering field.

Although MSCs offer many exciting applications for tissue regeneration, wound sites that would benefit from therapeutic augmentation from implanted cells are commonly inhospitable for their engraftment. Naturally, these injury sites are highly inflamed, possessing high concentrations of proteases and reactive oxygen species secreted by immune cells to combat invading pathogens (**Fig. 1.2**). This immunological battle within the body, coupled with low oxygen and nutrient availability following destruction of the local vasculature, leads to low cell survivability. This dissertation seeks to address this issue through leveraging the following tools: **1) Aggregating MSCs into spheroids to enhance viability and GF secretion; 2) Entrapping cells in engineered hydrogels to increase survival and tune cell function; and 3) Promoting and retaining the MSC secretome to enhance therapeutic output, regardless of cell viability**.

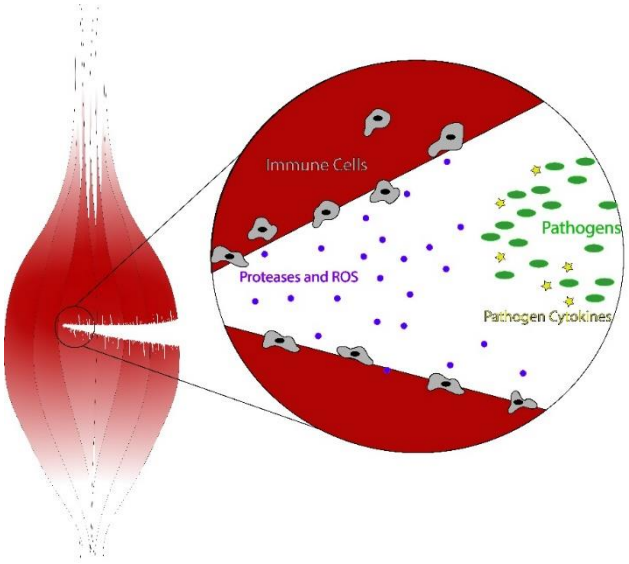

Figure 1.2. Fresh wound sites are characterized by inflammatory responses that propagate an inhospitable environment for implanted cells. This is due to immune cells attempting to clear the injured tissue of any potential pathogens from the environment.

The first method we will investigate is to use MSCs aggregated into multicell pellets, known as spheroids. Not only do MSCs exhibit higher viability when formed into

spheroids, but the therapeutic capacity of the MSC secretome is also amplified.[7, 8] Spheroid formation allows cells to attach and interact more effectively with each other and their extracellular matrix (ECM), as they would in a 3D tissue environment. Therefore, spheroid formation offers many advantages for tissue engineering, including increasing cell viability and promoting MSC ability to regulate function of vascular and immune cells through upregulation of secreted factors.[9] Although MSC spheroids offer many advantages compared to monodispersed cells, they do not address all concerns with implanted cell viability. MSC spheroid viability still decreases over time, and subsequently the secretome is also lost.[10]

Hydrogels have been utilized extensively in the tissue engineering field to further increase spheroid viability and dictate function. Biomaterials can increase entrapped cell viability by providing a physical buffer between delivered cells and the pro-inflammatory wound environment. Additionally, biomaterials enhance cell survival by providing instructional cues such as adhesion sites, growth factors, and protecting cells from mechanical stress associated with injection.[11] Beyond cell survival, substrate material properties influence cell function significantly. For example, material stiffness can dictate cell differentiation[12], stress-relaxation regulates cell spreading[13], and peptide presentation can influence cell survival and therapeutic potency[14]. Alginate, a naturally derived, tunable, FDA-approved biomaterial, can be modified to express properties for increasing the therapeutic potency of MSCs. Specifically, we demonstrate the ability of alginate to tune storage modulus and degradation rate independent of chemical properties such as peptide conjugation or chemical group functionalization. Through modification of these properties for biomaterials used in cell delivery, we have demonstrated improved regeneration of musculoskeletal tissues within a range of animal models.

The final strategy we will investigate is to retain or deliver bioactive molecules secreted by MSCs, allowing them to become the main influence of therapeutic impact regardless of MSC death. Alginate hydrogels are a promising platform to pursue this strategy, as these gels possess a small mesh size that leads to slow diffusion rates of large GFs and a negative charge that can

weakly bind positively charged GFs.[15] Within this thesis, we investigate the capacity of alginate to deliver the MSC spheroid secretome when transplanted into a rat femoral defect model. The secretome had a significant therapeutic benefit for bone regeneration, indicating promise for an acellular hydrogel strategy that would circumvent the need to prolong cell viability *in vivo*.[8] To further increase GF retention, we mimicked heparan sulfate, a molecule within the extracellular matrix that sequesters positively charged GFs, using negatively charged sulfate groups. In previous studies, recombinant GFs sequestered by heparan sulfate not only exhibit increased retention but also display increased bioactivity.[16]

Instead of using heparan sulfate itself, we studied sulfate-functionalized alginate that can bind GFs similarly to heparan sulfate. Heparan sulfate is a large, complex molecule that can be difficult to chemically bond to other polymeric substrata, and sulfated alginate facilitates more tunability in our platform. Sulfated alginate has been utilized by other groups to deliver individual recombinant GFs.[17, 18] However, to our knowledge, no group has explored the capacity of sulfated alginate hydrogels to efficiently deliver the complex mixture of secreted GFs contained within the MSC secretome.

Within this dissertation, alginate was functionalized with sulfate groups, and the GF binding ability, tunability and material properties were evaluated for this material. We then determined how the MSC spheroid secretome can be retained in sulfated alginate, thereby enhancing MSC spheroid therapeutic potency *in vitro* and *in vitro*.

1.2 HYPOTHESIS AND SPECIFIC AIMS

Hypothesis: The mesenchymal stromal cell (MSC) spheroid secretome can be used to enhance tissue regeneration through localized delivery from engineered materials.

Aim 1: Evaluate the regenerative and osteogenic differentiation potential of the MSC and myoblast secretome and evaluate efficacy of the secretome in a rat femoral defect model.

Aim 2: Engineer a sulfated alginate hydrogel for retention and increased bioactivity of MSC spheroid secretome.

Aim 3: Determine myoblast response in MSC spheroid -oaded sulfated alginate hydrogels and evaluate efficacy in a rat muscular crush injury.

1.3 SIGNIFICANCE

Current GF delivery strategies have potential for tissue regeneration but suffer from multiple drawbacks that diminish their effectiveness for clinical applications. Many GF therapies are already available in the clinic, including bone morphogenetic protein 2 (BMP-2) for spinal fusion and a truncated version of keratinocyte growth factor (KGF) used in combating the negative effects of chemotherapy.[19, 20] However, there are numerous disadvantages to these approaches, many stemming from the fact that supraphysiological levels of GF are required to achieve a therapeutic response *in vivo*. This is due to a combination of short GF half-lives and poor clinical delivery, which is often characterized by an undesired burst release within the first 24 hours. However, such high concentrations of these implanted GFs are prone to off-target effects. For example, VEGF (vascular endothelial growth factor) has been implicated in tumor growth and metastasis, leading to the development of drug Bevacizumab (Avastin; Genentech) as an anti-VEGF chemotherapy agent.[21] The delivery of a single recombinant GF also is not reflective of the diversity of GFs involved in tissue regeneration and homeostasis. Cells secrete a complex

Table 1.1.

Heparin binding growth factors and their corresponding binding constant to heparin.[3]

Growth Factor	K_A (M^{-1})
aFGF	$7.9x10^7$
bFGF	$1.68x10^7$
EGF	$8.38x10^6$
HGF	$1.19x10^8$
IGF	$5.55x10^7$
IL-6	$1.12x10^7$
PDGF-BB	$1.33x10^6$
SDF-1	$1.65x10^7$
VEGF	$8.14x10^5$

cocktail of GFs, while the majority of GF-based therapies rely on a single or only a few factors to influence cell function.

MSC spheroids themselves represent a promising alternative GF source to individual recombinant GF delivery. Spheroids secrete a complex secretome that can influence local cell function while limiting off-target effects. Our lab has previously characterized this extensively *in vitro* and *in vivo* for osteogenic applications.[8, 22] This strategy is clinically relevant and not as expensive as GF synthesis considering the GFs are secreted by the patient's own cells. MSC spheroids exhibit enhanced viability in harsh environmental conditions, thus, we would expect prolonged GF production for longer periods than monodisperse cells. This prolonged delivery will further enhance therapeutic outcome compared to the burst release of a few factors.

To combat the loss of bioactive GF upon diffusion away from the implant site, GF sequestering moieties will further enhance the therapeutic capacity of the MSC secretome. Bound GFs show enhanced retention and increased signal transduction in cells when coupled with adhesive moieties compared to freely injected GFs.[23] GFs are presented physiologically to cells while sequestered to the ECM through glycosaminoglycans (GAGs).[24] Heparan sulfate, a GAG that can bind GFs, is indicated as the primary molecule in this process. Heparan has negatively charged sulfate and carboxylate groups that can electrostatically bind to the positively charged amino acids arginine and lysine present in GFs.[25] Binding potential of any two molecules can be represented by the association constant (K_a), where a higher K_a indicates higher affinity and lower K_a implies higher dissociation. Heparin binding growth factors have higher K_a values for heparin compared to non-heparin binding GFs that exhibit no binding to heparin. While not all GFs are

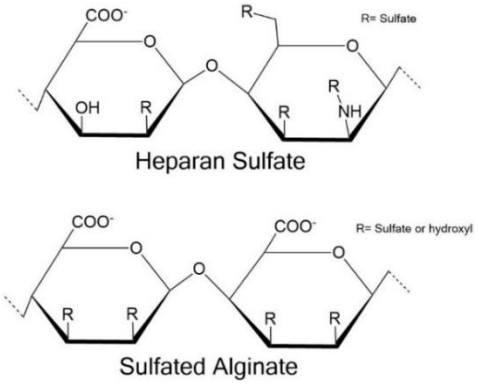

Figure 1.3. Heparan sulfate exhibits an analogous chemical structure to sulfated alginate, allowing it to similarly sequester heparin binding

heparan binding, many key tissue regenerative factors studied in tissue regeneration are heparin binding including VEGF, IGF, and EGF, among others in **Table 1.1**.[3]

Instead of focusing on large biological molecules like heparan, there are many advantages to using isolated GF sequestering sulfate groups. Heparin, a more biologically active derivative of heparan sulfate that is commonly used in the clinic to prevent blood clotting, has higher GF binding potential due to greater sulfation and more charge and has been investigated as a biomaterial for tissue engineering applications.[26, 27] However, the use of such a large, complex molecule that can cause unintended blood thinning is not ideal for biomaterial incorporation. Therefore, we propose a more direct approach by isolating the GF binding sulfate groups. Sulfate groups are simpler to chemically synthesize and eliminate many unintended effects that a larger heparin molecule may induce. Modification of alginate with sulfate groups yields a polymer that is structurally similar to heparan sulfate, GF binding, and remains mechanically and chemically tunable (**Fig. 1.3**).

With this platform, we engineered a cell and GF adhesive material to maintain the MSC spheroid secretome and maximize muscular repair. We hypothesized that a sulfated alginate hydrogel will retain factors secreted from MSCs, amplifying and retaining their therapeutic potential for a longer duration regardless of cell viability.

1.4 THESIS OVERVIEW

Chapter 2 is a review on MSC spheroids, including the engineering principles behind spheroid formation, an outline of different methods of spheroid formation, and a summary of their therapeutic applications and which biomaterials have been utilized to direct their function. Chapter 3 investigates the influence that MSC and myoblast secretome have on regeneration of a critically sized rat femoral bone defect. The combined secretome from two cell sources increased cell number and promoted osteogenic differentiation of pre-osteoblasts *in vitro*. *In vivo*, the secretome enhanced bone regeneration at 12 weeks post injury. Chapter 4 describes the synthesis and characterization of sulfated alginate. We showed that initial storage modulus, degradation rate

and sulfation are all characteristics that can be decoupled within our platform. We further demonstrated that sulfated alginate exhibited increased retention of a variety of heparan binding GFs, leading to increases in myoblast infiltration. Chapter 5 translates the MSC spheroid sulfated alginate into a rat soleus muscle crush injury. Hydrogels with either sulfated alginate alone, MSC spheroids in unmodified alginate, MSC spheroids in sulfated alginate, or MSC spheroid conditioned media in sulfated alginate were placed on top of the injured muscle. The regeneration of the muscle was evaluated through histological analysis, mechanical testing, and biochemical testing. Chapter 6 investigates an alginate biomaterial with hyaluronate, mineralized microspheres and autologous MSCs for regeneration of bone in the iliac crest of sheep. This study showed alginate implanted with MSCs enhanced bone repair in a large animal model. The conclusions of the thesis are presented in Chapter 7, summarizing the main findings of the dissertation, putting them in context with other work, and predicting future trends in the field.

1.5 REFERENCES

[1] F. Ng, S. Boucher, S. Koh, K.S. Sastry, L. Chase, U. Lakshmipathy, C. Choong, Z. Yang, M.C. Vemuri, M.S. Rao, V. Tanavde, PDGF, TGF-beta, and FGF signaling is important for differentiation and growth of mesenchymal stem cells (MSCs): transcriptional profiling can identify markers and signaling pathways important in differentiation of MSCs into adipogenic, chondrogenic, and osteogenic lineages, Blood 112(2) (2008) 295-307.

[2] C.K. Chan, E.Y. Seo, J.Y. Chen, D. Lo, A. McArdle, R. Sinha, R. Tevlin, J. Seita, J. Vincent-Tompkins, T. Wearda, W.J. Lu, K. Senarath-Yapa, M.T. Chung, O. Marecic, M. Tran, K.S. Yan, R. Upton, G.G. Walmsley, A.S. Lee, D. Sahoo, C.J. Kuo, I.L. Weissman, M.T. Longaker, Identification and specification of the mouse skeletal stem cell, Cell 160(1-2) (2015) 285-98.

[3] I. Freeman, A. Kedem, S. Cohen, The effect of sulfation of alginate hydrogels on the specific binding and controlled release of heparin-binding proteins, Biomaterials 29(22) (2008) 3260-8.

[4] A.I. Caplan, Are All Adult Stem Cells The Same?, Regenerative Engineering and Translational Medicine 1(1) (2015) 4-10.

[5] M. Brennan, P. Layrolle, D.J. Mooney, Biomaterials functionalized with MSC secreted extracellular vesicles and soluble factors for tissue regeneration, Adv Funct Mater 30(37) (2020).

[6] M. Ruiz, K. Toupet, M. Maumus, P. Rozier, C. Jorgensen, D. Noël, TGFBI secreted by mesenchymal stromal cells ameliorates osteoarthritis and is detected in extracellular vesicles, Biomaterials 226 (2020) 119544.

[7] J.M. Santos, S.P. Camões, E. Filipe, M. Cipriano, R.N. Barcia, M. Filipe, M. Teixeira, S. Simões, M. Gaspar, D. Mosqueira, D.S. Nascimento, P. Pinto-do-Ó, P. Cruz, H. Cruz, M. Castro, J.P. Miranda, Three-dimensional spheroid cell culture of umbilical cord tissue-derived mesenchymal stromal cells leads to enhanced paracrine induction of wound healing, Stem Cell Res Ther 6 (2015) 90.

[8] A.M. Saiz, Jr., M.A. Gionet-Gonzales, M.A. Lee, J.K. Leach, Conditioning of myoblast secretome using mesenchymal stem/stromal cell spheroids improves bone repair, Bone 125 (2019) 151-159.

[9] S. Aggarwal, M.F. Pittenger, Human mesenchymal stem cells modulate allogeneic immune cell responses, Blood 105(4) (2005) 1815-22.

[10] I.G. Kim, H. Cho, J. Shin, J.H. Cho, S.W. Cho, E.J. Chung, Regeneration of irradiation-damaged esophagus by local delivery of mesenchymal stem-cell spheroids encapsulated in a hyaluronic-acid-based hydrogel, Biomater Sci 9(6) (2021) 2197-2208.

[11] N. Mitrousis, A. Fokina, M.S. Shoichet, Biomaterials for cell transplantation, Nature Reviews Materials 3(11) (2018) 441-456.

[12] A.J. Engler, S. Sen, H.L. Sweeney, D.E. Discher, Matrix Elasticity Directs Stem Cell Lineage Specification, Cell 126(4) (2006) 677-689.

[13] O. Chaudhuri, L. Gu, M. Darnell, D. Klumpers, S.A. Bencherif, J.C. Weaver, N. Huebsch, D.J. Mooney, Substrate stress relaxation regulates cell spreading, Nat Commun 6(1) (2015) 1-7.

[14] A.Y. Clark, K.E. Martin, J.R. García, C.T. Johnson, H.S. Theriault, W.M. Han, D.W. Zhou, E.A. Botchwey, A.J. García, Integrin-specific hydrogels modulate transplanted human bone marrow-derived mesenchymal stem cell survival, engraftment, and reparative activities, Nat Commun 11(1) (2020) 114.

[15] M.C. Peters, B.C. Isenberg, J.A. Rowley, D.J. Mooney, Release from alginate enhances the biological activity of vascular endothelial growth factor, J Biomater Sci Polym Ed 9(12) (1998) 1267-78.

[16] M.H. Hettiaratchi, T. Miller, J.S. Temenoff, R.E. Guldberg, T.C. McDevitt, Heparin microparticle effects on presentation and bioactivity of bone morphogenetic protein-2, Biomaterials 35(25) (2014) 7228-38.

[17] J. Park, S.J. Lee, H. Lee, S.A. Park, J.Y. Lee, Three dimensional cell printing with sulfated alginate for improved bone morphogenetic protein-2 delivery and osteogenesis in bone tissue engineering, Carbohydr Polym 196 (2018) 217-224.

[18] B. Wang, P.J. Díaz-Payno, D.C. Browe, F.E. Freeman, J. Nulty, R. Burdis, D.J. Kelly, Affinity-bound growth factor within sulfated interpenetrate network bioinks for bioprinting cartilaginous tissues, Acta Biomater (2021).

[19] M.L. Radtke, J.M. Kolesar, Palifermin (Kepivance) for the treatment of oral mucositis in patients with hematologic malignancies requiring hematopoietic stem cell support, J Oncol Pharm Pract 11(3) (2005) 121-5.

[20] J.K. Burkus, M.F. Gornet, C.A. Dickman, T.A. Zdeblick, Anterior lumbar interbody fusion using rhBMP-2 with tapered interbody cages, J Spinal Disord Tech 15(5) (2002) 337-49.

[21] F. Kazazi-Hyseni, J.H. Beijnen, J.H. Schellens, Bevacizumab, Oncologist 15(8) (2010) 819-25.

[22] S.S. Ho, A.T. Keown, B. Addison, J.K. Leach, Cell migration and bone formation from mesenchymal stem cell spheroids in alginate hydrogels are regulated by adhesive ligand density, Biomacromolecules 18(12) (2017) 4331-4340.

[23] T.T. Chen, A. Luque, S. Lee, S.M. Anderson, T. Segura, M.L. Iruela-Arispe, Anchorage of VEGF to the extracellular matrix conveys differential signaling responses to endothelial cells, J Cell Biol 188(4) (2010) 595-609.

[24] G.S. Schultz, A. Wysocki, Interactions between extracellular matrix and growth factors in wound healing, Wound Repair Regen 17(2) (2009) 153-62.

[25] J.R. Fromm, R.E. Hileman, E.E. Caldwell, J.M. Weiler, R.J. Linhardt, Differences in the interaction of heparin with arginine and lysine and the importance of these basic amino acids in the binding of heparin to acidic fibroblast growth factor, Arch Biochem Biophys 323(2) (1995) 279-87.

[26] O. Jeon, C. Powell, L.D. Solorio, M.D. Krebs, E. Alsberg, Affinity-based growth factor delivery using biodegradable, photocrosslinked heparin-alginate hydrogels, J Control Release 154(3) (2011) 258-66.

[27] M. Ohta, Y. Suzuki, H. Chou, N. Ishikawa, S. Suzuki, M. Tanihara, Y. Mizushima, M. Dezawa, C. Ide, Novel heparin/alginate gel combined with basic fibroblast growth factor promotes nerve regeneration in rat sciatic nerve, J Biomed Mater Res A 71(4) (2004) 661-8.

CHAPTER 2: ENGINEERING PRINCIPLES FOR GUIDING SPHEROID FUNCTION IN THE REGENERATION OF BONE, CARTILAGE, AND SKIN

There is a critical need for strategies that effectively enhance cell viability and post-implantation performance in order to advance cell-based therapies. Spheroids, which are dense cellular aggregates, overcome many current limitations with transplanting individual cells. Compared to individual cells, the aggregation of cells into spheroids results in increased cell viability, together with enhanced proangiogenic, anti-inflammatory, and tissue-forming potential. Furthermore, the transplantation of cells using engineered materials enables localized delivery to the target site while providing an opportunity to guide cell fate *in situ*, resulting in improved therapeutic outcomes compared to systemic or localized injection. Despite promising early results achieved by freely injecting spheroids into damaged tissues, growing evidence demonstrates the advantages of entrapping spheroids within a biomaterial prior to implantation. This review will highlight the basic characteristics and qualities of spheroids, describe the underlying principles for how biomaterials influence spheroid behavior, with an emphasis on hydrogels, and provide examples of synergistic approaches using spheroids and biomaterials for tissue engineering applications.

Published as: M.A. Gionet-Gonzales, J.K. Leach, Engineering principles for guiding spheroid function in the regeneration of bone, cartilage, and skin, *Biomed Mater*. 13 (2018) 34109.

2.1 INTRODUCTION

Cell-based therapies are a promising therapeutic alternative to tissue grafts or pharmacological approaches for treating tissue loss due to trauma, disease, or congenital malformation. Indeed, the cell therapy market is projected to grow to nearly $330 million by 2020.[1] Several cell-based therapies are already used as effective treatments, including bone marrow [2] and umbilical cord stem cell transplants [3] to treat cancer and anemia. Adipose tissue is another readily accessible tissue compartment to harvest cells for regenerative therapies. Adipose stromal cells can be isolated in large numbers from the donor for autologous use, possess multilineage potential, and may be used with minimal manipulation,[4] potentially reducing the oversight required by regulatory bodies such as the United States Food and Drug Administration (FDA). In cases where it is difficult to procure sufficient quantities of cells, investigators have used *ex vivo* expansion prior to reinjection into the body. For example, chimeric antigen receptor T cell (CAR-T) therapy utilizes T cells harvested from the patient, which are genetically engineered to recognize and attack tumor cells and expanded *ex vivo* for infusion to the patient. This therapy achieved successful outcomes in clinical trials with more than 75% of B cell acute lymphoblastic leukemia patients treated with CAR-T classified as minimal residual disease negative[5], leading to FDA approval in 2017 for treatment of acute lymphoblastic leukemia and relapsed large B-cell lymphoma.

Mesenchymal stem cells (MSCs) are a widely studied candidate for cell-based therapies and tissue engineering. MSCs possess multilineage potential and a potent secretome that promotes tissue repair and modulates the local inflammatory microenvironment. More than 600 clinical trials are ongoing that utilize MSCs as an intervention for numerous diseases including arthritis, diabetes, cardiovascular disease, and lung disease (www.clinicaltrials.gov; accessed 11/3/2017). Despite exciting results when transplanting somatic or stem and progenitor cells into damaged tissues, numerous challenges remain for cell-based therapies to achieve their full clinical potential. The vast majority of cells transplanted into an injury site are no longer viable within days

due to the harsh microenvironment and limited cell-cell and cell-matrix interactions.[6-8] While short-term cell survival has resulted in detectable improvements, these effects may be insufficient when considering the costs associated with cell collection, expansion, and ensuring the purity and safety prior to transplantation. The therapeutic benefits of transplanting cells into damaged tissues will no doubt be enhanced by prolonging their survival and guiding their activity *in situ*.

Cellular spheroids represent one approach to address the shortcomings of individual cells freely injected or transplanted into the body (**Fig. 2.1**). Spheroids are dense aggregates formed when cells exhibit preferential cohesion to other cells over adhesion to the underlying matrix. Cells within spheroids are exposed to physical interactions that more closely reflect behavior in three-dimensional (3-D) native tissue.[9] Unlike individual cells liberated from the culture dish, spheroids retain their endogenous extracellular matrix (ECM), which has instructive potential to promote physiologically accurate connections with their environment, prolong cell survival, and direct differentiation.[10-13] Beyond cellular aggregation, the use of engineered carriers as cell delivery vehicles provides additional means to instruct cell function and enhance the effect of cell therapies. Cells that are intravenously or locally injected are rapidly cleared from the body or fail to remain at the intended target site following migration or death.[14, 15] Biomaterials present instructive cues to entrapped cells to potentiate their survival and guide cell fate over predetermined spatial and temporal time scales. The contribution of spheroids towards tissue repair, once entrapped and transplanted in engineered materials, is under investigation to pursue new opportunities and propel their therapeutic benefit in cell-based therapies. This review will describe the fundamental principles and strategies of spheroid formation, articulate the benefits of spheroids over individual cells, and highlight recent examples using spheroids with engineered materials, particularly hydrogels, for tissue engineering applications.

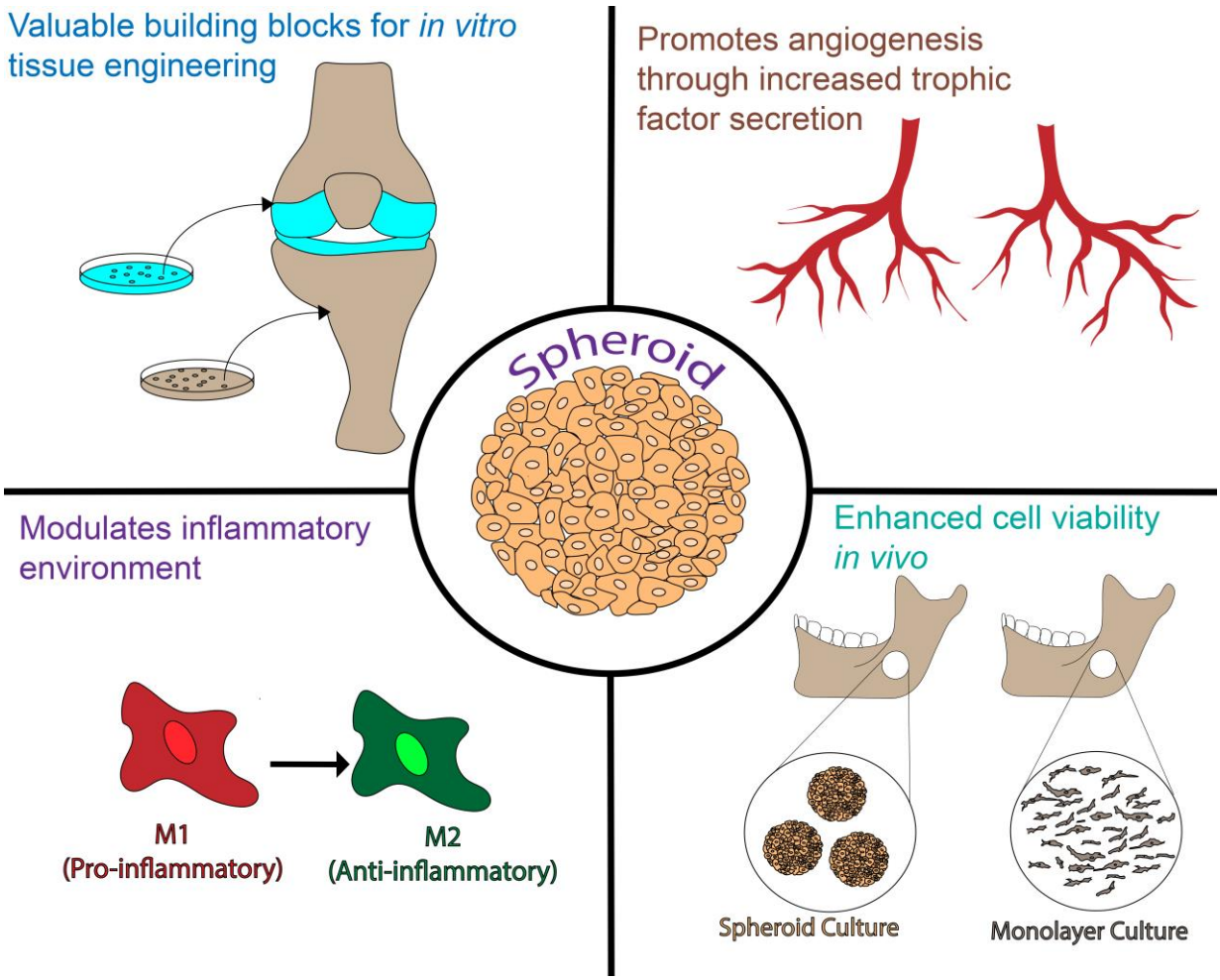

Figure 2.1. Spheroids overcome many shortcomings inherent with individual cells when used in cell-based therapies and tissue engineering. Compared to individual cells, spheroids secrete increased levels of trophic factors with proangiogenic and immunomodulatory potential, exhibit enhanced cell viability and persistence, and are valuable building blocks for tissue formation.

2.2 SPHEROIDS FOR DEVELOPMENT AND DRUG DISCOVERY

Individual cells, whether in monolayer culture or distributed in a 3-D environment, fail to mimic the complex cell-cell and cell-matrix interactions present within a tissue. The limited interaction between individual cells in culture hinders efforts to model early events in development, accurately test the potency of numerous chemotherapeutic molecules, and prepare cells for their intended

use in cell therapies. Spheroids directly address these concerns by promoting cell-to-cell contact and presenting more physiologically relevant characteristics. In 1944, Holtfreter pioneered the use of spheroids as a morphogenic model in his investigation of ectoderm and endoderm behavior during development.[16] Embryonic stem cell spatial positioning in a spheroid approximates that of a dividing fertilized egg by maintaining spherical geometry for several developmental stages.

Spheroids are also valuable tools in the understanding and experimental modeling of cancer.[17] Tumor cells within the spheroid central core experience reduced oxygen and nutrient availability, reflecting a hypoxic and nutrient-starved core evident in tumors.[18] Tumor cell spheroids are widely used as models to test the efficacy of antineoplastic drugs, while mathematical models devised to predict tumor response have further improved the design and dosing of these drugs.

Spheroids formed of other cell types are used to model cell function in various tissues, although with alternate rationales from studying embryological development or cancer. Spheroids are not normally found under physiological conditions in the postnatal organism, yet aggregates of neural cells and cardiomyocytes have revealed new findings in the behavior of these cell populations.

Neurospheres are commonly used for modeling neural tissues to study brain tumors and developmental neurotoxicity. Neurospheres exhibit many processes observed in brain development including cell proliferation, migration, and apoptosis.[19] Neurospheres can be used to model adverse chemical effects in a developing brain and the impact of the Zika virus.[20, 21] Following brain tumor excision, the incidence of tumor reoccurrence is extremely high, likely due to the retention of a subset of the tumor cell population that can regenerate the tumor after removal.[22] Neurospheres were employed as a model system to evaluate the behavior and function of these tumor cells and to assess lineage commitment and mitogenic potency.[23] Neurospheres have also been directly used for tissue engineering applications. Neural stem cells maintained as neurospheres in culture were transplanted into the brains of neonatal mice where

they engrafted and differentiated *in vivo*.[24] Cardiospheres of cardiac progenitor cells exhibit enhanced differentiation, increased ECM secretion, and in some cases, can functionally beat.[25, 26] Cardiomyocytes derived from cardiospheres can be directly grafted into infarcted cardiac muscle[27] and form new cardiac tissue in mice.[28] Although spheroids can accurately recapitulate some aspects of the physiological environment, they alone are still imperfect models. When multiple cell types are present, as occurs *in vivo*, cellular organization within a spheroid may not mimic physiological conditions. Furthermore the proper management of the physiochemical conditions for each individual spheroid can be challenging, often requiring the incorporation of more complex systems such as bioreactors or microfluidic devices.[29]

Spheroids are increasingly pursued as therapeutic agents in tissue engineering, due to their capacity to outperform individual cells in monolayer culture or suspended in a 3-D environment. Chondrocytes undergo rapid dedifferentiation in culture, and the micromass assay is a standard approach for generating small cartilaginous pellets.[30] Chondrogenic differentiation is enhanced in spheroids, possibly due to the activation of the Rho/Rho-associated kinase (ROCK) pathway.[31] Spheroids mimic mesenchymal condensation, an embryonic event that is prerequisite to chondrogenic differentiation.[32] Mesenchymal stem/stromal cells (MSCs) from bone marrow, adipose tissue (ASCs), and other tissue compartments are used in tissue engineering due to their multilineage potential and their potent secretome that stimulates angiogenesis and suppresses inflammation.[33-35] MSCs stimulated with transforming growth factor-β (TGF-β) formed aggregates and produced cartilage that was within range of physiological stiffness.[36] ASC spheroids stimulated the regeneration of cartilage and subchondral bone in microminipigs after one year of implantation.[37] MSC spheroids increased angiogenesis by enhanced secretion of endogenous proangiogenic growth factors, and injection of spheroids into ischemic hind limbs accelerated neovascularization in rodents.[38] Spheroids also upregulate production of prostaglandin E2 (PGE_2)[39, 40], which polarizes pro-inflammatory M1 macrophages toward a more anti-inflammatory, regenerative M2 phenotype.[41] Spheroids

formed of post-thawed human ASCs possessed greater cell viability compared to cells in monolayer, highlighting the clinical potential of spheroids in cell therapies.[42] Furthermore, cells within spheroids decrease their expression of several surface markers, making them less likely to trigger an immune response compared to individual cells.[43] Overall, spheroids possess many desirable qualities for tissue engineering applications that will be further discussed in subsequent sections.

2.3 CONSIDERATIONS FOR SPHEROID FORMATION

Spheroid formation requires compaction and protein accumulation that occur through self-assembly without the need for additional stimuli (**Fig. 2.2**).[44-47] While the precise sequence of events is likely related to the preparation and identity of selected cells, spheroid formation is dependent upon increased cadherin expression and the production and engagement of an endogenous ECM. Beyond cohesion, adhesion, and compaction, spheroids depict characteristics of self-organization by partitioning themselves based on cell type and adhesive strength. Cellular self-organization has been described by Foty and Steinberg using the differential adhesion

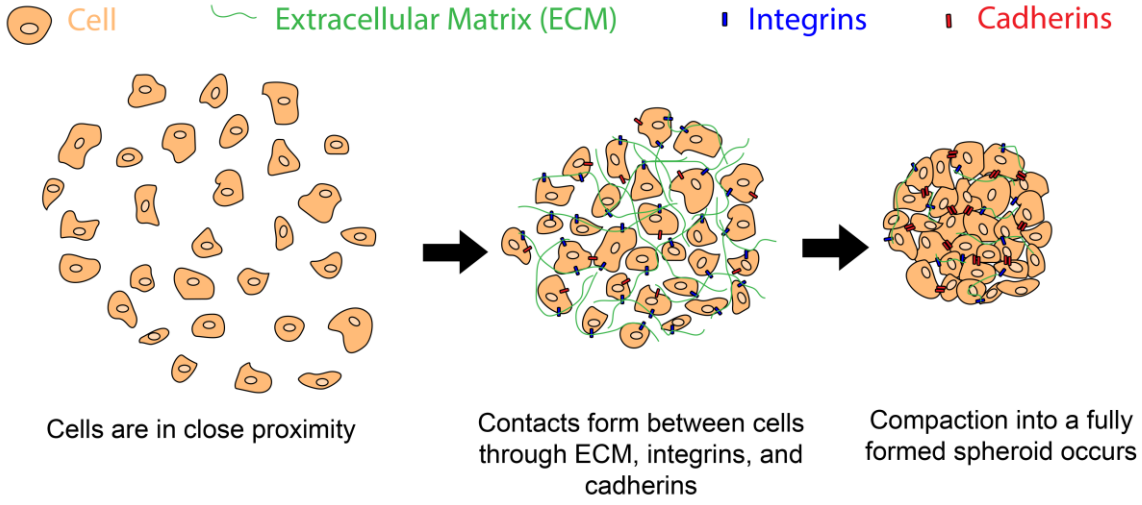

Figure 2.2. Cell suspensions assemble into spheroids upon cell-to-cell binding and establishing ligand-receptor interactions *via* cadherins and integrins, respectively. The cellular aggregate compacts into a fully formed spheroid over time.

hypothesis (DAH), demonstrating that cells of higher adhesive strength aggregate in the center, while less adhesive cells are displaced and surround them.[48, 49] Although the DAH seems to predict the behavior of embryonic tissues, interactions among other more differentiated cell populations such as non-random cell motion, cell traction, and excessive cell compaction may dictate organization and merit further consideration.[50]

Spheroids are a powerful tool for research and clinical application, and thus, reliable and cost-effective means are necessary for their rapid and reproducible production. The hanging drop method remains one of the most commonly used techniques for spheroid formation due to its relative ease and lack of required specialized equipment.[51] This gentle, gravity-driven approach is unlikely to adversely affect cells. However, the utility of this method is confined to smaller spheroids, as larger aggregates fall from the droplet. Furthermore, the hanging drop method is labor intensive with low throughput capacity, limiting the numbers of spheroids that can be produced for therapeutic purposes. Micromolded pellet culture was developed to address throughput limitations of the hanging drop method. In this approach, non-adhesive culture surfaces, commonly prepared from agarose, are generated from a mold.[52, 53] Upon addition of a cell suspension, cells are forced to aggregate, and this process can be accelerated by centrifugation. Although this strategy eliminates restrictions on spheroid size and increases production throughput, high or prolonged centrifugation can disrupt the spheroids and potentially alter their function. Spheroids have also been made in even greater quantities using spinner flasks, wherein cells are maintained in media with continual stirring. Since cells are continually moving, they cannot adhere to the surface and may only aggregate with other cells. Stirring speed is a key optimization parameter, as cells exposed to excessive shear may die. Insufficient shear allows multiple spheroids to coalesce into larger aggregates, resulting in irregular spheroids or large nutrient gradients that reduce cell viability.

The surface properties of biomaterials, namely surface tension and adhesivity, may also be manipulated to guide spheroid formation. Stromal vascular fraction (SVF) derived from

lipoaspirate was formed into spheroids by seeding on a hydrophobic/hydrophilic patterned surface using a bioprinter technology similar to extrusion 3D printing.[54] Compared to self-assembly based methods, bioprinting was faster, produced spheroids of similar size and shape, and enabled the precise positioning and patterning of cells. However, bioprinting requires specialized equipment and exposes cells to potentially harmful shear forces that must be optimized for each cell type. Chitosan, a material derived from crustaceans, presents no human cell-binding domains and encourages cell-cell binding, making chitosan membranes a popular material for spheroid formation.[55, 56] Spheroid diameter can be controlled by cell seeding density on the membrane and peptide modification of the surface. ASC spheroids formed on chitosan membranes exhibited enhanced pluripotent gene expression compared to cells in monolayer culture, representing a strategy to impair undesired differentiation during culture expansion.[57] While the use of chitosan to form spheroids is relatively inexpensive and facilitates high throughput spheroid production, the size of resulting spheroids is irregular, leading to batch inconsistencies.

Spheroid diameter is a key variable to consider when translating this approach into clinical use, as spheroids may be delivered to ischemic tissues. While MSC spheroids can be formed with diameters as large as 600 μm without a hypoxic core[58], spheroids formed of other cells may be more vulnerable to limitations in nutrient transport. Importantly, spheroid diameter did not correlate with the number of cells per spheroid, suggesting that cells adapt their packing density during spheroid formation. When evaluating a comparable total number of cells, MSC spheroids composed of 40,000 cells secreted more PGE_2 and VEGF compared to more numerous, yet smaller spheroids made from 25,000 or 10,000 cells.[40] Thus, the number of cells per spheroid represents an important element in the design of cell-based approaches using spheroids.

2.4 FABRICATION OF ENGINEERED TISSUES USING SPHEROIDS

Over the last two decades, spheroids have become increasingly relevant for tissue engineering applications. Papas *et al.* initially evaluated the insulin-secreting characteristics of AtT-20 spheroids for their potential as bioartificial endocrine organs.[59] Since that report, the use of spheroids in tissue engineering applications has expanded. Spheroids have been used to engineer bone[60-63], cartilage[64, 65], skin[66], heart[67], liver[68, 69], brain[24], and various other tissues or tissue mimetics.

As previously stated, spheroids may contribute indirectly or directly to tissue formation. Compared to individual cells, spheroids secrete increased concentrations of trophic factors that speed angiogenesis, promote cell migration, and modulate the local inflammatory microenvironment, making them ideal for tissue engineering.[39, 40] Beyond secretion of endogenous factors, spheroids are promising building blocks for fabricating engineered tissues, as they can be further aggregated into larger tissue constructs. The use of spheroids as building blocks is motivated by eliminating the interruptions in cell-cell interactions that may occur when cells are seeded in scaffolds, a challenge identified in vascular tissue engineering.[70] Spheroids formed of human pluripotent stem cells (hPSCs) exhibited higher fusion capacity than aggregates of differentiated cells, resulting in successful post-fusion differentiation into neural tissue.[71] These data suggest an optimal protocol exists regarding the sequence of fusion and differentiation for each cell source and engineered tissue.

The positioning of spheroids may be manipulated through magnetic forces. Magnetoferritin nanoparticles, a less toxic alternative to iron oxide nanoparticles, were successfully internalized by cells that were then incorporated into spheroids. Nanoparticle-loaded spheroids were then magnetically patterned and fused into rings for vascular tissue engineering, resulting in rings with a 250 μm inner diameter after 156 hours of fusion.[72, 73] Alternatively, microtissues of various geometries have been generated directly from cell suspensions using polydimethylsiloxane

(PDMS) molds through cell self-assembly methods, reducing delays associated with spheroid formation.[74]

The emerging field of 3D printing leverages spheroids as building blocks to fabricate engineered tissues. To make larger aggregate structures for tissues such as liver, the Bio Pick, Place and Perfuse (Bio-3P) was engineered to precisely place cell aggregates together into a tissue while maintaining perfusion. Aggregates were formed as spheroids, toroids, or honeycombs and then oriented into a large-scale tissue.[75] Alternatively, the Kenzan printing method, under investigation for robotic spheroid-based 3-D printing, forms spheroids within stainless steel microneedles and can spatially position the aggregates in the desired orientation.[76] Endothelial colony forming cells (ECFCs) and smooth-muscle forming cells (SMFCs) derived from induced pluripotent stem cells (iPSCs) were formed into spheroids and printed using the Kenzan method. These spheroids fused within 7 days, and spheroids derived from SMFCs yielded tubular structures with apparent ECM deposition.[77] Heterogeneous cell spheroids composed of umbilical vein endothelial cells, aortic smooth muscle cells, and dermal fibroblasts were similarly printed into a tubular shape to engineer 1.5 mm inner diameter blood vessels that underwent maturation when cultured in an *ex vivo* perfusion system.[78] After 5 days in the rat aorta, these engineered vessels remained patent and exhibited remodeling and endothelialization of the tube. However, the time required for vessel formation remains a caveat of this approach, requiring 4 days for fusion and another 4 days for maturation in the bioreactor. Spheroids have also been used to bioprint engineered blood vessels with complex geometry and multiple layers.[79] Investigators reported that bioprinting cylinders rather than spheroids was more efficient at increasing structure homogeneity, reducing the fusion time from 5-7 days to as little as 2-4 days.

The assembly of spheroids into engineered tissues provides an exciting strategy to build densely cellularized tissues from the bottom up. However, numerous limitations remain unsolved. Significant delays are often incurred when expanding biopsies to clinically relevant numbers in

culture. A massive number of cells is needed to construct a tissue, potentially eliminating the possibility for using autologous cells. When incorporating undifferentiated stem and progenitor cells, it may be necessary to provide prolonged instructional cues, whether as soluble growth factors or mechanical stimulation, to ensure proper differentiation and avoid aberrant tissue formation. The resulting tissues lack mechanical integrity until sufficient ECM is deposited to bridge the spheroids or adequate fusion occurs. Collectively, these challenges necessitate extended culture durations to make desired tissues, combined with costly recombinant growth factors and unique bioreactors, which may limit the translation of this approach to the clinical setting.

2.5 BIOMATERIALS TO INFLUENCE SPHEROID FUNCTION

The clinical use of spheroids for tissue regeneration and repair is primarily restricted to two approaches: 1) maintaining spheroids in culture to promote fusion and formation into a more coherent structure; or 2) transplanting the cell aggregates to the target site immediately after formation. The former requires extended *ex vivo* culture time, hence delaying delivery to the patient, while the latter relinquishes control of spheroid function to the surrounding environment that may be damaged or inhospitable to transplanted cells. As an alternative approach, the entrapment of spheroids into biomaterials is a promising strategy that can address many of these challenges while heightening the therapeutic potential of spheroids in tissue repair. Biomaterials can be engineered with target ligands to engage neighboring cells and possessing desired mechanical properties including stiffness, porosity, and degradation.[80] Spheroids may also be implanted at a lower cell density when delivered in a biomaterial in anticipation that cells in the construct will proliferate and host cells will infiltrate the material. This can eliminate the need for costly growth factors to induce differentiation while reducing the time before implantation. However, the introduction of a biomaterial represents another level of complexity to the implant that requires careful consideration.

Hydrogels formed of alginate, fibrin, hyaluronic acid (HA), gelatin, and polyethylene glycol (PEG) have many favorable characteristics for cell entrapment and delivery, and they have been broadly used in cell-based therapies for tissue engineering.[81] Their gelation characteristics enable facile entrapment of cell aggregates and direct injection to the target site. Spheroids may be entrapped in large numbers or as individual aggregates. Additionally, many characteristics of the native ECM can be recapitulated in engineered hydrogels including the presentation of native adhesive ligands, cell-responsive linkages that promote hydrogel remodeling and degradation, and known mechanical properties. These properties can then be manipulated to influence cell growth, differentiation and behavior.[81]

The vast majority of cells used in tissue engineering are anchorage-dependent, requiring adhesion to the surrounding ECM to remain viable and undergo instruction toward the desired lineage. Cells transplanted in biomaterials consistently outperform those simply injected into the damaged tissue site. Biomaterials facilitate the localized delivery of cells and provide adhesive cues to promote cell survival, differentiation, or increase trophic factor secretion.[82, 83] Similarly, spheroids entrapped in biomaterials possessing engineered biophysical properties may enhance their therapeutic potential. For example, spheroids entrapped in biomaterials engineered to control adhesion exhibited increased secretion of many proangiogenic growth factors, as well as high cell viability and differentiation potential.[57, 84] To engineer specific adhesive properties into the material's bulk, one strategy is to covalently couple ECM proteins or peptide sequences to the polymer backbone that engage cellular receptors. The most common peptide used in this approach is arginine-glycine-aspartic acid (Arg-Gly-Asp, RGD), present in numerous ECM proteins such as fibronectin and collagen that enable cell adhesion. Most cell types are able to bind to RGD, making this a widely employed peptide to provide adhesivity to alginate and other polymers.[83, 85]

Ho *et al.* demonstrated the importance of adhesion to MSC spheroids by presenting RGD ligands to cells entrapped in alginate hydrogels (**Fig. 2.3A**).[84] Compared to spheroids in

unmodified alginate, which preserved the spherical structure due to its non-fouling nature, the presentation of RGD significantly increased both cell viability and VEGF secretion by entrapped spheroids. MSC spheroids entrapped in RGD-modified alginate gels exhibited increased osteogenic markers such as alkaline phosphatase (ALP) activity and calcium deposition compared to spheroids entrapped in unmodified gels, translating to increased bone formation *in vivo* in the absence of additional cues. More recently, the effect of RGD density on entrapped osteogenically induced MSC spheroids was reported (**Fig. 2.3B**), with increased ligand density translating to improved maintenance of the osteoblastic phenotype and increased bone formation *in vivo*.[86] Conversely, poly-L-lysine coated alginate beads possessing no cell adhesion sites impaired cell spreading and promoted embryonic stem cell (ESC) spheroid pluripotency.[87] These reports demonstrate that engineering the adhesive nature of biomaterials is a key parameter for instructing spheroid survival and function.

The density and spatial positioning of adhesive ligands within a biomaterial are important properties to regulate cell outgrowth from spheroids. 3D patterning of RGD in a collagenase-sensitive poly(ethylene glycol) diacrylate (PEGDA) hydrogel was achieved using a two-photon laser scanning (TPLS) photolithography technique.[88] TPLS immobilized RGD ligands on the gel in prescribed 3D patterns and gradients. Fibroblast clusters encapsulated in these gels were able to successfully migrate only into the patterned regions of the gel. By controlling the total area of pathways radiating from the spheroid, one could maintain aggregate formation for a known duration to sustain the desired therapeutic effect, while still allowing cells to migrate into the native tissue where they could further enhance repair.

Implantable scaffolds formed of synthetic polymers are commonly used in bone tissue engineering due to their tailorability (*e.g.*, shape, porosity, and mechanical properties), ease of synthesis, stability, and predictable resorption profile. Poly(lactic-co-glycolic acid) (PLGA) is an FDA-approved biodegradable polyester widely used for drug delivery that can be easily fashioned

into porous biomaterial scaffolds.[12, 89-91] Poly(ε-caprolactone) (PCL) is another FDA-approved polyester possessing biodegradability and tailorability. PCL is commonly fabricated into scaffolds *via* electrospinning to mimic the fibrous structure of the native ECM.[92] Although spheroids cannot be formed *a priori* and entrapped in these dry scaffolds like hydrogels, the biophysical properties of the material can induce spheroid formation of dissociated cells within the scaffolds.[82] ASCs seeded into dried porous PLGA scaffolds exhibited spheroid formation and enhanced adipogenic differentiation and vascularization after subcutaneous implantation into mice.[93] This group pursued a similar approach using ASC spheroids in poly(L-glutamic acid)/chitosan scaffolds for cartilage repair.[94]

The encapsulation of therapeutic cells has been widely investigated for endocrine cells such as hepatocytes.[95, 96] Similar to many other cell types, hepatocyte function is enhanced when formed into spheroids versus cells in monolayer[97], motivating the exploration of hepatocyte spheroids for studies *in vitro* and upon implantation.[98] The immune response to transplanted cells can be suppressed by entrapping spheroids in a biomaterial before implantation to the patient, thereby addressing a primary challenge in cell transplantation. The semipermeable biomaterial enveloping the spheroids enables necessary exchange of small molecules between hepatocytes and the surrounding environment, allowing for continued albumin secretion and oxygen diffusion without the risk of immune response. Without immunoisolation of the hepatocytes, functional cells could only be maintained using long-term immunosuppression, which has numerous drawbacks.[99] Therefore, spheroid encapsulation offers a promising solution.[96] Advanced methods have emerged to efficiently entrap hepatocytes by using microfluidic devices that combine aggregation and encapsulation in a PEG hydrogel in a single step. PEG-entrapped hepatocyte spheroids exhibited greater albumin secretion compared to spheroids in AggreWells™, with only a 17% loss in viability.[100] This study demonstrated that

hepatocyte spheroids could achieve enhanced function when encapsulated, emphasizing the potential for other applications of this approach.

Although hydrogels are intuitive biomaterials for spheroid entrapment, microporous scaffolds such as PLGA have also been used for endocrine aggregate cell delivery and allow for better host tissue integration. Islet cells, spheroid-like clusters of endocrine cells that produce insulin, have been delivered via porous PLGA scaffolds, with properties of the scaffold having a direct effect on islet behavior *in vivo*. Greater pore interconnectivity of the scaffold showed faster reversal of diabetes when islet cells were implanted into the epidermal fat pad of mice.[101] This further enforces the conclusion that proper biomaterial manipulation has a profound effect on spheroids

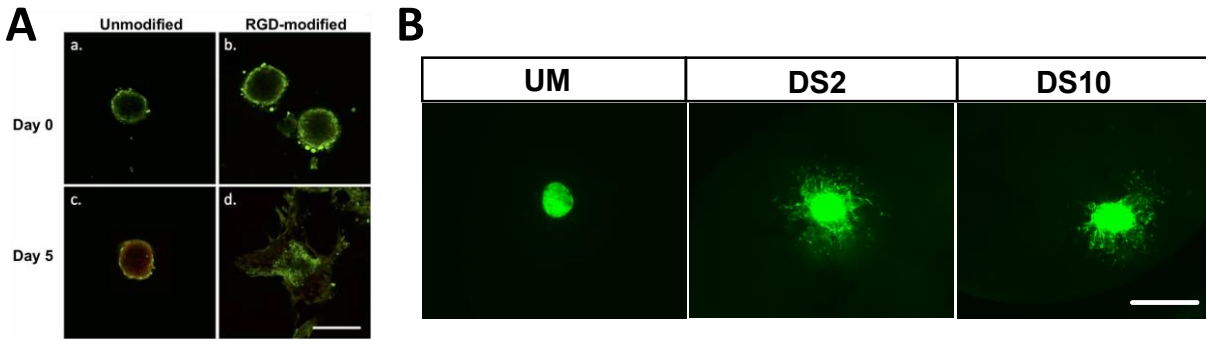

Figure 2.3. The presence and density of RGD in alginate hydrogels influence MSC spheroid viability and migration. (A) Live/dead stain reveals comparable viability and spherical morphology for spheroids at Day 0 in (**a**) unmodified and (**b**) RGD-modified gels when visualized with confocal microscopy. (**c**) Live/dead stain demonstrates increase in dead cells and retained spherical morphology for spheroids at Day 5 in unmodified alginate, while (**d**) spheroids in RGD-modified alginate gels have increased viability and migration from the aggregate. Scale bar = 200 µm. Reprinted with permission from (84), Copyright 2016 John Wiley and Sons. **(B)** Representative fluorescent images of spheroids in unmodified, DS2, and DS10 RGD-modified alginate gels at Day 10. Scale bar = 500 µm. Reprinted with permission from (86), Copyright 2017 American Chemical Society.

potential for tissue engineering. The potential of these scaffolds for use as drug delivery vehicles was demonstrated by sustained release of transforming growth factor-beta1 (TGF-β1). Islet cells face similar hurdles as hepatic transplants due to concerns regarding the immune response, and TGF-β1 is a potent growth factor that can combat the inflammation response occurring after implantation. Scaffolds delivering islet cells and releasing TGF-β1 exhibited improved graft survival and decreased leukocyte infiltration, thus reducing the immune response.[102]

Nanofibers have also been pursued as a favorable biomaterial for spheroid delivery due to their similar nanotopography to native ECM. Fibroblast spheroids were deployed for diabetic wound healing on 0.4 mm- (2D) or 4 mm-thick (3D) porous nanofiber mesh scaffolds made of PCL and gelatin.[103] Compared to 2D nanofiber scaffolds, fibroblasts had greater interaction with the pores in 3D scaffolds, suggesting an opportunity to improve cellularization of wound dressings. PLGA nanofibers coated with fibrin, collagen or no protein were placed on top of fibroblast spheroids for gingiva connective tissue engineering.[104] Fibers with collagen and fibrin prompted cell extensions protruding out of the spheroid, while uncoated fibers induced no spheroid migration. Further experiments showed collagen coated nanofibers allowed fibroblasts to migrate deeper into the scaffold and fuse into larger microtissues. Meanwhile, fibrin coated nanofibers promoted the disassembly of fibroblast spheroids, leading to scaffolds with highly dispersed fibroblasts Collectively, these examples of engineering nanofiber scaffolds for spheroid delivery exhibit the profound effect a properly designed scaffold may have on spheroid function. Through manipulation of fiber composition and structure, spheroids can remain as aggregates or become dissociated, ultimately dictating their therapeutic function.

Chitosan has been used to leverage the multilineage potential of MSCs for tissue engineering. Adipogenesis was enhanced in MSC spheroids after incubation on a chitosan coated amyloid fibril network for 7 days before induction[105], an effect potentially resulting from the nanotopography of the fibrils. Furthermore, ASC spheroids cultured on chitosan exhibited cardiac marker gene expression without additional inductive cues, potentially expanding the use of this

population in cardiac repair.[55] In another example, the differentiation capacity of ASCs was significantly enhanced after spheroid formation on chitosan membranes, pluripotency markers were upregulated, and transdifferentiation into neuronal and hepatocyte-like cells was reported.[57] Collectively, these reports demonstrate that the characteristics of the biomaterials have a profound effect on spheroid differentiation and function.

2.6 SPHEROIDS IN BIOMATERIALS FOR CELL-BASED TISSUE ENGINEERING

The entrapment and transplantation of spheroids in engineered materials with preferred adhesivity, stiffness, and degradation enables *in situ* control over spheroid function. The transplantation of MSCs in biomaterials has consistently yielded improved tissue formation compared to systemic or localized injection of cells, providing a strong motivation to study the therapeutic promise of entrapped MSC spheroids for tissue engineering. We provide some recent examples of this approach when applied toward bone and cartilage tissue engineering and wound healing.

2.6a Bone tissue engineering

Bone formation and repair is a delicate interplay between angiogenesis, driven by local VEGF signaling, and the local availability of bone-forming cells, which may be achieved by transplanting cells of the osteoblastic lineage or stimulating differentiation of host cells.[106] Cell-based approaches are widely studied for bone tissue engineering as viable alternatives to bone grafts, synthetic materials, and pharmacological approaches. Osteogenically-induced MSC spheroids entrapped in fibrin hydrogels exhibited enhanced osteogenesis, improved survival, and increased angiogenic potential compared to individual MSCs.[107] Platelet-rich plasma (PRP) is another promising cell carrier for use in bone tissue engineering, buoyed by its long-term use and safety profile in applications of wound healing.[108] PRP may be isolated for autologous use and formation into hydrogels that retain pro-regenerative growth factors or cytokines that suppress

local inflammation. Compared to individual MSCs on a ceramic construct, MSC spheroids within a PRP gel containing ceramic particles generated more bone when implanted in a murine ectopic site.[61] However, the variability of these naturally-derived hydrogels and challenges associated with independently modulating the mechanical properties limit their use as a research platform to explore the effect of various stimuli on spheroid function.

Adhesivity is a key design parameter to instruct the function of entrapped, anchorage-dependent cells, and this is commonly manipulated by the incorporation of adhesive proteins or peptides onto the polymer backbone. When entrapping osteogenically-induced MSC spheroids in alginate gels, the density of the adhesive peptide was a crucial aspect to maintain their osteogenic phenotype.[86] Bone formation was increased in gels that limited MSC migration from the spheroids, whether unmodified gels or alginate gels with high RGD density, suggesting that restricting the migration of cells from the spheroidal structure is a viable strategy to enhance bone formation with MSCs.

Pullulan and dextran are naturally-derived polysaccharides that can form hydrogels or solid scaffolds upon crosslinking under aqueous conditions. The incorporation of hydroxyapatite enhanced the osteogenic potential of such composite hydrogels when freeze-dried into macroporous scaffolds, thus recapitulating the nanostructure and mineralized environment of bone tissue.[62] These scaffolds successfully induced cell aggregation and spheroid formation of implanted human MSCs, improving bone formation in the rat femoral condyles. However, these materials require modification to present adhesion sites necessary for spreading, proliferation, and osteogenic differentiation.[109, 110] Additionally, the commercial production of dextran remains inefficient, presently limiting its widespread use as a biomaterial for bone tissue engineering.[111]

In addition to the materials already discussed, nanofibrous mesh scaffolds formed of PCL have been used as a carrier for osteoblast spheroids. Compared to scaffolds seeded with individual human primary osteoblasts, calvarial bone defects treated with spheroid-loaded

scaffolds exhibited enhanced bone regeneration, particularly within the core region of the scaffold.[112]

2.6b Cartilage tissue engineering

In light of the self-assembling nature of cartilage during development [113], cartilage tissue engineering is being pursued by entrapping spheroids in biomaterials that promote signaling present during these events.[114] Biomaterials can potentiate the condensation processes that promote cartilage formation while providing an effective delivery method of spheroids to damaged tissue. Preferred biomaterials are sufficiently non-adhesive to inhibit cell spreading and dedifferentiation from the chondrogenic phenotype, yet also possess sufficient porosity to enable diffusive nutrient transport to entrapped spheroids.

Hydrophilic, non-fouling biomaterials provide characteristics ideal for retaining spheroid morphology and preventing adhesion and migration from the aggregate. Among these materials, alginate has been used due to its hydrophilic nature and lack of native cell binding sites. Spheroid formation was achieved by entrapping ASCs in unmodified alginate and culturing in chondrogenic media, which maintained expression of chondrogenic markers after subcutaneous implantation in mice.[115] By 12 weeks, entrapped spheroids produced substantial cartilaginous ECM. Polyurethane (PU) and hyaluronic acid (HA) are other biomaterials that have been investigated for cartilage tissue engineering. Using a water-based 3-D printing technique, PU-HA scaffolds were seeded with MSCs that aggregated into spheroids within the construct and underwent chondrogenesis. When implanted into rabbit chondral defects, the PU-HA scaffolds induced significantly more cartilage regeneration compared to PLGA scaffolds.[116]

PLGA and chitosan have been used to deliver spheroids for cartilage engineering despite their tendency to adsorb plasma proteins that provide adhesion sites for associated cells. Both PLGA and chitosan can crosslink *via* amide bonds, forming a hydrophilic network that can then be dried into a porous scaffold. Individual ASCs were seeded into PLGA-chitosan hybrid scaffolds,

resulting in spheroids with a diameter of 80-110 μm.[94] When compared to scaffolds that failed to sustain spheroid morphology, leporine cartilage defects treated with spheroid-maintaining scaffolds exhibited better organized repair tissue with perpendicularly aligned cells similar to neocartilage. Conversely, PLGA-chitosan scaffolds made using solid freeform fabrication failed to induce differences in cartilage repair within rabbit chondral defects when seeded with MSC spheroids over individual MSCs.[65]

Chitosan has been used in combination with other biomaterials such as silk fibroin, a fibrous protein found in silk. Biphasic scaffolds were successfully engineered with silk fibroin and chitosan for cartilage tissue engineering. The top of the scaffolds was composed of a silk fibroin film to prevent cells from leaving the defect site, while the bottom half of the scaffold was made of a silk fibroin and chitosan sponge that could be seeded with cells. Composite materials that induced spheroid formation by MSCs, attained by manipulating the ratio of silk fibroin to chitosan, resulted in enhanced cell survival and glycosaminoglycan secretion.[117]

As an alternative to entrapping spheroids in the material itself, chondrogenic differentiation of MSCs can be enhanced by presenting chondroinductive cues to responsive cells. For example, MSC chondrogenic differentiation was enhanced by delivering TGF-β to cells within the aggregate using gelatin microspheres, resulting in enhanced chondrogenic differentiation of the MSCs.[64] MSC spheroids were then formed into a tube structure, resulting in cartilage possessing similar mechanical properties to native trachea.

2.6c Wound healing

Chronic or non-healing wounds of the skin are a significant clinical problem, occurring in 7 million patients each year in the United States alone.[118] Chronic wounds have been treated using recombinant growth factors such as VEGF, platelet-derived growth factor (PDGF), basic fibroblast growth factor (bFGF), and others, to speed neovascularization and epithelialization.[119] Due to the short half-lives of these molecules, cell-based therapies are

under investigation to provide cells that jumpstart wound closure or secrete the numerous signals necessary for coordinated healing.[120] MSCs can significantly enhance granulation tissue formation, angiogenesis, and reduce inflammation through their potent secretome.[121, 122] Moreover, the quantity of endogenous factors secreted by MSCs increases when formed into spheroids compared to an equivalent number of individual cells.[40, 84] The composition of the MSC secretome can be tailored by the culture conditions employed during spheroid formation. VEGF[38, 123] and PGE_2 [41] are present within the MSC secretome and signal resident endothelial cells and macrophages to initiate wound repair. Importantly, both VEGF and PGE_2 promote re-epithelialization by stimulating keratinocyte migration and proliferation.[35, 124] To sustain the advantages of spheroids over individual cells *in situ*, the transplantation of spheroids within biomaterials that potentiate growth factor secretion will advance their therapeutic potential for wound healing.

The entrapment of spheroids in engineered biomaterials represents an exciting approach to regulate and even potentiate spheroid function in wound healing and tissue regeneration. Fibrin gels are FDA-approved wound dressings that can be engineered by modulating the composition of clotting proteins and other additives. Murphy *et al.* demonstrated that the biophysical properties of fibrin gels, modulated by altering composition, can guide the simultaneous secretion of robust concentrations of VEGF and PGE_2 (**Fig. 2.4**).[125] Importantly, fibrin gels could be tuned to independently or simultaneously enhance secretion of VEGF and PGE_2 from entrapped MSC spheroids, providing a tailorable platform for use in specific applications of wound healing and

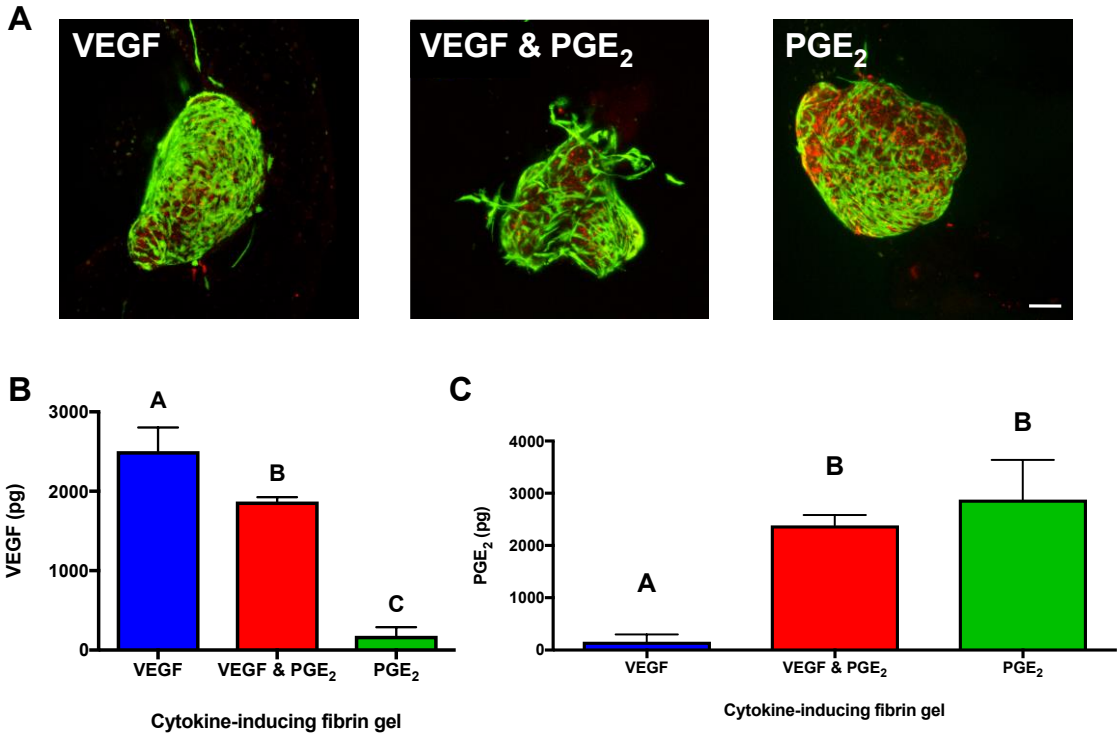

Figure 2.4. The biophysical properties of fibrin gels can be tailored to promote the wound healing potential of entrapped MSC spheroids. (A) Representative confocal microscopy images of live (green)/dead (red) assay revealing MSC spheroid viability when entrapped in a fibrin gel optimized for VEGF secretion, VEGF & PGE_2 secretion, and PGE_2 secretion after 7 days of culture. Scale bar is 100 μm. **(B)** Proangiogenic potential as measured by VEGF secretion by MSC spheroids entrapped in engineered fibrin gels designed to promote growth factor secretion. **(C)** Anti-inflammatory potential as measured by PGE_2 secretion by MSC spheroids entrapped in fibrin gels designed to promote growth factor secretion. Reprinted from (125) Copyright 2017 with permission from Elsevier.

tissue repair. Stiffer gels induced secretion of VEGF by entrapped spheroids, while more compliant gels preferentially stimulated PGE_2 secretion. The mechanical properties and degradation rate can be further tuned by addition of crosslinking agents or inhibitors of degradative enzymes. As another example, ASC spheroids entrapped in composite hydrogels of chitosan and HA yielded more vascularized tissue compared to spheroids exposed to HA alone.[126]

In clinical applications, transplantation of spheroids using biomaterials improves critical aspects of handling and localizing cells at the target site. When properly designed, biomaterials can promote regenerative properties in the cells and enhance repair of the surrounding tissue.

2.7 FUTURE OUTLOOK

Spheroids formed of somatic or stem and progenitor cells are a promising tool to propel the therapeutic efficacy of cell-based therapies and enhance our understanding of morphological development. Numerous examples can be found in the literature which demonstrate the benefits of spheroids over individual cells, yet there is no consensus on the ideal density of cells per spheroid to achieve a desired outcome. We anticipate that new techniques to form spheroids will yield higher throughput technologies to accommodate the vast number of cells required for clinical use. Similar to individual cells, the transplantation of spheroids in biomaterials localizes cells at the target site and facilitates *in situ* instruction. Despite early successes reported when simply injecting spheroids into damaged tissues,[38] the engineering of materials that direct the behavior of entrapped spheroids and respond to the localized environment is an exciting strategy to potentiate the efficacy of spheroids.

The advancement of spheroids for clinical use will be realized through advancements on several fronts including 1) reducing the time required for formation; 2) transplantation of co-culture spheroids; and 3) engineering materials that respond to changes in aggregate size or metabolic

activity. To reduce the time required for spheroid formation, high density aliquots of cells could be entrapped in non-adhesive materials that promote cell-cell adhesion and degrade in a few hours. Various microfluidic approaches have been used to successfully entrap individual cells[127, 128], opening the door to larger payloads for encapsulation. Hydrogels formed of low molecular weight alginate, HA, or PEG may be acceptable platforms, provided they contain enzymatically responsive linkages or are not heavily crosslinked. Secondly, the transplantation of a heterogeneous cell population or co-cultures may provide valuable contributions to promote tissue formation.[129-131] Accessory cells such as endothelial and hematopoietic cells secrete bioactive factors to support parenchymal cells and form nascent capillaries to enhance nutrient delivery. Finally, analyte-responsive materials may be used to capitalize on the changing metabolic profile of entrapped spheroids.[132] As spheroids undergo differentiation, the surrounding material may degrade or alter its biophysical properties upon secretion of new biomacromolecules by entrapped cells. The use of such materials as cell delivery vehicles would provide untapped potential to instruct spheroid fate upon implantation (**Fig. 2.5**).

This review highlights recent efforts to develop and apply biomaterials to guide spheroid function and their contributions to tissue repair. To extend the use of spheroids beyond preclinical studies, their advancement into clinical use will require additional testing to demonstrate safety and efficacy and to determine the minimum number of required cells. Since cells within spheroids exhibit improved cell viability, it is possible that spheroid-based therapies may be available to patients directly off-the-shelf. This concept is not so far from reality, as MSC spheroids have retained their function in ambient conditions for up to 7 days.[133] Among their promising characteristics, the improved cell survival observed when cells are formed into spheroids is one of the most exciting qualities for translation into the clinic, as this addresses a major hurdle of many cell based approaches. Numerous studies have recognized the fact that a high percentage of cells implanted do not survive, severely diluting the regeneration potential of the implant.[134]

Spheroids could result in marked improvements in potency for many cell-based methods, making them more clinically feasible by requiring fewer cells for similar or improved therapeutic outcomes.

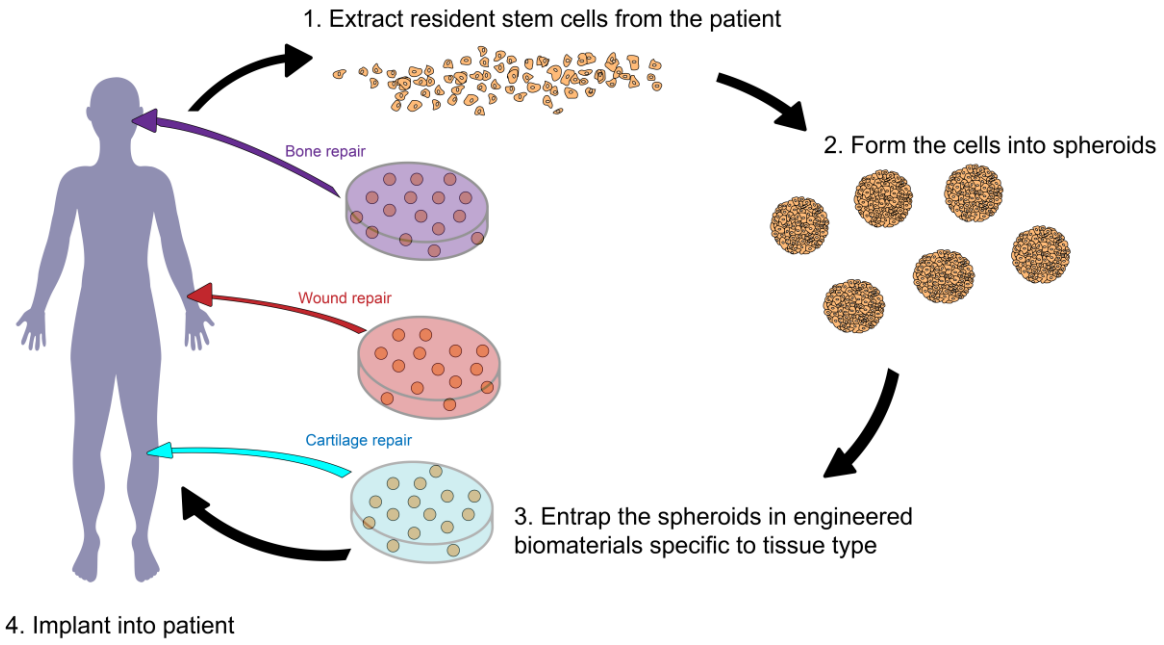

Figure 2.5. Advanced spheroid-based therapies may benefit from entrapping spheroids derived from the patient's stem cells into biomaterials known to promote a specific lineage. This approach would increase the off-the-shelf potential for using spheroids in tissue regeneration.

High throughput methods of spheroid formation are ideal for use in a clinical setting, as they require less specialized equipment and skilled labor. Future applications that require spheroids of autologous cells will be facilitated by improving the capacity to quickly and easily produce them. Moreover, hydrogels are commonly used in tissue engineering approaches. They are easily tailorable, can be delivered in a minimally invasive manner, and there are FDA-approved hydrogels for use in the clinic. Therefore, pursuing these promising results with spheroids entrapped in engineered hydrogels could further accelerate the translational use of spheroids. The value of biomaterials-based delivery of spheroids over free injection or pharmacological

approaches of delivering recombinant growth factors will be established by minimizing costs associated with this cell-based approach and demonstrating reproducibility of their application in blinded studies. By combining such strategies with existing knowledge of biomaterial properties to instruct cell phenotype, spheroids may become an even more powerful tool in advancing our knowledge of morphogenesis and the repair and regeneration of damaged tissues.

2.8 REFERENCES

[1] Stem cell therapy market by treatment mode (autologous & allogeneic), therapeutic applications (CNS, CVS, GIT, wound healing, musculoskeletal, eye, & immune system)—regulatory landscape, pipeline analysis & global forecasts to 2020, MarketsandMarkets.

[2] E.A. Copelan, Hematopoietic stem-cell transplantation, N Engl J Med 354(17) (2006) 1813-1826.

[3] J.N. Barker, J.E. Wagner, Umbilical-cord blood transplantation for the treatment of cancer, Nat Rev Cancer 3(7) (2003) 526-32.

[4] P.A. Zuk, M. Zhu, H. Mizuno, J. Huang, J.W. Futrell, A.J. Katz, P. Benhaim, H.P. Lorenz, M.H. Hedrick, Multilineage cells from human adipose tissue: implications for cell-based therapies, Tissue Eng 7(2) (2001) 211-28.

[5] M.L. Davila, I. Riviere, X. Wang, S. Bartido, J. Park, K. Curran, S.S. Chung, J. Stefanski, O. Borquez-Ojeda, M. Olszewska, J. Qu, T. Wasielewska, Q. He, M. Fink, H. Shinglot, M. Youssif, M. Satter, Y. Wang, J. Hosey, H. Quintanilla, E. Halton, Y. Bernal, D.C. Bouhassira, M.E. Arcila, M. Gonen, G.J. Roboz, P. Maslak, D. Douer, M.G. Frattini, S. Giralt, M. Sadelain, R. Brentjens, Efficacy and toxicity management of 19-28z CAR T cell therapy in B cell acute lymphoblastic leukemia, Sci Transl Med 6(224) (2014) 224ra25.

[6] M. Manassero, J. Paquet, M. Deschepper, V. Viateau, J. Retortillo, M. Bensidhoum, D. Logeart-Avramoglou, H. Petite, Comparison of survival and osteogenic ability of human mesenchymal stem cells in orthotopic and ectopic sites in mice, Tissue Eng Part A 22(5-6) (2016) 534-44.

[7] B. Sharma, S. Fermanian, M. Gibson, S. Unterman, D.A. Herzka, B. Cascio, J. Coburn, A.Y. Hui, N. Marcus, G.E. Gold, J.H. Elisseeff, Human cartilage repair with a photoreactive adhesive-hydrogel composite, Sci Transl Med 5(167) (2013) 167ra6.

[8] S.S. Tseng, M.A. Lee, A.H. Reddi, Nonunions and the potential of stem cells in fracture-healing, J Bone Joint Surg Am 90 Suppl 1 (2008) 92-8.

[9] M.W. Laschke, M.D. Menger, Life is 3D: boosting spheroid function for tissue engineering, Trends Biotechnol 35(2) (2017) 133-144.

[10] A.I. Hoch, V. Mittal, D. Mitra, N. Vollmer, C.A. Zikry, J.K. Leach, Cell-secreted matrices perpetuate the bone-forming phenotype of differentiated mesenchymal stem cells, Biomaterials 74 (2016) 178-87.

[11] K.C. Murphy, A.I. Hoch, J.N. Harvestine, D. Zhou, J.K. Leach, Mesenchymal stem cell spheroids retain osteogenic phenotype through α2β1 signaling, Stem Cells Transl Med 5(9) (2016) 1229-37.

[12] J.N. Harvestine, N.L. Vollmer, S.S. Ho, C.A. Zikry, M.A. Lee, J.K. Leach, Extracellular matrix-coated composite scaffolds promote mesenchymal stem cell persistence and osteogenesis, Biomacromolecules 17(11) (2016) 3524-3531.

[13] R.O. Hynes, The extracellular matrix: not just pretty fibrils, Science 326(5957) (2009) 1216.

[14] M.T. Harting, F. Jimenez, H. Xue, U.M. Fischer, J. Baumgartner, P.K. Dash, C.S. Cox, Intravenous mesenchymal stem cell therapy for traumatic brain injury, J Neurosurg 110(6) (2009) 1189-97.

[15] M. Zhang, D. Methot, V. Poppa, Y. Fujio, K. Walsh, C.E. Murry, Cardiomyocyte grafting for cardiac repair: graft cell death and anti-death strategies, J Mol Cell Cardiol 33(5) (2001) 907-21.

[16] J. Holtfreter, A study of the mechanics of gastrulation, J Exp Zool 95(2) (1944) 171-212.

[17] W. Mueller-Klieser, Three-dimensional cell cultures: from molecular mechanisms to clinical applications, Am J Physiol 273(4 Pt 1) (1997) C1109-23.

[18] C. Wenzel, B. Riefke, S. Gründemann, A. Krebs, S. Christian, F. Prinz, M. Osterland, S. Golfier, S. Räse, N. Ansari, M. Esner, M. Bickle, F. Pampaloni, C. Mattheyer, E.H. Stelzer, K. Parczyk, S. Prechtl, P. Steigemann, 3D high-content screening for the identification of compounds that target cells in dormant tumor spheroid regions, Exp Cell Res 323(1) (2014) 131-43.

[19] M. Salama, A. Lotfy, K. Fathy, M. Makar, M. El-Emam, A. El-Gamal, M. El-Gamal, A. Badawy, W.M. Mohamed, M. Sobh, Developmental neurotoxic effects of Malathion on 3D neurosphere system, Appl Transl Genom 7 (2015) 13-8.

[20] E.J. Hill, E.K. Woehrling, M. Prince, M.D. Coleman, Differentiating human NT2/D1 neurospheres as a versatile in vitro 3D model system for developmental neurotoxicity testing, Toxicology 249(2-3) (2008) 243-50.

[21] P.P. Garcez, J.M. Nascimento, J.M. de Vasconcelos, R. Madeiro da Costa, R. Delvecchio, P. Trindade, E.C. Loiola, L.M. Higa, J.S. Cassoli, G. Vitória, P.C. Sequeira, J. Sochacki, R.S. Aguiar, H.T. Fuzii, A.M. de Filippis, J.L. da Silva Gonçalves Vianez Júnior, A. Tanuri, D. Martins-de-Souza, S.K. Rehen, Zika virus disrupts molecular fingerprinting of human neurospheres, Sci Rep 7 (2017) 40780.

[22] H. Guerrero-Cázares, K.L. Chaichana, A. Quiñones-Hinojosa, Neurosphere culture and human organotypic model to evaluate brain tumor stem cells, Methods Mol Biol 568 (2009) 73-83.

[23] I. Singec, R. Knoth, R.P. Meyer, J. Maciaczyk, B. Volk, G. Nikkhah, M. Frotscher, E.Y. Snyder, Defining the actual sensitivity and specificity of the neurosphere assay in stem cell biology, Nat Methods 3(10) (2006) 801-6.

[24] N. Uchida, D.W. Buck, D. He, M.J. Reitsma, M. Masek, T.V. Phan, A.S. Tsukamoto, F.H. Gage, I.L. Weissman, Direct isolation of human central nervous system stem cells, Proc Natl Acad Sci U S A 97(26) (2000) 14720-5.

[25] T.S. Li, K. Cheng, S.T. Lee, S. Matsushita, D. Davis, K. Malliaras, Y. Zhang, N. Matsushita, R.R. Smith, E. Marbán, Cardiospheres recapitulate a niche-like microenvironment rich in stemness and cell-matrix interactions, rationalizing their enhanced functional potency for myocardial repair, Stem Cells 28(11) (2010) 2088-98.

[26] E. Messina, L. De Angelis, G. Frati, S. Morrone, S. Chimenti, F. Fiordaliso, M. Salio, M. Battaglia, M.V. Latronico, M. Coletta, E. Vivarelli, L. Frati, G. Cossu, A. Giacomello, Isolation and expansion of adult cardiac stem cells from human and murine heart, Circ Res 95(9) (2004) 911-21.

[27] D.R. Davis, R. Ruckdeschel Smith, E. Marbán, Human cardiospheres are a source of stem cells with cardiomyogenic potential, Stem Cells 28(5) (2010) 903-4.

[28] P.V. Johnston, T. Sasano, K. Mills, R. Evers, S.T. Lee, R.R. Smith, A.C. Lardo, S. Lai, C. Steenbergen, G. Gerstenblith, R. Lange, E. Marbán, Engraftment, differentiation, and functional benefits of autologous cardiosphere-derived cells in porcine ischemic cardiomyopathy, Circulation 120(12) (2009) 1075-83.

[29] V.E. Santo, S.P. Rebelo, M.F. Estrada, P.M. Alves, E. Boghaert, C. Brito, Drug screening in 3D in vitro tumor models: overcoming current pitfalls of efficacy read-outs, Biotechnol J 12(1) (2017).

[30] A.E. Denker, S.B. Nicoll, R.S. Tuan, Formation of cartilage-like spheroids by micromass cultures of murine C3H10T1/2 cells upon treatment with transforming growth factor-β1, Differentiation 59(1) (1995) 25-34.

[31] S.H. Hsu, G.S. Huang, S.Y. Lin, F. Feng, T.T. Ho, Y.C. Liao, Enhanced chondrogenic differentiation potential of human gingival fibroblasts by spheroid formation on chitosan membranes, Tissue Eng Part A 18(1-2) (2012) 67-79.

[32] S. Ghosh, M. Laha, S. Mondal, S. Sengupta, D.L. Kaplan, In vitro model of mesenchymal condensation during chondrogenic development, Biomaterials 30(33) (2009) 6530-40.

[33] M.F. Pittenger, A.M. Mackay, S.C. Beck, R.K. Jaiswal, R. Douglas, J.D. Mosca, M.A. Moorman, D.W. Simonetti, S. Craig, D.R. Marshak, Multilineage potential of adult human mesenchymal stem cells, Science 284(5411) (1999) 143-7.

[34] J.Y. Oh, M.K. Kim, M.S. Shin, H.J. Lee, J.H. Ko, W.R. Wee, J.H. Lee, The anti-inflammatory and anti-angiogenic role of mesenchymal stem cells in corneal wound healing following chemical injury, Stem Cells 26(4) (2008) 1047-55.

[35] J.M. Santos, S.P. Camões, E. Filipe, M. Cipriano, R.N. Barcia, M. Filipe, M. Teixeira, S. Simões, M. Gaspar, D. Mosqueira, D.S. Nascimento, P. Pinto-do-Ó, P. Cruz, H. Cruz, M. Castro, J.P. Miranda, Three-dimensional spheroid cell culture of umbilical cord tissue-derived mesenchymal stromal cells leads to enhanced paracrine induction of wound healing, Stem Cell Res Ther 6 (2015) 90.

[36] S. Bhumiratana, R.E. Eton, S.R. Oungoulian, L.Q. Wan, G.A. Ateshian, G. Vunjak-Novakovic, Large, stratified, and mechanically functional human cartilage grown in vitro by mesenchymal condensation, Proc Natl Acad Sci USA 111(19) (2014) 6940-6945.

[37] D. Murata, S. Tokunaga, T. Tamura, H. Kawaguchi, N. Miyoshi, M. Fujiki, K. Nakayama, K. Misumi, A preliminary study of osteochondral regeneration using a scaffold-free three-dimensional construct of porcine adipose tissue-derived mesenchymal stem cells, J Orthop Surg Res 10 (2015) 35.

[38] S.H. Bhang, S. Lee, J.Y. Shin, T.J. Lee, B.S. Kim, Transplantation of cord blood mesenchymal stem cells as spheroids enhances vascularization, Tissue Eng Part A 18(19-20) (2012) 2138-47.

[39] T.J. Bartosh, J.H. Ylöstalo, A. Mohammadipoor, N. Bazhanov, K. Coble, K. Claypool, R.H. Lee, H. Choi, D.J. Prockop, Aggregation of human mesenchymal stromal cells (MSCs) into 3D

spheroids enhances their antiinflammatory properties, Proc Natl Acad Sci U S A 107(31) (2010) 13724-9.

[40] K.C. Murphy, J. Whitehead, P.C. Falahee, D. Zhou, S.I. Simon, J.K. Leach, Multifactorial experimental design to optimize the anti-inflammatory and proangiogenic potential of mesenchymal stem cell spheroids, Stem Cells 35(6) (2017) 1493-1504.

[41] J.H. Ylostalo, T.J. Bartosh, K. Coble, D.J. Prockop, Human mesenchymal stem/stromal cells cultured as spheroids are self-activated to produce prostaglandin E2 that directs stimulated macrophages into an anti-inflammatory phenotype, Stem Cells 30(10) (2012) 2283-96.

[42] X. Guo, S. Li, Q. Ji, R. Lian, J. Chen, Enhanced viability and neural differential potential in poor post-thaw hADSCs by agarose multi-well dishes and spheroid culture, Hum Cell 28(4) (2015) 175-89.

[43] J.E. Frith, B. Thomson, P.G. Genever, Dynamic three-dimensional culture methods enhance mesenchymal stem cell properties and increase therapeutic potential, Tissue Eng Part C Methods 16(4) (2010) 735-49.

[44] R.-Z. Lin, L.-F. Chou, C.-C.M. Chien, H.-Y. Chang, Dynamic analysis of hepatoma spheroid formation: roles of E-cadherin and β1-integrin, Cell and Tissue Res 324(3) (2006) 411-422.

[45] A.P. Napolitano, P. Chai, D.M. Dean, J.R. Morgan, Dynamics of the self-assembly of complex cellular aggregates on micromolded nonadhesive hydrogels, Tissue Eng 13(8) (2007) 2087-94.

[46] G.M. Whitesides, B. Grzybowski, Self-assembly at all scales, Science 295(5564) (2002) 2418.

[47] K.R. Vadivelu, H. Kamble, J.M. Shiddiky, N.-T. Nguyen, Microfluidic technology for the generation of cell spheroids and their applications, Micromachines 8(4) (2017) 94.

[48] R.A. Foty, M.S. Steinberg, Cadherin-mediated cell-cell adhesion and tissue segregation in relation to malignancy, Int J Dev Biol 48(5-6) (2004) 397-409.

[49] R.A. Foty, M.S. Steinberg, The differential adhesion hypothesis: a direct evaluation, Dev Biol 278(1) (2005) 255-263.

[50] S. Pawlizak, W.F. Anatol, S. Grosser, D. Ahrens, T. Thalheim, S. Riedel, T.R. Kießling, L. Oswald, M. Zink, M.L. Manning, J.A. Käs, Testing the differential adhesion hypothesis across the epithelial−mesenchymal transition, New J Phys 17(8) (2015) 083049.

[51] R. Foty, A simple hanging drop cell culture protocol for generation of 3D spheroids, J Vis Exp (51) (2011).

[52] X. Gong, C. Lin, J. Cheng, J. Su, H. Zhao, T. Liu, X. Wen, P. Zhao, Generation of multicellular tumor spheroids with microwell-based agarose scaffolds for drug testing, PLoS One 10(6) (2015) e0130348.

[53] J. Dahlmann, G. Kensah, H. Kempf, D. Skvorc, A. Gawol, D.A. Elliott, G. Dräger, R. Zweigerdt, U. Martin, I. Gruh, The use of agarose microwells for scalable embryoid body formation and cardiac differentiation of human and murine pluripotent stem cells, Biomaterials 34(10) (2013) 2463-71.

[54] B.C. Gettler, J.S. Zakhari, P.S. Gandhi, S.K. Williams, Formation of adipose stromal vascular fraction cell-laden spheroids using a three-dimensional bioprinter and superhydrophobic surfaces, Tissue Eng Part C Methods 23(9) (2017) 516-524.

[55] B.H. Liu, H.Y. Yeh, Y.C. Lin, M.H. Wang, D.C. Chen, B.H. Lee, S.H. Hsu, Spheroid formation and enhanced cardiomyogenic potential of adipose-derived stem cells grown on chitosan, Biores Open Access 2(1) (2013) 28-39.

[56] G.S. Huang, L.G. Dai, B.L. Yen, S.H. Hsu, Spheroid formation of mesenchymal stem cells on chitosan and chitosan-hyaluronan membranes, Biomaterials 32(29) (2011) 6929-45.

[57] N.-C. Cheng, S. Wang, T.-H. Young, The influence of spheroid formation of human adipose-derived stem cells on chitosan films on stemness and differentiation capabilities, Biomaterials 33(6) (2012) 1748-1758.

[58] K.C. Murphy, B.P. Hung, S. Browne-Bourne, D. Zhou, J. Yeung, D.C. Genetos, J.K. Leach, Measurement of oxygen tension within mesenchymal stem cell spheroids, J R Soc Interface 14(127) (2017) 20160851.

[59] K.K. Papas, I. Constantinidis, A. Sambanis, Cultivation of recombinant, insulin-secreting AtT-20 cells as free and entrapped spheroids, Cytotechnology 13(1) (1993) 1-12.

[60] T. Anada, T. Sato, T. Kamoya, Y. Shiwaku, K. Tsuchiya, T. Takano-Yamamoto, K. Sasaki, O. Suzuki, Evaluation of bioactivity of octacalcium phosphate using osteoblastic cell aggregates on a spheroid culture device, Regen Therapy 3 (2016) 58-62.

[61] A. Chatterjea, V.L. LaPointe, A. Barradas, H. Garritsen, H. Yuan, A. Renard, C.A. van Blitterswijk, J. de Beor, Cell aggregation enhances bone formation by human mesenchymal stromal cells, Eur Cell Mater 33 (2017) 121-129.

[62] J.C. Fricain, S. Schlaubitz, C. Le Visage, I. Arnault, S.M. Derkaoui, R. Siadous, S. Catros, C. Lalande, R. Bareille, M. Renard, T. Fabre, S. Cornet, M. Durand, A. Léonard, N. Sahraoui, D. Letourneur, J. Amédée, A nano-hydroxyapatite – Pullulan/dextran polysaccharide composite macroporous material for bone tissue engineering, Biomaterials 34(12) (2013) 2947-2959.

[63] L. Keller, Y. Idoux-Gillet, Q. Wagner, S. Eap, D. Brasse, P. Schwinté, M. Arruebo, N. Benkirane-Jessel, Nanoengineered implant as a new platform for regenerative nanomedicine using 3D well-organized human cell spheroids, Int J Nanomed 12 (2017) 447-457.

[64] A.D. Dikina, H.A. Strobel, B.P. Lai, M.W. Rolle, E. Alsberg, Engineered cartilaginous tubes for tracheal tissue replacement via self-assembly and fusion of human mesenchymal stem cell constructs, Biomaterials 52 (2015) 452-62.

[65] G.S. Huang, C.S. Tseng, B. Linju Yen, L.G. Dai, P.S. Hsieh, S.H. Hsu, Solid freeform-fabricated scaffolds designed to carry multicellular mesenchymal stem cell spheroids for cartilage regeneration, Eur Cell Mater 26 (2013) 179-94; discussion 194.

[66] J. Feng, K. Mineda, S.-H. Wu, T. Mashiko, K. Doi, S. Kuno, K. Kinoshita, K. Kanayama, R. Asahi, A. Sunaga, K. Yoshimura, An injectable non-cross-linked hyaluronic-acid gel containing therapeutic spheroids of human adipose-derived stem cells, Sci Rep 7 (2017) 1548.

[67] K. Nakajima, J. Fujita, S. Tohyama, R. Ohno, H. Kanazawa, T. Seki, Y. Kishino, M. Okada, S. Kawaguchi, S. Tanosaki, S. Someya, H. Shimizu, Y. Tabata, E. Kobayashi, K. Fukuda, The regenerative therapy of human induced pluripotent stem cells-derived pure cardiac spheroids with gelatin hydrogel restores cardiac function and has weak arrhythmogenic property in heart failure, Eur Heart J 38(suppl_1) (2017) ehx502.P2542-ehx502.P2542.

[68] C.M. Hwang, S. Sant, M. Masaeli, N.N. Kachouie, B. Zamanian, S.H. Lee, A. Khademhosseini, Fabrication of three-dimensional porous cell-laden hydrogel for tissue engineering, Biofabrication 2(3) (2010) 035003.

[69] K.H. Lee, d.Y. No, S.H. Kim, J.H. Ryoo, S.F. Wong, S.H. Lee, Diffusion-mediated in situ alginate encapsulation of cell spheroids using microscale concave well and nanoporous membrane, Lab Chip 11(6) (2011) 1168-73.

[70] S.L. Dahl, C. Rhim, Y.C. Song, L.E. Niklason, Mechanical properties and compositions of tissue engineered and native arteries, Ann Biomed Eng 35(3) (2007) 348-55.

[71] L. Haishuang Lin and Qiang Li and Yuguo, Three-dimensional tissues using human pluripotent stem cell spheroids as biofabrication building blocks, Biofabrication 9(2) (2017) 025007.

[72] B. Mattix, T.R. Olsen, Y. Gu, M. Casco, A. Herbst, D.T. Simionescu, R.P. Visconti, K.G. Kornev, F. Alexis, Biological magnetic cellular spheroids as building blocks for tissue engineering, Acta Biomater 10(2) (2014) 623-9.

[73] T.R. Olsen, B. Mattix, M. Casco, A. Herbst, C. Williams, A. Tarasidis, D. Simionescu, R.P. Visconti, F. Alexis, Manipulation of cellular spheroid composition and the effects on vascular tissue fusion, Acta Biomater 13 (2015) 188-98.

[74] R. Noguchi, K. Nakayama, M. Itoh, K. Kamohara, K. Furukawa, J.-i. Oyama, K. Node, S. Morita, Development of a three-dimensional pre-vascularized scaffold-free contractile cardiac patch for treating heart disease, J Heart Lung Transplant 35(1) (2016) 137-145.

[75] A.M. Blakely, K.L. Manning, A. Tripathi, J.R. Morgan, Bio-pick, place, and perfuse: a new instrument for three-dimensional tissue engineering, Tissue Eng Part C Methods 21(7) (2015) 737-46.

[76] N. Moldovan, I., N. Hibino, K. Nakayama, Principles of the Kenzan method for robotic cell spheroid-based three-dimensional bioprinting, Tissue Eng Part B Rev, 2017, pp. 237-244.

[77] L. Moldovan, A. Barnard, C.H. Gil, Y. Lin, M.B. Grant, M.C. Yoder, N. Prasain, N.I. Moldovan, iPSC-derived vascular cell spheroids as building blocks for scaffold-free biofabrication, Biotechnol J (2017).

[78] M. Itoh, K. Nakayama, R. Noguchi, K. Kamohara, K. Furukawa, K. Uchihashi, S. Toda, J.-i. Oyama, K. Node, S. Morita, Scaffold-free tubular tissues created by a bio-3d printer undergo remodeling and endothelialization when implanted in rat aortae, PLoS ONE 10(9) (2015) e0136681.

[79] C. Norotte, F.S. Marga, L.E. Niklason, G. Forgacs, Scaffold-free vascular tissue engineering using bioprinting, Biomaterials 30(30) (2009) 5910-7.

[80] J.K. Leach, J. Whitehead, Materials-directed differentiation of mesenchymal stem cells for tissue engineering and regeneration, ACS Biomater Sci Eng (2017).

[81] S.R. Caliari, J.A. Burdick, A practical guide to hydrogels for cell culture, Nat Methods 13(5) (2016) 405-14.

[82] T.H. Qazi, D.J. Mooney, G.N. Duda, S. Geissler, Biomaterials that promote cell-cell interactions enhance the paracrine function of MSCs, Biomaterials 140 (2017) 103-114.

[83] M.P. Lutolf, P.M. Gilbert, H.M. Blau, Designing materials to direct stem-cell fate, Nature 462(7272) (2009) 433-41.

[84] S.S. Ho, K.C. Murphy, B.Y.K. Binder, C.B. Vissers, J.K. Leach, Increased survival and function of mesenchymal stem cell spheroids entrapped in instructive alginate hydrogels, Stem Cells Transl Med 5(6) (2016) 773-781.

[85] J.L. Drury, D.J. Mooney, Hydrogels for tissue engineering: scaffold design variables and applications, Biomaterials 24(24) (2003) 4337-51.

[86] S.S. Ho, A.T. Keown, B. Addison, J.K. Leach, Cell migration and bone formation from mesenchymal stem cell spheroids in alginate hydrogels are regulated by adhesive ligand density, Biomacromolecules (2017).

[87] J.L. Wilson, M.A. Najia, R. Saeed, T.C. McDevitt, Alginate encapsulation parameters influence the differentiation of microencapsulated embryonic stem cell aggregates, Biotechnol Bioeng 111(3) (2014) 618-31.

[88] S.H. Lee, J.J. Moon, J.L. West, Three-dimensional micropatterning of bioactive hydrogels via two-photon laser scanning photolithography for guided 3D cell migration, Biomaterials 29(20) (2008) 2962-8.

[89] C.A.B. Vissers, J.N. Harvestine, J.K. Leach, Pore size regulates mesenchymal stem cell response to bioglass-loaded composite scaffolds, J Mater Chem B 3(44) (2015) 8650-8658.

[90] J. He, D.C. Genetos, J.K. Leach, Osteogenesis and trophic factor secretion are influenced by the composition of hydroxyapatite/poly(lactide-co-glycolide) composite scaffolds, Tissue Eng Part A 16(1) (2010) 127-37.

[91] R.A. Jain, The manufacturing techniques of various drug loaded biodegradable poly(lactide-co-glycolide) (PLGA) devices, Biomaterials 21(23) (2000) 2475-90.

[92] G.C. Ingavle, J.K. Leach, Advancements in electrospinning of polymeric nanofibrous scaffolds for tissue engineering, Tissue Eng Part B Rev 20(4) (2014) 277-93.

[93] K. Zhang, L. Song, J. Wang, S. Yan, G. Li, L. Cui, J. Yin, Strategy for constructing vascularized adipose units in poly(l-glutamic acid) hydrogel porous scaffold through inducing in-situ formation of ASCs spheroids, Acta Biomater 51 (2017) 246-257.

[94] K. Zhang, S. Yan, G. Li, L. Cui, J. Yin, In-situ birth of MSCs multicellular spheroids in poly(l-glutamic acid)/chitosan scaffold for hyaline-like cartilage regeneration, Biomaterials 71 (2015) 24-34.

[95] J.A. Steele, J.P. Hallé, D. Poncelet, R.J. Neufeld, Therapeutic cell encapsulation techniques and applications in diabetes, Adv Drug Deliv Rev 67-68 (2014) 74-83.

[96] A.J. Ryan, H.S. O'Neill, G.P. Duffy, F.J. O'Brien, Advances in polymeric islet cell encapsulation technologies to limit the foreign body response and provide immunoisolation, Curr Opin Pharmacol 36 (2017) 66-71.

[97] N. Koide, T. Shinji, T. Tanabe, K. Asano, M. Kawaguchi, K. Sakaguchi, Y. Koide, M. Mori, T. Tsuji, Continued high albumin production by multicellular spheroids of adult rat hepatocytes formed in the presence of liver-derived proteoglycans, Biochem Biophys Res Commun 161(1) (1989) 385-91.

[98] T.T. Chang, M. Hughes-Fulford, Monolayer and spheroid culture of human liver hepatocellular carcinoma cell line cells demonstrate distinct global gene expression patterns and functional phenotypes, Tissue Eng Part A 15(3) (2009) 559-67.

[99] R.D. Hughes, R.R. Mitry, A. Dhawan, Current status of hepatocyte transplantation, Transplantation 93(4) (2012) 342-7.

[100] C. Siltanen, M. Diakatou, J. Lowen, A. Haque, A. Rahimian, G. Stybayeva, A. Revzin, One step fabrication of hydrogel microcapsules with hollow core for assembly and cultivation of hepatocyte spheroids, Acta Biomater 50 (2017) 428-436.

[101] R.F. Gibly, X. Zhang, M.L. Graham, B.J. Hering, D.B. Kaufman, W.L. Lowe, L.D. Shea, Extrahepatic islet transplantation with microporous polymer scaffolds in syngeneic mouse and allogeneic porcine models, Biomaterials 32(36) (2011) 9677-84.

[102] J.M.H. Liu, J. Zhang, X. Zhang, K.A. Hlavaty, C.F. Ricci, J.N. Leonard, L.D. Shea, R.M. Gower, Transforming growth factor-beta 1 delivery from microporous scaffolds decreases inflammation post-implant and enhances function of transplanted islets, Biomaterials 80 (2016) 11-19.

[103] L. Fu, J. Xie, M.A. Carlson, D.A. Reilly, Three-dimensional nanofiber scaffolds with arrayed holes for engineering skin tissue constructs, MRS Commun 7(3) (2017) 361-366.

[104] G. Kaufman, R.A. Whitescarver, L. Nunes, X.L. Palmer, D. Skrtic, W. Tutak, Effects of protein-coated nanofibers on conformation of gingival fibroblast spheroids: potential utility for connective tissue regeneration, Biomed Mater 13(2) (2018) 025006.

[105] J. Gilbert, N.P. Reynolds, S.M. Russell, D. Haylock, S. McArthur, M. Charnley, O.G. Jones, Chitosan-coated amyloid fibrils increase adipogenesis of mesenchymal stem cells, Mater Sci Eng C Mater Biol Appl 79 (2017) 363-371.

[106] T.A. Einhorn, L.C. Gerstenfeld, Fracture healing: mechanisms and interventions, Nat Rev Rheumatol 11(1) (2015) 45-54.

[107] K.C. Murphy, S.Y. Fang, J.K. Leach, Human mesenchymal stem cell spheroids in fibrin hydrogels exhibit improved cell survival and potential for bone healing, Cell Tissue Res 357(1) (2014) 91-9.

[108] K.M. Lacci, A. Dardik, Platelet-rich plasma: support for its use in wound healing, Yale J Biol Med 83(1) (2010) 1-9.

[109] R.S. Singh, N. Kaur, V. Rana, J.F. Kennedy, Recent insights on applications of pullulan in tissue engineering, Carbohydr Polym 153 (2016) 455-462.

[110] S.P. Massia, J. Stark, D.S. Letbetter, Surface-immobilized dextran limits cell adhesion and spreading, Biomaterials 21(22) (2000) 2253-61.

[111] M.H.P.B. Vettoria, K. Blanco, M. Cortezi, C.J.B. de Lima, J. Contiero, Dextran: effect of process parameters on production, purification and molecular weight and recent applications, Diálogos & Ciência 31 (2012) 171-186.

[112] L. Keller, Y. Idoux-Gillet, Q. Wagner, S. Eap, D. Brasse, P. Schwinté, M. Arruebo, N. Benkirane-Jessel, Nanoengineered implant as a new platform for regenerative nanomedicine using 3D well-organized human cell spheroids, Int J of Nanomedicine 12 (2017) 447-457.

[113] P.V. Thorogood, J.R. Hinchliffe, An analysis of the condensation process during chondrogenesis in the embryonic chick hind limb, J Embryol Exp Morphol 33(3) (1975) 581-606.

[114] H.H. Yoon, S.H. Bhang, J.Y. Shin, J. Shin, B.S. Kim, Enhanced cartilage formation via three-dimensional cell engineering of human adipose-derived stem cells, Tissue Eng Part A 18(19-20) (2012) 1949-56.

[115] G.R. Erickson, J.M. Gimble, D.M. Franklin, H.E. Rice, H. Awad, F. Guilak, Chondrogenic potential of adipose tissue-derived stromal cells in vitro and in vivo, Biochem Biophys Res Commun 290(2) (2002) 763-9.

[116] K.C. Hung, C.S. Tseng, L.G. Dai, S.H. Hsu, Water-based polyurethane 3D printed scaffolds with controlled release function for customized cartilage tissue engineering, Biomaterials 83 (2016) 156-68.

[117] K. Panjapheree, S. Kamonmattayakul, J. Meesane, Biphasic scaffolds of silk fibroin film affixed to silk fibroin/chitosan sponge based on surgical design for cartilage defect in osteoarthritis, Mater Des 141 (2018) 323-332.

[118] S. Malhotra, E. Bello, S. Kominsky, Diabetic foot ulcerations: biomechanics, charcot foot, and total contact cast, Semin Vasc Surg 25(2) (2012) 66-9.

[119] L.I. Moura, A.M. Dias, E. Carvalho, H.C. de Sousa, Recent advances on the development of wound dressings for diabetic foot ulcer treatment--a review, Acta Biomater 9(7) (2013) 7093-114.

[120] L. Chen, E.E. Tredget, P.Y. Wu, Y. Wu, Paracrine factors of mesenchymal stem cells recruit macrophages and endothelial lineage cells and enhance wound healing, PLoS One 3(4) (2008) e1886.

[121] Y. Wu, L. Chen, P.G. Scott, E.E. Tredget, Mesenchymal stem cells enhance wound healing through differentiation and angiogenesis, Stem Cells 25(10) (2007) 2648-59.

[122] P.J. Amos, S.K. Kapur, P.C. Stapor, H. Shang, S. Bekiranov, M. Khurgel, G.T. Rodeheaver, S.M. Peirce, A.J. Katz, Human adipose-derived stromal cells accelerate diabetic wound healing: impact of cell formulation and delivery, Tissue Eng Part A 16(5) (2010) 1595-606.

[123] P. Bao, A. Kodra, M. Tomic-Canic, M.S. Golinko, H.P. Ehrlich, H. Brem, The role of vascular endothelial growth factor in wound healing, J Surg Res 153(2) (2009) 347-358.

[124] J. Michaels, M. Dobryansky, R.D. Galiano, K.A. Bhatt, R. Ashinoff, D.J. Ceradini, G.C. Gurtner, Topical vascular endothelial growth factor reverses delayed wound healing secondary to angiogenesis inhibitor administration, Wound Repair Regen 13(5) (2005) 506-12.

[125] K.C. Murphy, J. Whitehead, D. Zhou, S.S. Ho, J.K. Leach, Engineering fibrin hydrogels to promote the wound healing potential of mesenchymal stem cell spheroids, Acta Biomater 64 (2017) 176-186.

[126] S.-h. Hsu, P.-S. Hsieh, Self-assembled adult adipose-derived stem cell spheroids combined with biomaterials promote wound healing in a rat skin repair model, Wound Repair Regen 23(1) (2015) 57-64.

[127] S. Utech, R. Prodanovic, A.S. Mao, R. Ostafe, D.J. Mooney, D.A. Weitz, Microfluidic generation of monodisperse, structurally homogeneous alginate microgels for cell encapsulation and 3D cell culture, Adv Healthc Mater 4(11) (2015) 1628-33.

[128] A.S. Mao, J.W. Shin, S. Utech, H. Wang, O. Uzun, W. Li, M. Cooper, Y. Hu, L. Zhang, D.A. Weitz, D.J. Mooney, Deterministic encapsulation of single cells in thin tunable microgels for niche modelling and therapeutic delivery, Nat Mater 16(2) (2017) 236-243.

[129] S.H. Hsu, T.T. Ho, N.C. Huang, C.L. Yao, L.H. Peng, N.T. Dai, Substrate-dependent modulation of 3D spheroid morphology self-assembled in mesenchymal stem cell-endothelial progenitor cell coculture, Biomaterials 35(26) (2014) 7295-307.

[130] G.G.Y. Chiew, N. Wei, S. Sultania, S. Lim, K.Q. Luo, Bioengineered three-dimensional co-culture of cancer cells and endothelial cells: A model system for dual analysis of tumor growth and angiogenesis, Biotechnol Bioeng 114(8) (2017) 1865-1877.

[131] R. Walser, W. Metzger, A. Görg, T. Pohlemann, M.D. Menger, M.W. Laschke, Generation of co-culture spheroids as vascularisation units for bone tissue engineering, Eur Cell Mater 26 (2013) 222-33.

[132] H.R. Culver, J.R. Clegg, N.A. Peppas, Analyte-responsive hydrogels: intelligent materials for biosensing and drug delivery, Acc Chem Res 50(2) (2017) 170-178.

[133] B. Jiang, L. Yan, Z. Miao, E. Li, K.H. Wong, R.H. Xu, Spheroidal formation preserves human stem cells for prolonged time under ambient conditions for facile storage and transportation, Biomaterials 133 (2017) 275-286.

[134] D.J. Mooney, H. Vandenburgh, Cell delivery mechanisms for tissue repair, Cell Stem Cell 2(3) (2008) 205-13.

CHAPTER 3: MESENCHYMAL STEM CELL SPHEROIDS ENHANCE THE MYOBLAST SECRETOME FOR ENHANCED BONE REPAIR

Local muscle loss associated with open fractures remains an obstacle to functional recovery and bone healing. Muscle cells secrete bioactive myokines that elicit autocrine and paracrine effects and initiate signaling pathways for regenerating damaged muscle and bone. Mesenchymal stem cells (MSCs) are under investigation for the regeneration of both muscle and bone through their potent secretome. Compared to monodisperse cells, MSC spheroids exhibit a more complex secretome with heightened therapeutic potential. We hypothesized that the osteogenic potential of myokines would be enhanced when myoblasts were exposed to MSC spheroids. Conditioned media from MSC spheroids increased osteogenic response of MC3T3 pre-osteoblasts compared to myokines from L6 myoblasts alone. This effect was synergistically enhanced when conditioned media of MSC spheroids was serially exposed to myoblasts and then osteoprogenitor cells *in vitro*. We then delivered myoblast-conditioned media in the presence or absence of syngeneic rat bone marrow stromal cells (rBMSCs) from alginate hydrogels to a rat critical-sized femoral defect. Bone formation was greatest in defects treated with conditioned media and rBMSCs over 12 weeks, while we observed markedly increased bone formation in defects treated with conditioned media compared to syngeneic bone marrow stromal cells alone. This foundational study demonstrates a novel approach for capitalizing on the paracrine signaling of muscle cells to promote bone repair and provides additional evidence of the synergistic interaction between muscle and bone.

Published as: A.M. Saiz*, Jr., M.A. Gionet-Gonzales*, M.A. Lee, J.K. Leach, Conditioning of myoblast secretome using mesenchymal stem/stromal cell spheroids improves bone repair, *Bone* 125 (2019) 151-159.

3.1 INTRODUCTION

Open fractures, denoted by injury to both the bone and musculature, are associated with increases in delayed union, nonunion, rehospitalization, infection, revision surgery and worse functional outcomes compared to closed fractures.[1,2] Full bridging is not observed in the presence of a large muscle defect, even when stimulated by potent osteoinductive cues such as bone morphogenetic proteins.[3] Even short-term muscle atrophy, modeled by local injection of botulinum toxin, impairs fracture healing in rodents.[4] Autologous muscle flap transplantation remains the gold standard treatment of large volumetric muscle loss injuries. While this approach can improve fracture repair, it is associated with short- and long-term functional deficits, donor site morbidity, and potential limb loss.[5,6] Cellular therapies, including injection of satellite cells, myogenic progenitor cells, and mesenchymal stromal cells (MSCs) are promising strategies but are plagued by limitations including low viability and poor integration into damaged muscle.[7,8] While muscle contributes necessary mechanical loading and enables ambulation, it also acts as an endocrine organ, secreting myokines that stimulate surrounding cells in adjacent muscle and bone.[10] Thus, new strategies that mimic the endocrine and paracrine signaling activities of muscle may provide an opportunity to stimulate bone repair.

MSCs from various tissue compartments enhance bone healing in numerous preclinical bone defect models[11], while bone marrow aspirate, a rich source of MSCs, promoted fracture healing in human patients afflicted by delayed unions or non-unions.[12] Despite their multilineage potential *in vitro*, there is limited evidence that transplanted MSCs differentiate into osteoblasts *in situ* and directly form bone when used to treat bone defects. Instead, MSCs may have a greater therapeutic effect *in vivo via* indirect contributions to tissue repair. MSCs possess a potent secretome containing bioactive factors that stimulate angiogenesis, prolong cell viability, induce cell migration, and modulate the local inflammatory environment.[13,14] However, the translational potential of cell therapy is limited by the high death rate and poor engraftment of cells in ischemic conditions[15], motivating the need for strategies that potentiate the effect of the

secretome. For example, MSC transplantation into damaged muscle increased muscle repair indirectly through local secretome activity instead of direct differentiation into new muscle cells.[9] Compared to monodisperse cells, MSC spheroids exhibit improved survival in harsh microenvironments and increased secretion of bioactive trophic factors, resulting in improved tissue repair.[16–19] While the benefits of MSC transplantation are apparent for both muscle and bone repair, no studies have reported the effect of myokine activity on bone regeneration generated by serial exposure of muscle cells to MSCs.

We hypothesized that bone formation would be enhanced by local myokine presentation, and the myoblast secretome would be augmented by exposure to factors secreted by MSC spheroids. Our aims were three-fold: (1) evaluate the potential of myokines to stimulate osteogenic differentiation of osteoprogenitor cells, (2) identify key bioactive cues involved in stimulating osteogenesis, and (3) translate this strategic approach to promote bone healing by locally delivering the myoblast secretome to a rat femoral segmental defect model.

3.2 MATERIALS AND METHODS

3.2a Cell culture

Human bone marrow-derived MSCs from a single donor were purchased from RoosterBio (Frederick, MD). Cells were expanded in α-MEM (Invitrogen, Carlsbad, CA) supplemented with 10% v/v fetal bovine serum (FBS, JR Scientific, Woodland, CA), 100 units/mL penicillin, and 100 µg/mL streptomycin (Gemini Bio-Products, Sacramento, CA) under standard culture conditions until use at passage 4-5. MC3T3-E1 pre-osteoblasts (ATCC, Manassas, VA) and rat bone marrow stromal cells (rBMSCs) (Cyagen Biosciences Inc, Santa Clara, CA) were cultured in similar conditions. L6 rat myoblasts (ATCC) were maintained in DMEM supplemented with 10% v/v FBS, 100 units/mL penicillin, and 100 µg/mL streptomycin under standard culture conditions. Myoblasts were kept below 70% confluency to prevent differentiation and myofibril formation.

3.2b Fabrication of MSC spheroids, conditioning, and media collection

MSC spheroids of 5,000 (5K); 15,000 (15K); and 40,000 cells/spheroid (40K) were formed using a forced aggregation technique.[18,20] Media was exchanged with fresh media supplemented with 100 mM $CoCl_2$ (Sigma, St. Louis, MO) and maintained for 3 days. Spheroids in standard culture conditions and monolayer cultured MSCs served as controls. Spheroids were then washed with PBS, and media was replaced with fresh α-MEM for culture in ambient conditions for 24 h and designated as spheroid-conditioned media (SPH). Media from MSCs in monolayer treated identically was designated as monolayer-conditioned media (MCM). Conditioned media from L6 myoblasts was termed myoblast-conditioned media (MYO). Finally, monolayer L6 myoblasts were exposed to SPH for 24 h, after which the media was collected and termed spheroid-myoblast-conditioned media (SPH-MYO). For *in vivo* experiments, conditioned media (6 mL) was lyophilized for 48 h until dry for subsequent entrapment in alginate.

3.2c Evaluation of conditioned media on viability and function

MC3T3-E1 murine pre-osteoblasts were plated at $1.0x10^5$ cells/cm^2 in complete media and allowed to attach for 24 h. Cells were then exposed to a 50:50 mixture of osteogenic media (10 mM β-glycerophosphate, 50 μg/mL ascorbate-2-phosphate; both from Sigma) and conditioned media for 3 days. Subsequent media changes were performed every 3 days with complete α-MEM. Cell survival and apoptosis was measured using a Caspase-Glo 3/7 assay (Promega, Madison, WI).[21] The osteogenic response of MC3T3-E1s and rBMSCs to conditioned media was assessed by quantifying cell number, DNA content, intracellular alkaline phosphatase (ALP) activity from a *p*-nitrophenyl phosphate assay, and calcium deposition by *o*-cresolphthalein assay and Alizarin red staining.[22–24] The concentration and identification of growth factors

and cytokines within conditioned media was evaluated using a protein array (Ray Biotech, Norcross, GA).[17]

3.2d Preparation and characterization of RGD-modified alginate

RGD-modified alginate was prepared as described previously.[18] Briefly, G_4RGDSP (Commonwealth Biotechnologies, Richmond, VA) was covalently coupled to UltraPure VLVG sodium alginate and 1% oxidized UltraPure MVG (Pronova, Lysaker, Norway) using standard carbodiimide chemistry, yielding hydrogels containing 0.8 mM RGD. The resulting RGD-alginate was sterile filtered and lyophilized for 4 days. Lyophilized alginate was reconstituted in serum-free α-MEM (840 µL) at a 25:75 VLVG:MVG ratio to obtain a 2% (w/v) solution. We then mixed lyophilized SPH-MYO into the alginate, with or without rBMSCs (5×10^6 cells/mL), and gels (60 µL) were crosslinked by dialyzing with 200 mM $CaCl_2$ for 10 min.[18]

We measured gel storage modulus using a Discovery HR2 Hybrid Rheometer (TA Instruments, New Castle, DE). An 8.0-mm-diameter Peltier plate geometry was used with an oscillatory strain sweep protocol ranging from 0.004% to 4% strain.[25] We evaluated myokine release from the alginate gels using 2 µg of VEGF (PeproTech, Rocky Hill, NJ) as a model protein. VEGF elution into serum-free media was measured using a VEGF-specific ELISA (R&D Systems, Minneapolis, MN). We confirmed cell viability in gels using a Live/Dead Assay and confocal microscopy.

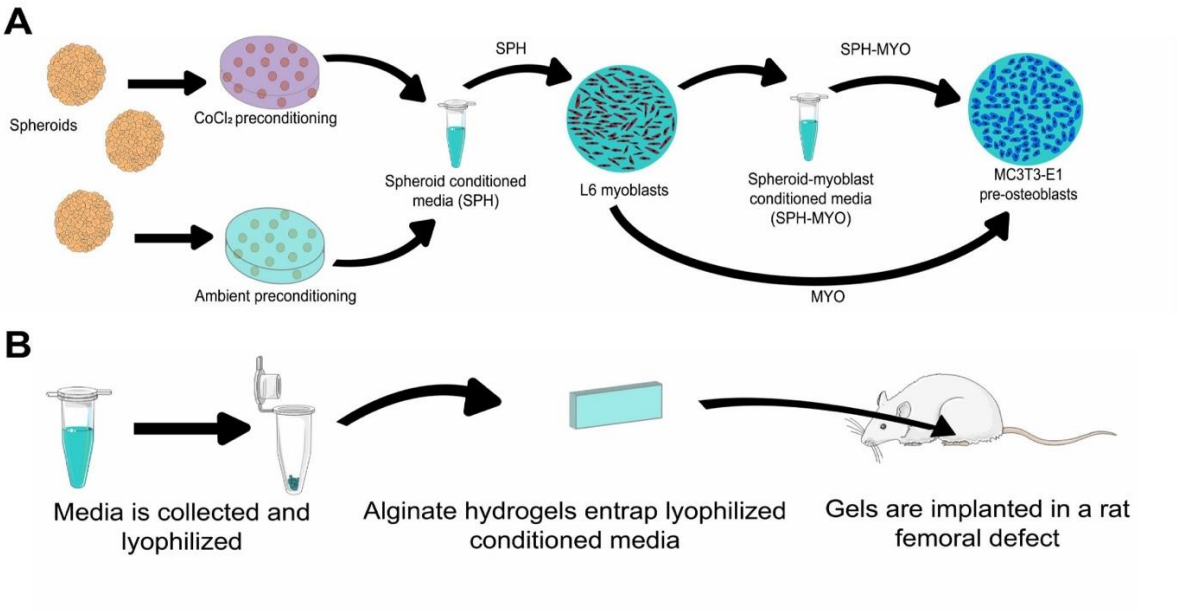

Figure 3.1. Schematic of experimental procedure. (A) MSC spheroids were preconditioned in either $CoCl_2$ or ambient conditions for 72 h and then maintained in growth media for 24 h. Conditioned media was then collected as spheroid-conditioned media (SPH). In some cases, SPH was incubated with L6 myoblasts for 24 h, yielding spheroid-myoblast conditioned media (SPH-MYO). (B) Schematic of experiments to investigate the therapeutic potential of conditioned media *in vivo*.

3.2e Segmental bone defect model

Treatment of experimental animals was in accordance with the UC Davis animal care guidelines and all National Institutes of Health animal handling procedures. SPH-MYO, with or without rBMSCs ($30x10^6$ cells/mL), was entrapped in alginate hydrogels (60 µL, 3 mm height, 3 mm width, 6 mm length) and kept in complete media in standard culture conditions for 18 h before implantation. Sprague-Dawley rats (male and female, 10 weeks old, Taconic, Hudson, NY) were anesthetized and maintained under a 3-4% isoflurane/O_2 mixture delivered through a nose cone. We created six-millimeter diaphyseal critical-size defects in the right femora of each animal and stabilized these defects with a radiolucent polyetheretherketone (PEEK) plate and 6 angular stable bicortical titanium screws (RISystem AG, Davos, Switzerland).[18,26] We immediately filled these defects with one of four RGD-modified alginate constructs: 1) acellular gels containing SPH-MYO only; 2) rBMSC-loaded gels; 3) gels containing both SPH-MYO and rBMSCs (SPH-MYO + rBMSCs); or 4) empty gels.

3.2f Quantification of bone formation and assessment of mechanical properties of repair tissue

We monitored bone formation noninvasively using contact high-resolution radiographs (20 kVp, 3 mA, 2 min exposure time, 61 cm source-film distance) taken in a cabinet radiograph unit (Faxitron 43805 N, Field Emission Corporation, Tucson, AZ) with high-resolution mammography film (Oncology Film PPL-2, Kodak, Rochester, NY) and digitized using a high-resolution flatbed scanner. Three blinded, independent reviewers scored these radiographs at 2, 4, 8, and 12 weeks on a scale of 0 (no bone formation) to 6 (homogeneous bone structure). At 12 weeks post-surgery, animals were euthanized, and femurs were explanted, wrapped in sterile gauze, submerged in PBS, and stored at -20°C until analysis. We imaged explanted femurs (45 kVp, 177 µA, 400 µs integration time, average of four images) at 6 µm resolution using a high-resolution microCT specimen scanner (µCT 35; Scanco Medical, Brüttisellen, Switzerland). Bone volume within the

tissue defect and bone mineral density (BMD) were determined from resulting images. We then analyzed explants *via* torsional testing to ascertain mechanical properties of repair tissue.[18,26] Prior to testing, we cut all PEEK plates to ensure stress was concentrated in the defect.

Explants were then demineralized in Calci-Clear Rapid (National Diagnostics, Atlanta, GA), processed, paraffin-embedded, and sectioned at 5 μm thickness. We stained sections with hematoxylin and eosin (H&E) and imaged using a Nikon Eclipse TE2000U microscope and Andor Zyla 5.5 sCMOS digital camera (Concord, MA). We stained tissue sections with Masson's trichrome to visualize collagen deposition within newly formed tissue, while Safranin O/Fast green staining was used to determine if negatively charged substances such as alginate or cartilage were present. Immunohistochemistry for human osteocalcin (1:200, product #AB13420, Abcam), was performed using an HRP detection kit (AB64261, Abcam) per the manufacturer's instructions.

3.2g Statistical analysis

Data are presented as means ± standard deviation. All experiments represent at least three independent experiments unless otherwise noted. Statistical analysis was performed using a one-way analysis of variance with Bonferroni correction for multiple comparisons in Prism 7 software (GraphPad, San Diego, CA); *p*-values less than 0.05 were considered statistically significant. Significance is denoted by alphabetical letterings; groups with no significance are linked by the same letters, while groups with significance do not share the same letters.

3.3 RESULTS

3.3a Myokines induce pre-osteoblast proliferation and early osteogenic response

MC3T3-E1 pre-osteoblasts exposed to MYO exhibited greater cell proliferation compared to cells maintained in growth media (**Fig. 3.2B**). Additionally, MC3T3s treated with MYO for 3 days had greater ALP activity at Day 7 than cells maintained in osteogenic media alone (**Fig. 3.2C**).

However, calcium deposition at Day 14 was not significantly different between the two groups (**Fig. 3.2D**), suggesting that MYO alone lacks sufficient potency to induce long-term osteogenic differentiation.

3.3b MSC spheroids synergistically enhance myokine bioactivity

MSC spheroids exhibited similar viability regardless of cell density (5K, 15K, or 40K) or preconditioning regimen ($CoCl_2$, 1% O_2, or ambient conditions) by live/dead staining (*data not shown*). In preliminary studies, we observed similar osteogenic response of MC3T3-E1 pre-osteoblasts when exposed to preconditioned media from MSCs in $CoCl_2$ or 1% O_2. Due to increased reproducibility of supplementing culture media with small molecules versus regulating the local oxygen microenvironment, all subsequent preconditioning was performed using $CoCl_2$. Compared to 5K and 15K spheroids, conditioned media from an identical number of MSCs formed into 40K spheroids induced a greater osteogenic response in MC3T3-E1 pre-osteoblasts (**Fig. 3.3**), motivating the use of 40K spheroids for all subsequent experiments.

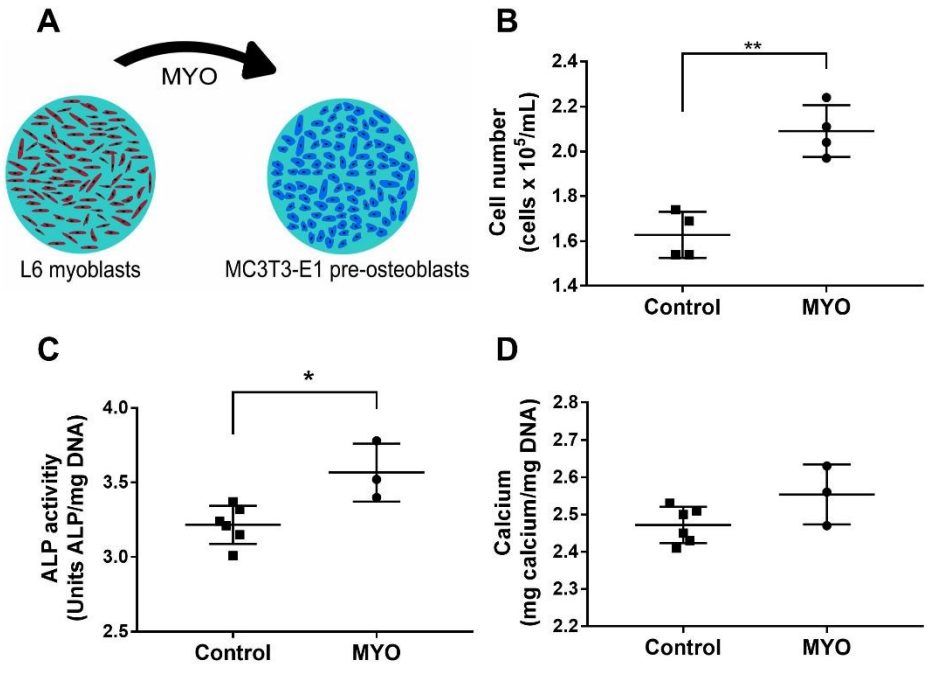

Figure 3.2. Myokines induce early osteogenic response in pre-osteoblasts. (A) L6 myoblast-conditioned media (MYO) was added to MC3T3-E1 pre-osteoblasts in monolayer culture. (B) Cell number at day 3, (C) ALP activity at day 7, and (D) calcium deposition at day 14 for MC3T3s after exposure to MYO. Control groups maintained in osteogenic media alone; *p<0.05, **p<0.01; n = 3-6.

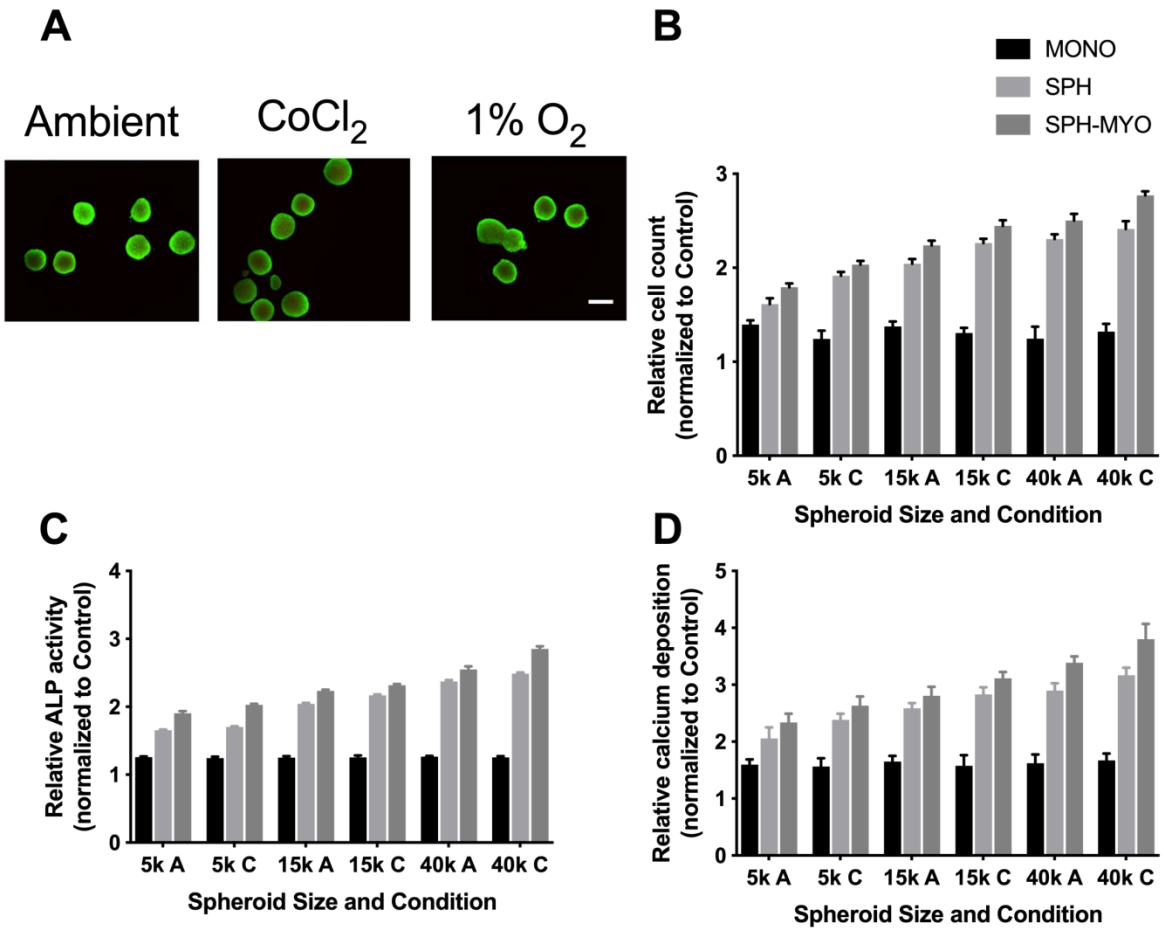

Figure 3.3. Osteogenic potential of conditioned media from MSC spheroids of different cell density. (A) Live/dead staining of spheroids at 72 hours in different conditions reveals similar viability. **(B)** Cell number, **(C)** ALP activity, and **(D)** calcium deposition of MC3T3s after 7 days (n=3) when stimulated by various conditioned media. A = ambient; C = $CoCl_2$ conditioned.

In agreement with previous reports in which MSC spheroids outperform equal numbers of individual MSCs[17], conditioned media from MSC spheroids induced greater osteogenic response in MC3T3s compared to MSCs in monolayer culture. MC3T3s exposed to SPH-MYO exhibited the greatest proliferation when compared to the SPH and MYO groups (**Fig. 3.4A**). The secretome of MSC spheroids preconditioned in $CoCl_2$ resulted in greater ALP activity, an early marker of osteogenic differentiation (**Fig. 3.4B**)**,** compared to SPH from spheroids in ambient air.

In the $CoCl_2$ group, ALP activity increased by more than 90% in SPH and 120% in SPH-MYO groups compared to MONO ($p<0.0001$). Calcium deposition, a late-stage functional marker of osteogenic differentiation, was also increased in pre-osteoblasts exposed to SPH-MYO by 120% compared to MONO ($p<0.0001$), while SPH induced nearly 90% increase ($p<0.0001$) (**Fig. 3.4C**). We confirmed these quantitative increases in calcium deposition by Alizarin Red staining (**Fig. 3.4D**). For both markers, the largest increase in osteogenic markers was induced by exposure to the secretome of MSC spheroids (SPH), and these markers were further increased when exposed to SPH-MYO.

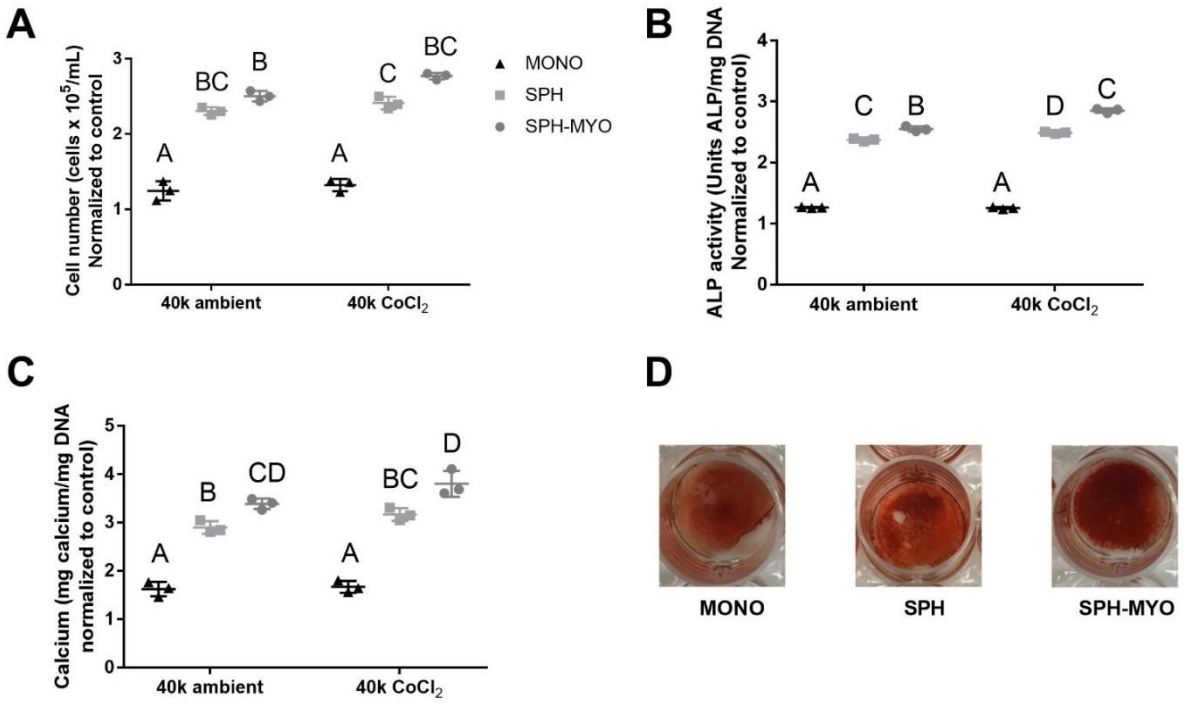

Figure 3.4. Investigation of the osteogenic response of conditioned media on pre-osteoblasts. The osteogenic response of spheroid-myoblast conditioned media (SPH-MYO), spheroid conditioned media (SPH) and MSC monolayer conditioned media (MONO) on MC3T3s was investigated by analyzing (A) cell number at day 3, (B) ALP activity at day 7, and (C) calcium deposition and (D) Alizarin red staining at day 14. Data are normalized to the response of MC3T3s in osteogenic media alone (n=3).

To interrogate potential differences in the composition and quantity of cytokines in each secretome, we analyzed the cytokine profiles of each formulation using a protein array (**Fig. 3.5**). The complexity and quantity of bioactive factors were also enhanced in conditioned media from $CoCl_2$-preconditioned spheroids compared to spheroids maintained in ambient conditions. Among the secreted factors examined, we detected appreciable increases in the quantity and complexity of SPH-MYO compared to SPH or MYO alone. We measured nearly a 30% increase IGF-1 and 20% increase in SDF-1α in SPH-MYO compared to SPH, and both factors were increased by more than 200% compared to MYO. Of particular interest, the preconditioned SPH-MYO media contained increased concentrations of IGF-1, IL-8, TIMP1, FGF-6, SDF-1α, and IL-6 compared to SPH and MYO media alone.

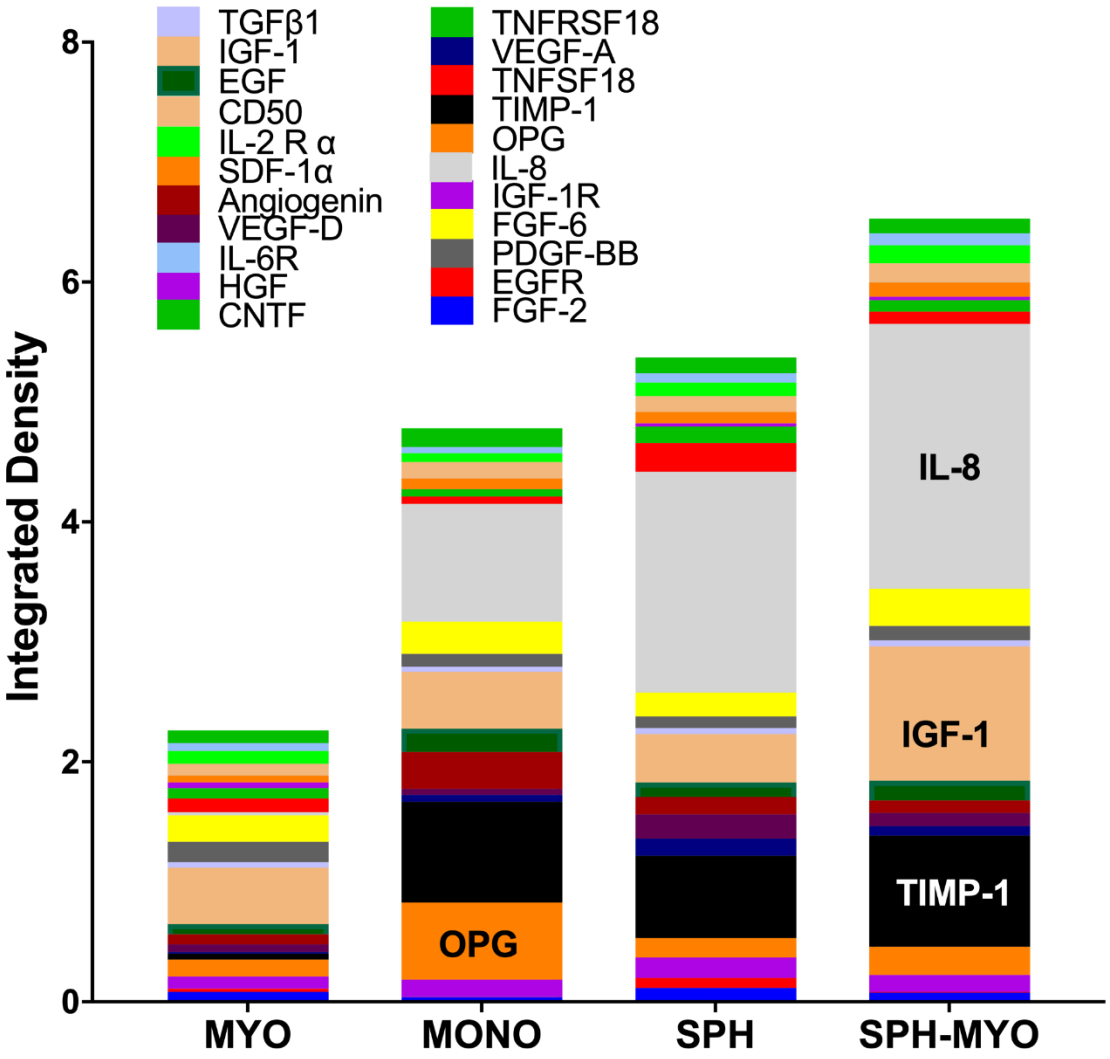

Figure 3.5. Protein array of conditioned media from myoblasts and MSCs. The composition of conditioned media was analyzed using a growth factor protein array (n=2).

3.3c Conditioned media entrapped in alginate hydrogels

Gels were formed to fill surgically created voids when press fit into the femoral defect (**Fig. 3.6A**). Entrapped rBMSCs evaluated after overnight incubation exhibited high viability and homogeneous distribution throughout the gel (**Fig. 3.6B**). Upon fabrication, gels could be easily handled and exhibited a decrease in storage modulus after 3 days that remained constant over

10 days (**Fig. 3.6C**). The majority of VEGF, serving as a model protein to mimic release of entrapped trophic factors in conditioned media, eluted from the gel over the first 72 hours (**Fig. 3.6D**).

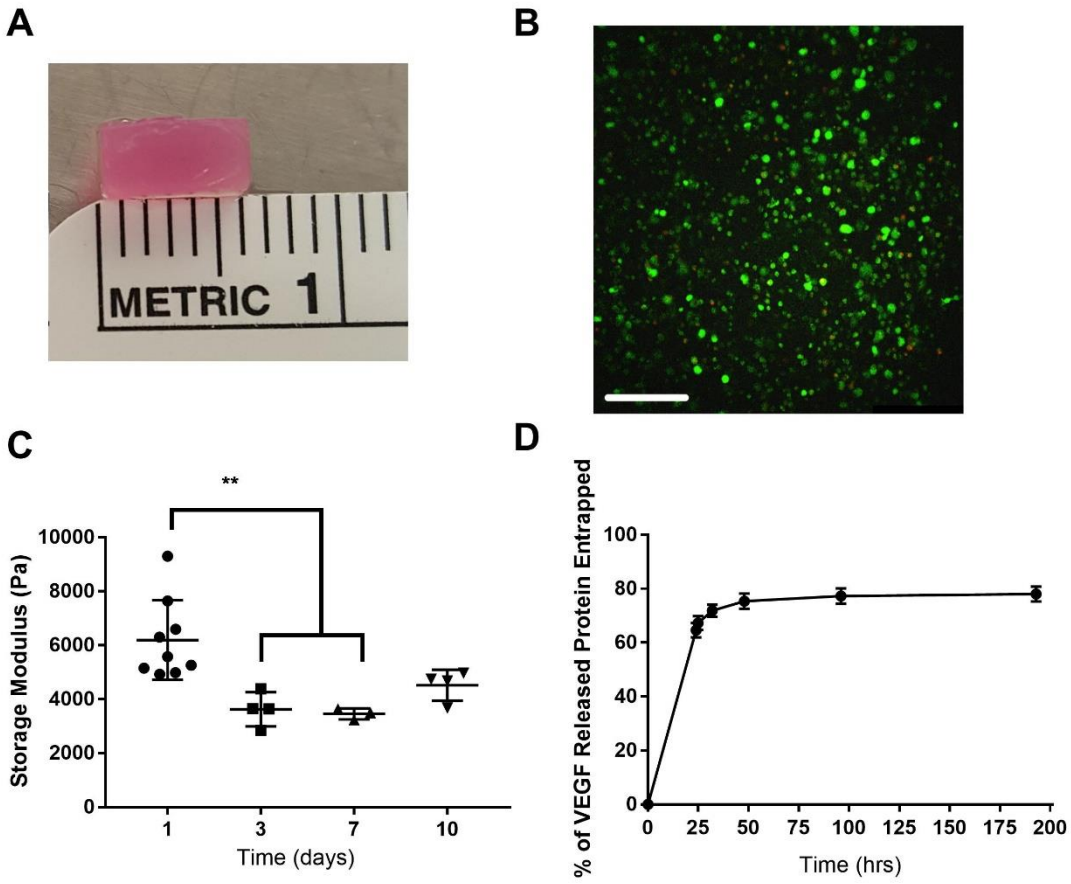

Figure 3.6. Characterization of alginate hydrogel properties and delivery of growth factor. (A) Image of MYO-SPH loaded hydrogel. (B) Live/dead stain of rBMSCs in hydrogel before implantation. Scale bar represents 250 µm. (C) Storage modulus of MYO-SPH-loaded hydrogel over 10 days (**p<0.01; n=3-4). (D) Percent release of loaded VEGF over 193 h.

3.3d Local presentation of myokine-conditioned media increases bone formation in vivo

The local presentation of SPH-MYO from alginate gels, in the presence and absence of rBMSCs, increased bone formation compared to empty hydrogels as measured by blinded radiograph evaluation (**Fig. 3.7** and **Fig. 3.8A)**. Importantly, the combined delivery of rBMSCs with SPH-MYO resulted in the greatest bone regeneration among the groups analyzed, which was more than 1.6-fold greater than acellular SPH-MYO-containing hydrogels ($p<0.05$) and more than 35-fold greater than rBMSCs alone ($p<0.0001$). We observed increased bone formation and vascularization within femoral defects treated with SPH-MYO-containing gels by macroscopic tissue images of the defect upon explantation (**Fig. 3.8B)**. Quantitative measurements of bone volume and bone mineral density using microCT were in agreement with radiography and gross tissue observations, with defects treated with SPH-MYO-containing gels exhibiting the highest bone volume and bone mineral density (**Fig. 3.8C-E)**. The resultant repair tissue within bone defects treated with SPH-MYO also possessed the most robust mechanical properties. Femoral defects treated with SPH-MYO-containing gels, particularly those gels also containing rBMSCs, demonstrated the greatest torsional stiffness and torque to failure (**Fig. 3.9A-B**), which was 1.5 times greater than SPH ($p<0.0003$) and 11 times greater than rBMSCs alone ($p<0.0001$). H&E staining revealed higher cell density in the groups without rBMSCs, while defects treated with rBMSCs contained more organized, dense tissue **(Fig. 3.10A)**. Masson's trichrome staining of repair tissue confirmed bony tissue formation within the femoral defect with integration with native bone ends. Intense Masson's trichome staining in defects treated with SPH-MYO + rBMSCs indicated robust collagen deposition, while porous pink regions revealed the formation of marrow spaces (**Fig. 3.10B**). Safranin O/Fast green staining indicated the presence of negatively charged material through red staining in the empty and SPH-MYO group, potentially corresponding to residual alginate or neocartilage. Bone defects treated with SPH-MYO + rBMSCs exhibited red staining on the outer layer of the blue-stained regenerated bone (**Fig. 3.10C**)**.** Osteocalcin IHC

further confirmed these data, revealing darker staining in the groups containing rBMSCs and indicating bone formation was occurring **(Fig. 3.10D**).

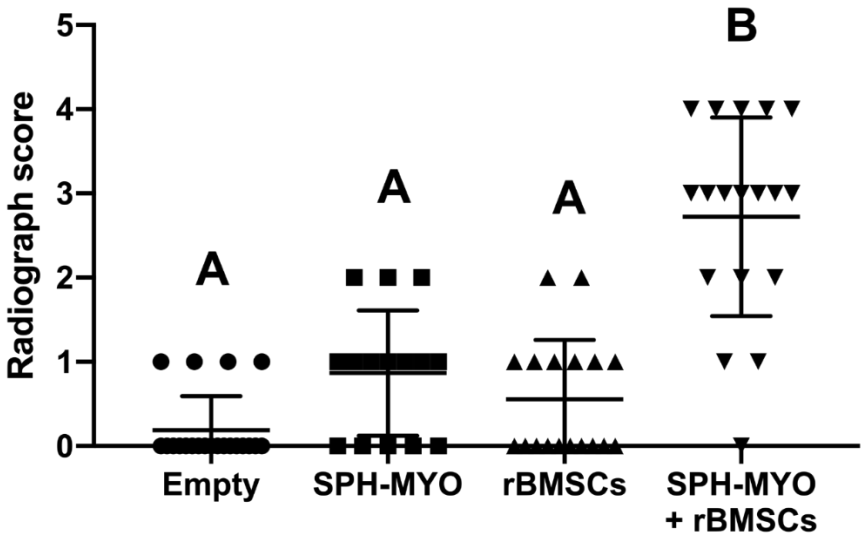

Figure 3.7. Blinded radiograph scores of treated femurs at 12 weeks (n=15-21).

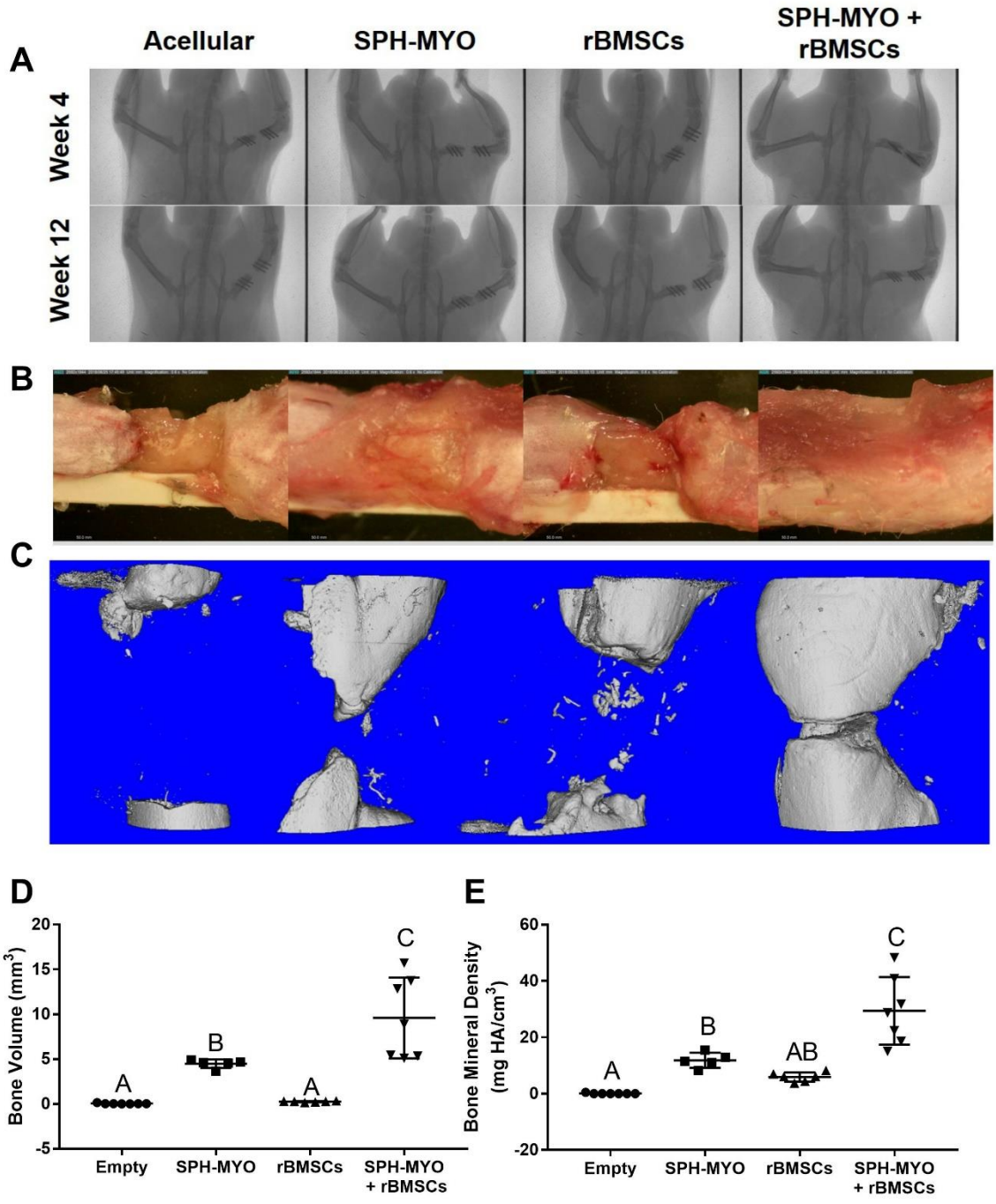

Figure 3.8. Repair of rat femoral defect when treated with conditioned media. (A) Week 4 and 12 x-rays of the defect. **(B)** Images of explanted femurs at week 12. **(C)** MicroCT images of bone mineralization at week 12 and quantitative microCT data for **(D)** bone volume and **(E)** bone mineral density. Bars that do not share letters are statistically significant from each other (n=5-7).

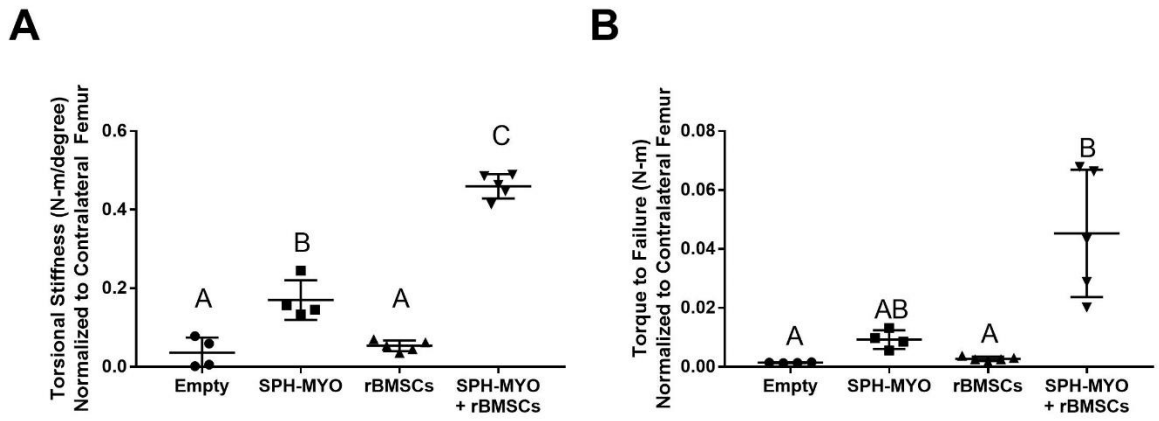

Figure 3.9. Mechanical testing of explanted femurs at week 12. Measurement of **(A)** torsional stiffness and **(B)** torque to failure on explanted femurs. Bars that do not share letters are statistically significant from each other (n=4-5).

3.4 DISCUSSION

Fractures with associated volumetric muscle loss pose a severe clinical challenge yet to be fully addressed, and insufficient healing of these defects demonstrates the importance of muscle-bone crosstalk in bone repair.[27] Autologous muscle flap transplantation, the current standard of treatment, increases the rate of fracture healing but has several limitations including restricted donor site availability, significant donor site morbidity, decreased function of donor and recipient sites, need for further surgery, and a high rate of complications including complete failure of the graft. This study demonstrated the promise of delivering myokines as a potent osteoinductive cue to upregulate osteogenic differentiation and support the function of transplanted stromal cells in bone repair. To our knowledge, this is the first demonstration of the synergistic interaction between the paracrine milieu of the MSC spheroid on the myoblast secretome. The translational clinical potential of this therapy is extremely high, as the growth factors are non-immunogenic and possess a prolonged half-life when stored as a lyophilized powder.

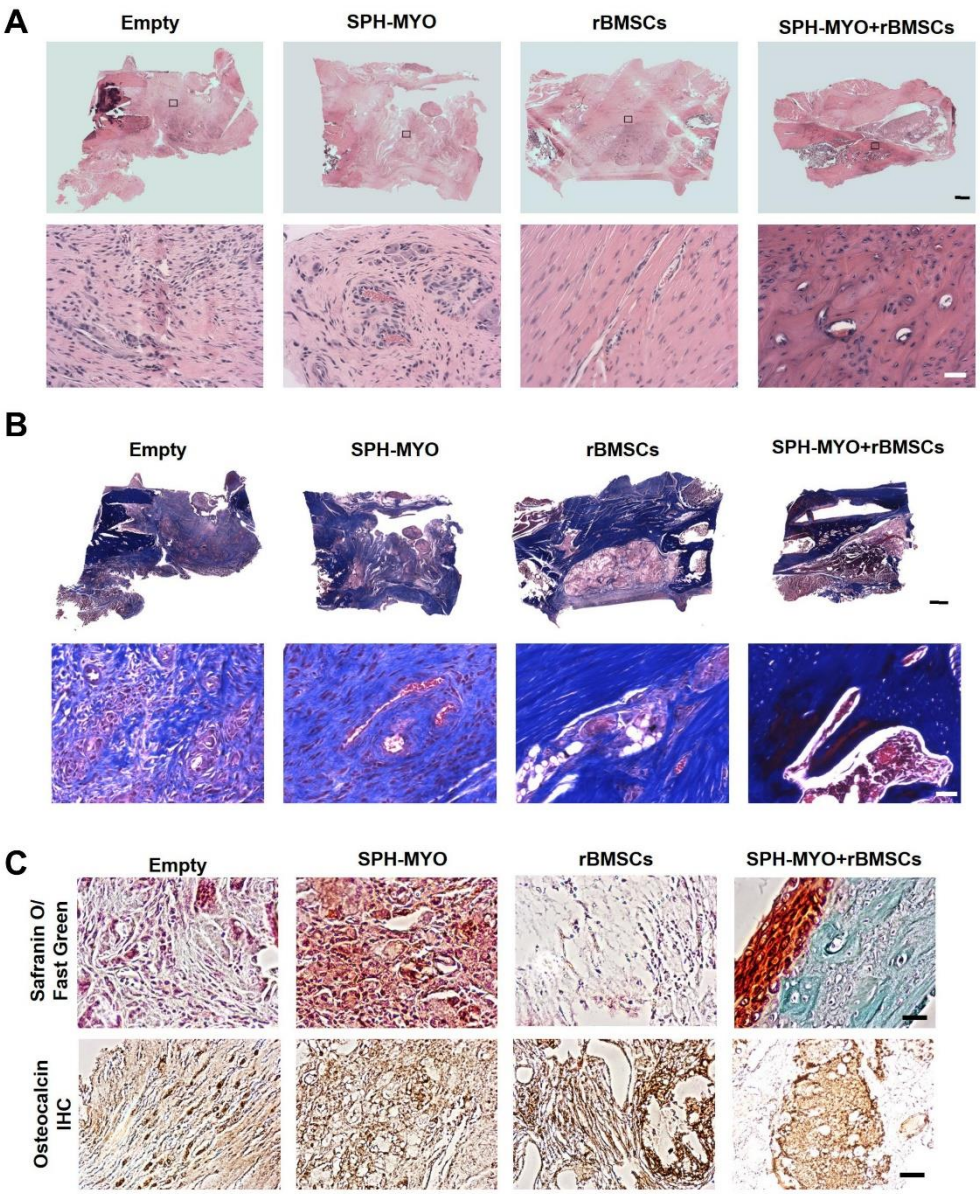

Figure 3.10. Histological analysis of regenerated bone tissue. (A) Hematoxylin and Eosin (H&E) staining of tissue at the defect site reveals more dense, organized tissue in defects treated with SPH-MYO + rBMSCs. Top images are the entire section, while images below are insets at 20x magnification. (B) Masson's Trichrome staining with large scan on top and inset images below at 20x magnification reveals more intense collagen staining in SPH-MYO + rBMSCs compared to other groups. (C) 20x magnification images of Safranin O/Fast Green- and osteocalcin-stained sections. Scale bar in large scan is 1 mm; scale bar in 20x images is 50 μm.

Effective bone repair is reliant on healthy musculature. Fractures involving damaged muscle rarely exhibit bridging compared to fractures in which the muscle remains intact, even with BMP-2 delivery to the defect site.[3,28–30] The observation of impaired bone healing in the presence of damaged or missing muscle has led to investigation of crosstalk between the two tissues. Muscle enables mechanical loading of the skeleton, which is key to provide sufficient nutrients and induce differentiation of bone cells through fluid flow. As an alternative to its mechanical loading contributions, the focus of this study was aimed at the endocrine activity of muscle. Although there are over 200 cytokines in the muscle secretome that are implicated in bone repair including IGF-1, BMPs, various interleukins, and several others, [31] there are limited studies that describe their direct therapeutic potency on bone formation. This study confirms the potency of these myokines by identifying them in the conditioned media of myoblasts and MSC spheroids. Myoblasts were used as individual cells that were not fused into myotubes to produce myoblast-conditioned media (MYO), as more mature myofibers secrete growth factors such as ciliary neurotrophic factor (CNTF) that may impair osteogenesis.[32] Each of our groups contained similar concentrations of CNTF, suggesting that other myokines compensated for any downregulation of osteogenesis by this factor.

Compared to MSCs in monolayer culture, MSC spheroids secrete an enhanced secretome that aids in osteogenesis, inflammatory modulation, and cell engraftment and survival.[17,33–35] Data from these *in vitro* studies are in agreement with previous studies, as conditioned media from spheroids (SPH) induced greater cell proliferation, ALP activity, and calcium deposition compared to MONO and MYO groups. Furthermore, the number and relative concentrations of myokines was greater in SPH compared to MONO and MYO. Spheroid therapeutic potential can be modulated *via* cell density and pre-conditioning, as spheroids with higher cell density and maintained under hypoxic, pro-inflammatory conditions secrete more vascular endothelial growth factor (VEGF) and PGE_2.[33] Prostaglandin E2 (PGE_2) is a critical factor for muscle repair,[36]

and our previous work demonstrates that PGE_2 secretion is upregulated by MSC spheroids that promote migration of host cells and catalyze bone healing.[36,37] We further demonstrated that the secretome from $CoCl_2$-preconditioned MSC spheroids induced a greater osteogenic response from MC3T3s compared to spheroids in ambient conditions. Hypoxic preconditioning of MSCs, whether as monolayer cells or spheroids, results in prolonged viability,[38] increased VEGF secretion,[18] and expression of chondrogenic markers[39], demonstrating the value of oxygen preconditioning to influence cell function.

Although the MSC spheroid secretome has high therapeutic value, the paracrine activity of muscle for bone repair should not be undervalued. Myoblasts exposed to MSC spheroid-conditioned media produced enriched myokines, resulting in increased osteogenic differentiation *in vitro* for bone marrow-derived stem cells and pre-osteoblasts, as well as enhanced bone growth *in vivo*. The cytokine portfolio was more complex than that of MSC spheroids or myoblasts alone, thereby demonstrating a synergistic and augmented relationship. IGF-1 and FGF-2 are potent myokines that promote bone repair[40], and we detected more than a 2-fold increase of IGF-1 in MYO-SPH compared to MYO or SPH alone. We stimulated rat myoblasts with conditioned media from human MSC spheroids, and it is unclear if similar therapeutic benefit would be observed using cells from the same species. However, human recombinant growth factors are highly effective when used in preclinical animal models, and the genetic structure of growth factors such as IGF-1 are well-conserved among mammalian species.[41]

To leverage the enhanced osteogenic potential of myokines from serially-stimulated myoblasts, we entrapped conditioned media from stimulated myoblasts in alginate gels for local presentation at the defect site. Alginate is commonly used as a carrier for cells and macromolecules in tissue regeneration.[9,29,42] While the conditioned media of MSCs has been used to treat other tissues[43,44], this is the first report of efficacy from conditioned media from serially-stimulated cells. Conditioned media was lyophilized for efficient entrapment in small

volumes with no apparent adverse effects on growth factor bioactivity or gel stability. Compared to acellular gels or gels containing rBMSCs in RGD-modified alginate gels, we observed increased bone formation in acellular defects treated with SPH-MYO alone. This is in agreement with studies demonstrating that bone marrow-derived MSCs, whether monodisperse or spheroids, are insufficient to repair large bone defects without preconditioning or osteoinductive stimuli.[26,45] Importantly, the synergistic presentation of SPH-MYO and rBMSCs resulted in significant increases in bone volume and near complete bridging in 12 weeks, demonstrating the potent nature of these myokines on promoting cell function and resultant bone formation. However, we were unable to determine the specific function of transplanted rBMSCs in this model. The role of myokines on promoting cell survival, cell differentiation or trophic factor secretion *in situ*, or how myokines may influence the surrounding microenvironment merit further investigation. These data represent the first evidence of myokines locally presented from a carrier in promoting significant bone formation, demonstrating translational potential for use in personalized medicine. This approach facilitates the use of donor cells to manufacture the myokines, and the complexity of cytokine cocktails may achieve improved results compared to a single recombinant factor.

3.5 CONCLUSION

This study demonstrates the therapeutic potential of myokines in bone healing. Specifically, these data reveal the capacity of myokines from myoblasts stimulated by MSC spheroids to induce osteogenic differentiation *in vitro*, stimulate bone healing *in vivo*, and synergistically support bone marrow stromal cells to bridge critical-sized bone defects. These data emphasize the importance of muscle in bone healing, providing evidence that deficient bone healing in the presence of muscle loss may be due to insufficient myokines secreted from surrounding tissues. Strategies that capitalize on the muscle secretome represent a promising approach to speed the

treatment of open fractures with volumetric muscle loss or closed fractures that may suffer from slow or impaired healing due to other comorbidities and complications.

3.6 REFERENCES

[1] S.S. Tseng, M.A. Lee, A.H. Reddi, Nonunions and the potential of stem cells in fracture-healing, J Bone Jt. Surg Am. 90 Suppl 1 (2008) 92–98.

[2] C.M. Court-Brown, K.E. Bugler, N.D. Clement, A.D. Duckworth, M.M. McQueen, The epidemiology of open fractures in adults. A 15-year review, Injury. 43 (2012) 891–897.

[3] N.J. Willett, M.-T.A. Li, B.A. Uhrig, J.D. Boerckel, N. Huebsch, T.L. Lundgren, G.L. Warren, R.E. Guldberg, Attenuated human bone morphogenetic protein-2-mediated bone regeneration in a rat model of composite bone and muscle injury., Tissue Eng. Part C. Methods. 19 (2013) 316–25.

[4] Y. Hao, Y. Ma, X. Wang, F. Jin, S. Ge, Short-term muscle atrophy caused by botulinum toxin-A local injection impairs fracture healing in the rat femur, J. Orthop. Res. 30 (2012) 574–580.

[5] M.J. Bosse, E.J. MacKenzie, J.F. Kellam, A.R. Burgess, L.X. Webb, M.F. Swiontkowski, R.W. Sanders, A.L. Jones, M.P. McAndrew, B.M. Patterson, M.L. McCarthy, T.G. Travison, R.C. Castillo, An Analysis of Outcomes of Reconstruction or Amputation after Leg-Threatening Injuries, N. Engl. J. Med. 347 (2002) 1924–1931.

[6] M.D. Helgeson, B.K. Potter, T.C. Burns, R.A. Hayda, D.A. Gajewski, Risk Factors for and Results of Late or Delayed Amputation Following Combat-Related Extremity Injuries, Orthopedics. 33 (2010) 669.

[7] D. Montarras, J. Morgan, C. Collins, F. Relaix, S. Zaffran, A. Cumano, T. Partridge, M. Buckingham, Direct Isolation of Satellite Cells for Skeletal Muscle Regeneration, Science (80-.). 309 (2005) 2064–2067.

[8] B. Péault, M. Rudnicki, Y. Torrente, G. Cossu, J.P. Tremblay, T. Partridge, E. Gussoni, L.M. Kunkel, J. Huard, Stem and Progenitor Cells in Skeletal Muscle Development, Maintenance, and Therapy, Mol. Ther. 15 (2007) 867–877.

[9] M. Pumberger, T.H. Qazi, M.C. Ehrentraut, M. Textor, J. Kueper, G. Stoltenburg-Didinger, T. Winkler, P. von Roth, S. Reinke, C. Borselli, C. Perka, D.J. Mooney, G.N. Duda, S. Geißler, Synthetic niche to modulate regenerative potential of MSCs and enhance skeletal muscle regeneration, Biomaterials. 99 (2016) 95–108.

[10] M. Brotto, L. Bonewald, Bone and muscle: Interactions beyond mechanical, Bone. 80 (2015) 109–114.

[11] J.N. Harvestine, H. Orbay, J.Y. Chen, D.E. Sahar, J.K. Leach, Cell-secreted extracellular matrix, independent of cell source, promotes the osteogenic differentiation of human stromal vascular fraction, J. Mater. Chem. B. 6 (2018) 4104–4115.

[12] R. Katare, F. Riu, J. Rowlinson, A. Lewis, R. Holden, M. Meloni, C. Reni, C. Wallrapp, C. Emanueli, P. Madeddu, Perivascular Delivery of Encapsulated Mesenchymal Stem Cells Improves Postischemic Angiogenesis Via Paracrine Activation of VEGF-A, Arterioscler. Thromb. Vasc. Biol. 33 (2013) 1872–1880.

[13] S.H. Ranganath, O. Levy, M.S. Inamdar, J.M. Karp, Harnessing the Mesenchymal Stem Cell Secretome for the Treatment of Cardiovascular Disease, Cell Stem Cell. 10 (2012) 244–258.

[14] M. Pumberger, T.H. Qazi, M.C. Ehrentraut, M. Textor, J. Kueper, G. Stoltenburg-Didinger, T. Winkler, P. von Roth, S. Reinke, C. Borselli, C. Perka, D.J. Mooney, G.N. Duda, S. Geißler, Synthetic niche to modulate regenerative potential of MSCs and enhance skeletal muscle regeneration, Biomaterials. 99 (2016) 95–108.

[15] B. Assmus, J. Honold, V. Schächinger, M.B. Britten, U. Fischer-Rasokat, R. Lehmann, C. Teupe, K. Pistorius, H. Martin, N.D. Abolmaali, T. Tonn, S. Dimmeler, A.M. Zeiher, Transcoronary Transplantation of Progenitor Cells after Myocardial Infarction, N. Engl. J. Med. 355 (2006) 1222–1232.

[16] K.C. Murphy, A.I. Hoch, J.N. Harvestine, D. Zhou, J.K. Leach, Mesenchymal stem cell spheroids retain osteogenic phenotype through α2β1 signaling, Stem Cells Transl Med. 5 (2016) 1229–1237.

[17] S.S. Ho, K.C. Murphy, B.Y.K.K. Binder, C.B. Vissers, J.K. Leach, Increased survival and function of mesenchymal stem cell spheroids entrapped in instructive alginate hydrogels, Stem Cells Transl Med. 5 (2016) 773–781.

[18] S.S. Ho, B.P. Hung, N. Heyrani, M.A. Lee, J.K. Leach, Hypoxic Preconditioning of Mesenchymal Stem Cells with Subsequent Spheroid Formation Accelerates Repair of Segmental Bone Defects, Stem Cells. 36 (2018) 1393–1403.

[19] H. Liu, W. Xue, G. Ge, X. Luo, Y. Li, H. Xiang, X. Ding, P. Tian, X. Tian, Hypoxic preconditioning advances CXCR4 and CXCR7 expression by activating HIF-1α in MSCs, Biochem. Biophys. Res. Commun. 401 (2010) 509–515.

[20] C.E. Vorwald, S.S. Ho, J. Whitehead, J.K. Leach, High-Throughput Formation of Mesenchymal Stem Cell Spheroids and Entrapment in Alginate Hydrogels, in: Methods Mol. Biol., 2018: pp. 139–149.

[21] B.Y.K. Binder, D.C. Genetos, J.K. Leach, Lysophosphatidic acid protects human mesenchymal stromal cells from differentiation-dependent vulnerability to apoptosis., Tissue Eng. Part A. 20 (2014) 1156–64.

[22] A. Bhat, A.I. Hoch, M.L. Decaris, J.K. Leach, Alginate hydrogels containing cell-interactive beads for bone formation, FASEB J. 27 (2013) 4844–4852.

[23] H.E. Davis, B.Y.K. Binder, P. Schaecher, D.D. Yakoobinsky, A. Bhat, J.K. Leach, Enhancing osteoconductivity of fibrin gels with apatite-coated polymer microspheres., Tissue Eng. Part A. 19 (2013) 1773–82.

[24] M.L. Decaris, B.Y. Binder, M.A. Soicher, A. Bhat, J.K. Leach, Cell-derived matrix coatings for polymeric scaffolds., Tissue Eng. Part A. 18 (2012) 2148–57.

[25] S.S. Ho, A.T. Keown, B. Addison, J.K. Leach, Cell Migration and Bone Formation from Mesenchymal Stem Cell Spheroids in Alginate Hydrogels Are Regulated by Adhesive Ligand Density, Biomacromolecules. 18 (2017) 4331–4340.

[26] S.S. Ho, N.L. Vollmer, M.I. Refaat, O. Jeon, E. Alsberg, M.A. Lee, J.K. Leach, Bone Morphogenetic Protein-2 Promotes Human Mesenchymal Stem Cell Survival and Resultant Bone Formation When Entrapped in Photocrosslinked Alginate Hydrogels, Adv. Healthc. Mater. 5 (2016) 2501–2509.

[27] L.E. Harry, A. Sandison, E.M. Paleolog, U. Hansen, M.F. Pearse, J. Nanchahal, Comparison of the healing of open tibial fractures covered with either muscle or fasciocutaneous tissue in a murine model, J. Orthop. Res. 26 (2008) 1238–1244.

[28] J.D. Boerckel, Y.M. Kolambkar, K.M. Dupont, B.A. Uhrig, E.A. Phelps, H.Y. Stevens, A.J. García, R.E. Guldberg, Effects of protein dose and delivery system on BMP-mediated bone regeneration, Biomaterials. 32 (2011) 5241–5251.

[29] Y.M. Kolambkar, K.M. Dupont, J.D. Boerckel, N. Huebsch, D.J. Mooney, D.W. Hutmacher, R.E. Guldberg, An alginate-based hybrid system for growth factor delivery in the functional repair of large bone defects, Biomaterials. 32 (2011) 65–74.

[30] Y.M. Kolambkar, J.D. Boerckel, K.M. Dupont, M. Bajin, N. Huebsch, D.J. Mooney, D.W. Hutmacher, R.E. Guldberg, Spatiotemporal delivery of bone morphogenetic protein enhances functional repair of segmental bone defects, Bone. 49 (2011) 485–492.

[31] H. Li, J.J. Hicks, L. Wang, N. Oyster, M.J. Philippon, S. Hurwitz, M. V. Hogan, J. Huard, Customized platelet-rich plasma with transforming growth factor β1 neutralization antibody to reduce fibrosis in skeletal muscle, Biomaterials. 87 (2016) 147–156.

[32] R.W. Johnson, J.D. White, E.C. Walker, T.J. Martin, N.A. Sims, Myokines (muscle-derived cytokines and chemokines) including ciliary neurotrophic factor (CNTF) inhibit osteoblast differentiation, Bone. 64 (2014) 47–56.

[33] K.C. Murphy, J. Whitehead, P.C. Falahee, D. Zhou, S.I. Simon, J.K. Leach, Multifactorial experimental design to optimize the anti-inflammatory and proangiogenic potential of mesenchymal stem cell spheroids, Stem Cells. 35 (2017) 1493–1504.

[34] J.H. YlÖstalo, T.J. Bartosh, K. Coble, D.J. Prockop, Human Mesenchymal Stem/Stromal Cells Cultured as Spheroids are Self-activated to Produce Prostaglandin E2 that Directs Stimulated Macrophages into an Anti-inflammatory Phenotype, Stem Cells. 30 (2012) 2283–2296.

[35] M.A. Gionet-Gonzales, J.K. Leach, Engineering principles for guiding spheroid function in the regeneration of bone, cartilage, and skin, Biomed Mater. 13 (2018) 34109.

[36] A.T. V Ho, A.R. Palla, M.R. Blake, N.D. Yucel, Y.X. Wang, K.E.G. Magnusson, C.A. Holbrook, P.E. Kraft, S.L. Delp, H.M. Blau, Prostaglandin E2 is essential for efficacious skeletal muscle stem-cell function, augmenting regeneration and strength., Proc. Natl. Acad. Sci. U. S. A. 114 (2017) 6675–6684.

[37] K.C. Murphy, J. Whitehead, P.C. Falahee, D. Zhou, S.I. Simon, J.K. Leach, Multifactorial experimental design to optimize the anti-inflammatory and proangiogenic potential of mesenchymal stem cell spheroids, Stem Cells. 35 (2017) 1493–1504.

[38] J. Beegle, K. Lakatos, S. Kalomoiris, H. Stewart, R.R. Isseroff, J.A. Nolta, F.A. Fierro, Hypoxic Preconditioning of Mesenchymal Stromal Cells Induces Metabolic Changes, Enhances Survival, and Promotes Cell Retention In Vivo, Stem Cells. 33 (2015) 1818–1828.

[39] S. Khajeh, V. Razban, T. Talaei-Khozani, M. Soleimani, R. Asadi-Golshan, F. Dehghani, A. Ramezani, Z. Mostafavi-Pour, Enhanced chondrogenic differentiation of dental pulp-derived mesenchymal stem cells in 3D pellet culture system: effect of mimicking hypoxia, Biologia

(Bratisl). 73 (2018) 715–726.

[40] M.W. Hamrick, P.L. McNeil, S.L. Patterson, Role of muscle-derived growth factors in bone formation., J. Musculoskelet. Neuronal Interact. 10 (2010) 64–70.

[41] P. Rotwein, Diversification of the insulin-like growth factor 1 gene in mammals., PLoS One. 12 (2017) e0189642.

[42] J.K. Leach, J. Whitehead, Materials-directed differentiation of mesenchymal stem cells for tissue engineering and regeneration, ACS Biomater Sci Eng. (2017).

[43] M. Osugi, W. Katagiri, R. Yoshimi, T. Inukai, H. Hibi, M. Ueda, Conditioned media from mesenchymal stem cells enhanced bone regeneration in rat calvarial bone defects., Tissue Eng. Part A. 18 (2012) 1479–89.

[44] B. Ritschka, M. Storer, A. Mas, F. Heinzmann, M.C. Ortells, J.P. Morton, O.J. Sansom, L. Zender, W.M. Keyes, The senescence-associated secretory phenotype induces cellular plasticity and tissue regeneration, Genes Dev. 31 (2017) 172–183.

[45] A.B. Allen, J.A. Zimmermann, O.A. Burnsed, D.C. Yakubovich, H.Y. Stevens, Z. Gazit, T.C. McDevitt, R.E. Guldberg, Environmental manipulation to promote stem cell survival in vivo: use of aggregation, oxygen carrier, and BMP-2 co-delivery strategies, J. Mater. Chem. B. 4 (2016) 3594–3607.

CHAPTER 4: SULFATED ALGINATE HYDROGELS PROLONG THE THERAPEUTIC POTENTIAL OF MSC SPHEROIDS BY RETAINING THE SECRETOME

Cell-based approaches to tissue repair suffer from rapid cell death upon implantation, limiting the window for therapeutic intervention. Despite robust lineage-specific differentiation potential in vitro, the function of transplanted mesenchymal stromal cells (MSCs) in vivo is largely attributed to their potent secretome comprised of a variety of growth factors (GFs). Furthermore, GF secretion is markedly increased when MSCs are formed into spheroids. Native GFs are sequestered within the extracellular matrix (ECM) via sulfated glycosaminoglycans, increasing the potency of GF signaling compared to their unbound form. To address the critical need to prolong the efficacy of transplanted cells, we modified alginate hydrogels with sulfate groups to sequester endogenous heparin-binding GFs secreted by MSC spheroids. We assessed the influence of crosslinking method and alginate modification on mechanical properties, degradation rate, and degree of sulfate modification. Sulfated alginate hydrogels sequestered a mixture of MSC secreted endogenous biomolecules, thereby prolonging the therapeutic effect of MSC spheroids for tissue regeneration. GFs were sequestered for longer durations within sulfated hydrogels and retained their bioactivity to regulate endothelial cell tubulogenesis and myoblast infiltration. This platform has the potential to prolong the therapeutic benefit of the MSC secretome and serve as a valuable tool for investigating GF sequestration.

Under revision as: M. Gionet-Gonzales, D. Diloretto, C. Ginnell, A. Casella, A. Bigot, J. K. Leach, Sulfated alginate hydrogels prolong the therapeutic potential of MSC spheroids by sequestering the secretome, *Adv. Healthc. Mater.*

4.1 INTRODUCTION

Cells are the building blocks of new and replacement tissues that offer a therapeutic benefit often unmatched by cell-free approaches. Consequently, a multitude of tissue engineering strategies have employed the delivery of cells to wound sites for improved regeneration.[1] Mesenchymal stromal cells (MSCs) are commonly used for this application due to their ease of harvest from adult patients, trilineage potential, and their therapeutic secretome that recruits host cells to the tissue site, promotes angiogenesis, and modulates the local inflammatory microenvironment.[2] The MSC secretome is composed of a complex mixture of tissue-reparative cytokines and endogenous growth factors (GFs) including VEGFA, IGF-1 and IL-8. Despite their robust differentiation potential *in vitro*, it is widely assumed that MSCs primarily contribute to tissue regeneration and repair via this potent secretome.[3]

Cell-based tissue engineering approaches are limited by rapid cell death upon implantation into a harsh microenvironment, thereby reducing the duration and overall potential of this strategy.[4-6] In contrast to monodisperse cells, the aggregation of MSCs into spheroids results in prolonged cell viability and enhanced secretion of endogenous GFs.[7-9] The behavior of MSC spheroids can be further influenced by the biophysical properties of carriers used to transplant cells. For example, hydrogel stiffness and adhesivity can be tuned to upregulate GF production by MSC spheroids.[9, 10] However, the therapeutic effects of MSC spheroids are limited by their survival and rapid diffusion of endogenous GFs from many cell carriers and delivery vehicles.

To address the challenge of short-term cellular contributions to cell-based therapies, there is a critical need for the development of advanced biomaterials that prolong or retain the bioactivity of endogenous GFs or other bioactive moieties.[11, 12] Beyond tuning the morphological and mechanical properties of biomaterials, one strategy is designed to mimic a key role of the native extracellular matrix (ECM): retention and presentation of endogenous GFs secreted by neighboring cells. The presentation and release of GFs from biomaterials can be regulated by controlling pore density and gel composition, covalently tethering GFs to materials, and

sequestering GFs via charged polymers.[13-16] Heparan sulfate (HS), a negatively charged glycosaminoglycan that reversibly binds positively charged GFs, is a key GF binding constituent of the native ECM. HS function has been mimicked using naturally occurring sulfated polymers (e.g., heparin) or modifying polymers such as polyethylene glycol (PEG) and alginate with functional sulfate groups.[17, 18] Sulfated alginate has been used as a GF delivery vehicle for applications in hind limb ischemia and myocardial infarction, demonstrating a 3-fold greater retention of entrapped GFs compared to unmodified alginate.[19, 20] However, this platform is designed to deliver a single GF for a therapeutic application, which severely limits the potential of endogenous GFs to be retained in the platform. MSC spheroids are under investigation for the utility of their secretome,[21] a complex mixture of endogenous GFs, and cells are commonly transplanted using engineered hydrogels.[22, 23] Thus, it is imperative to develop and characterize the ability of biomaterial platforms to sequester the endogenous secretome produced by entrapped MSC spheroids.

We hypothesized that alginate hydrogels could be modified to support survival of entrapped MSC spheroids and sequester components of the endogenous secretome as a means to prolong their therapeutic potential. We sought to independently control initial moduli, degradation rate, and degree of sulfation of these modified hydrogels to tune the production and retention of endogenous GFs. We then investigated the capacity of sulfated alginate hydrogels to capture the bioactive MSC spheroid secretome and enhance cell infiltration to demonstrate the utility of this platform.

4.2 MATERIALS AND METHODS

4.2a Modification of alginate with functional groups

PRONOVA UP VLVG alginate (< 75,000 g/mol; NovaMatrix Sandvika, Norway) was modified with sulfate groups on the polymer backbone as described.[24] Briefly, dried VLVG was dissolved in formamide at 2.5% (w/v). Chlorosulfonic acid (HSO3Cl; Sigma Chemical, St. Louis, MO) at 0-2% (v/v) was added to the solution and incubated at 60oC for 2.5 hrs while stirring. Alginate was

then precipitated out of solution in cold acetone and dissolved in ultrapure water overnight. Sodium hydroxide was added dropwise to the alginate solution until each sample reached a neutral pH (~7). The solutions were pipetted into 3500 Da molecular weight cut off (MWCO) dialysis tubing (Spectrum Laboratories, New Brunswick, NJ). The tubes were maintained in 2 L of 100 mM sodium chloride solution for 12 hrs and then ultrapure water the next 2.5 days, with water changes every 6-12 hrs. The alginate was then recovered from the dialysis tubing, filtered through a 0.22 μm pore filter, and lyophilized for up to 7 days until dry.

PRONOVA UP MVG (> 200,000 g/mol; NovaMatrix Sandvika) was oxidized as previously described.[25] Alginate was dissolved overnight in ultrapure water at a 1% (w/v) solution and reacted with 1 mM of sodium periodate for 1% oxidation or 5 mM for 5% oxidation. The reaction was then quenched after 17 hrs in darkness with stirring using an equimolar amount of ethylene glycol. The alginate was dialyzed in ultrapure water, filtered, and lyophilized.

PRONOVA UP VLVG and oxidized PRONOVA UP MVG were modified with Arg-Gly-Asp (RGD) through standard carbodiimide chemistry.[26] Alginate was first dissolved in a 1% (w/v) solution in MES buffer (0.1 M MES, 0.3 M NaCl pH 6.5) overnight. The next day, N-(3-Dimethylaminopropyl)-N'-ethylcarbodiimide hydrochloride (EDC) and N-Hydroxysulfosuccinimide sodium salt (Sulfo-NHS) were added to the reaction at a ratio of 2:1 per gram of alginate. The peptide G4RGDSP (Commonwealth Biotechnologies, Richmond, VA) was then added to the reaction to achieve a degree of substitution (DS) of 2. The resulting RGD-alginate was put in a dialysis tube (6-8 kDa MWCO, Spectrum Laboratories) in a water bath for three days. The solution was then sterile filtered and lyophilized for 4 days.

4.2b Detection of sulfate groups tethered to the alginate polymer

The modification of alginate with sulfate groups was confirmed via 1H NMR as described.[26] Briefly, lyophilized alginate samples were dissolved in D2O at 3.33% (w/v) concentration and were recorded using an 800 MHz Bruker Avance III NMR spectrometer. Alginate sulfate

modification was further verified through 1,9-Dimethyl-Methylene Blue zinc chloride double salt (DMMB) assay.[27] The DMMB solution pH was reduced to 1.5 to eliminate false readings from the negatively charged alginate polymer. Sulfated alginate was compared via DMMB assay with a sample of decellularized ECM derived from human MSCs and commercially available heparin sodium salt (Fisher Scientific, Hampton, NH). ECM was decellularized as previously described, including treatment with a detergent solution and deoxyribonuclease.[28]

4.2c Sulfated hydrogel synthesis

All alginate was dissolved at a concentration of 25 mg/mL in PBS. Alginate hydrogels were produced by combining sulfated alginate with non-sulfated alginate in a ratio of 1:7 (sulfated:non-sulfated). The sulfated alginate consisted of VLVG alginate reacted with 0, 1 or 2% chlorosulfonic acid. The non-sulfated alginate was composed of 1 part RGD-modified VLVG alginate and 1 part oxidized (either 1% or 5%) RGD-modified MVG, as described in Table 1. A visual representation of the gel composition can be seen in Figure 2A. After mixing via gentle tube rotation for 10 min, the alginate mixture was pipetted into 8 mm diameter circular silicone molds sandwiched between two dialysis membranes (6-8 kDa MWCO, Spectrum Laboratories). A solution of either 6 mM $BaCl_2$ and 200mM $CaCl_2$ (high elastic moduli) or 3 mM $BaCl_2$ and 100 mM $CaCl_2$ (low elastic moduli) was pipetted onto the top dialysis membrane for 5 min. The gels were then flipped, and the ionic solution was pipetted onto the other dialysis membrane for an additional 5 min. Both dialysis membranes were removed, and the gels were put in a bath of the same ionic solution for an additional 10 min. Gels were then removed from the mold and used immediately.

4.2d Mechanical testing and degradation

We tested the shear storage moduli of 8 mm diameter gels using a Discovery HR2 Hybrid Rheometer (TA Instruments, New Castle, DE) with a stainless steel, cross hatched, 8 mm plate geometry. We performed an oscillatory strain sweep ranging from 0.004% to 4% strain on each

gel to obtain the linear viscoelastic region (LVR) before failure.[26] At least 5 data points were collected for the LVR and averaged to obtain gel shear storage modulus. Gels were measured after 1 or 14 days in serum-free αMEM at standard sterile culture conditions (37°C, 21% O2, 5% CO2). After testing, gels were frozen and lyophilized for 24 hrs or until dry. The dry mass of the gels was determined using a Mettler Toledo XPR2 Microbalance (Mettler-Toledo, Columbus, OH).

4.2e Cell culture and MSC spheroid formation

Human MSCs (RoosterBio, Frederick, MD) were cultured in αMEM (Invitrogen, Carlsbad, CA) with 10% fetal bovine serum (FBS) (Biotechne, Minneapolis, MN) and 1% penicillin-streptomycin (pen/strep) (Gemini Bio Products, West Sacramento, CA) in standard conditions. MSCs were used at passage 3-5 for all experiments. TdTomato-expressing human hTERT/cdk4 immortalized myoblasts (Institute of Myology, Paris, France) were cultured in 1:4 ratio of Media 199 (Thermo Fisher, Chicago, IL) and DMEM (Invitrogen) supplemented with 20% FBS, 1% pen/strep, 25 µg/mL fetuin, 5 ng/mL of hEGF, 0.5 ng/mL of bFGF, 5 µg/mL of insulin, and 0.2 µg/mL dexamethasone (all from Millipore Sigma, Burlington, MA) under the same conditions.[29] Myoblasts were cultured in flask until 80% confluence or lower to discourage cell fusion and myotube formation. Human dermal microvascular endothelial cells (HDMECs, Lot #437592; Lonza, Basel, Switzerland) were cultured in complete endothelial cell growth media (EGM2-MV). HDMECs were cultured for 6 days under standard conditions or until 75-80% confluent before use, and cells were used between passage 4-5 for all experiments.

MSC spheroids were produced using the forced aggregation technique as we described.[26, 30] Once cultured to confluence, MSCs were trypsinized and centrifuged down into 2,000 µm pores made out of 1.5% agarose to form 40,000 cell spheroids. After 48 hrs in static conditions to enable spheroid formation, MSC spheroids were pipetted into the alginate solutions at 800,000 cells per gel and crosslinked into hydrogels as described above.

4.2f Testing retention of proteins in modified alginate gels

Hydrogels were loaded with 1 µg HGF (PeproTech, Rocky Hill, NJ) as a model protein to verify that sulfate groups bind heparin-binding GFs. As a control experiment, another set of hydrogels was loaded with 1 µg IGF-1 (PeproTech), a non-heparin binding GF, to verify GF retention was specific for heparin binding GFs. All gels were cultured in serum-free media that was collected at various time points for GF quantification. HGF and IGF detection was quantified using Human Quantikine ELISA Kits specific for each GF (R&D Systems, Minneapolis, MN) and assessed on a Synergy HTX Multi-Mode Reader (BioTek, Winooski, VT) at 450 nm. To quantify hydrogel-retained cytokines, MSC spheroids were cultured in sulfated or non-sulfated hydrogels for 3 days, then collected in 1 mg/mL alginate lyase (Millipore Sigma) in a 1.4 M NaCl solution. MSC spheroid-secreted GFs were quantified and identified using the IsoLight System (IsoPlexis, Branford, CT) with the Human Innate Immune cytokine panel.

4.2g Endothelial cell tubulogenesis assay

MSC spheroids were entrapped in alginate sulfated with either 0, 1, or 2% HSO_3Cl and cultured for 21 days. The media was refreshed every 2-3 days and subsequently stored at -20°C for later use. Before use, the conditioned media was thawed on ice, vortexed briefly, then centrifuged at 700xg for 8 min to pellet any cell debris or ECM. Immediately before use, the media was warmed to 37°C, and 200 µL of supernatant was used for experimentation.

Matrigel (Corning, Corning, NY) was pipetted into a 48-well plate and incubated at 37°C for 1 hr to ensure gelation. HDMECs were trypsinized and resuspended at a concentration of 30,000 cells per well in either complete EGM2 as the positive control, GF-deficient media as the negative control, or conditioned media for the experimental groups. Tubule formation proceeded for 6 hrs. The media was then removed, a 2 mM calcein AM solution was added to each well, and plates were incubated for an additional 30 min. Each well was imaged in 3 different locations; network length and branch number were quantified using the ImageJ Angiogenesis Analyzer plugin.

Network length was quantified as the sum of all segments in the network, and branches were defined as segments linked to one junction, a bifurcation point, and one extremity, a segment with a free end.[31]

4.2h Myoblast infiltration into hydrogels

MSC spheroids were loaded into sulfated alginate hydrogels at 800,000 cells per gel (20 spheroids per gel; concentration). The gels were cultured in complete αMEM for 4 days to allow for accumulation of the secretome within the hydrogel. To test the potential of GFs retained after cell death, gels were frozen at -80°C for 2 weeks, while live spheroid hydrogels were used immediately after the 4-day culture. Hydrogels were then placed in non-tissue culture treated 24-well plates and seeded with $1x10^6$ td myoblasts in a 50:50 αMEM-myoblast media mixture. Hydrogels were moved to new plates after 24 hrs and media was refreshed every 2-3 days to prevent GFs secreted from non-adherent myoblasts to confound results. After 8 days, myoblast infiltration was characterized via confocal imaging. Z stacks of 100-300 μm depth were analyzed using Imaris software to quantify myoblast infiltration depth and sphericity.

4.2i Statistical analysis

Data are presented as means ± standard deviation. All experiments represent at least three independent experiments unless otherwise noted. Statistical analysis was performed using a one-way or two-way analysis of variance with Bonferroni correction for multiple comparisons in Prism 9 software (GraphPad, San Diego, CA); *p*-values less than 0.05 were considered statistically significant. Significance is denoted by alphabetical letterings; groups with no significance are linked by the same letters, while groups with significance do not share the same letters.

4.3 RESULTS

4.3a Addition of sulfate groups to alginate hydrogels increases retention of growth factors

Alginate was reacted with chlorosulfonic acid (HSO_3Cl), resulting in the substitution of hydroxyl groups with sulfate groups (**Fig. 4.1A**). The success of this reaction was evaluated using ^1H NMR analysis to verify peak shifts. Protons on the 1 and 5 positions on the G block of alginate (G1, G5) and the proton in the 1 position on the M block (M1) were identified and labeled. We observed increased substitution of sulfate groups on the alginate backbone with increasing concentration of HSO_3Cl. All peaks exhibited a shift upfield with increasing sulfate modification, indicative of shielding or increase in electron density (**Fig. 4.1B**). This verifies that increasing the concentration of HSO_3Cl in the reaction results in alginate possessing higher negative charges due to the addition of sulfate groups. Subsequently, three concentrations were explored (0%, 1%, and 2% HSO_3Cl) and identified as non-sulfated, low-sulfated, and high-sulfated alginate, respectively.

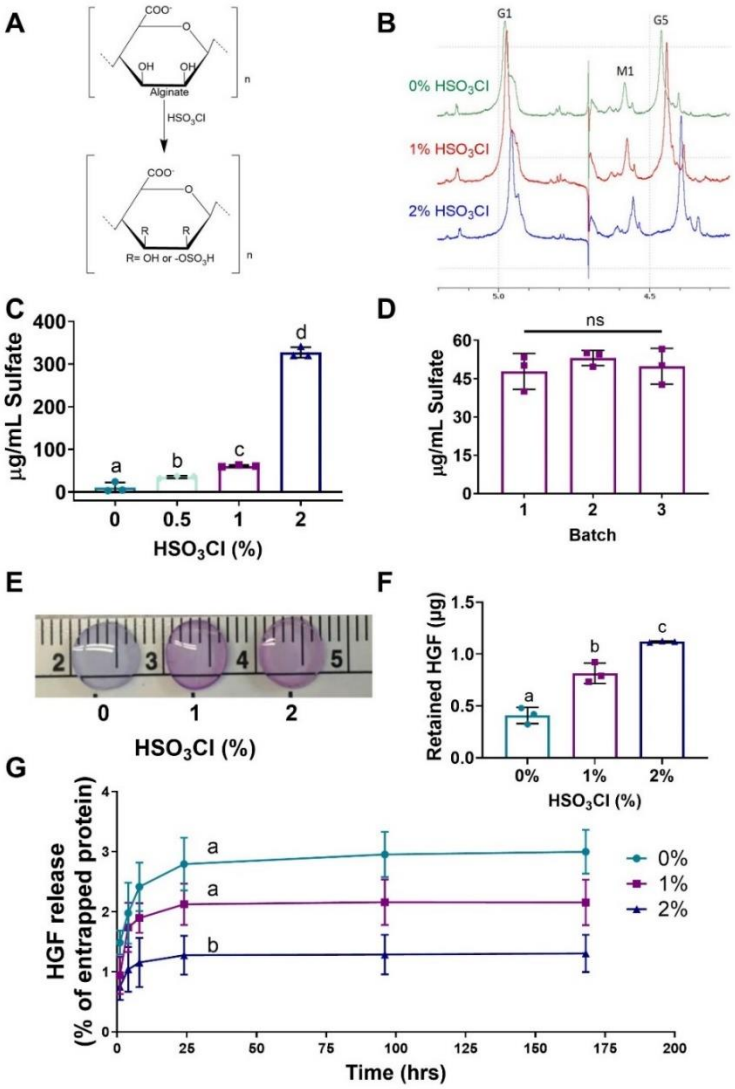

Figure 4.1. Quantification of the amount and functionality of sulfate modified alginate. (A) The reaction of alginate with chlorosulfonic acid yields sulfated alginate. (B) Sulfate modification of alginate was verified by ^{1}H NMR. (C, D) Sulfate modification was quantified at different chlorosulfonic acid concentrations and between different batches *via* DMMB assay. (E) DMMB staining of crosslinked hydrogels exhibited uniform staining throughout the gel. (F) Recombinant HGF was entrapped in sulfated alginate hydrogels and the amount retained after 7 days was quantified. (G) HGF release curves confirm that sulfate groups are functional and retain this heparin binding GF. Data are mean ± SD (n=3-4). Groups with statistically significant differences do not share the same letters; ns denotes no significance among all groups.

Sulfate modification was further confirmed using a DMMB assay, a protocol used to determine the GAG content in physiological samples. In agreement with ^{1}H NMR analysis, increases in the HSO_3Cl correlated with greater sulfate modification of the alginate. Differences among the hydrogels were apparent with as low as 0.5% HSO_3Cl, indicating the efficiency of this reaction (**Fig. 4.1C**). To further validate this sulfate modification method, we evaluated batch-to-batch variation of modification with 1% HSO_3Cl using the DMMB assay. The presence of sulfate was similar among three batches, confirming the reproducibility of this modification method (**Fig. 4.1D**). Crosslinked hydrogels were stained with DMMB to qualitatively observe the spatial distribution of sulfate in a 3D hydrogel. DMMB exhibits a blue color until it is bound to sulfate and turns pink. Gels exhibited relatively homogenous staining, with sulfate-bound pink staining most apparent in the 2% HSO_3Cl gels, 0% HSO_3Cl gels exhibiting minimal blue staining, and 1% HSO_3Cl exhibiting a combination of both blue and pink staining (**Fig. 4.1E**). The sulfate concentration detected on the alginate was also compared to heparin and decellularized ECM via DMMB assay (**Fig. 4.2**). All sulfated alginate groups exhibited lower sulfate modification than heparin but higher sulfate concentrations than decellularized ECM secreted by human MSCs. Collectively, these data demonstrate the efficiency, reproducibility, and tunability of this method to modify alginate with sulfate groups.

Upon verification of sulfate modification of the alginate, we sought to demonstrate that the sulfate groups were functional and could sequester GFs. We loaded all hydrogels with known quantities of HGF and monitored its release over 7 days. Compared to the non-sulfated control, HGF was retained within the sulfated alginate longer, exhibiting slower release curves over 7 days (**Fig. 4.1F,G**). We confirmed the functionality of sulfated alginate to retain GFs by studying the encapsulation and release of a non-heparin binding GF, IGF-1. These curves showed no statistical significance in release, indicating sulfation had no effect on the retention of non-heparin binding GFs (**Fig. 4.3**). These data demonstrate the sulfate-modified alginate can effectively retain

heparin binding growth factors, while non-heparin binding growth factors readily diffuse from the gel into the surrounding environment.

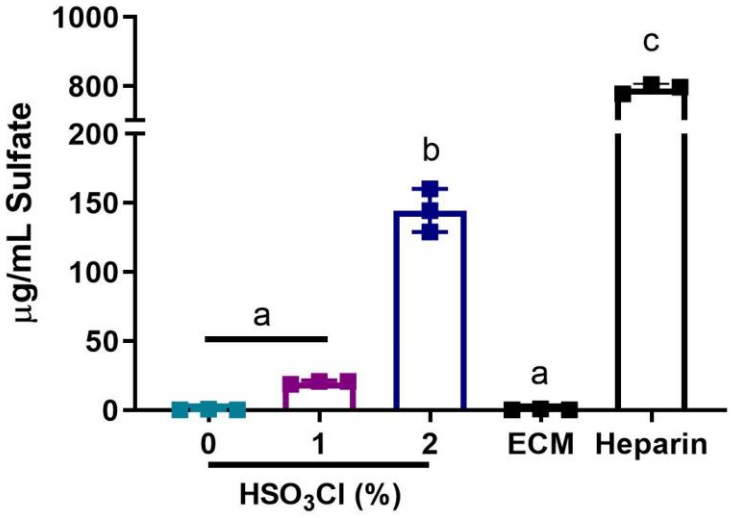

Figure 4.2. Analysis of sulfated alginate compared to heparin and native ECM. Comparison of percentage of sulfate quantification *via* DMMB assay between sulfated alginate, decellularized ECM and heparin. Data are mean ± SD (n=3). Groups with statistically significant differences do not share the same letters; ns denotes no significance among all groups.

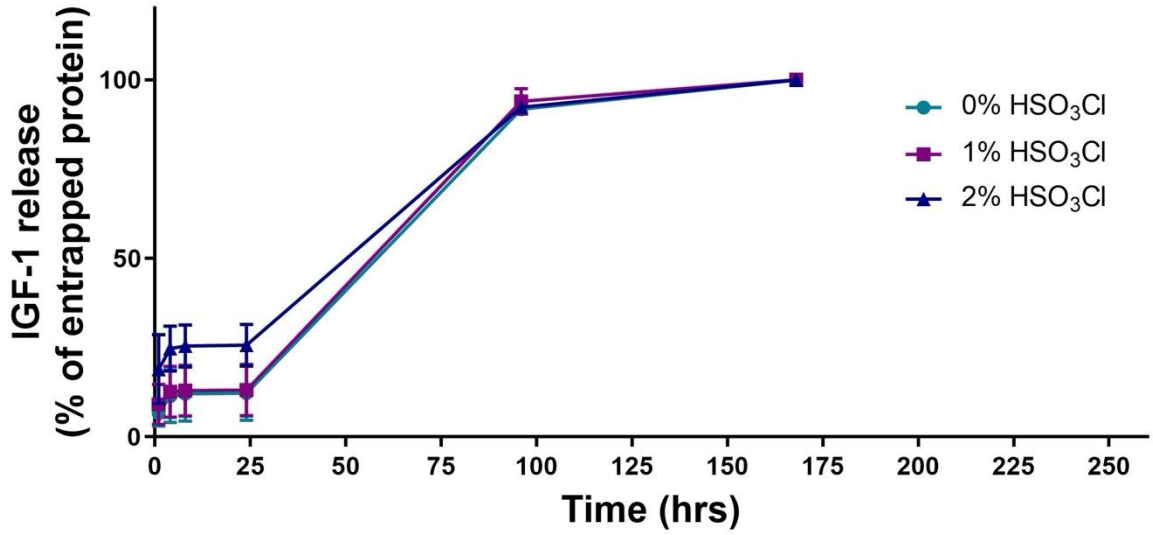

Figure 4.3. IGF-1 release from sulfated hydrogels. Non-heparin binding growth factor IGF-1 released at the same rate for both sulfated and non-sulfated alginate hydrogels. Data are mean ± SD (n=4). Groups with statistically significant differences do not share the same letters; ns denotes no significance among all groups

4.3b Sulfate modification, degradation and initial moduli can be decoupled

Hydrogels were prepared from a mixture of sulfated VLVG, non-sulfated VLVG, and oxidized non-sulfated MVG alginates (**Fig. 4.4A**). 1% oxidized MVG gels were dual-crosslinked using either 6 mM $BaCl_2$ and 200 mM $CaCl_2$ to achieve a high initial modulus, or 3 mM $BaCl_2$ and 100 mM $CaCl_2$ for a low initial modulus (**Table 4.1**). Since sulfate groups can inhibit the formation of ionic crosslinks, $BaCl_2$ was used to strengthen hydrogel formation as it is able to crosslink both guluronic (G) and mannuronic (M) acid blocks in alginate, while $CaCl_2$ primarily crosslinks only G blocks.[32] A higher concentration of $CaCl_2$ was supplemented with $BaCl_2$ to further increase crosslinking since higher concentrations of $BaCl_2$ can be cytotoxic.[33] On day 1, we observed significant differences in initial elastic moduli between the high moduli (14.5 ± 3.2 kPa) and low moduli groups (7.5 ± 2.4 kPa; $p<0.0001$) regardless of the level of sulfation (**Fig. 4.4B**). Next, we

assessed hydrogel degradation by quantifying changes in moduli at day 14 (**Fig. 4.4C-D**) and measuring dry mass over time (**Fig. 4.5**). Both groups exhibited significant reductions in moduli compared to initial elastic modulus by day 14, with the low moduli group decreasing to 1.8 ± 0.9 kPa and the high moduli decreasing to 3.3 ± 0.9 kPa ($p<0.0001$ for both groups). We did not detect differences in modulus as a function of sulfate modification at either time point. These data confirm we can control the degree of sulfate modification on the backbone of alginate without sacrificing the ability to tune initial moduli.

In order to decouple the interplay between sulfate modification and degradation, we incorporated our sulfated alginate into a faster degrading hydrogel composed of 5% oxidized MVG (**Table 4.1**). The initial moduli for these hydrogels were 13.2 ± 3.7 kPa for the high moduli group and 7.1 ± 2.4 kPa for the low moduli group, similar to moduli for the slower degrading 1% oxidized gels. As expected, the moduli of the 5% oxidized high group decreased more by 14 days to 1 ± 0.5 kPa (**Fig. 4.4E-F**). These changes were further confirmed by measuring the dry mass degradation of the high initial moduli group (**Fig. 4.5A,B**). The dry mass decreased significantly for all gels from day 1 to 14 in the low moduli group except those modified with 1% HSO_3Cl (**Figure 4.5B**). To verify that degradation did not significantly influence the availability of sulfate groups, we performed a DMMB assay on gels after 14 days to determine if degrees of sulfate modification could be detected. All formulations exhibited clear differences in sulfate modification between 0% and 2% HSO_3Cl groups, with all except the high moduli 1% oxidation group exhibiting statistical differences between all groups (**Fig. 4.6**). We also measured swelling ratio and mesh size of sulfated hydrogels. Sulfation did not appreciably influence these parameters, confirming that hydrogel physical properties are independent of modification with sulfate groups (**Fig. 4.7**). These data verify that the degree of sulfate modification, degradation rate, and initial modulus can be independently tuned. For the remainder of the study, we used the high moduli, slow degrading hydrogels (1% oxidized MVG crosslinked with 6 mM $BaCl_2$ and 200 mM $CaCl_2$), as they exhibited the best durability for long term *in vitro* culture.

Table 4.1. Composition of the different hydrogel groups.

	Hydrogel component (percent volume in gel)			
Hydrogel Group	*MVG (43.75%)*	*VLVG (43.75%)*	*Sulfated VLVG (12.5%)*	*Crosslinker*
High moduli slow degrading	1% oxidized RGD modified	RGD modified	Sulfate modified	6mM $BaCl_2$ 200mM $CaCl_2$
Low moduli slow degrading	1% oxidized RGD modified	RGD modified	Sulfate modified	3mM $BaCl_2$ 100mM $CaCl_2$
High moduli fast degrading	5% oxidized RGD modified	RGD modified	Sulfate modified	6mM $BaCl_2$ 200mM $CaCl_2$
Low moduli fast degrading	5% oxidized RGD modified	RGD modified	Sulfate modified	3mM $BaCl_2$ 100mM $CaCl_2$

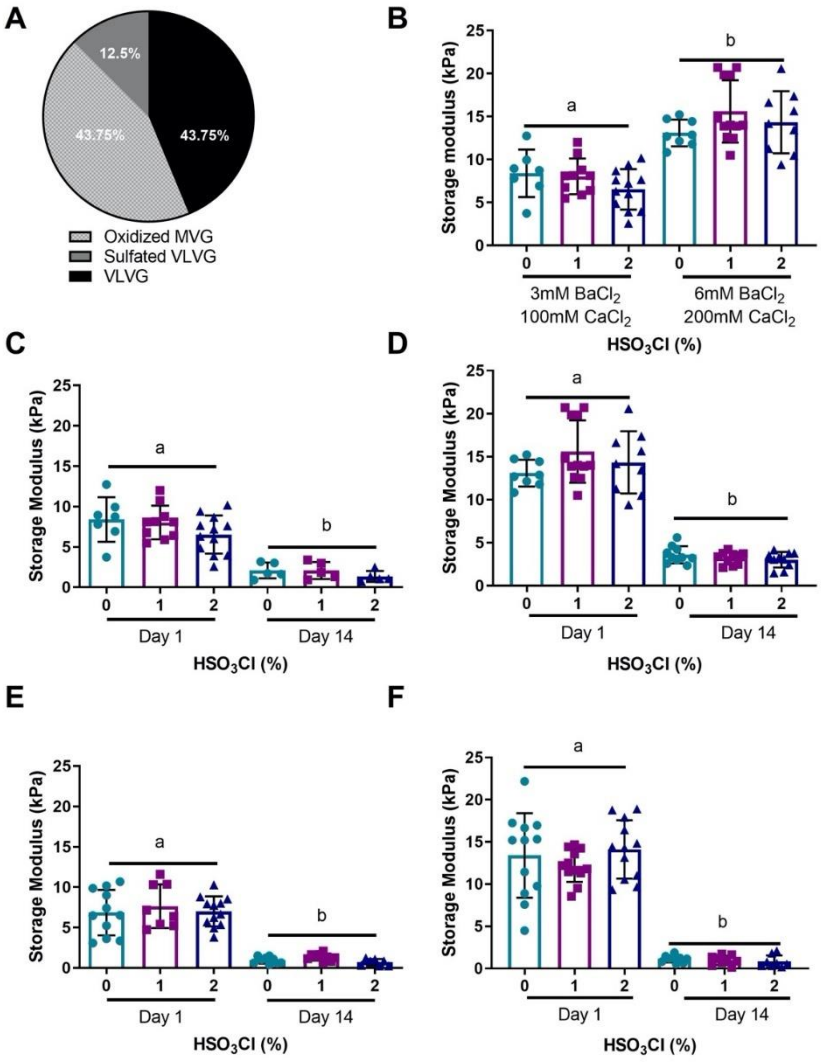

Figure 4.4. Hydrogel formulation and modulation of mechanical and degradation properties. (a) Composition of sulfated alginate hydrogels. (b) Initial moduli of sulfated alginate can be regulated by varying the concentration of ionic crosslinkers. A 3mM $BaCl_2$ and 100mM $CaCl_2$ concentration produced a hydrogel with low initial moduli, and 6mM $BaCl_2$ and 200mM $CaCl_2$ produced a high initial modulus. The moduli for 1% oxidized (c) low initial moduli, and (d) high initial moduli decreases over time at a similar rate. Increasing the oxidation percentage of the MVG alginate from 1% to 5% increases the degradation rate for both (e) low and (f) high initial moduli groups without affecting initial moduli. Data are mean ± SD (n=7-12). Groups with statistically significant differences do not share the same letters.

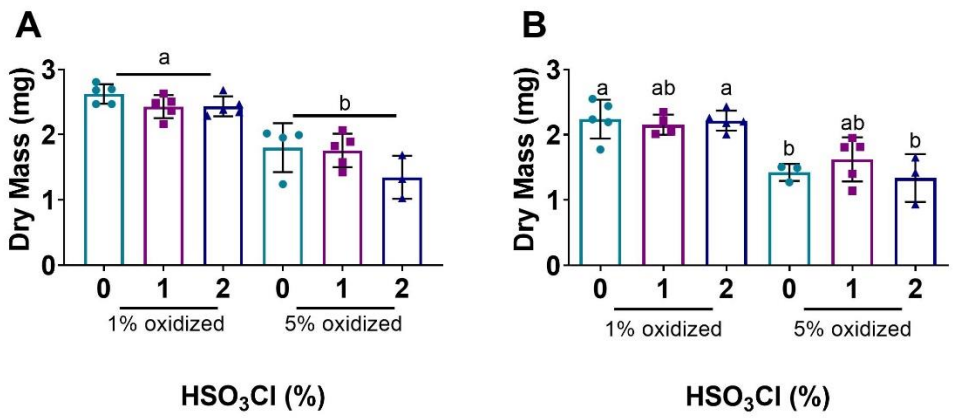

Figure 4.5. Dry mass degradation of 1% vs 5% oxidized alginate. Dry mass of the (a) high initial moduli group and (b) low initial moduli group at day 14 between 1% and 5% oxidized groups. Data are mean ± SD (n=3-5). Groups with statistically significant differences do not share the same letters.

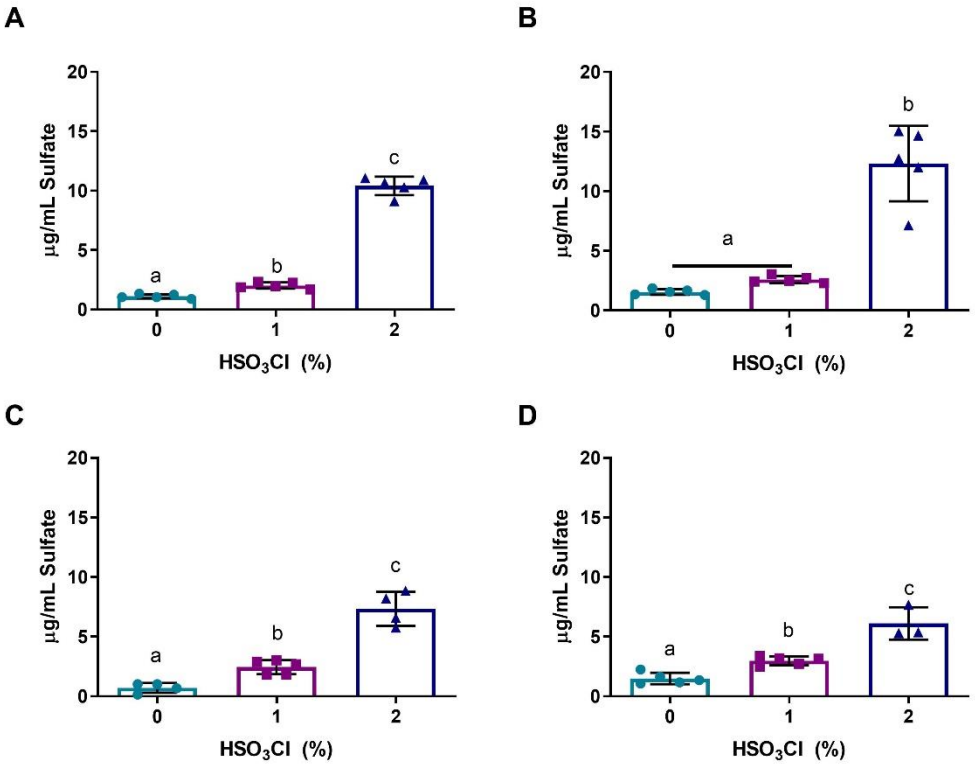

Figure 4.6. Detection of sulfate groups *via* DMMB assay on day 14 gels. DMMB data from (a) Low moduli 1% oxidized, (b) high moduli 1% oxidized (c) low moduli 5% oxidized and (d) high moduli 5% oxidized day 14 gels. Data are mean ± SD (n=3-5). Groups with statistically significant differences do not share the same letters.

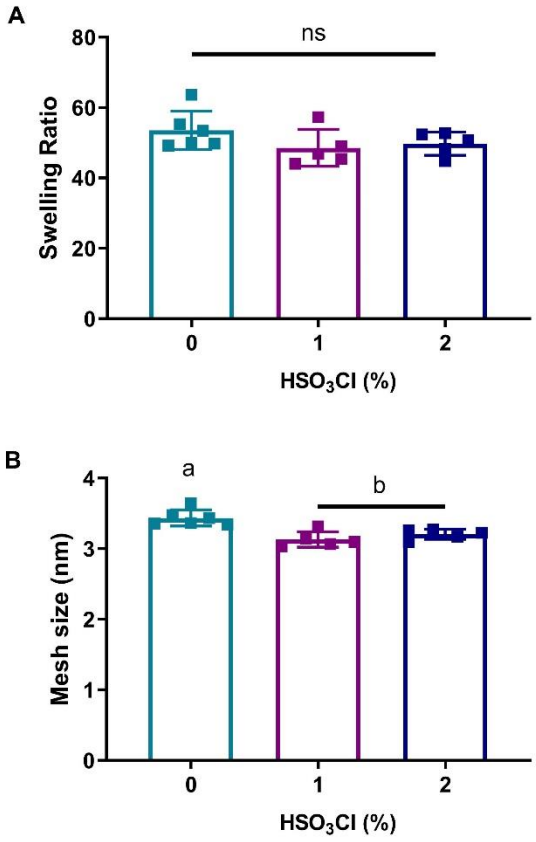

Figure 4.7. Analysis of sulfated alginate swelling ratio and mesh size. (a) Swelling ratio and (b) mesh size was quantified for alginate hydrogels crosslinked with 200mM $CaCl_2$ and 6mM $BaCl_2$ after 24 hrs of formation. Data are mean ± SD (n=5-6). Groups with statistically significant differences do not share the same letters.

4.3c MSC spheroids entrapped in sulfated alginate are viable and secreted GFs are retained

To verify that our dual ionic crosslinking method did not adversely affect cell viability, we entrapped human MSC spheroids within our hydrogels and evaluated viability after 8 and 21 days (**Fig. 4.8A**). At both time points, we observed high viability of the MSC spheroids and no observable differences between sulfated and non-sulfated groups when stained with LIVE/DEAD stain, indicating that neither the exposed sulfate groups nor ionic crosslinking method were

detrimental toward cell viability (**Fig. 4.8B**). We detected comparable metabolic activity *via* alamarBlue between groups at day 21 (**Fig. 4.8C**).

We then sought to determine if sulfated alginate could retain cell-secreted GFs. After 24 hours, the retained MSC-secreted VEGF in all gels was equivalent. However, the amount of VEGF retained in the 1% and 2% gels increased significantly from day 1 to day 4, whereas the 0% group exhibited no change in VEGF retention (**Fig. 4.8D**). These data confirm the functionality of sulfated hydrogels to sequester both recombinant GFs as well as endogenous, cell-secreted VEGF at higher levels than non-sulfated hydrogels. We examined the diversity of GF and cytokines within sulfated gels to assess the efficiency of MSC secretome retention. A variety of factors were retained at higher levels in sulfated alginate compared to unmodified gels. The greatest cytokine signals were derived from IL-8, IL-6, and VEGF, with sulfated gels exhibiting significantly higher levels of VEGF compared to their non-sulfated counterparts (**Fig. 4.8E**). Cytokines detected at lower concentrations exhibited similar trends, with heparin binding factors such as interferon gamma (IFN-γ) displaying significantly increased concentrations in sulfated gels. However, non-heparin binding GFs such as epidermal growth factor (EGF) exhibited no increase in retention (**Fig. 4.8F**). These data indicate that sulfated alginate hydrogels can retain an array of cytokines secreted my MSC spheroids.

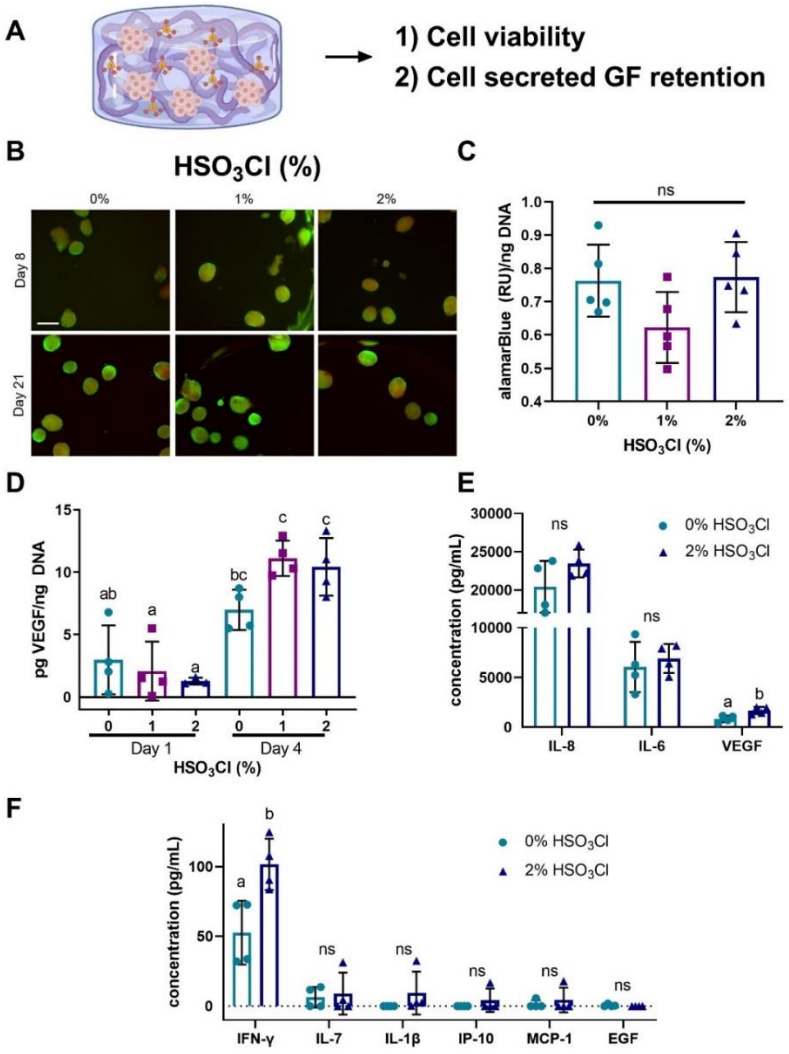

Figure 4.8. Spheroid-produced GFs are retained within sulfated alginate hydrogels. (a) MSC spheroids were entrapped in sulfated alginate hydrogels. (b) No apparent differences were observed in cell viability by LIVE/DEAD stain of MSC spheroids entrapped in sulfated and non-sulfated alginate on day 8 (scale bar = 500μm). (c) Metabolic activity is comparable for MSC spheroids entrapped in sulfated and non-sulfated alginate on day 8. (d) MSC-secreted VEGF is retained in sulfated alginate hydrogels on days 1 and 4. (e-f) Retained MSC spheroid cytokines in sulfated and non-sulfated hydrogels. Data are mean ± SD (n=4-5). Groups with statistically significant differences do not share the same letters; ns denotes no significance among all groups.

4.3d MSC spheroid-secreted GFs are effectively retained in sulfated hydrogels

We indirectly assessed the bioactivity of sequestered factors within sulfated alginate gels by collecting conditioned media from loaded sulfated alginate hydrogels with entrapped MSC spheroids at 4 and 21 days. We stimulated HDMECs seeded on Matrigel with this media, and tubule formation was quantified after 6 hours (**Fig. 4.9A**). We hypothesized that sulfated alginate hydrogels would sequester more GFs, resulting in fewer GFs in the conditioned media and thus inferior tubule formation. Tubule formation was most visibly affected when stimulated by 21-day conditioned media. Tubule formation was greatest using conditioned media from unmodified alginate, followed by 1% sulfated gels and virtually no tubule formation was observed using media from 2% sulfated hydrogels (**Fig. 4.9B**). Day 4 conditioned media elicited no statistical differences in tubule length among conditioned media from the different gels, though HDMECs stimulated by media from the 2% sulfated gels trended lower. The day 21 conditioned media showed clearer results, with statistically greater tubule length for the unmodified gels compared to 2% sulfated alginate (**Fig. 4.9C**). Tubule branch number exhibited similar trends to the tubule length data, although no significant differences were observed among alginates (**Fig. 4.9D**). These data indicate that GFs are retained for longer durations in more sulfated alginate gels, while non- or lower-sulfated hydrogels elute factors that enhance HDMEC tubule formation.

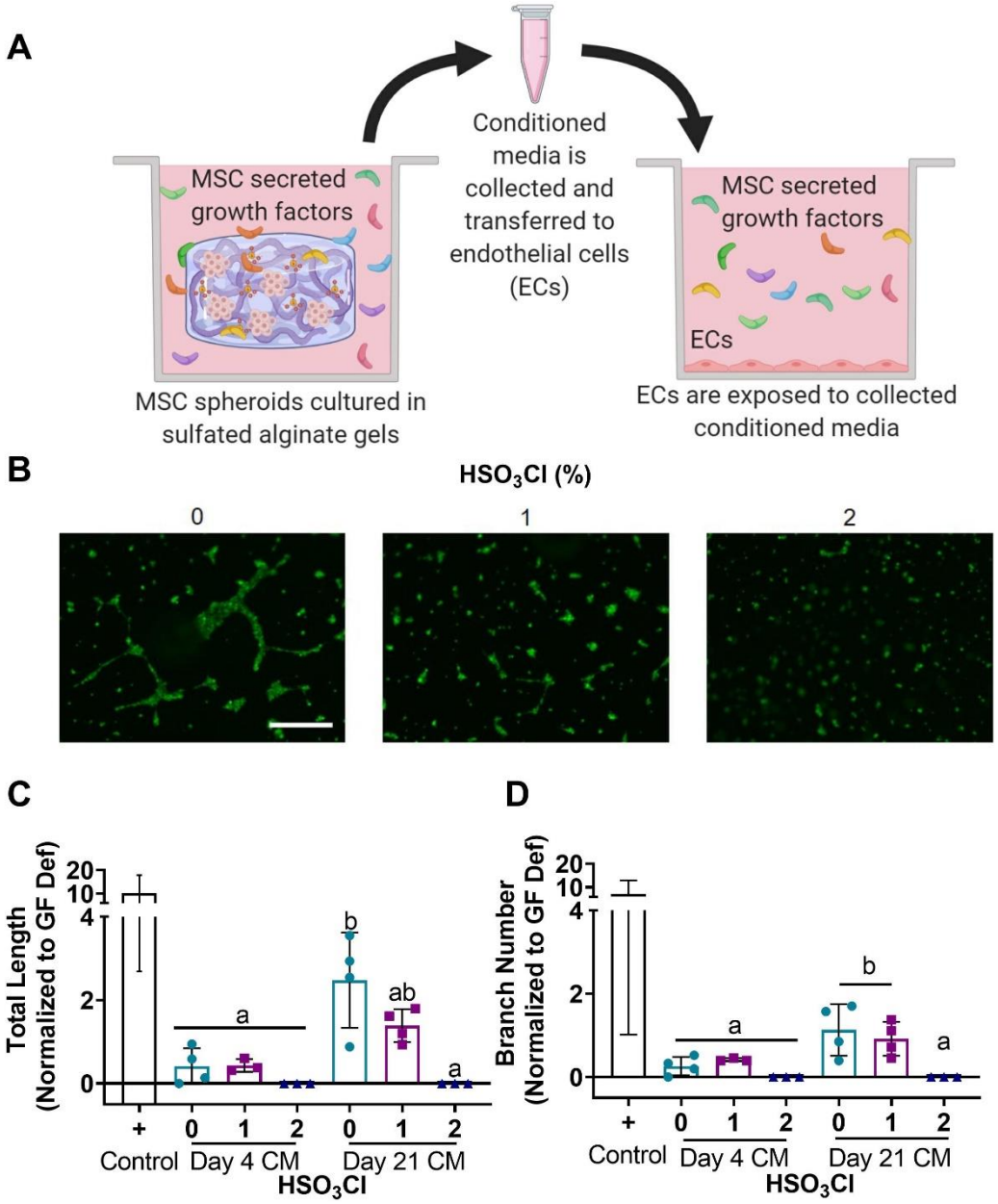

Figure 4.9. GFs eluting from sulfated alginate are functional and stimulate tubule formation. (a) Conditioned media was collected from sulfated hydrogels loaded with MSC spheroids and pipetted on HDMECs to establish the retention of function GFs indirectly by determining tubule formation. (b) Calcein AM stain of HDMECs exposed to day 21 conditioned media (scale bar = 500 μm). Quantification of (c) total tubule length and (d) branch number from HDMEC images confirm that more GFs are eluted from non- and low-sulfated alginate hydrogels. Data are mean ± SD (n=3-4). Groups with statistically significant differences do not share the same letters; ns denotes no significance among all groups.

4.3e MSC spheroids entrapped in sulfated alginate stimulate myoblast infiltration

Having established differences in the bioactivity of secreted GFs from sulfated hydrogels, we investigated the bioactivity of GFs retained within the hydrogel. We cultured MSC spheroids for 4 days to enable accumulation of the MSC spheroid secretome within the sulfated hydrogels. We then assessed the invasion of tdTomato-expressing human myoblasts into the gels over 8 days *via* confocal microscopy. Confocal z-stack images confirmed greater numbers of myoblasts within 2% sulfated hydrogels that also exhibited a more elongated morphology. In contrast, myoblasts in unmodified and 1% hydrogels were sparse, rounded, and often remained at the periphery of the hydrogel (**Fig. 4.10B**). Image quantification of myoblast invasion confirmed these visual observations, with 2% sulfated hydrogels resulting in significantly higher fluorescence, corresponding to higher myoblast infiltration, compared to other groups (**Fig. 4.10C**). We determined significant increases in the depth of myoblast invasion as a function of sulfate modification (**Fig. 4.10D**). Myoblasts that invaded the 2% sulfated alginate gels exhibited significantly lower sphericity compared to lower sulfated and non-sulfated groups, in agreement with representative images of increased spreading and elongation in 2% gels (**Fig. 4.10E**), suggestive of the migratory activities of these cells.

To further verify that the effect of infiltration was due to GFs sequestered by the sulfated alginate and not the MSC spheroids themselves, we repeated the experiment by killing the MSC spheroids *via* flash freezing after 4 days in culture. Hydrogels were thawed, and myoblasts were introduced in the same manner as the previous experiment (**Fig. 4.10F**). After 8 days, we observed similar infiltration in gels containing dead MSC spheroids, with myoblast infiltration and elongation corresponding to the degree of sulfate modification (**Fig. 4.10G**). Quantification of these images indicated increased myoblast infiltration in higher sulfated hydrogels, with trends mirroring those studies using viable MSC spheroids (**Fig. 4.10H**). Z-position and sphericity were in agreement with data using live cells, evidenced by significant increases in infiltration depth and myoblast elongation within 2% sulfated hydrogels (**Fig. 4.10I-J**). We performed a control

experiment using acellular sulfated hydrogels to investigate if myoblast infiltration was influenced by the sulfate groups themselves in the absence of MSC spheroids (**Fig. 4.11**). These data indicated sulfation alone induced myoblast infiltration, although not to the same degree. Additionally, penetration depth of the myoblasts increased when spheroids were absent. Thus, sulfate groups may sequester cytokines from neighboring that induced myoblast migration. These data support the hypothesis that sulfated alginate sequesters endogenous, cell-secreted GFs, and these bound GFs retain their bioactivity.

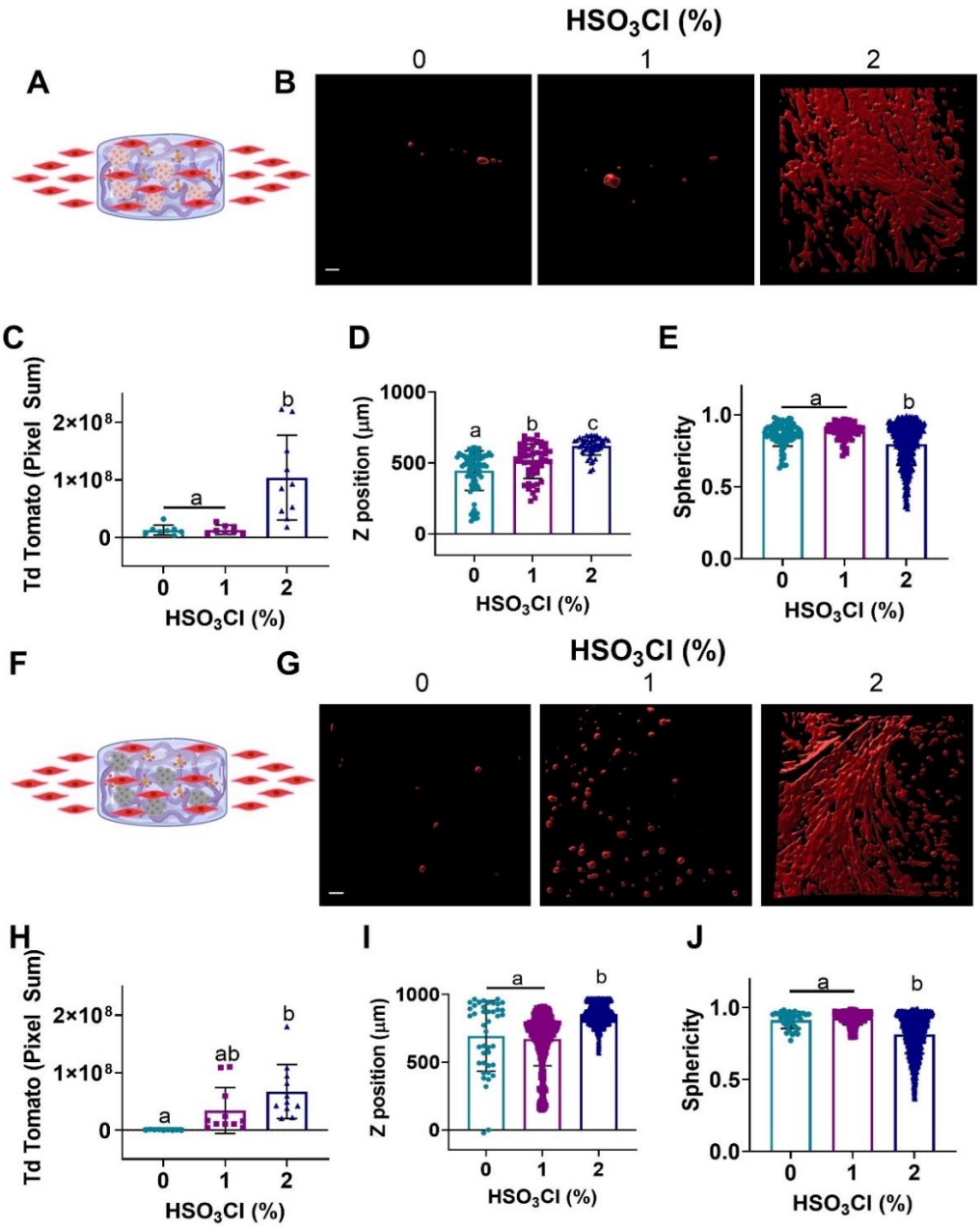
A
B
HSO3Cl (%)
0
1
2
C
Td Tomato (Pixel Sum)
2×10^8
1×10^8
0
a
b
HSO3Cl (%)
D
Z position (µm)
1000
500
0
a
b
c
HSO3Cl (%)
E
Sphericity
1.0
0.5
0.0
a
b
HSO3Cl (%)
F
G
HSO3Cl (%)
H
Td Tomato (Pixel Sum)
2×10^8
1×10^8
0
a
ab
b
HSO3Cl (%)
I
Z position (µm)
1000
500
0
a
b
HSO3Cl (%)
J
Sphericity
1.0
0.5
0.0
a
b
HSO3Cl (%)

Figure 4.10. MSC spheroids entrapped in sulfate-modified alginate hydrogels enhance myoblast infiltration. (a) MSC spheroids were entrapped and cultured in alginate hydrogels for 4 days, then td expressing myoblasts were introduced to the media and cultured for an additional 8 days. (b) Representative z stack images of Td myoblast within MSC spheroid gels on day 8 (scale bar=100 μm). (c) Pixel sum of td tomato fluorescence, (d) depth of penetration and (e) sphericity of the infiltrating myoblasts were quantified from the z stacks, confirming greater myoblast invasion and elongation in 2% sulfated gels. (f-j) The experiment was repeated with spheroids that were killed after 4 days of culture to confirm that GF retention induced myoblast infiltration. Data are mean ± SD (n=9-1145). Groups with statistically significant differences do not share the same letters; ns denotes no significance among all groups.

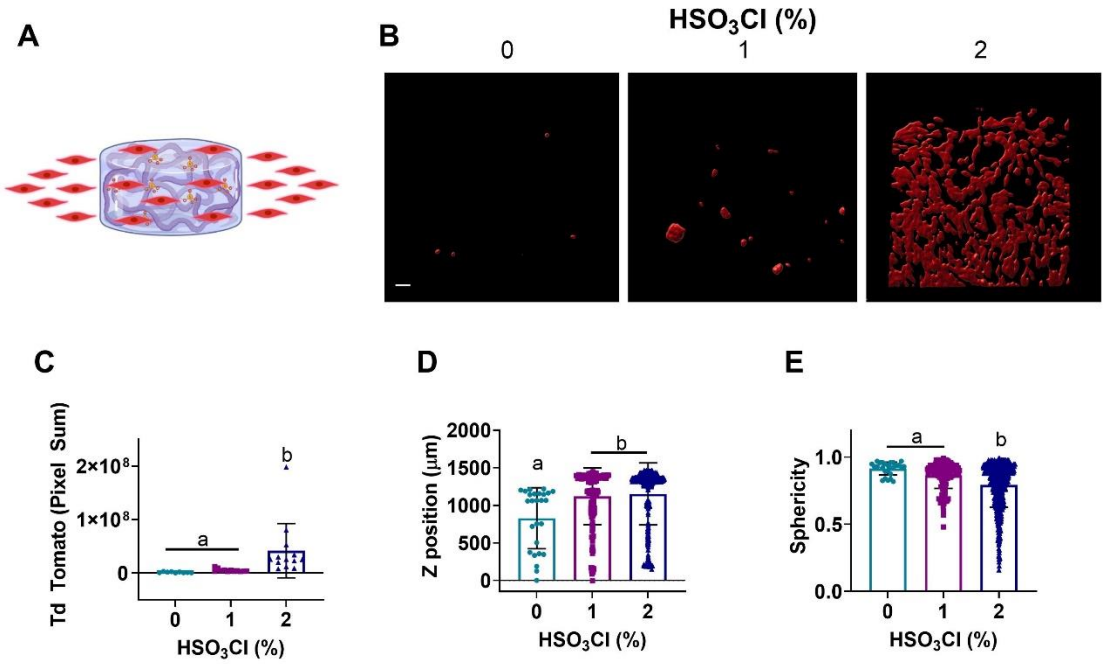

Figure 4.11. Myoblast invasion of acellular sulfated hydrogels. (a) Td expressing myoblasts were cultured on acellular sulfated hydrogels for 8 days. (b) Representative z stack images of Td myoblast within MSC spheroid gels on day 8 (scale bar=100 µm) demonstrate greater myoblast invasion in sulfated alginate, which is a function of sulfate concentration. (c) The pixel sum of td tomato fluorescence, (d) depth of penetration, and (e) sphericity of the infiltrating myoblasts was quantified from the z stacks. Data are mean ± SD (n=9-693). Groups with statistically significant differences do not share the same letters; ns denotes no significance among all groups.

4.4 DISCUSSION

Poor cell viability upon transplantation remains a critical challenge for the success of cell-based approaches to tissue repair and regeneration. MSCs are widely acknowledged to support tissue repair upon implantation through their potent secretome, yet the utility of MSCs persists only while cells remain viable. We developed a biomaterial platform that supports the viability of entrapped MSC spheroids while sequestering a variety of endogenous secreted GFs for prolonged presentation. To our knowledge, this is the first study to explore utilizing GF

sequestering moieties to retain and prolong the therapeutic benefit of the MSC spheroid secretome. We designed a unique crosslinking method that facilitates the tunable regulation of initial elastic moduli, degradation, and degree of sulfate modification within alginate hydrogels. Our results demonstrate that increasing the sulfate modification of alginate increases the retention of MSC spheroid-secreted GFs. Importantly, sulfated hydrogels enhanced myoblast infiltration even when MSC spheroids were no longer viable. These findings highlight how our platform could aid in solving challenges related to rapid cell death upon transplantation in cellular therapies.

The addition of GF sequestering moieties to biomaterials has been reported by several groups.[34, 35] Heparin is a well-characterized anticoagulant that has been thoroughly investigated in the biomedical field as a GF delivery agent. Foundational studies of heparin immobilization were initially motivated by increasing blood compatibility on the surface of biomaterials. These methods leveraged both the localized, sustained release of heparin[36] and direct covalent binding to the material surface[37, 38], though the latter was more advantageous for long-term results. These studies ultimately led to the successful design of adhesion methods for bioactive heparin that have been implemented commercially in polytetrafluoroethylene (PTFE) vascular grafts.[39]

Heparin has been used for GF delivery due to its ability to bind bioactive factors strongly and reversibly. Heparin has been incorporated into various hydrogel polymers, including polyethylene glycol (PEG)[40, 41], fibrin[42], poly(lactic-co-glycolic) acid (PLGA)[43] and alginate[44, 45] for effective delivery of a variety of therapeutic GFs for tissue engineering applications. Notably, heparin was co-polymerized with PEG to form hydrogels that delivered basic fibroblast growth factor (bFGF) to MSCs for up to five weeks, resulting in increased cellular proliferation, adhesion, and osteogenic differentiation.[46] Although heparin incorporation is an effective method for GF sequestration, alternative approaches have been evaluated to avoid the complexity, cost, and antithrombotic effects of using the full heparin molecule. For example, the modification of alginate macromer with sulfate groups derived from sulfonic acid treatment capitalizes on the polymer's

high degree of material tunability.[17, 24, 47] Like heparin, sulfated alginate can be used for controlled GF delivery. The formulation has been successfully used to sequester and release BMP-2[48] and FGF-2[49], resulting in increased cell differentiation and response compared to GFs released from unmodified alginate.

GF delivery alone is often insufficient for tissue regeneration due to unintended side effects when using GFs at supraphysiological concentrations, prohibitive cost of these GFs, and poor replication of endogenous signaling that occurs with a multitude of GFs presented to neighboring cells. MSCs produce a complex secretome composed of multiple GFs at lower concentrations than routinely used for therapeutic applications. Although the incorporation of sulfate groups onto polymers such as alginate has been reported, previous studies have focused on delivering a single recombinant GF, while neglecting to capitalize on the complex and physiologically tuned MSC secretome. The true innovation of our work is in sequestering a diverse array of factors secreted by MSC spheroids, as opposed to pre-loading individual recombinant GFs for delivery.

To investigate this aspect further, we characterized MSC spheroid-secreted factors retained in sulfated and non-sulfated hydrogels. We found increased retention of an array of heparin binding cytokines in sulfated hydrogels, verifying that this platform is capable of retaining several therapeutic cytokines. These included extremely high levels of heparin binding cytokines IL-8, IL-6 and VEGF, in agreement with other reports describing the composition of the MSC spheroid secretome.[50, 51] We also detected increased retention of INF-γ in sulfated hydrogels, corresponding with previous work indicating that INF-γ has high heparin affinity.[52] This is especially promising considering INF-γ sequestered by heparin and collagen has enhanced ability to increase MSC cytokine secretion and integrin binding.[53] Identification of these cytokines indicates MSC spheroid loaded sulfated alginate has high therapeutic potential, which we further evaluated through a series of *in vitro* studies.

Upon accumulation of endogenous factors of the MSC secretome, we observed increased adherence, spreading and migration of myoblasts into sulfated alginate compared to unmodified

hydrogels. It is important to note that the sulfate-modified alginate is likely retaining MSC spheroid-secreted GFs as well as myokines that may further contribute to myoblast infiltration. Indeed, we observed myoblast infiltration from the acellular sulfated hydrogel control groups, indicating myokine and serum GF retention is likely contributing to our results. These results are in agreement with previous observations of the bioactivity of sequestered GF within hydrogels.[46] A possible limitation to this platform is that the sulfated alginate will retain proinflammatory cytokines produced by the injured tissue when implanted in a wound site. Future studies are required to evaluate the efficacy of sulfated alginate *in vivo* and determine if preloading hydrogels with MSC secretome is necessary so endogenous GFs produced by the tissue do not dominate the hydrogel.

When formed into spheroids, MSCs exhibit enhanced viability, differentiation and increased secretion of immunomodulatory and reparative GFs compared to monodisperse MSCs. [51, 54-56] The MSC secretome can also be influenced by the biophysical properties of the surrounding ECM. Fibrin hydrogels were designed to increase the concentration of VEGF or PGE_2 within the MSC spheroid secretome [21], and degree of alginate RGD modification influences MSC spheroid migration, GF secretion and differentiation.[26] These findings highlight the importance of the mechanical and chemical tunability of sulfated alginate, as these properties can be leveraged to manipulate secretome and cell function for different applications which can be further amplified through GF sequestration.

We used a dual ionic crosslinking technique to independently modulate the physical and chemical properties of sulfated alginate hydrogels. Few studies have directly measured and established this tunability using an ionically crosslinked sulfated alginate hydrogel, likely because the negatively charged sulfate groups can interfere with ionic crosslinking, influencing hydrogel degradation and moduli. By crosslinking with both $CaCl_2$ and $BaCl_2$, we produced a divalent cation combination strong enough to overcome these issues. $CaCl_2$ and $BaCl_2$ have been successfully utilized for bio-printing applications of alginate[57], although not with this reported simultaneous

crosslinking technique. One possible limitation of using $BaCl_2$ as a crosslinker is that it can injury myofibers, and injection of the chemical has been well established as a muscle injury model.[58] Our crosslinker concentration is well below that of the concentration used for muscle injury, however we have not yet tested our hydrogel on *in vivo* tissue to verify the $BaCl_2$ will not exhibit any adverse effects. Using this method, we demonstrated that sulfate modification can be modulated independently of initial elastic moduli and degradation. Although not explicitly explored in this paper, modification with different adhesion sites and densities could further be pursued as another independent factor, as adhesion peptide degree of substitution does not influence alginate mechanical properties.[26, 59]

These studies establish an exciting platform of study, facilitating the independent regulation of mechanical properties, adhesive moiety type and concentration, and sulfate modification within alginate hydrogels using simple and well-established chemical modifications. This platform can be further used to interrogate the effect of higher sulfate modification levels, as previous studies indicate sulfate concentration on the alginate backbone increases using up to 3.5% HSO_3Cl.[60] Sulfated alginate also exhibits promising translational potential, as alginate is FDA approved for wound healing and as a food additive. The sulfated alginate described herein requires significantly lower concentrations of sulfate than that contained in heparin (**Fig. 4.2**) while still inducing significant biological differences. This is advantageous, as heparin levels that exceed the effective threshold for VEGF delivery correlated with reductions in network formation by endothelial cells.[61] These data emphasize the importance of striking a balance between sequestration and delivery of GF.

4.5 CONCLUSION

We established and characterized a sulfated alginate hydrogel platform with independent tunability of sulfate modification, initial elastic moduli, and degradation rate. We determined that sulfated alginate could bind both recombinant and cell-secreted GFs. Sulfated alginate

sequestered a multitude of bioactive GFs from the secretome of entrapped MSC spheroids. These studies indicate that sulfate groups aid in retaining and increasing the therapeutic effect of the MSC spheroid secretome within the hydrogel, potentially prolonging the therapeutic effect of cells transplanted for their secretome.

4.6 REFERENCES

[1] X. Wang, N. Rivera-Bolanos, B. Jiang, G.A. Ameer, Advanced functional biomaterials for stem cell delivery in regenerative engineering and medicine, Adv Funct Mater 29(23) (2019) 1809009.

[2] A.I. Caplan, Adult mesenchymal stem cells for tissue engineering versus regenerative medicine, J Cell Physiol 213(2) (2007) 341-7.

[3] M.E. Wechsler, V.V. Rao, A.N. Borelli, K.S. Anseth, Engineering the MSC secretome: a hydrogel focused approach, Adv Healthc Mater 10(7) (2021) 2001948.

[4] E. Eggenhofer, V. Benseler, A. Kroemer, F.C. Popp, E.K. Geissler, H.J. Schlitt, C.C. Baan, M.H. Dahlke, M.J. Hoogduijn, Mesenchymal stem cells are short-lived and do not migrate beyond the lungs after intravenous infusion, Front Immunol 3(26) (2012) 297.

[5] E. Potier, E. Ferreira, A. Meunier, L. Sedel, D. Logeart-Avramoglou, H. Petite, Prolonged hypoxia concomitant with serum deprivation induces massive human mesenchymal stem cell death, Tissue Eng 13(6) (2007) 1325-1331.

[6] M.T. Lam, A. Nauta, N.P. Meyer, J.C. Wu, M.T. Longaker, Effective delivery of stem cells using an extracellular matrix patch results in increased cell survival and proliferation and reduced scarring in skin wound healing, Tissue Eng Part A 19(5-6) (2013) 738-47.

[7] T.J. Bartosh, J.H. Ylöstalo, A. Mohammadipoor, N. Bazhanov, K. Coble, K. Claypool, R.H. Lee, H. Choi, D.J. Prockop, Aggregation of human mesenchymal stromal cells (MSCs) into 3D spheroids enhances their antiinflammatory properties, Proc Natl Acad Sci U S A 107(31) (2010) 13724-9.

[8] K.C. Murphy, S.Y. Fang, J.K. Leach, Human mesenchymal stem cell spheroids in fibrin hydrogels exhibit improved cell survival and potential for bone healing, Cell Tissue Res 357(1) (2014) 91-9.

[9] S.S. Ho, B.P. Hung, N. Heyrani, M.A. Lee, J.K. Leach, Hypoxic preconditioning of mesenchymal stem cells with subsequent spheroid formation accelerates repair of segmental bone defects, Stem Cells 36(9) (2018) 1393-1403.

[10] A. Abdeen, J. Weiss, J. Lee, K. Kilian, Matrix composition and mechanics direct proangiogenic signaling from mesenchymal stem cells, Tissue Eng Part A 20(19-20) (2014).

[11] T.N. Lamichhane, S. Sokic, J.S. Schardt, R.S. Raiker, J.W. Lin, S.M. Jay, Emerging roles for extracellular vesicles in tissue engineering and regenerative medicine, Tissue Eng Part B Rev 21(1) (2015) 45-54.

[12] T. Gotterbarm, W. Richter, M. Jung, S. Berardi Vilei, P. Mainil-Varlet, T. Yamashita, S.J. Breusch, An in vivo study of a growth-factor enhanced, cell free, two-layered collagen-tricalcium phosphate in deep osteochondral defects, Biomaterials 27(18) (2006) 3387-95.

[13] A.K. Silva, C. Richard, M. Bessodes, D. Scherman, O.W. Merten, Growth factor delivery approaches in hydrogels, Biomacromolecules 10(1) (2009) 9-18.

[14] J.M. Mejia Oneto, M. Gupta, J.K. Leach, M. Lee, J.L. Sutcliffe, Implantable biomaterial based on click chemistry for targeting small molecules, Acta Biomater 10(12) (2014) 5099-5105.

[15] Y. Brudno, M.J. Pezone, T.K. Snyder, O. Uzun, C.T. Moody, M. Aizenberg, D.J. Mooney, Replenishable drug depot to combat post-resection cancer recurrence, Biomaterials 178 (2018) 373-382.

[16] A.M. Bratt-Leal, A.H. Nguyen, K.A. Hammersmith, A. Singh, T.C. McDevitt, A microparticle approach to morphogen delivery within pluripotent stem cell aggregates, Biomaterials 34(30) (2013) 7227-35.

[17] I. Freeman, A. Kedem, S. Cohen, The effect of sulfation of alginate hydrogels on the specific binding and controlled release of heparin-binding proteins, Biomaterials 29(22) (2008) 3260-8.

[18] D.S. Benoit, A.R. Durney, K.S. Anseth, The effect of heparin-functionalized PEG hydrogels on three-dimensional human mesenchymal stem cell osteogenic differentiation, Biomaterials 28(1) (2007) 66-77.

[19] E. Ruvinov, J. Leor, S. Cohen, The effects of controlled HGF delivery from an affinity-binding alginate biomaterial on angiogenesis and blood perfusion in a hindlimb ischemia model, Biomaterials 31(16) (2010) 4573-82.

[20] E. Ruvinov, J. Leor, S. Cohen, The promotion of myocardial repair by the sequential delivery of IGF-1 and HGF from an injectable alginate biomaterial in a model of acute myocardial infarction, Biomaterials 32(2) (2011).

[21] K.C. Murphy, J. Whitehead, D. Zhou, S.S. Ho, J.K. Leach, Engineering fibrin hydrogels to promote the wound healing potential of mesenchymal stem cell spheroids, Acta Biomater 64 (2017) 176-186.

[22] J. Whitehead, K.H. Griffin, M. Gionet-Gonzales, C.E. Vorwald, S.E. Cinque, J.K. Leach, Hydrogel mechanics are a key driver of bone formation by mesenchymal stromal cell spheroids, Biomaterials 269 (2021) 120607.

[23] J.K. Leach, J. Whitehead, Materials-directed differentiation of mesenchymal stem cells for tissue engineering and regeneration, ACS Biomater Sci Eng 4(4) (2017) 1115-1127.

[24] Ø. Arlov, G. Skjåk-Bræk, A.M. Rokstad, Sulfated alginate microspheres associate with factor H and dampen the inflammatory cytokine response, Acta Biomater 42 (2016) 180-188.

[25] K.H. Bouhadir, K.Y. Lee, E. Alsberg, K.L. Damm, K.W. Anderson, D.J. Mooney, Degradation of partially oxidized alginate and its potential application for tissue engineering, Biotechnol Prog 17(5) (2001) 945-50.

[26] S.S. Ho, A.T. Keown, B. Addison, J.K. Leach, Cell migration and bone formation from mesenchymal stem cell spheroids in alginate hydrogels are regulated by adhesive ligand density, Biomacromolecules 18(12) (2017) 4331-4340.

[27] C. Zheng, M.E. Levenston, Fact versus artifact: avoiding erroneous estimates of sulfated glycosaminoglycan content using the dimethylmethylene blue colorimetric assay for tissue-engineered constructs, Eur Cell Mater 29 (2015) 224-36.

[28] J.N. Harvestine, T. Gonzalez-Fernandez, A. Sebastian, N.R. Hum, D.C. Genetos, G.G. Loots, J.K. Leach, Osteogenic preconditioning in perfusion bioreactors improves vascularization and bone formation by human bone marrow aspirates, Sci Adv 6(7) (2020) 2387.

[29] M. Thorley, S. Duguez, E.M.C. Mazza, S. Valsoni, A. Bigot, K. Mamchaoui, B. Harmon, T. Voit, V. Mouly, W. Duddy, Skeletal muscle characteristics are preserved in hTERT/cdk4 human myogenic cell lines, Skelet Muscle 6(1) (2016) 1-12.

[30] J. Whitehead, A. Kothambawala, J.K. Leach, Morphogen delivery by osteoconductive nanoparticles instructs stromal cell spheroid phenotype, Adv Biosyst 3(12) (2019) 1900141.

[31] C.E. Vorwald, K.C. Murphy, J.K. Leach, Restoring vasculogenic potential of endothelial cells from diabetic patients through spheroid formation, Cell Mol Bioeng 11(4) (2018) 267-278.

[32] Ý.A. Mørch, I. Donati, B.L. Strand, G. Skjåk-Bræk, Effect of Ca2+, Ba2+, and Sr2+ on alginate microbeads, Biomacromolecules 7(5) (2006) 1471-1480.

[33] D. Dietz, M. Elwell, W. Davis, E. Meirhenry, Subchronic toxicity of barium chloride dihydrate administered to rats and mice in the drinking water, Fundam Appl Toxicol 19(4) (1992) 527-37.

[34] N.A. Impellitteri, M.W. Toepke, S.K. Lan Levengood, W.L. Murphy, Specific VEGF sequestering and release using peptide-functionalized hydrogel microspheres, Biomaterials 33(12) (2012) 3475-84.

[35] A.K. Jha, K.M. Tharp, J. Ye, J.L. Santiago-Ortiz, W.M. Jackson, A. Stahl, D.V. Schaffer, Y. Yeghiazarians, K.E. Healy, Enhanced survival and engraftment of transplanted stem cells using growth factor sequestering hydrogels, Biomaterials 47 (2015) 1-12.

[36] K. Sung Ho, K. Sung Wan, Heparin release from hydrophobic polymers: (I) In vitro studies, Arch Pharm Res 9(4) (2020) 193-199.

[37] K. Park, T. Okano, C. Nojiri, S. Kim, Heparin immobilization onto segmented polyurethane-urea surfaces--effect of hydrophilic spacers, J Biomed Mater Res 22(11) (1988) 977-92.

[38] G. Schmer, The biological activity of covalently immobilized heparin, Trans Am Soc Artif Intern Organs 18(0) (1972) 321-4.

[39] P. Begovac, R. Thomson, J. Fisher, A. Hughson, A. Gällhagen, Improvements in GORE-TEX vascular graft performance by Carmeda BioActive surface heparin immobilization, Eur J Vasc Endovasc Surg 25(5) (2003) 432-7.

[40] G. Tae, M. Scatena, P. Stayton, A. Hoffman, PEG-cross-linked heparin is an affinity hydrogel for sustained release of vascular endothelial growth factor, J Biomater Sci Polym Ed 17(1-2) (2006) 187-97.

[41] K. Chwalek, M.V. Tsurkan, U. Freudenberg, C. Werner, Glycosaminoglycan-based hydrogels to modulate heterocellular communication in in vitro angiogenesis models, Sci Rep 4(1) (2014) 1-8.

[42] O. Jeon, S. Ryu, J. Chung, B. Kim, Control of basic fibroblast growth factor release from fibrin gel with heparin and concentrations of fibrinogen and thrombin, J Control Release 105(3) (2005) 249-59.

[43] H.J. Chung, H.K. Kim, J.J. Yoon, T.G. Park, Heparin immobilized porous PLGA microspheres for angiogenic growth factor delivery, Pharm Res 23(8) (2006) 1835-41.

[44] M. Tanihara, Y. Suzuki, E. Yamamoto, A. Noguchi, Y. Mizushima, Sustained release of basic fibroblast growth factor and angiogenesis in a novel covalently crosslinked gel of heparin and alginate, J Biomed Mater Res 56(2) (2001) 216-221.

[45] M. Ohta, Y. Suzuki, H. Chou, N. Ishikawa, S. Suzuki, M. Tanihara, Y. Mizushima, M. Dezawa, C. Ide, Novel heparin/alginate gel combined with basic fibroblast growth factor promotes nerve regeneration in rat sciatic nerve, J Biomed Mater Res A 71(4) (2004) 661-8.

[46] D.S.W. Benoit, K.S. Anseth, Heparin functionalized PEG gels that modulate protein adsorption for hMSC adhesion and differentiation, Acta Biomater 1(4) (2005) 461-70.

[47] Ø. Arlov, G. Skjåk-Bræk, Sulfated alginates as heparin analogues: a review of chemical and functional properties, Molecules 22(5) (2017).

[48] J. Park, S.J. Lee, H. Lee, S.A. Park, J.Y. Lee, Three dimensional cell printing with sulfated alginate for improved bone morphogenetic protein-2 delivery and osteogenesis in bone tissue engineering, Carbohydr Polym 196 (2018) 217-224.

[49] R. Mhanna, J. Becher, M. Schnabelrauch, R.L. Reis, I. Pashkuleva, Sulfated alginate as a mimic of sulfated glycosaminoglycans: binding of growth factors and effect on stem cell behavior, Adv Biosyst 1(7) (2017) 1700043.

[50] L. Xie, M. Mao, L. Zhou, L. Zhang, B. Jiang, Signal factors secreted by 2D and spheroid mesenchymal stem cells and by cocultures of mesenchymal stem cells derived microvesicles and retinal photoreceptor neurons, Stem Cells Int 2017 (2017) 2730472.

[51] A.M. Saiz, Jr., M.A. Gionet-Gonzales, M.A. Lee, J.K. Leach, Conditioning of myoblast secretome using mesenchymal stem/stromal cell spheroids improves bone repair, Bone 125 (2019) 151-159.

[52] H. Lortat-Jacob, P. Esterre, J.A. Grimaud, Interferon-gamma, an anti-fibrogenic cytokine which binds to heparan sulfate, Pathol Res Pract 190(9-10) (1994) 920-2.

[53] D.A. Castilla-Casadiego, J.R. García, A.J. García, J. Almodovar, Heparin/Collagen coatings improve human mesenchymal stromal cell response to interferon gamma, ACS Biomater Sci Eng 5(6) (2019) 2793-2803.

[54] K.C. Murphy, J. Whitehead, P.C. Falahee, D. Zhou, S.I. Simon, J.K. Leach, Multifactorial experimental design to optimize the anti-inflammatory and proangiogenic potential of mesenchymal stem cell spheroids, Stem Cells 35(6) (2017) 1493-1504.

[55] L. Guo, Y. Zhou, S. Wang, Y. and Wua, Epigenetic changes of mesenchymal stem cells in three-dimensional (3D) spheroids, J Cell Mol Med 18(10) (2014) 2009-2019.

[56] S.S. Ho, K.C. Murphy, B.Y.K. Binder, C.B. Vissers, J.K. Leach, Increased survival and function of mesenchymal stem cell spheroids entrapped in instructive alginate hydrogels, Stem Cells Transl Med 5(6) (2016) 773-781.

[57] A. Tabriz, M. Hermida, N. Leslie, W. Shu, Three-dimensional bioprinting of complex cell laden alginate hydrogel structures, Biofabrication 7(4) (2015) 045012.

[58] A.B. Morton, C.E. Norton, N.L. Jacobsen, C.A. Fernando, D.D.W. Cornelison, S.S. Segal, Barium chloride injures myofibers through calcium-induced proteolysis with fragmentation of motor nerves and microvessels, Skelet Muscle 9(1) (2019) 1-10.

[59] B.P. Hung, T. Gonzalez-Fernandez, J.B. Lin, T. Campbell, Y.B. Lee, A. Panitch, E. Alsberg, J.K. Leach, Multi-peptide presentation and hydrogel mechanics jointly enhance therapeutic duo-potential of entrapped stromal cells, Biomaterials 245 (2020) 119973.

[60] Ø. Arlov, F.L. Aachmann, A. Sundan, T. Espevik, G. Skjåk-Bræk, Heparin-Like properties of sulfated alginates with defined sequences and sulfation degrees, Biomacromolecules 15(7) (2014) 2744-2750.

[61] Y.D.P. Limasale, P. Atallah, C. Werner, U. Freudenberg, R. Zimmermann, Tuning the local availability of VEGF within glycosaminoglycan-based hydrogels to modulate vascular endothelial cell morphogenesis, Adv Funct Mater 30(44) (2020) 2000068.

CHAPTER 5: TREATMENT WITH MSC SPHEROIDS ENTRAPED IN SULFATED ALGINATE RESULTS IN ENHANCED REGENERATION AND DECREASED FIBROSIS OF SOLEUS CRUSH INJURIES IN RATS

The therapeutic efficacy of mesenchymal stromal cells (MSCs) for tissue regeneration is critically linked to the potency of their secretome, the complex mixture of growth factors, cytokines, exosomes, and other biological proteins that they secrete. The duration of cell-based approaches is limited by rapid loss of cells upon implantation, motivating the need to prolong cell viability and extend the therapeutic influence of the secretome. We and others demonstrated that the secretome is upregulated when MSCs are formed into spheroids. Although the efficacy of the MSC secretome has been characterized in the literature, no studies have reported the *in situ* sequestration of the secretome within a wound site using engineered biomaterials. We previously demonstrated the capacity of sulfated alginate hydrogels to sequester components of the MSC secretome for prolonged presentation *in vitro*, yet the efficacy of this platform has not been evaluated *in vivo*. In this study, we used sulfated alginate hydrogels loaded with MSC spheroids to aid in the regeneration of a rat muscle crush injury. We hypothesized that the use of sulfated alginate to bind therapeutically relevant growth factors within the MSC spheroid secretome would enhance muscle regeneration by increasing immune modulation, vascularization, and nerve restoration within the tissue site. We found that crushed muscles treated with the combination of sulfate groups and MSC spheroids resulted in decreased fibrosis at 2 and 6 weeks and increased neuromuscular junctions 2 weeks after injury. These data indicate that MSC spheroids delivered in sulfated alginate represent a promising approach for decreased fibrosis and increased functional regeneration of muscle.

5.1 INTRODUCTION

Mesenchymal stromal cells (MSCs) offer several therapeutic benefits for regeneration of a variety of tissues including bone, cartilage, and muscle. However, the therapeutic capacity of these cells is severely decreased by their low viability after implantation into inhospitable wound sites.[1, 2] Several strategies have been employed to keep cells alive longer for regenerative applications including delivery of cells within an engineered biomaterial[3], preconditioning of cells at low oxygen tension[4], and dense aggregation into more robust cellular constructs[5]. These methods have resulted in increased cellular viability and engraftment of transplanted MSCs.[6] Although viability of cells is improved under these circumstances, it has been shown to still decrease over time.[7]

MSCs themselves have a variety of therapeutic attributes, including their ability to directly integrate into and support regenerating tissues tissues.[8-11] However, MSCs promote regeneration at a much larger scale indirectly through their secretion of growth factors, cytokines, and exosomes, collectively known as the MSC secretome. The MSC secretome has been well characterized and is known to contain a vast variety of factors implicated in tissue regeneration for a vast array of applications.[12] The growth factors identified in the MSC secretome enhance angiogenesis, modulate the immune system, and increase resident cell proliferation, migration, and differentiation.[13, 14] Importantly, the secretome increase in potency when MSCs are aggregated into multicell spheroids, further amplifying their regenerative abilities.[15, 16]

Unfortunately, MSC spheroids still suffer low viability over time *in vivo*[17], and the permanence of these bioactive factors within any given wound site is short lived due to degradation and diffusion.[18, 19] Entrapment in a biomaterial can increase retention for certain factors longer depending on mesh size and charge. However, many standard materials used for cell entrapment still exhibit rapid growth factor elution. To address this issue, we synthesized a sulfated alginate hydrogel platform to sequester MSC spheroid secreted factors for enhanced tissue regeneration. Sulfate modification enables sequestration of heparin binding growth factors

through ionic interactions, prolonging the bioavailability of endogenous growth factors both by retaining them in the designated site of injury and protecting them from degradation.[20] Although previous groups have investigated the growth factor delivery applications of sulfated alginate, these studies have exclusively focused on seeding hydrogels with specific recombinant growth factors rather than cell secreted factors.[21, 22] The use of cell-secreted growth factors has a number of benefits over their recombinant counterparts, including lower cost, fewer off target effects, increased diversity of growth factors, and reduced concentrations required to achieve a desired biological response.

Within chapter 4 of this dissertation, we previously observed increased retention of bioactive growth factors when MSC spheroids were entrapped in sulfated alginate hydrogels that aid in tubulogenesis of endothelial cells as well as increased invasion of myoblasts *in vitro*. Herein, we translated this approach in order to promote the repair and regeneration of damaged skeletal muscle. We quantified the proliferation and differentiation of invading myoblasts in MSC spheroid loaded sulfated alginate gels *in vitro*. Additionally, we evaluated the efficacy of this platform *in vivo* through use of a crushed rat soleus muscle injury model. We hypothesized that the combined use of MSC spheroids and sulfated alginate would promote muscular regeneration by sequestering therapeutic components of MSC spheroid secretome *via* ionic interactions with sulfate functional groups.

5.2 MATERIALS AND METHODS

5.2a Modification of alginate with functional groups

Sulfate groups were conjugated to PRONOVA UP VLVG alginate (< 75,000 g/mol; NovaMatrix Sandvika, Norway) using chlorosulfonic acid.[23] Briefly, VLVG was reacted with chlorosulfonic acid (HSO_3Cl; Sigma Chemical, St. Louis, MO) at 2% (v/v) and incubated at 60^{o}C for 2.5 hrs. The alginate was precipitated in cold acetone and redissolved in ultrapure water and

neutralized. The solution was then dialyzed in 3500 Da molecular weight cut off (MWCO) dialysis tubing (Spectrum Laboratories, New Brunswick, NJ) in a 100 mM sodium chloride solution for 12 hrs and then ultrapure water the next 2.5 days, with water changes every 6-12 hrs. The alginate was sterile filtered through a 0.22 µm pore filter and lyophilized until dry.

Oxidation of PRONOVA UP MVG (> 200,000 g/mol; NovaMatrix Sandvika) was conducted as previously described.[24] Alginate was reacted with 1 mM of sodium periodate to produce 1% oxidized alginate. The reaction was then quenched with ethylene glycol, dialyzed in ultrapure water, filtered, and lyophilized. Both VLVG and oxidized MVG alginates were modified with Arg-Gly-Asp (RGD) through carbodiimide chemistry.[25] Alginate was first dissolved at 1% (w/v) in MES buffer. The next day, N-(3-Dimethylaminopropyl)-N'-ethylcarbodiimide hydrochloride (EDC) and N-Hydroxysulfosuccinimide sodium salt (Sulfo-NHS) were added to the reaction at a ratio of 2:1 per gram of alginate. The peptide G4RGDSP (Commonwealth Biotechnologies, Richmond, VA) was then added to the reaction for a degree of substitution (DS) of 2. The resulting RGD-alginate was put in a dialysis tube as previously described (6-8 kDa MWCO, Spectrum Laboratories) for three days. The solution was then sterile filtered and lyophilized.

5.2b Hydrogel crosslinking

Modified alginate was dissolved at 25 mg/mL in PBS. Hydrogels were composed of a 1:7 ratio of sulfated alginate to non-sulfated alginate. The non-sulfated alginate was a mixture of 1 part RGD-modified VLVG alginate and 1 part 1% oxidized RGD-modified MVG. After mixing *via* gentle tube rotation for at least 10 min, the alginate mixture was pipetted into 8 mm diameter circular silicone molds sandwiched between two dialysis membranes (6-8 kDa MWCO, Spectrum Laboratories). A solution of 6 mM $BaCl_2$ and 200mM $CaCl_2$ was liberally pipetted onto the top dialysis membrane for 5 min. The mold, gels and membranes were then flipped upside down so the ionic solution could be pipetted onto the dialysis membrane on the other side for an additional 5 min. Dialysis membranes were then removed, and the gels were put in a bath of ionic solution

for an additional 10 min. Gels were then recovered from the mold and used for experimentation after 24 hrs in media.

5.2c Cell culture and MSC spheroid formation

Sprague Dawley bone marrow MSCs (Cyagen Biosciences, Santa Clara, CA) were cultured in αMEM (Invitrogen, Carlsbad, CA) supplemented with 10% fetal bovine serum (FBS) (Biotechne, Minneapolis, MN) and 1% penicillin-streptomycin (pen/strep) (Gemini Bio Products, West Sacramento, CA) in standard conditions. MSCs were used at passage 3-5 for all experiments. L6 rat myoblasts (ATCC, Manassas, VA) were cultured in DMEM (Invitrogen) also supplemented with 10% FBS, 1% pen/strep. Myoblasts were cultured in flask until 80% confluence or lower to discourage cell fusion and myotube formation. The cells were used between passage 4-5 for all experiments.

MSC spheroids were produced using the forced aggregation technique as we described.[26] Once cultured to confluence, MSCs were trypsinized and centrifuged down into 2,000 μm pores made from 1.5% agarose to form 40,000 cell spheroids. After 48 hrs in static conditions to enable spheroid formation, MSC spheroids were pipetted into the alginate solutions and crosslinked into hydrogels as described above.

5.2d Polarized light microscopy

A complete cross-section of PSR-stained muscle was imaged with a 10X objective with brightfield illumination on a Leica DMi8 microscope and DFC9000GTC camera. Sections were also imaged under linearly polarized light by inserting a rotating polarizer into the beam path before and after the slide. To evaluate collagen architecture, a custom script in MATLAB (Mathworks) was used to evaluate the tissue birefringence from the polarized light images.

5.2e PCR analysis

Soleus muscles were measured, harvested, cut in half, and snap frozen in liquid nitrogen. Muscles were immersed in 1 mL of TRIzol Reagent (Invitrogen, Waltham, MA) and homogenized using a Tissue-tearor (BioSpec, Bartlesville, OK) at maximum capacity for 20 seconds. RNA was isolated following TRIzol reagent instructions per the manufacturer. 1000 ng of RNA was reverse transcribed using the QuantiTect Reverse Transcription Kit (Qiagen, Hilden, Germany) and normalized to a final concentration of 13 ng/ul. qPCR was performed using Taq PCR Master Mix (Qiagen, Hilden, Germany) in a QuantStudio 5 real-time PCR system (ThermoFisher, Waltham, MA). Rat specific primers for *Gapdh* (Rn01775763_g1)*, Myod* (Rn00598571_m1)*, Myog (*Rn00567418_m1) and *MyhcII (*Rn01470656_m1*)* were purchased from ThermoFisher. Results were normalized to the housekeeping gene, *Gapdh*, to yield a ΔCt value for each time point.

5.2f Soleus crush injury model

All animal studies were conducted in accordance with UC Davis animal care guidelines and all National Institutes of Health animal handling procedures. Male and female Sprague Dawley rats aged 8-12 weeks, between 200-250g in weight, were used. Rats were anesthetized using 2-3% isoflurane and 1% oxygen, then maintained at 0-3% isoflurane and 1% oxygen through a nose cone for the duration of the surgery. The surgical procedure was conducted on the right leg of the animal. An initial incision was performed, the skin was pulled back and the fascia of the gastrocnemius was separated to reach the soleus. Upon soleus isolation, clamps were placed on the muscle to crush the tissue for 10 s, which was repeated along the entire length of the muscle. The hydrogel was implanted on the muscle adjacent to the soleus. The muscle on top of the soleus was sutured to keep the gel in place. The initial incision on the skin was then closed with sutures and wound clips.

5.2g Histology Analysis

Muscle sections were fixed in 4% PFA then paraffin embedded and cryosectioned at 5µm thickness. Sections were stained with hematoxylin and eosin (H&E) and picrosirius red (PSR). H&E slides were imaged with 10X and 20X objectives using a Nikon Eclipse TE2000U microscope. For immunohistochemistry staining, slides were rehydrated and exposed to heat mediated antigen retrieval with a sodium citrate buffer. Samples were then incubated in blocking buffer composed of 10% goat serum and 10 mg/mL Bovine Serum Albumin (BSA) for 1 hr at room temperature. CD31 stained slides were incubated with recombinant anti-CD31 antibody (Abcam, Cambridge MA, ab182981) at a concentration of 1:200 overnight at 4°C. Slides were then treated with a secondary goat anti rabbit antibody conjugated to Alexa fluor 488 (Abcam, Cambridge, MA, ab150083) at a concentration of 1:300 for 1 hr at room temperature. Slides were then counterstained with Wheat Germ Agglutinin (WGA) conjugated to Alexa Fluor 680 and DAPI (Thermo Fisher, Chicago, IL). For the α-bungarotoxin stain, slides were rehydrated and treated for antigen retrieval as described above, then stained with Tetramethylrhodamine α-bungarotoxin at a concentration of 5 µg/mL. Slides were then counterstained with WGA conjugated to Alexa Fluor 488 and DAPI. Quantification of blood vessels was conducted on 3 field of views on n of 4 different slides per group by a blinded observer. Stained α-bungarotoxin slides were quantified using the Analyze Particles function in ImageJ and normalized to the total area of the section.

5.2h Soleus mechanical testing

Halved soleus muscles were stored in a solution of potassium-propionate, imidazole, EGTA, and magnesium chloride hexahydrate.[27] Elastic and dynamic stiffness was quantified using a method previously described.[28, 29] Briefly, muscles were removed from storage solution and immersed in a dilute storage solution supplemented with 2mM adenosine 5′-triphosphate disodium salt hydrate (ATP) adjusted to a pH of 7.[27] Muscles were pinned and loops were secured to each end of the soleus using 10-0 monofilament nylon suture. Distances between

sutures was measured and related to the fraction of total length of muscle as measured prior to resection. This value was then used as the starting length when loading for mechanical testing. Sutures were secured to a force transducer (Model 405A, sensitivity 10 V g−1, Aurora Scientific, Ontario, Canada) on one end and to a titanium wire rigidly attached to a rotational bearing (Newport MT-RS; Irvine, CA, USA) on the other end. Preconditioning of the muscle was accomplished with cyclical strain of 1 Hz for 5 s. Muscle halves underwent a ramp strain of 5, 10, 15, and 20% with each strain held for 2 minutes. The maximum stress reached during stress relaxation is referred to as the dynamic stress and the steady state stress after the 2-minute relaxation is referred to as the elastic stress. Elastic stiffness was determined from the tangent of the quadratic fit of the elastic stress to strain at 10% strain.[29]

5.3 RESULTS

5.3a MSC spheroids in sulfated and non-sulfated hydrogels had similar viability at 6 weeks

We tested the therapeutic potential of MSC spheroid sequestered *via* sulfated alginate using soleus crush injury model in Sprague Dawley rats, as depicted in **Fig. 5.1A** and **5.2A-H**. The implanted hydrogels are described in **Table 5.1**. These included: acellular sulfated alginate, spheroid loaded non-sulfated alginate, conditioned media loaded sulfated alginate and spheroid loaded sulfated alginate. All hydrogels looked morphologically similar once crosslinked, with the conditioned media loaded group appearing slightly more opaque than the others due to being dissolved in α-MEM and not PBS (**Figure 5.3**).

After injury and implantation of these hydrogels, rat soleus muscles were collected after 2 or 6 weeks to evaluate regeneration. After collection at 6 weeks, MSCs were present at similar levels in both sulfated and non-sulfated hydrogels, as determined by IVIS imaging (**Fig. 5.1B-C**). This also corresponds well with our *in vitro* data that verified viability of MSC spheroids in sulfated and non-sulfated alginate was the same (**Fig. 5.4**). These data confirm that sulfate groups do not impair spheroid viability, further strengthening the fact that any differences between groups are because of the sequestered secretome and not the MSCs themselves. Gross images of explanted muscle at 6 weeks appeared largely similar between groups, with the groups containing MSC spheroids exhibiting slightly thicker and darker muscle (**Fig. 5.1D**). In some explants, parts of the hydrogel could be seen embedded on top of the muscle tissue, indicated by the black arrows. At 2 weeks, H&E imaging showed increased areas of dense fibrotic tissue in sulfated acellular and non-sulfated spheroid groups, indicated by the red dotted lines (**Fig. 5.1E**). The sulfated spheroid group also had some fibrotic tissue, but it was less dense and had more blood vessels, indicated by the black arrows. At 6 weeks the fibrotic tissue decreased for the sulfated spheroid group, while the other groups appeared to maintain similar fibrotic area. Additionally, the muscle fibers appeared thicker and more organized in the sulfated spheroid group compared to the others, indicating more robust regeneration.

Table 5.1 Hydrogel formulations used for *in vivo* study.

Group	Alginate	Cells	Secretome source
Sulfated Acellular	Sulfated	Acellular	No secretome
Non-Sulfated spheroid	Unmodified	Spheroid	Cell secreted
Sulfated CM	Sulfated	Acellular	Conditioned media
Sulfated Spheroids	Sulfated	Spheroid	Cell secreted

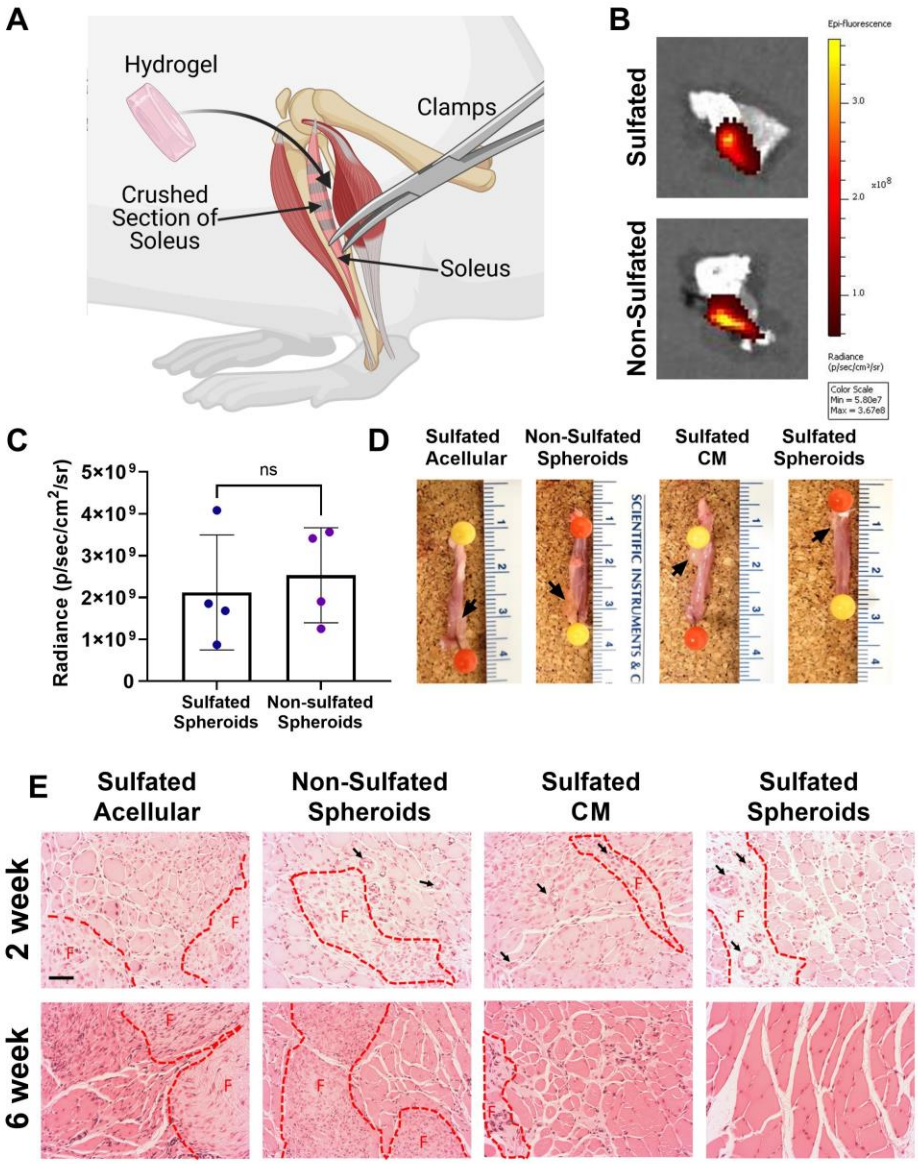

Figure 5.1 Sulfated hydrogels support transplanted cell viability. (a) Schematic of *in vitro* myoblast invasion experiment. (b) Representative near Infrared images of explanted soleus 6 weeks post injury of sulfated and non-sulfated spheroid groups. (c) Quantification of near infrared images. (d) Gross images of explanted muscles at 6 weeks post injury. Black arrows indicate residual alginate. (e) H&E stain of soleus at 2 weeks and 6 weeks post injury. Red dotted lines outline fibrosis, black arrows point to blood vessels. Scale bar= 50μm, data are mean ± SD (n=4); ns denotes no significance among all groups.

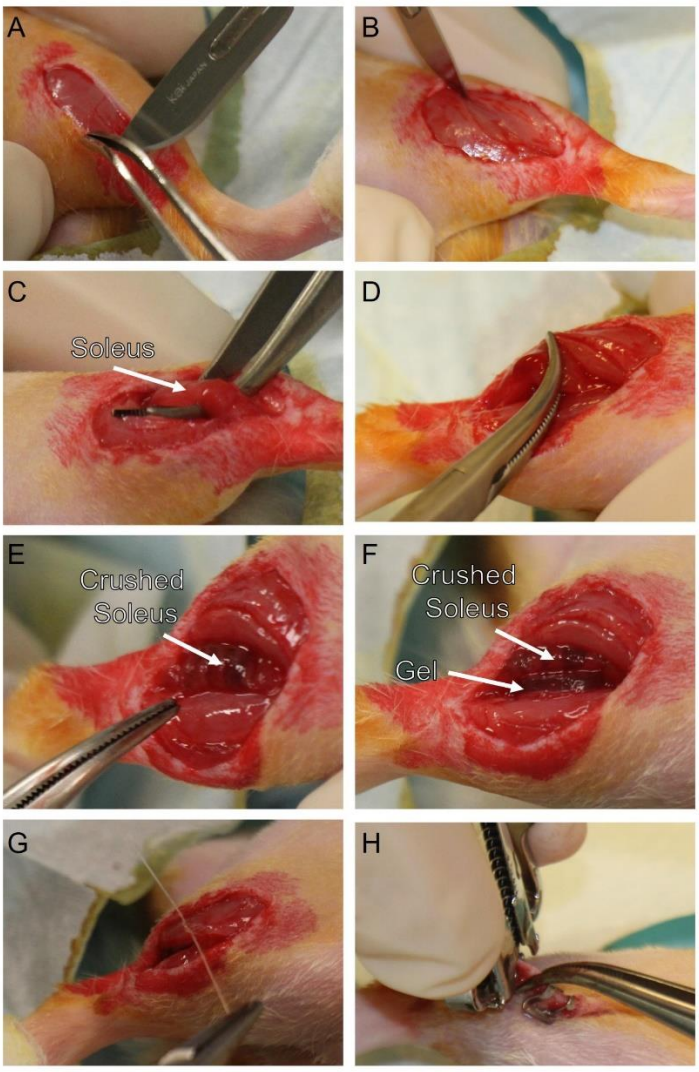

Figure 5.2 Surgical images from soleus crush injury model. (a) The right leg of the animal was opened. (b) The fascia was cut (c) and the soleus was found. (d,e) the soleus was crushed with clamps, (f) then a gel was implanted on top of the injured tissue. (G) The fascia was sutured shut, (h) and the skin was closed using a combination of wound clips and sutures.

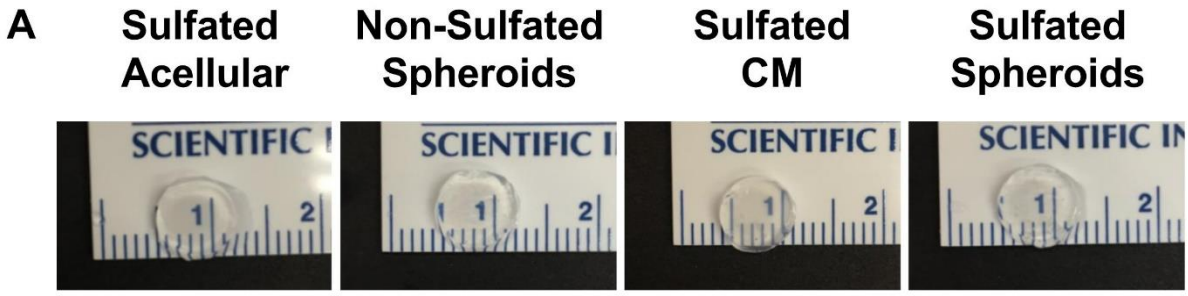

Figure 5.3 Characterization of hydrogels used for in vivo implantation. (a) Gross images of the hydrogels used for *in vivo* implantation.

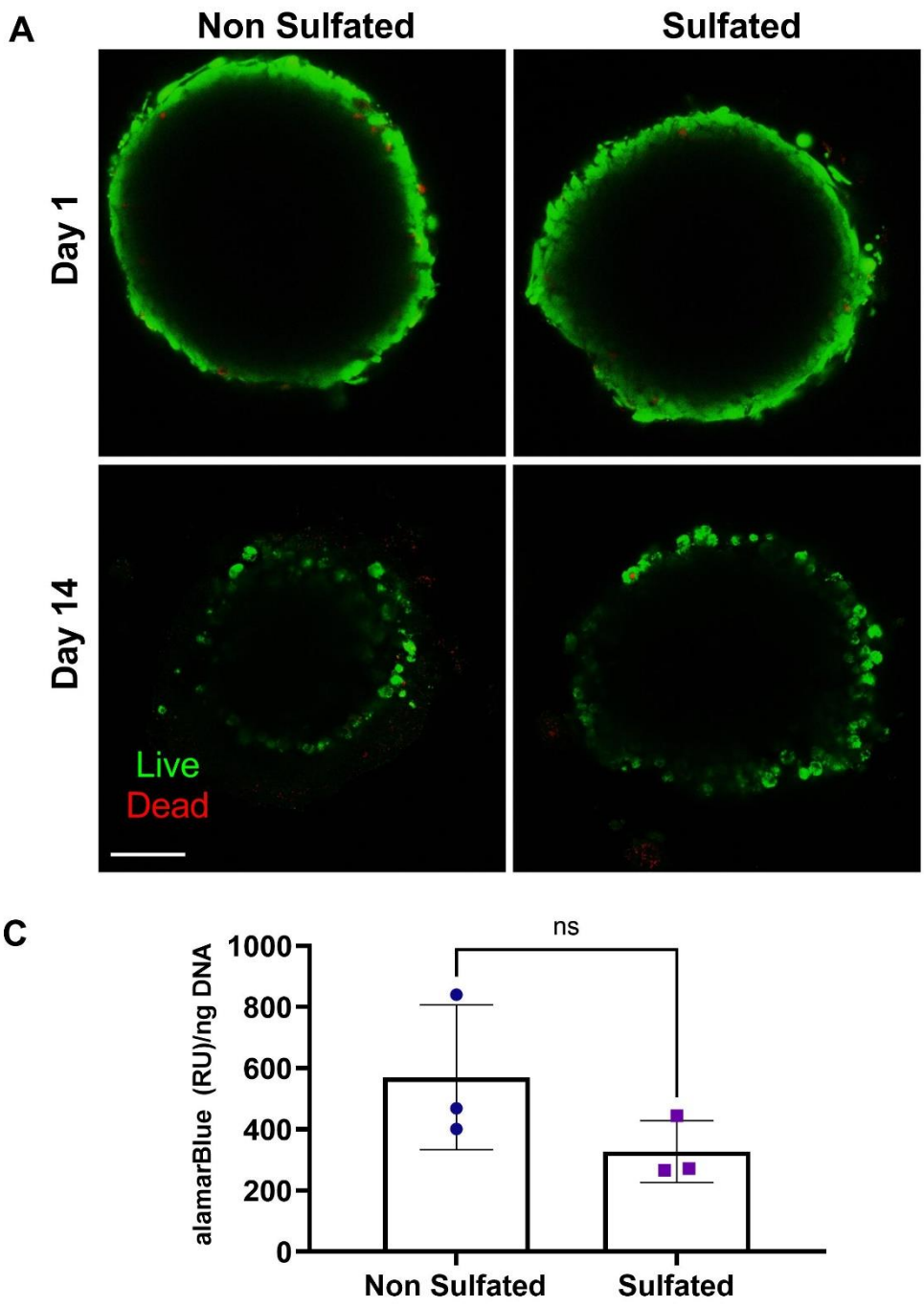

Figure 5.4. Spheroid viability in sulfated and non-sulfated hydrogels. (a) Live/Dead stain of MSC spheroids cultured in sulfated and non-sulfated hydrogels on day 1 and 14 (b) Alamarblue of MSC spheroids in non-sulfated and sulfated hydrogels on day 1 and 14 normalized to DNA. Data are mean ± SD (n=3); ns denotes no significance among all groups.

5.3b Hallmarks of fibrosis, including collagen content and fiber compaction decreases in sulfated spheroid hydrogels

Fibrosis is characterized by the buildup of biological matrix, in particularly collagen, after wound affliction and can decrease the functionality of muscle. Once explanted, we quantified the amount of collagen within explanted muscle tissue to further confirm the fibrotic response we saw in the H&E images. Through analysis *via* hydroxyproline assay, we determined that at 2 weeks the collagen content of the sulfated conditioned media group and the sulfated spheroids group were non-statistically different from the contralateral muscle (**Fig. 5.5A**). This indicates that these groups are producing less excess collagen and therefore likely exhibiting a limited fibrotic response compared to the sulfated acellular and spheroid non-sulfated groups. At 6 weeks this trend continued, as all groups except the sulfated acellular group were not statistically different than the contralateral. Additionally, the sulfated conditioned media group exhibited significantly lower collagen than the sulfated acellular control (**Fig. 5.5B**). We further quantified the percent insoluble collagen, as this investigates the amount of densely crosslinked collagen associated with fibrosis. At the 2-week time point, we found all groups had higher percentage of insoluble collagen than the contralateral, which is consistent with early injured muscle (**Fig. 5.5C**). However, by 6 weeks the sulfated spheroids group was the only group exhibiting no statistically significant differences with the contralateral (**Fig, 5.5D**). This further reinforces the conclusion that the sulfated spheroid group exhibited less fibrotic response compared to the other groups.

To further investigate the quality of this collagen, we analyzed picrosirius red stained slides using polarized light microscopy. This method allows us to determine the compaction of the collagen, with highly compact collagen fibers appearing red, mildly compact fibers appearing yellow, and loose fibers appearing green. Fibrotic tissue is characterized by higher concentrations of highly compacted collagen. Representative images indicate that muscle tissue treated with sulfated spheroids and sulfated conditioned media groups appear to have the thinnest fibers at both the 2- and 6-week time point, indicating the smallest amount of connective tissue and lowest

fibrotic response, which correlates well with the hydroxyproline data (**Fig. 5.5E**). We also noticed birefringence from the muscle fibers, seen in the blue coloring of the polarized light image of the sulfated spheroid group at 6-weeks, which was an artifact that was not taken into account for the analysis. We then analyzed the polarized light images to determine the fraction of collagen fibers exhibiting red, yellow, or green intensities, relating to the compaction of the collagen. At the two-week time point we found that the non-sulfated spheroid group exhibited a significantly higher number of red fibers compared to the acellular hydrogels (**Fig. 5.5F**). Week 6 data exhibited no significance, however, the sulfated spheroid hydrogel group appeared to line up the closest with the contralateral values for the red and yellow fibers. These data indicate that collagen compaction is nearest to that of uninjured muscle (**Fig. 5.5G**). Overall, these data suggest that the sulfated spheroid group induced lower amounts of collagen deposition and induced collagen compaction the most similarly to uninjured muscle compared to other groups.

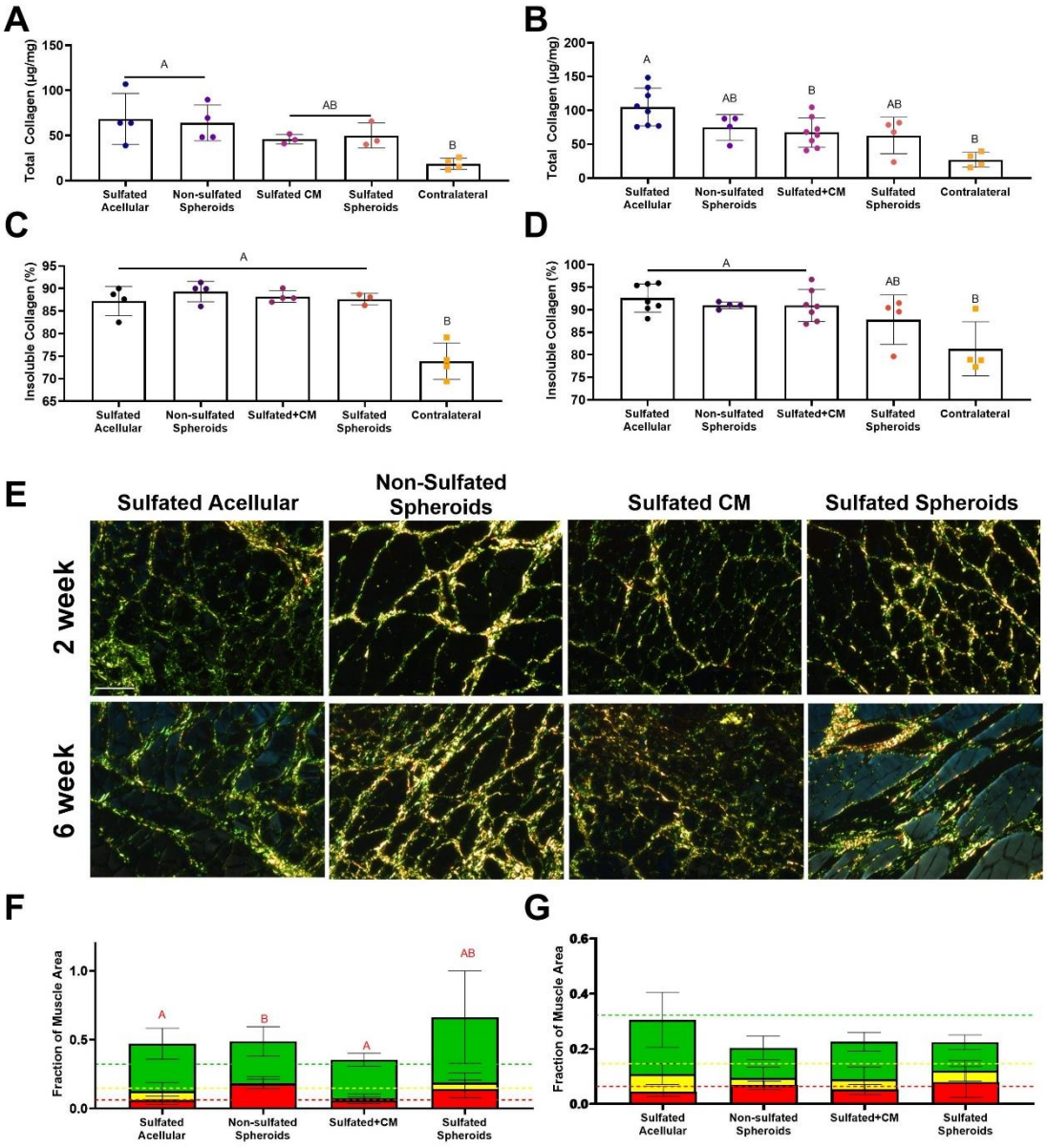

Figure 5.5 Sulfated hydrogels with MSC spheroids exhibit lower collagen deposition. (a) Hydroxyproline assay depicting total collagen levels in explanted muscle at (a) 2 weeks and (b) 6 weeks, and percent insoluble collagen at (c) 2 weeks and (d) 6 weeks. (e) Polarized light microscopy of picrosirius red sections quantified at (f) 2 weeks and (g) 6 weeks. Dotted lines denotate contralateral values. Data are mean ± SD (n=3-8). Groups with statistically significant differences do not share the same letters; ns denotes no significance among all groups.

5.3c Neuromuscular junctions and blood vessel formation are upregulated in muscle when treated with spheroid hydrogels

Blood vessels were identified *via* CD31 immunohistochemistry stain (**Fig. 5.6A**). More blood vessels were apparent in the sulfated spheroid group compared to the others, as indicated by the white arrows, indicating increased vascularization response. To interrogate nerve regeneration, we stained tissue sections with α-bungarotoxin, a stain specific for neuromuscular junctions, identified by the white arrows (**Fig. 5.6B**). When quantified, we identified increased number of neuromuscular junctions in muscle tissues treated with sulfated spheroid group compared to sulfated acellular and sulfated conditioned media groups at 2-weeks (**Fig. 5.6C**). This indicates a more robust neuromuscular junction regeneration response in the cellular groups with the highest response exhibited by the sulfated spheroid group. By 6-weeks we saw a trend of sulfated spheroids and sulfated conditioned media group exhibited higher numbers of neuromuscular junctions compared to the sulfated acellular and non-sulfated spheroid groups (**Fig. 5.6D**). This is likely due to the nerve regeneration being completed at this time point, which occurs within 6-12 weeks after injury. This indicated that the sulfated spheroid group had a jumpstart on the vascularized and innervation processes at 2 weeks.

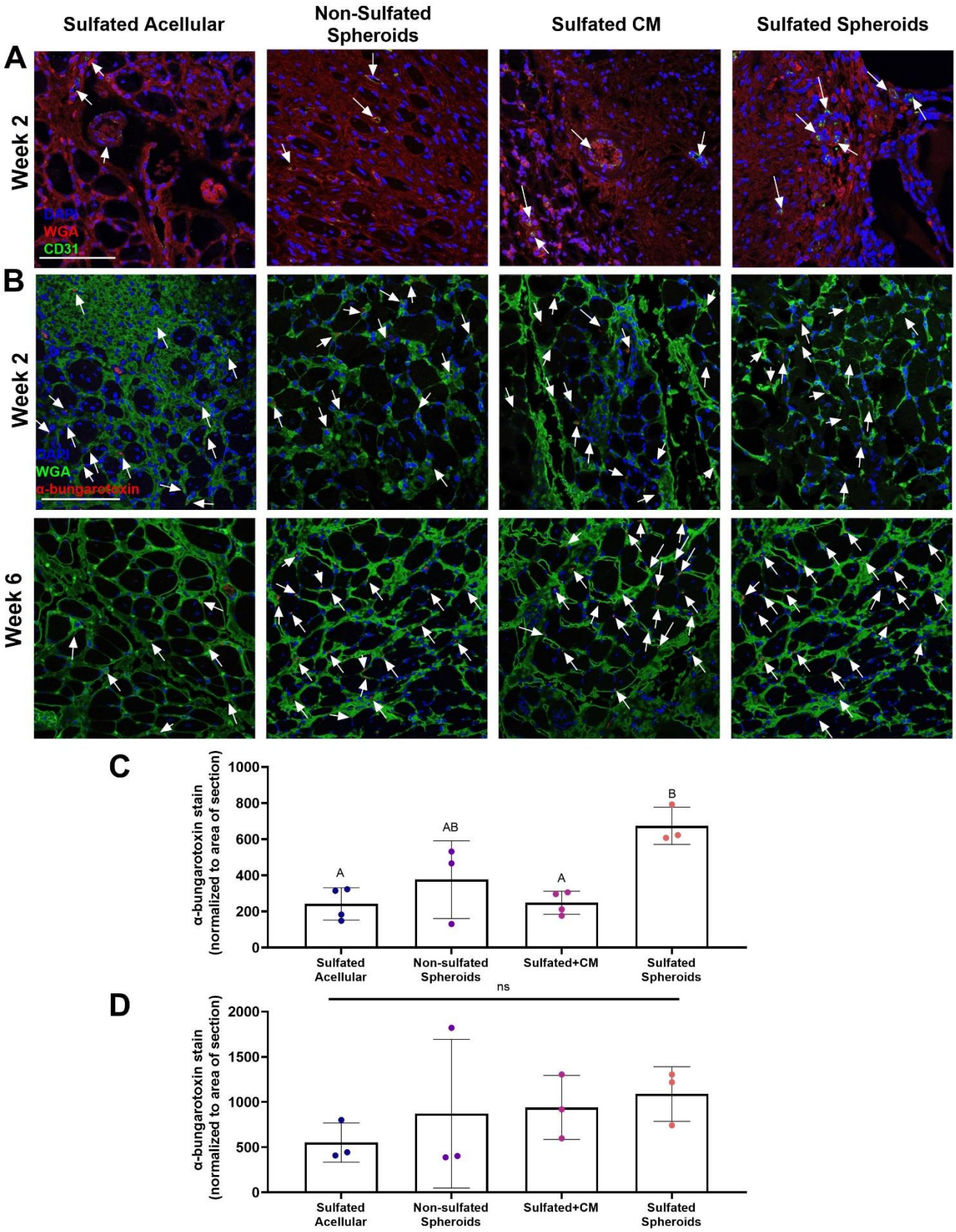
Sulfated Acellular
Non-Sulfated Spheroids
Sulfated CM
Sulfated Spheroids
A
Week 2
DAPI
WGA
CD31
B
Week 2
DAPI
WGA
α-bungarotoxin
Week 6
C
α-bungarotoxin stain (normalized to area of section)
1000
800
600
400
200
0
A
AB
A
B
Sulfated Acellular
Non-sulfated Spheroids
Sulfated+CM
Sulfated Spheroids
ns
D
α-bungarotoxin stain (normalized to area of section)
2000
1500
1000
500
0
Sulfated Acellular
Non-sulfated Spheroids
Sulfated+CM
Sulfated Spheroids

Figure 5.6 Spheroid hydrogels exhibit increased number of neuromuscular junctions and blood vessels. (a) CD31 staining of week 2 samples, blood vessels are identified by white arrows. (b) α-Bungarotoxin staining of week-2 and week-6 explants, stained neuromuscular junctions are identified by white arrows. Quantification of α-Bungarotoxin stain at (c)2-weeks and (d)6-weeks. Data are mean ± SD (n=3-4). Groups with statistically significant differences do not share the same letters; ns denotes no significance among all groups.

5.3d Mechanical properties for all groups exhibited similar values to contralateral muscle

We then examined the physical properties of the 6-week explanted muscle to further evaluate its regeneration quality. The muscle mass of all groups was non-significantly different from the contralateral muscle tissue (**Fig. 5.7A**). When measuring the elastic stiffness of the muscle, we again observed no significant differences between our experimental groups and the contralateral muscle (**Fig. 5.7B**). However, we did notice that the sulfated acellular treated group had the lowest average, indicating lower quality muscle formation, followed by the sulfated spheroids and non-sulfated spheroid groups. The sulfated conditioned media group had the highest mean elastic stiffness, surpassing that of the contralateral, but also the largest variability. Before explanation, we measured the range of motion of the injured and contralateral limb and plotted the difference of those values (**Fig. 5.7C**). Overall, the range of motion at 2-weeks was more variable than the range of motion at 6-weeks. This indicated limb range of motion improved over time, as 6-week time points were closer to zero, verifying closer range of motion to that of the contralateral. Range of motion in muscle tissues treated with each group were not significantly different, yet the non-sulfated spheroid control had values closest to zero. These data indicate that all injuries were near full regeneration regarding their physical properties after 6 weeks of regeneration.

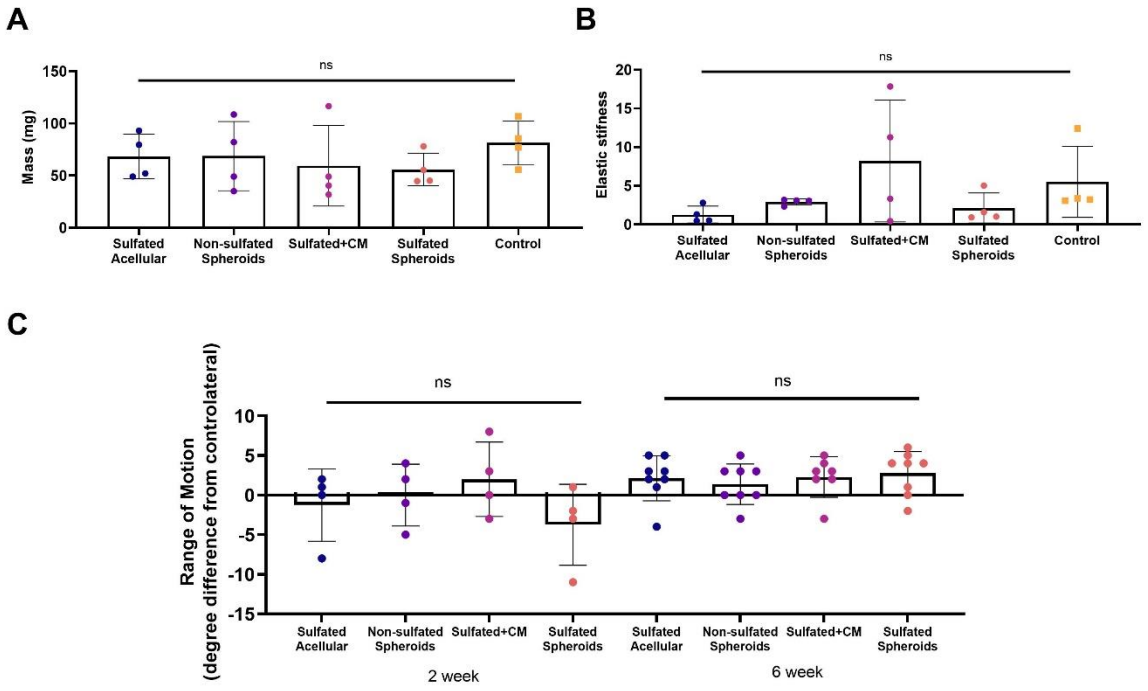

Figure 5.7. Physical and mechanical properties of regenerated muscle were comparable to uninjured muscle at 6-weeks. (a) Mass and (b) elastic stiffness of explanted soleus at 6-weeks regeneration. (c) range of motion difference from contralateral at 2- and 6-weeks post injury. Data are mean ± SD (n=3-8). Groups with statistically significant differences do not share the same letters; ns denotes no significance among all groups.

5.3e PCR muscle differentiation markers suggest improved myogenic differentiation when treated with spheroids in sulfated alginate

In order to further characterize the maturity of the regenerated muscle fibers, we measured differentiation markers *via* PCR. In muscle regeneration, the proliferation, activation and differentiation of muscle stem cells, termed satellite cells, is a necessary step. Myogenin is a transcription factor specific for muscle differentiation and is necessary for myofiber growth and satellite cell homeostasis.[30] At 2 weeks post injury, we observed a trend of increasing expression of MYOG, the gene for myogenin, in muscle tissues treated with sulfated conditioned media and sulfated spheroid groups, although this was not statistically significant (**Fig. 5.8A**).

Myosin heavy chain is a vital protein for muscle contraction; therefore, we investigated the expression of this gene at 6 weeks post injury as a later differentiation muscle marker. Although not statistically significant, we observed a similar trend as with myogenin, with tissues treated with conditioned media and spheroids in sulfated gels exhibiting higher expression on average (**Fig. 5.8B**). These data indicate that the sulfated conditioned media and sulfated spheroid group exhibited marginally higher expression of differentiation markers at both early and late time points, indicating slight increases in maturation of muscle fibers.

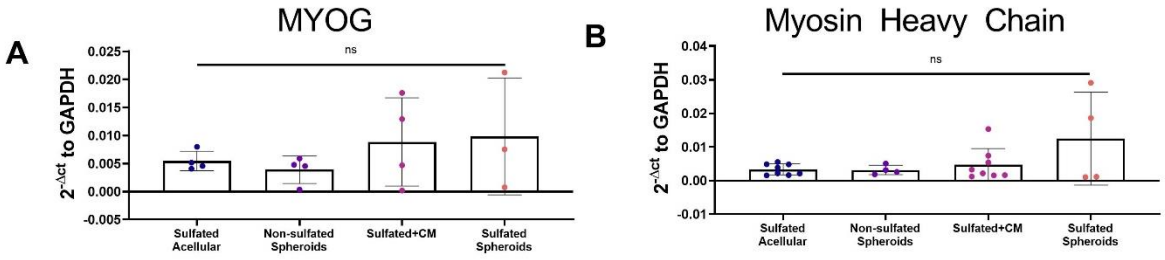

Figure 5.8 PCR analysis of muscle differentiation markers MYOG and myosin heavy chain. PCR determined the (a) MYOG expression at 2 weeks as an early muscle differentiation marker, and (b) myosin heavy chain as a marker of late muscle differentiation. Data are mean ± SD (n=4-8). Groups with statistically significant differences do not share the same letters; ns denotes no significance among all groups.

5.4 DISCUSSION

The MSC secretome presents an exciting tool for the tissue engineering field and has already been studied for several applications.[14, 31] However, little work has been done to investigate methods to prolong the presence of bioactive factors within the secretome to further promote its regenerative capacity. This is especially important considering cell survival dramatically declines when implanted within the inhospitable microenvironment of the body. This study aimed to sequester growth factors within the MSC spheroid secretome using a heparan mimetic sulfated alginate biomaterial. We evaluated the capacity of this material to repair a rat soleus crush injury,

through a novel approach using growth factor sequestering hydrogel to retain MSC spheroid secreted factors.

After muscle injury, a cascade of steps occurs in the muscle regeneration process. Several of these processes can be spurred and manipulated by growth factors. Indeed, there are several known growth factors secreted by MSC spheroids that can aid in muscle regeneration, including VEGF, IGF-1, HGF, and b-FGF.[32, 33] For example, concurrent delivery of VEGF and IGF-1 from alginate hydrogels increased vascularization, innervation and myogenic differentiation in an ischemic muscle injury. [34] Unloaded heparan sulfate mimetics have also previously shown increased regeneration of soleus crush injuries.[35] These groups further showed that heparan sulfate, or their heparan sulfate analogs, were able to stimulate growth and differentiation of satellite cells, which they hypothesized occurred through the sequestering of endogenous growth factors.[36] Therefore, utilizing a growth factor sequestering material in a muscle crush injury is well motivated and in line with many works in the field.

One common dysregulation in the muscle regeneration cascade is the formation of fibrotic scar tissue, mainly composed of collagen, that is not remodeled into functional muscle fibers. This can severely limit the functional capacity of muscle, and therefore is an important pitfall to avoid. To evaluate the fibrotic nature of our regenerated muscle, we quantified the amount of total collagen and insoluble collagen within each muscle. Insoluble collagen indicates an increase in crosslinking, which is characteristic of fibrotic collagen. We found that muscle injuries treated with sulfated hydrogels and spheroids had collagen levels closer to that of the contralateral at 2 weeks, and concentrations of insoluble collagen comparable to the contralateral by 6 weeks.

The collagen was further characterized through polarized light microscopy, which indicated that at 2 weeks the spheroid treated muscle exhibited the highest red, or tightly compact collagen associated with fibrosis. The sulfated spheroid group also had upregulated red collagen, but this was lower than the spheroid group and not statistically higher than any other group. This is an interesting finding, considering, although MSCs are immunoprivileged, they may be spurring a

low immune response that is not seen in the acellular groups. However, it is possible the sulfated alginate allowed for increased retention of anti-inflammatory factors known to be secreted by MSC spheroids, resulting in this muted effect in comparison with the spheroid group. Overall, this in-depth characterization of the collagen indicates that the sulfated spheroid group better regulated the fibrotic response, resulting in lower concentrations of total collagen, and higher concentrations of healthy non-fibrotic collagen.

Within our study, the number of neuromuscular junctions was increased within muscles treated with sulfated hydrogels containing spheroids compared to the acellular groups at 2 weeks. This shows that the sequestering of MSC spheroid produced growth factors is likely increasing the innervation rate. This is likely due to the growth factors secreted from MSC spheroids that are pro-regenerative for nerves such as nerve growth factor (NGF). By 6 weeks we saw no significant differences in neuromuscular junction expression, which correlates well with the literature, indicating innervation repair is likely completed at that time point.[34, 37] Innervation is an important step in the regeneration of functional muscle that is often overlooked in muscle tissue engineering. Therefore, ensuring nerve regeneration is occurring by quantifying the number of neuromuscular junctions is an important first step, considering muscle would not only be unfunctional without nerve regeneration, but would eventually atrophy.

It is interesting to note that the sulfated conditioned media group did not perform as well compared to the spheroid loaded sulfated group. This is likely because, as seen in the IVIS data, our spheroids were still present at 6-weeks, indicating they are likely still secreting growth factors. Alternatively, the conditioned media group consists of one load of growth factors with no way to replenish them over time. A limitation of this work is that we did not verify the mechanism of action for regeneration. We hypothesize that the improved soleus healing is due to sequestration of MSC spheroid growth factors *via* sulfate groups, however we did not explicitly investigate if this was the case. Future studies determining the bioactivity of the MSC spheroid factors sequestered in sulfated alginate are important to pursue. One of the main limitations of this work is that for much

of our data we did not see very large differences between groups. This could be because the muscle injury we pursued only focused on injury of the soleus muscle, while keeping it surrounded by healthy muscle during the healing processes. Previous studies have shown that the myokines myoblasts secrete are beneficial for the regeneration of musculoskeletal injuries. Therefore, it is possible that the concentration of growth factors is significantly upregulated within that physiologically area, muting the differences between secretome and non-secretome loaded groups. Future research is warranted in determining the effect spheroid loaded sulfated alginate has in more detrimental, growth factor deficient injury sites, such as volumetric muscle injuries.

5.5 CONCLUSION

Through this study, we found that spheroid loaded sulfated alginate shows significant reduction in fibrotic response within a soleus muscle crush injury. We further showed that this group exhibited larger neuromuscular junction and blood vessel formation at 2 weeks. Week 6 data indicated encouraging trends for myoblast differentiation markers and decreased fibrosis, however a higher number of animals is needed in order to see significant differences. These results are likely due to sulfated alginate's ability to retain the MSC spheroid secretome, which is known to consist of immune modulatory, vasculogenic and neurogenic heparin-binding growth factors.

5.7 REFERENCES

[1] L.M. McGinley, J. McMahon, A. Stocca, A. Duffy, A. Flynn, D. O'Toole, T. O'Brien, Mesenchymal Stem Cell Survival in the Infarcted Heart Is Enhanced by Lentivirus Vector-Mediated Heat Shock Protein 27 Expression, Hum Gene Ther2013, pp. 840-51.

[2] K.S. Dhada, D.S. Hernandez, L.J. Suggs, Photoacoustic Tracking of Mesenchymal Stem Cell Viability, ACS Nano 13(7) (2019) 7791-7799.

[3] E.T. Roche, C.L. Hastings, S.A. Lewin, D. Shvartsman, Y. Brudno, N.V. Vasilyev, F.J. O'Brien, C.J. Walsh, G.P. Duffy, D.J. Mooney, Comparison of biomaterial delivery vehicles for improving acute retention of stem cells in the infarcted heart, Biomaterials 35(25) (2014) 6850-6858.

[4] I. Rosová, M. Dao, B. Capoccia, D. Link, J.A. Nolta, Hypoxic preconditioning results in increased motility and improved therapeutic potential of human mesenchymal stem cells, Stem Cells 26(8) (2008) 2173-82.

[5] S.S. Ho, B.P. Hung, N. Heyrani, M.A. Lee, J.K.L. 1, Hypoxic Preconditioning of Mesenchymal Stem Cells with Subsequent Spheroid Formation Accelerates Repair of Segmental Bone Defects, Stem Cells 36(9) (2018) 1393-1403.

[6] J.N. Harvestine, T. Gonzalez-Fernandez, A. Sebastian, N.R. Hum, D.C. Genetos, G.G. Loots, J.K. Leach, Osteogenic preconditioning in perfusion bioreactors improves vascularization and bone formation by human bone marrow aspirates, Sci Adv 6(7) (2020) eaay2387.

[7] S. Khatab, M.J. Leijs, G. van Buul, J. Haeck, N. Kops, M. Nieboer, P.K. Bos, J.A.N. Verhaar, M. Bernsen, G.J.V.M. van Osch, MSC encapsulation in alginate microcapsules prolongs survival after intra-articular injection, a longitudinal in vivo cell and bead integrity tracking study, Cell Biol Toxicol 36(6) (2020) 553-570.

[8] F. Ng, S. Boucher, S. Koh, K.S. Sastry, L. Chase, U. Lakshmipathy, C. Choong, Z. Yang, M.C. Vemuri, M.S. Rao, V. Tanavde, PDGF, TGF-beta, and FGF signaling is important for differentiation and growth of mesenchymal stem cells (MSCs): transcriptional profiling can identify markers and signaling pathways important in differentiation of MSCs into adipogenic, chondrogenic, and osteogenic lineages, Blood 112(2) (2008) 295-307.

[9] C.K. Chan, E.Y. Seo, J.Y. Chen, D. Lo, A. McArdle, R. Sinha, R. Tevlin, J. Seita, J. Vincent-Tompkins, T. Wearda, W.J. Lu, K. Senarath-Yapa, M.T. Chung, O. Marecic, M. Tran, K.S. Yan, R. Upton, G.G. Walmsley, A.S. Lee, D. Sahoo, C.J. Kuo, I.L. Weissman, M.T. Longaker, Identification and specification of the mouse skeletal stem cell, Cell 160(1-2) (2015) 285-98.

[10] M. Crisan, S. Yap, L. Casteilla, C.W. Chen, M. Corselli, T.S. Park, G. Andriolo, B. Sun, B. Zheng, L. Zhang, C. Norotte, P.N. Teng, J. Traas, R. Schugar, B.M. Deasy, S. Badylak, H.J. Buhring, J.P. Giacobino, L. Lazzari, J. Huard, B. Péault, A perivascular origin for mesenchymal stem cells in multiple human organs, Cell Stem Cell 3(3) (2008) 301-13.

[11] C.M. Ghajar, S. Kachgal, E. Kniazeva, H. Mori, S.V. Costes, S.C. George, A.J. Putnam, Mesenchymal cells stimulate capillary morphogenesis via distinct proteolytic mechanisms, Exp Cell Res 316(5) (2010) 813-25.

[12] M.E. Wechsler, V.V. Rao, A.N. Borelli, K.S. Anseth, Engineering the MSC Secretome: A Hydrogel Focused Approach, Adv Healthc Mater (2021) e2001948.

[13] S. Aggarwal, M.F. Pittenger, Human mesenchymal stem cells modulate allogeneic immune cell responses, Blood 105(4) (2005) 1815-22.

[14] F.G. Teixeira, K.M. Panchalingam, R. Assunção-Silva, S.C. Serra, B. Mendes-Pinheiro, P. Patrício, S. Jung, S.I. Anjo, B. Manadas, L. Pinto, N. Sousa, L.A. Behie, A.J. Salgado, Modulation of the Mesenchymal Stem Cell Secretome Using Computer-Controlled Bioreactors: Impact on Neuronal Cell Proliferation, Survival and Differentiation, Sci Rep 6 (2016) 27791.

[15] A.M. Saiz, Jr., M.A. Gionet-Gonzales, M.A. Lee, J.K. Leach, Conditioning of myoblast secretome using mesenchymal stem/stromal cell spheroids improves bone repair, Bone 125 (2019) 151-159.

[16] S.S. Ho, K.C. Murphy, B.Y.K. Binder, C.B. Vissers, J.K. Leach, Increased survival and function of mesenchymal stem cell spheroids entrapped in instructive alginate hydrogels, Stem Cells Transl Med 5(6) (2016) 773-781.

[17] I.G. Kim, H. Cho, J. Shin, J.H. Cho, S.W. Cho, E.J. Chung, Regeneration of irradiation-damaged esophagus by local delivery of mesenchymal stem-cell spheroids encapsulated in a hyaluronic-acid-based hydrogel, Biomater Sci 9(6) (2021) 2197-2208.

[18] D.F. Lazarous, M. Shou, M. Scheinowitz, E. Hodge, V. Thirumurti, A.N. Kitsiou, J.A. Stiber, A.D. Lobo, S. Hunsberger, E. Guetta, S.E. Epstein, E.F. Unger, Comparative effects of basic fibroblast growth factor and vascular endothelial growth factor on coronary collateral development and the arterial response to injury, Circulation 94(5) (1996) 1074-82.

[19] H. Keshaw, A. Forbes, R.M. Day, Release of angiogenic growth factors from cells encapsulated in alginate beads with bioactive glass, Biomaterials 26(19) (2005) 4171-9.

[20] F. Munarin, C. Kabelac, K.L.K. Coulombe, Heparin-modified alginate microspheres enhance neovessel formation in hiPSC-derived endothelial cells and heterocellular in vitro models by controlled release of vascular endothelial growth factor, J Biomed Mater Res A (2021).

[21] B. Wang, P.J. Díaz-Payno, D.C. Browe, F.E. Freeman, J. Nulty, R. Burdis, D.J. Kelly, Affinity-bound growth factor within sulfated interpenetrate network bioinks for bioprinting cartilaginous tissues, Acta Biomater (2021).

[22] J. Park, S.J. Lee, H. Lee, S.A. Park, J.Y. Lee, Three dimensional cell printing with sulfated alginate for improved bone morphogenetic protein-2 delivery and osteogenesis in bone tissue engineering, Carbohydr Polym 196 (2018) 217-224.

[23] O. Arlov, G. Skjak-Braek, A.M. Rokstad, Sulfated alginate microspheres associate with factor H and dampen the inflammatory cytokine response, Acta Biomater 42 (2016) 180-188.

[24] K.H. Bouhadir, K.Y. Lee, E. Alsberg, K.L. Damm, K.W. Anderson, D.J. Mooney, Degradation of partially oxidized alginate and its potential application for tissue engineering, Biotechnol Prog 17(5) (2001) 945-50.

[25] S.S. Ho, A.T. Keown, B. Addison, J.K. Leach, Cell migration and bone formation from mesenchymal stem cell spheroids in alginate hydrogels are regulated by adhesive ligand density, Biomacromolecules (2017).

[26] C.E. Vorwald, S.S. Ho, J. Whitehead, J.K. Leach, High-Throughput Formation of Mesenchymal Stem Cell Spheroids and Entrapment in Alginate Hydrogels, Methods Mol Biol 1758 (2018) 139-49.

[27] S.M. Roche, J.P. Gumucio, S.V. Brooks, C.L. Mendias, D.R. Claflin, Measurement of Maximum Isometric Force Generated by Permeabilized Skeletal Muscle Fibers, J Vis Exp (100) (2015) e52695.

[28] L.R. Smith, K.S. Lee, S.R. Ward, H.G. Chambers, R.L. Lieber, Hamstring contractures in children with spastic cerebral palsy result from a stiffer extracellular matrix and increased in vivo sarcomere length, J Physiol 589(Pt 10) (2011) 2625-39.

[29] L.R. Smith, E.R. Barton, Collagen content does not alter the passive mechanical properties of fibrotic skeletal muscle in mdx mice, Am J Physiol Cell Physiol 306(10) (2014) C889-98.

[30] M. Ganassi, S. Badodi, K. Wanders, P.S. Zammit, S.M. Hughes, Myogenin is an essential regulator of adult myofibre growth and muscle stem cell homeostasis, Elife 9 (2020).

[31] S.H. Ranganath, O. Levy, M.S. Inamdar, J.M. Karp, Harnessing the mesenchymal stem cell secretome for the treatment of cardiovascular disease, Cell Stem Cell 10(3) (2012) 244-58.

[32] J. Menetrey, C. Kasemkijwattana, C.S. Day, P. Bosch, M. Vogt, F.H. Fu, M.S. Moreland, J. Huard, Growth factors improve muscle healing in vivo, J Bone Joint Surg Br 82(1) (2000) 131-7.

[33] S.M. Sheehan, R. Tatsumi, C.J. Temm-Grove, R.E. Allen, HGF is an autocrine growth factor for skeletal muscle satellite cells in vitro, Muscle Nerve 23(2) (2000) 239-45.

[34] C. Borselli, H. Storrie, F. Benesch-Lee, D. Shvartsman, C. Cezar, J. Lichtman, H. Vandenburgh, D. Mooney, Functional muscle regeneration with combined delivery of angiogenesis and myogenesis factors, Proc Natl Acad Sci U S A 107(8) (2010) 3287-92.

[35] A. Aamiri, G.S. Butler-Browne, I. Martelly, D. Barritault, J. Gautron, Influence of a dextran derivative on myosin heavy chain expression during rat skeletal muscle regeneration, Neurosci Lett 201(3) (1995) 243-6.

[36] D. Stockholm, C. Barbaud, S. Marchand, F. Ammarguellat, D. Barritault, I. Richard, J. Beckmann, I. Martelly, Studies on calpain expression during differentiation of rat satellite cells in primary cultures in the presence of heparin or a mimic compound, Exp Cell Res 252(2) (1999) 392-400.

[37] B. Vannucci, K.B. Santosa, A.M. Keane, A. Jablonka-Shariff, C.Y. Lu, Y. Yan, M. MacEwan, A.K. Snyder-Warwick, What is Normal? Neuromuscular junction reinnervation after nerve injury, Muscle Nerve 60(5) (2019) 604-612.

CHAPTER 6: INJECTABLE MINERALIZED MICROSPHERE-LOADED COMPOSITE HYDROGELS FOR BONE REPAIR IN A SHEEP BONE DEFECT MODEL

The efficacy of cell-based therapies as an alternative to autologous bone grafts requires biomaterials to localize cells at the defect and drive osteogenic differentiation. Hydrogels are ideal cell delivery vehicles that can provide instructional cues via their composition or mechanical properties but commonly lack osteoconductive components that nucleate mineral. To address this challenge, we entrapped mesenchymal stromal cells (MSCs) in a composite hydrogel based on two naturally derived polymers (alginate and hyaluronate) containing biomineralized polymeric microspheres. Mechanical properties of the hydrogels were dependent upon composition. The presentation of the adhesive tripeptide Arginine-Glycine-Aspartic Acid (RGD) from both polymers induced greater osteogenic differentiation of ovine MSCs in vitro compared to gels formed of RGD-alginate or RGD-alginate/hyaluronate alone. We then evaluated the capacity of this construct to stimulate bone healing when transplanting autologous, culture-expanded MSCs into a surgical induced, critical-sized ovine iliac crest bone defect. At 12 weeks post-implantation, defects treated with MSCs transplanted in composite gels exhibited significant increases in blood vessel density, osteoid formation, and bone formation compared to acellular gels or untreated defects. These findings demonstrate the capacity of osteoconductive hydrogels to promote bone formation with autologous MSCs in a large animal bone defect model and provide a promising vehicle for cell-based therapies of bone healing.

Published as: G.C. Ingavle*, M. Gionet-Gonzales*, C.E. Vorwald, L.K. Bohannon, K. Clark, L.D. Galuppo, J.K. Leach. Injectable mineralized microsphere-loaded composite hydrogels for bone repair in a sheep bone defect model. *Biomaterials*. (2019) 197:119-128.

6.1 INTRODUCTION

Cell-based therapies are an exciting strategy to stimulate bone healing in large bone defects resulting from trauma, disease, or malformation. The transplantation of mesenchymal stromal cells (MSCs), adult-derived progenitor cells commonly derived from bone marrow or other tissue compartments, increases bone volume in multiple defect models.[1] However, the effectiveness of this approach requires the transplantation of MSCs using a biomaterial to localize cells at the defect, limit migration away from the target site, and potentially include instructional signals to drive cellular behavior.[2]

Hydrogels have attracted intense interest as a cell carrier because of their tailorability and potential for minimally invasive administration to the defect site.[3,4] Alginate is broadly used in forming hydrogels due to its chemically-controlled material properties and presentation of specific cues that regulate cell adhesion and phenotype.[2,5] The tripeptide Arginine-Glycine-Aspartic Acid (RGD) is widely employed to engage integrins by mimicking the adhesive binding properties of matricellular proteins such as fibronectin.[6] Hyaluronate is another promising platform in tissue engineering due to its intrinsic viscosity, engagement with cells through CD44-specific interactions, and tunability.[7] Beyond its use as a cell carrier, hyaluronate is under investigation as a biomacromolecule to stimulate repair of connective tissues, making it a promising adjuvant for local delivery.[8] These two polymers were previously combined to form composite hydrogels for cartilage regeneration, capitalizing on the CD44 expression of chondrocytes to address their limited engagement and impaired responsiveness to RGD.[9,10] The inclusion of hyaluronate enabled cell-mediated crosslinking within the composite gels that was not observed with RGD-modified alginate alone.

Hydrogels provide an ideal platform to efficiently entrap cells for delivery to the defect site, yet these materials generally lack sufficient osteoconductivity to nucleate calcium, integrate with surrounding bone, and promote bone formation. Carbonated apatite coatings exhibiting characteristics similar to native bone have been applied to various materials to enhance

osteoconductivity and contribute to bone repair.[11–13] We previously demonstrated the potential to enhance the osteoconductivity of fibrin hydrogels by supplementation with mineralized poly(lactide-co-glycolide) (PLG) microspheres, resulting in significant increases in bone mineral density over non-mineralized gels when implanted in a rodent calvarial defect.[14] Polymeric microspheres are less dense than other bioceramics (*e.g.*, β-tricalcium phosphate, hydroxyapatite), thus allowing for more homogenous distribution throughout the gel and improved spatial interaction with entrapped cells. However, these osteoconductive gels were not transplanted with bone-forming cells, resulting in relatively low quantities of new bone and motivating a critical need to evaluate this approach for stimulating bone repair using MSCs.

We hypothesized that the transplantation of autologous MSCs within peptide-modified composite hydrogels containing mineralized polymeric microspheres would enhance hydrogel osteoconductivity, increase its osteogenic potential, and promote bone healing in a large animal bone defect model. We further hypothesized that the inclusion of hyaluronate would enhance osteogenesis due to its promise in stimulating repair of connective tissues. We characterized the physical properties of these composite gels and the osteogenic response of ovine MSCs *in vitro*. We then examined the ability of composite hydrogels transplanting autologous MSCs to promote repair of critical-sized iliac crest bone defects using an ovine model.

6.2 MATERIALS AND METHODS

6.2a Isolation and culture of ovine MSCs

Treatment of experimental animals was in accordance with the UC Davis animal care guidelines and all National Institutes of Health animal handling procedures. Bone marrow collection from 12 adult female Swiss Alpine sheep (approximately 60-80 kg) was performed under general anesthesia. After aseptic preparation and draping of the sternum, a 13.5-gauge 2.5-inch bone marrow aspiration needle was inserted through the skin into the medullary cavity of a sternebra, and bone marrow aspirate (40-60 mL total volume) was collected into a

heparinized 60 mL syringe (**Supplementary Fig. 6.1A**). Animals were returned to small pens during stem cell isolation and expansion (approximately 3 weeks). After removal of plasma and red blood cells, cells were passaged at a low density into successively larger tissue culture flasks with culture media comprised of α-MEM supplemented with 10% fetal bovine serum (JR Scientific, Woodland, CA), 1% penicillin/streptomycin and 0.1% fungizone (Mediatech, Manassas, VA). Medium was replaced every 2-3 days to achieve an adherent cell population with fibroblastic morphology. Cells were used at passage 3-4.

To validate that the recovered cells were indeed MSCs, we performed flow cytometry for known MSC surface markers (CD90, CD105, CD44, CD45) and characterized their trilineage potential (*i.e.*, osteogenesis, chondrogenesis, adipogenesis) in monolayer culture using lineage-specific media for up to 3 weeks.[15,16] Characterization and all *in vitro* studies were performed with MSCs from a single donor.

6.2b Fabrication of apatite-coated PLG microspheres

Poly(lactide-*co*-glycolide) (PLG) microspheres were formed from PLG pellets (85:15 DLG 7E; Lakeshore Biomaterials, Birmingham, AL) using a standard double-emulsion process and lyophilized to form a free-flowing powder.[14] Microspheres were hydrolyzed for 10 min in 0.5 M NaOH to functionalize the polymer surface and then rinsed in distilled H_2O. Modified simulated body fluid (mSBF) was prepared as previously described[17] and consisted of the following reagents dissolved in distilled H_2O: 141 mM NaCl, 5.0 mM $CaCl_2$, 4.2 mM $NaHCO_3$, 4.0 mM KCl, 2.0 mM KH_2PO_4, 1.0 mM $MgCl_2$, and 0.5 mM $MgSO_4$. The solution was held at pH 6.8 to avoid homogeneous precipitation of CaP phases. Microspheres were placed in mSBF and incubated at 37ºC for 7 days, making sure to exchange the solution daily to maintain appropriate ion concentrations, frozen overnight at -80ºC, and lyophilized for 3 days. Microparticles possessed diameters in the range of 50-100 □m as previously reported.[14,18] Microspheres were sterilized under ultraviolet light for 16-18 hours prior to use.

6.2c Preparation and seeding of composite hydrogels

Sodium alginate (PRONOVA UP MVG, approximate M_w = 2.7x10^5 g/mol, G/M ratio: ≥ 1.5, FMC Biopolymer, Princeton, NJ) was gamma (γ) irradiated with a cobalt-60 source for 4 h at a γ-dose of 5.0 Mrad for faster degradation[19], resulting in alginate with M_w = 5.3x10^4 g/mol. Alginate was then covalently modified with G_4RGDSP (Celtek Peptides, Nashville, TN) using standard carbodiimide chemistry.[20] Sodium hyaluronan (approximately 1200-1900 kDa, FMC Biopolymer) was covalently coupled with G_4RGDSP using similar protocols. The resulting RGD-modified polymers were sterile filtered, lyophilized, and stored at -20°C until use. Control groups formed of unmodified polymers were prepared identically but lacking peptide addition.

RGD-alginate and RGD-hyaluronate were reconstituted separately in α-MEM to obtain 2% (w/v) and 1% (w/v) solutions, respectively. Sterile 0.22 μm filtered RGD-alginate solution was mixed with sterile filtered RGD-hyaluronate solution at 9:1 (v/v) ratio with mineralized microspheres (3 mg/mL final concentration). This solution was then mixed with 100 μL MSCs (10x10^6 cells/mL final concentration in α-MEM). Composite gels were ionically crosslinked by adding 50 μL of supersaturated $CaSO_4$ to 850 μL composite hydrogel mixture and mixed with 100 □L of the cell suspension. The solution was mixed between two 1-mL syringes (Becton-Dickinson, Franklin Lakes, NJ) coupled with a 3-way stopcock syringe connector with Luer-Lok fittings to minimize air bubbles. The mixture was dispensed between sterile parallel glass plates with 1 mm spacers, allowed to gel for 60 min in a standard CO_2 incubator, and circular gel disks were cut with 8 mm biopsy punches, with each gel containing approximately 5x10^5 cells. The osteogenic potential of this system was evaluated *in vitro* upon transferring constructs to 24-well plates and culturing for 1, 7, 14 or 21 days under standard conditions in osteogenic media (α-MEM supplemented with 10% FBS, 1% P/S, 10 mM β-glycerophosphate, 50 μg/mL ascorbate-2-phosphate, 10 nM dexamethasone), which was replaced every 2-3 days.

6.2d Measurement of hydrogel biophysical properties

Covalent modification was confirmed by NMR.[188] ^{1}H NMR spectra were recorded at 800 MHz using D_2O as a solvent with an NMR spectrometer (Bruker Avance 600). The concentration of RGD conjugated to alginate and hyaluronate was determined using the LavaPep Fluorescent Protein and Peptide Quantification Kit per the manufacturer's instructions (Gel Company, San Francisco, CA). The morphological characteristics of cells seeded in composite mineralized microsphere-loaded hydrogels were observed by scanning electron microscopy (Philips XL30 TMP field emission SEM, FEI Company, Eindhoven, Netherlands).

Acellular composite hydrogels were prepared as described above, and gels (5 mm diameter and 2 mm height thickness) were cut from a hydrogel sheet and allowed to equilibrate in DI water for 24 h before use. To measure the swelling potential, equilibrated gel samples were weighed, lyophilized for 48 h, and weighed again. The swelling ratio, Q, was determined by calculating the ratio of the equilibrated hydrogel weight to its dry weight (n=3 for all samples). Hydrogel dry mass was measured from MSC-loaded hydrogels cultured for up to 28 days in osteogenic media that were lyophilized for 48 h before weighing with a microbalance.

The compressive modulus of composite hydrogels was determined using an Instron 3345 compressive testing system (Norwood, MA). Gels were equilibrated in PBS for 24 h at room temperature prior to measurement. Excess fluid was blotted from the gel surface and then loaded between two flat platens. Hydrogel disks were compressed with a 10 N load cell at 1 mm/min. The compressive elastic modulus, defined as the slope of the linear region of the stress–strain curve of a material under compression, was calculated from the initial linear portion of the curve (0-5% strain, n=5 for all groups).[21]

6.2e MSC viability and spreading

MSC-loaded composite gels were rinsed with PBS, minced with a scalpel, homogenized, and collected in passive lysis buffer (Promega). Immediately following one freeze-thaw cycle, lysates

were sonicated briefly, centrifuged for 5 min at 10,000 rpm, and the supernatant was used to determine DNA content and intracellular alkaline phosphatase activity (ALP). Total DNA present in each hydrogel construct was quantified using the Quant-iT PicoGreen dsDNA kit (Invitrogen) in comparison to a known standard curve. The remaining homogenized gels were then incubated overnight in H_2SO_4 to solubilize surface calcium deposits. ALP activity and total calcium within composite hydrogels was determined using a *p*-nitrophenyl phosphate (PNPP) colorimetric assay at 405 nm and *o*-cresolphthalein colorimetric assay, respectively.[188] Calcium in acellular gels was quantified and subtracted at each time point to account for calcium present in the mineralized microspheres. After 21 days, some gels were paraffin-embedded, sectioned at 5 μm, and stained with hematoxylin and eosin (H&E) to assess microsphere morphology and distribution or immunostained for osteocalcin (ab13420, 1:200; Abcam, Cambridge, MA). Viability was assessed *via* the live/dead assay (Invitrogen) and visualized with confocal microscopy on Day 1 and 7 of culture.

6.2f Ovine iliac crest bone defect model

Bilateral critical-sized iliac crest bone defects were surgically created in 12 adult female Swiss Alpine sheep as previously described[22] (**Supplementary Figure 6.1B-I**). Animals received preoperative intramuscular antibiotics (naxcel, 2.2 mg/kg) and analgesia (banamine, 1.1 mg/kg) prior to induction of anesthesia. After aseptic preparation and draping, a 10 cm incision was made over the dorsal aspect of each iliac wing. Bilateral full-thickness defects were created in the iliac crest (15 mm diameter, 5 mm depth) using a 15 mm drill bit and custom-made jig fixed in position using locating screws to ensure the correct location. Approximately 1 mL hydrogel was injected in the defect core using a 21g needle. Three groups were studied (n=5-6 per group): 1) untreated bone defects (sham/empty); 2) acellular composite hydrogels formed of RGD-alginate/RGD-hyaluronate with biomineralized microspheres; or 3) autologous MSCs ($10x10^6$ cells/mL) delivered in composite hydrogels with biomineralized microspheres. Groups were

assigned to the right and left iliac wings to evenly distribute pairs of groups and obtain a balanced experimental design. The periosteum, muscle, and skin were sutured over the iliac crest in layers immediately after the defect filling. After surgery, the animals were allowed to recover and move freely. Animals received an intramuscular injection of banamine (1.0-2.2 mg/kg) postoperatively once a day for 5 days and then as needed for pain control.

6.2g Assessment of bone healing

Radiographs of the sheep ilium were taken at 12 weeks after the surgery to qualitatively assess bone regeneration, while microcomputed tomography (microCT) was performed at 12 weeks from bone explants to quantitatively evaluate bone healing. The original defect site was harvested by collecting a 20 mm diameter and 5-13 mm long bone core cylinder, fixed in formalin overnight and moved to 70% ethanol, and samples with a 15 mm region of interest (ROI) were imaged at 15 μm resolution (70 kVp, 114 μA, 300 ms integration time, average of 3 images) using a high-resolution microCT scanner (μCT 35, Scanco Medical; Brüttisellen, Switzerland). Bone tissue in the reconstructed images was determined by thresholding (191-3000 mg HA/cc) to partition mineralized tissue from fluid and soft-tissues, and bone volume fraction (BVF) and bone mineral density (BMD) were calculated from the images.

After imaging, scaffolds were demineralized (Calciclear, National Diagnostics) overnight, bisected, paraffin-embedded, and sectioned at 5 μm for staining with H&E. Vascularization within the defect area was assessed from H&E-stained sections by counting circular structures with well-defined lumens containing erythrocytes at 100X magnification.[23] Blood vessels were quantified from 3 distinct slides of 4 treated iliac crests per group, and the presence of vessels was confirmed by immunostaining for von Willebrand factor (1:200, ab6994; Abcam). Tissue sections were also stained by Masson's trichrome to detect collagen deposition and osteoid as an indicator of new bone formation and Safranin O/Fast green to detect residual hydrogel.

6.2h Statistical analysis

Data are presented as mean ± standard deviation for at least three replicates. Statistical significance was assessed by Student's t-test, one-way ANOVA followed by a Tukey's post-hoc test for swelling and mechanical testing, or two-way ANOVA with Bonferroni post-hoc testing for calcium and ALP when appropriate. Statistical analysis was performed using GraphPad Prism® 8 analysis software (GraphPad Software, San Diego, CA). *p*-values < 0.05 were considered statistically significant.

6.3 RESULTS

6.3a Biophysical properties of composite hydrogels are composition dependent

Gross morphological dimensions and swelling ratio of hydrogels were similar, regardless of composition (**Fig. 6.1A, 6.1E**). RGD conjugation was more efficient on alginate than on hyaluronate, demonstrated by a significant reduction (~40%) in RGD concentration on the backbone of hyaluronate gels (**Fig. 6.1B**). RGD conjugation to alginate and hyaluronate was verified by ^{1}H NMR, which detected characteristic proton peaks at 2.8 and 3.2 ppm for aspartic acid and arginine, respectively (**Fig. 6.1C-D**). Pure polymers did not exhibit the presence of these peaks. The addition of hyaluronate, regardless of RGD modification, significantly reduced the compressive modulus compared to RGD-alginate gels alone (Fig. 1F). Quantification of degradation of MSC-containing hydrogels *in vitro* demonstrated a rapid mass loss over the first 7 days in culture that remained constant over the remaining 28 days (**Supplementary Fig. 6.3A**).

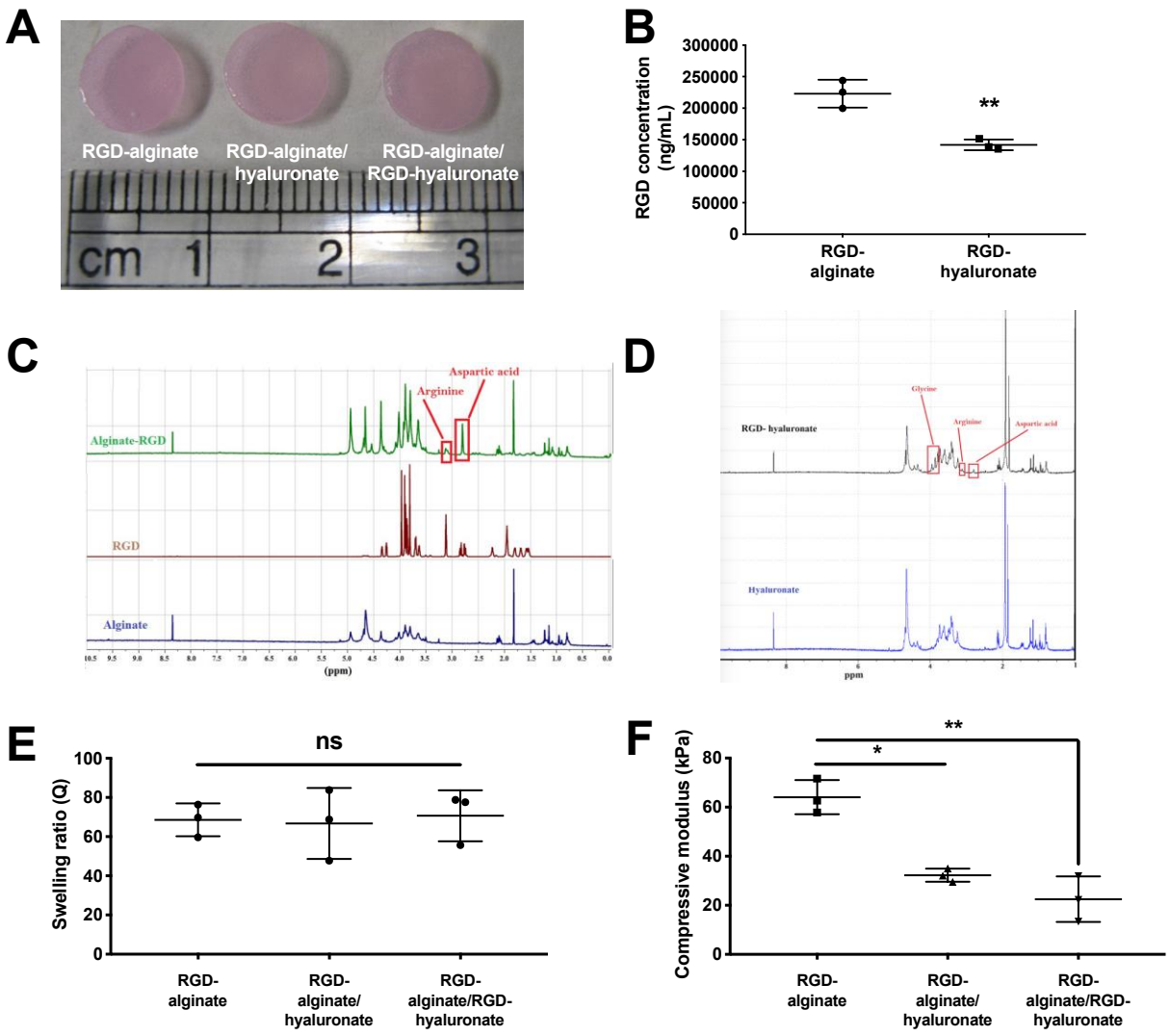

Figure 6.1. Morphologic and mechanical characterization of composite hydrogels formed of alginate, hyaluronate, and biomineralized microspheres. (A) Macroscopic morphology of ionically crosslinked cellular hydrogel disks in culture medium after 24 h. **(B)** Quantification of RGD concentration in RGD-alginate or RGD-hyaluronate (n=3; ***p*<0.01). ^{1}H NMR spectra of RGD-modified **(C)** alginate and **(D)** hyaluronate. **(E)** Swelling ratio in deionized water and **(F)** compressive moduli (**p*<0.05, ***p*<0.01; n=3).

6.3b In vitro osteogenic response of entrapped MSCs

Ovine MSCs exhibited trilineage potential by differentiation toward the osteoblastic, chondrogenic, and adipogenic lineages when maintained in lineage-specific media for 3 weeks (**Supplementary Fig. 6.2A**). MSCs also expressed characteristic cell surface markers when analyzed by flow cytometry (CD90+CD105+CD44+CD45-) (**Supplementary Fig. 6.2B**).

Intracellular ALP activity was significantly increased for all gels over 3 weeks in culture (**Fig. 6.2A**). MSCs entrapped within RGD-alginate/RGD-hyaluronate exhibited the most rapid increase in ALP activity, which was higher than the other groups at day 14 and higher than RGD-alginate/hyaluronate at day 21. MSCs entrapped in RGD-alginate exhibited a significant increase in ALP activity from day 14 and beyond compared to day 1, ultimately reaching a level 80% of MSCs in RGD-alginate/RGD-hyaluronate. MSCs in RGD-alginate/hyaluronate demonstrated a more cyclical ALP expression profile, reaching the highest level at 3 weeks. For calcium deposition, we observed non-significant increases by MSCs in all gels over time (**Fig. 6.2B**). MSCs entrapped in RGD-alginate/RGD-hyaluronate gels exhibited the greatest and only statistically significant increase in calcium at week 3. MSCs entrapped in RGD-alginate/RGD-hyaluronate gels secreted nearly 19-fold more calcium at 3 weeks relative to Day 1 values. DNA content, an indicator of cell number, increased in all gels over three weeks, yet we did not observe differences in DNA content after 3 weeks in culture (*data not shown*). Microspheres appeared randomly distributed and could be observed throughout the hydrogels after 21 days in culture (**Fig. 6.2C**). Positive staining for osteocalcin further confirmed that entrapped MSCs were undergoing osteogenic differentiation (**Fig. 6.2D**). MSCs remained viable and spread in all gels, with apparent increases in spreading by MSCs in RGD-alginate/RGD-hyaluronate hydrogels (**Fig. 6.3A, B**). In light of increases in early and late osteogenic markers by MSCs entrapped in RGD-alginate/RGD-hyaluronate hydrogels containing biomineralized microspheres, we selected this single formulation for examination in the ovine iliac crest defect.

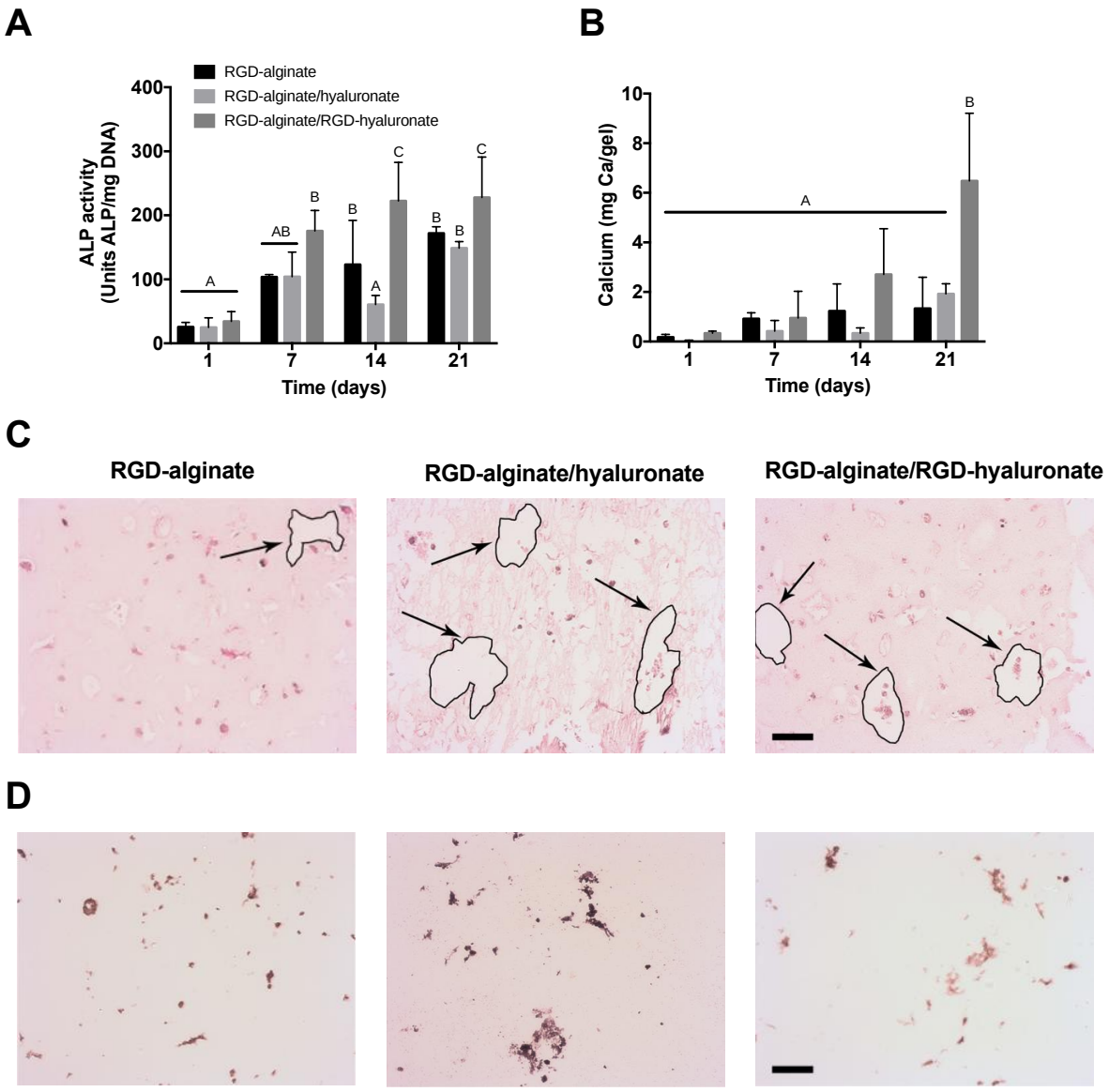

Figure 6.2. Quantification of *in vitro* osteogenic potential. (A) ALP activity and **(B)** total calcium deposition by ovine MSCs entrapped in RGD-alginate, RGD-alginate/hyaluronate, and RGD-alginate/RGD-hyaluronate composite gels over 3 weeks (n=3 for ALP activity, n=4 for total calcium; bars that are statistically different from one another do not share a letter). **(C)** H&E and **(D)** osteocalcin staining of gels after 21 days in culture. Arrows and outlines denote location and shape of microspheres, respectively. Scale bar = 50 µm.

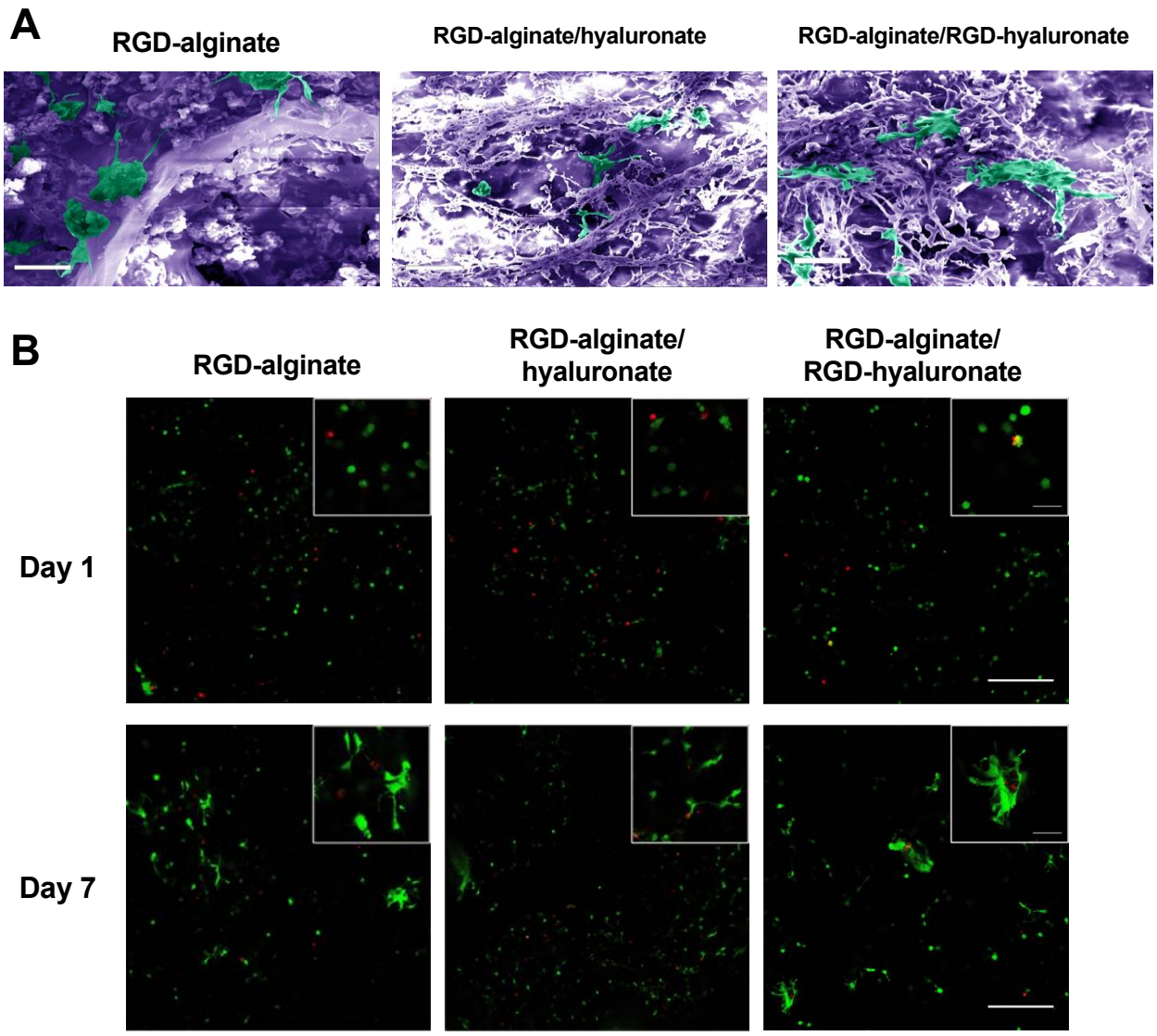

Figure 6.3. Ovine MSCs spread and are viable in composite hydrogels (A) False-colored SEM images of MSCs in RGD-alginate, RGD-alginate/hyaluronate, and RGD-alginate/RGD-hyaluronate composite hydrogels (150X) after 21 days in culture. Ovine MSCs are highlighted in green, while purple indicates hydrogel scaffold. Scale bar = 100 µm. **(B)** Live/dead staining of MSCs entrapped in RGD-alginate, RGD-alginate/hyaluronate, and RGD-alginate/RGD-hyaluronate composite gels over 7 days visualized by confocal microscopy reveal increased spreading in RGD-alginate and RGD-alginate/RGD-hyaluronate at 7 days. Scale bars of original images and inserts are 250 and 50 µm, respectively.

6.3c Assessment of iliac crest bone healing

Locating screws were placed adjacent to the defect at the time of surgery to observe repair from a consistent position. New bone formation within the defect was observed in all animals (**Fig. 6.4A**). The untreated sheep showed minimal bone formation within the defect, while defects treated with acellular or MSC-containing RGD-alginate/RGD-hyaluronate gels consistently exhibited formation of new tissue.

Bone explants were harvested to assess the extent of new bone formation by microCT (**Fig. 6.4B**). Images of the explants confirm more bone formation occurred in acellular and MSC-loaded composite hydrogels compared to untreated defects. When quantified, we detected significant increases in bone volume fraction for defects treated with MSC-containing composite gels compared to acellular hydrogels or sham-treated defects (**Fig. 6.4C**). Bone volume fraction within the defect was similar for sham and acellular hydrogel-treated defects. Similar trends were observed when quantifying bone mineral density (BMD) in the bone defects (**Fig. 6.4D**).

Tissue formation was further evaluated by histological evaluation of 12-week tissue explants. We detected significant increases in vascular density of defects treated with MSC-laden constructs compared to acellular gels or sham-treated defects (**Fig. 6.5A, 6.5B**). Clear differences in tissue formation were evident between treatment groups following H&E (**Fig. 6.5C**) and trichrome staining (**Fig. 6.5D**) when evaluating the entire defect site, with numerous visible areas of osteoid and dense connective tissue.

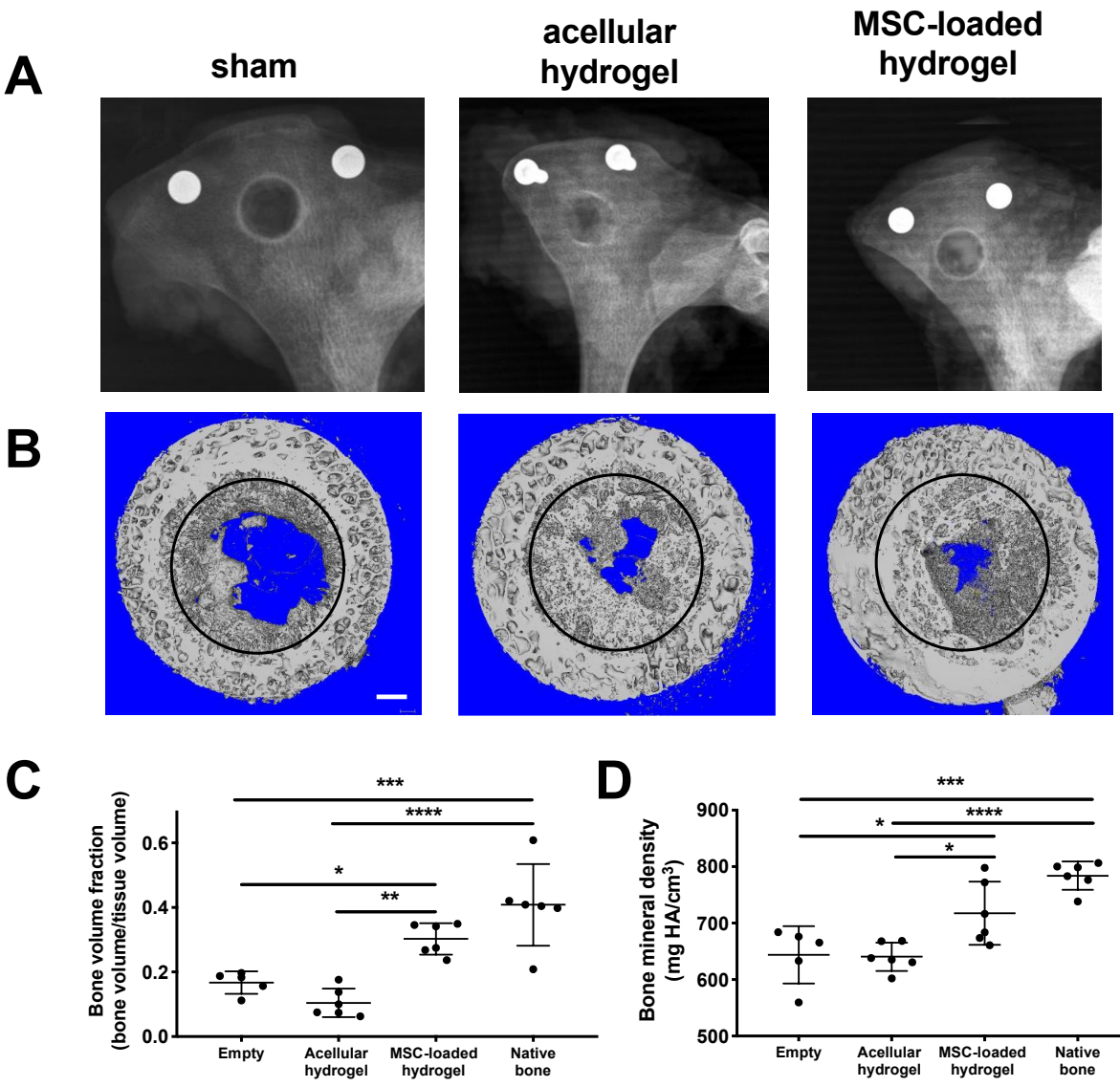

Figure 6.4. Bone formation in iliac crest defects is increased with MSC-laden composite hydrogels. (A) Representative radiographs of the ovine iliac crest *in vivo* when left untreated (sham) or treated with acellular or MSC-containing RGD-alginate/RGD-hyaluronate composite hydrogels. **(B)** Representative high resolution microCT images of explants at 12 weeks. Circles denote repair tissue within the 15 mm surgical defect. Scale bar = 2 mm. **(C)** Bone volume fraction and **(D)** bone mineral density within the tissue defects (N=5-6 per group). *p<0.05, **p<0.01, ***p<0.001, ****p<0.0001.

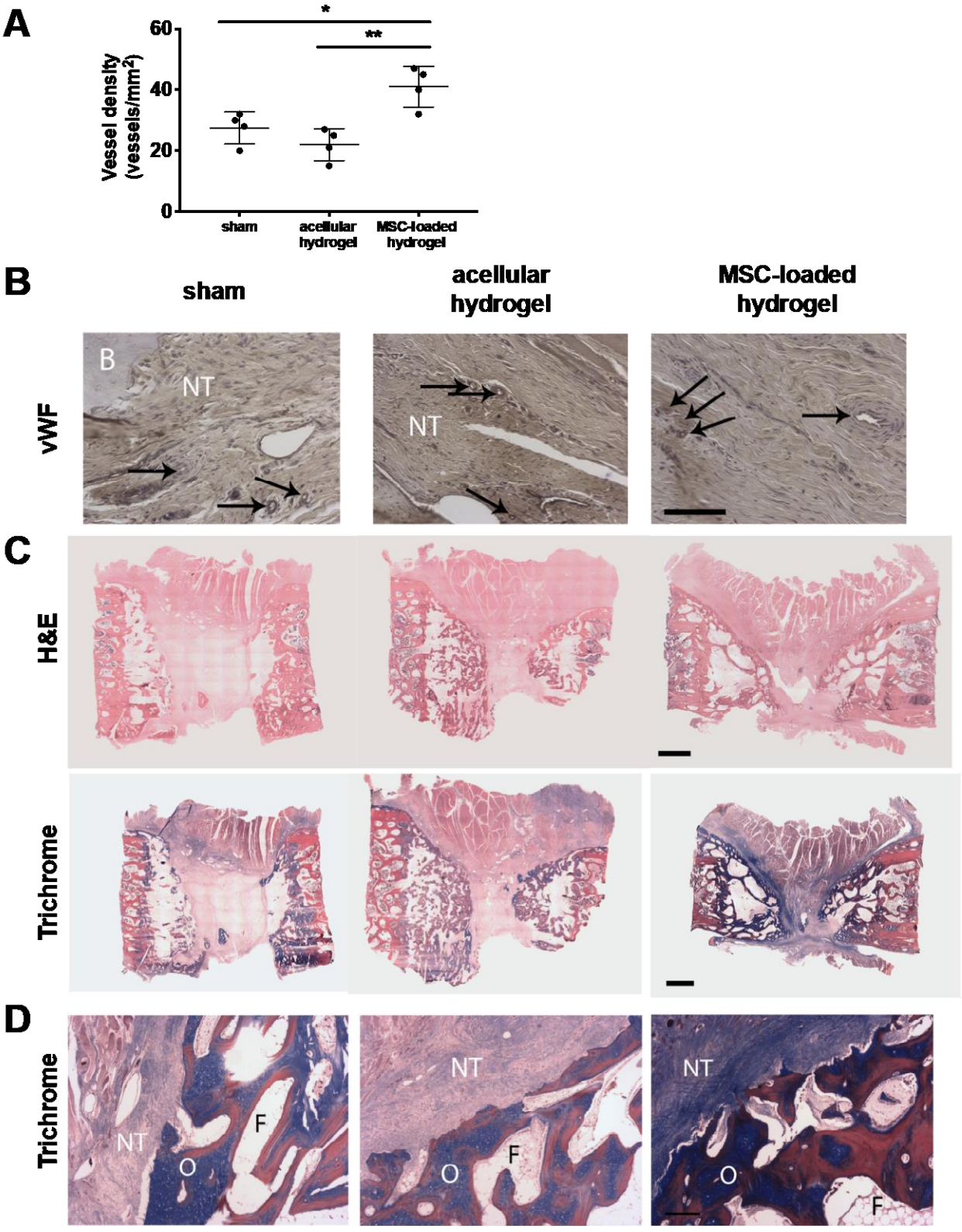
A
Vessel density (vessels/mm²)
60
40
20
0
*
**
sham
acellular hydrogel
MSC-loaded hydrogel
B
sham
acellular hydrogel
MSC-loaded hydrogel
vWF
B
NT
NT
C
H&E
Trichrome
D
Trichrome
NT
O
F
NT
O
F
NT
O
F

Figure 6.5. Tissue formation is enhanced with MSC-loaded composite hydrogels. (A) Quantification of vessel density within repair tissue at 12 weeks (N=4, *p<0.05, **p<0.01). **(B)** Representative vWF staining of explants at 20X magnification. Arrows denote vessels; scale bar = 100 µm. **(C)** Representative H&E (top) and Masson's trichrome staining (bottom) of entire explants in cross-section. Osteoid is visible in dark pink, collagen fibers are stained blue, and native bone tissue is visible in red. Scale bar = 5 mm. **(D)** Higher magnification of Masson's trichrome-stained sections. B= bone, O = osteoid, F = fat, NT = new tissue. Scale bar = 100 µm.

Higher magnification images of the explants confirmed increased tissue formation and osteoid staining in MSC-loaded hydrogels compared to control or sham defects (**Fig. 6.5D**). Collagen fibers, visualized in blue by Masson's trichrome staining, were apparent in all explants. Osteoid formation (dark pink staining) was strongly evident in MSC-laden hydrogels, while more dense, organized tissue was appreciated in defects treated with acellular hydrogels compared to sham controls. Residual hydrogel was not detected in either acellular and MSC-loaded composite hydrogels, as indicated by Safranin O/Fast green staining (**Supplementary Fig. 6.3B**), and we observed no histological evidence of a persistent inflammatory response.

6.4 DISCUSSION

Cell-based approaches to bone healing require the transplantation of cells in carriers that instruct desired cell fate and integrate with surrounding tissues. Hydrogels are ideal vehicles for cell transplantation due to their hydrated nature, tunability, and capacity to gel slowly in order to support cell survival. However, few hydrogels possess the necessary osteoconductive characteristics required to integrate with host bone and nucleate cell-secreted calcium in order to accelerate bone formation. The goal of this study was to test the hypothesis that supplementation of a composite hydrogel with biomineralized substrata would enhance hydrogel osteoconductivity,

promote osteogenic differentiation of MSCs, and enhance bone formation in an ovine iliac crest bone defect.

Herein, we describe the development and characterization of composite hydrogels formed of RGD-modified alginate and hyaluronate and containing apatite-coated polymeric microspheres. The swelling ratio, an indicator of the capacity of hydrogels to imbibe water, was not affected by the addition of hyaluronate to alginate hydrogels. However, we detected a significant decrease in the elastic modulus of alginate gels upon addition of hyaluronate. Bone-associated therapies often require stiffer materials, and hydrogels possessing greater elastic moduli are effective for inducing MSCs towards the osteoblastic lineage.[24,25] However, the addition of hyaluronate to this system compensated for the slight reduction in modulus through its other chemical properties that promote osteogenesis. While degradation and associated reductions in mechanical properties were evident after 7 days, we observed a stable and even small increase in dry weight of the hydrogel after 28 days, suggesting that cells were depositing new ECM that compensated for hydrogel degradation.

The hydrophilic nature of alginate does not permit protein adsorption or cell adhesion and requires the covalent incorporation and presentation of adhesion ligands such as RGD. The RGD sequence is the cell attachment site of a large number of adhesive extracellular matrix and cell surface proteins, and nearly half of the over 20 known integrins recognize this sequence in their adhesion protein ligands.[26] RGD modification of hyaluronate was less efficient than alginate (~40%), making the total RGD concentration inconsistent and representing a limitation of our study. However, the small overall volume contribution of hyaluronate used in the composite gel represents a relatively small difference in overall RGD content. Using covalently crosslinked polyethylene glycol hydrogels, increases in RGD concentration correlated with increases in MSC osteogenic differentiation.[27] Similar results were reported for murine and human MSCs in covalently crosslinked alginate gels.[28] However, the gels studied herein were ionically crosslinked and possess dynamic mechanical properties that cells sense, together with ligand

concentration, to undergo osteogenic differentiation.[29] When studying ionically crosslinked alginate gels, adhesion and cell proliferation were increased with increasing RGD concentration, but the dose dependence of osteogenic differentiation on RGD concentration was not reported[30]. In this study, we observed increased osteogenic differentiation in composite gels presenting similar RGD concentrations but weaker mechanical properties, further strengthening the beneficial role of hyaluronate in this system. Collectively, this suggests that differences in osteogenesis are derived from other aspects of the composite hydrogel.

Hyaluronate can also function as a cell adhesion molecule, and CD44 can participate in hyaluronate recognition.[31] CD44 is a cluster of differentiation protein commonly used to identify MSCs[16] and enables MSCs to adhere to hyaluronate. Flow cytometry confirmed that ovine MSCs express CD44, providing an additional opportunity for entrapped MSCs to engage both polymers in the composite gel. However, outside of CD44, hyaluronate is unable to engage other cell receptors or integrins, severely limiting its ability to promote adhesion and enable mechanotransduction to regulate MSC phenotype. To enhance adhesivity in composite gels, we covalently modified both polymers with RGD. Robust cell spreading and viability by MSCs in these composite gels, together with increases in early and late osteogenic markers by ovine MSCs, demonstrate the cooperative effects of integrin and CD44 engagement and are in agreement with other studies using RGD-modified hyaluronate gels.[32,33] We hypothesize that MSCs bind to both polymers more uniformly when entrapped in RGD-alginate/RGD-hyaluronate compared to RGD-alginate/hyaluronate (**Fig. 6**). The composite gel was ionically crosslinked using divalent calcium ions, physically entrapping the hyaluronate within the crosslinked alginate network. The long-term stability of hyaluronate within this composite hydrogel is unknown and represents an area of future investigation.

To enhance the limited osteoconductivity of this hydrogel formulation, we incorporated polymer microspheres coated with bone-like mineral within the hydrogel to act as a calcium nucleation site. Coating of synthetic polymers such as PLG with carbonated apatite alters cell

spreading in 2D[34] and enhances osteoconductivity in 3D porous scaffolds[35]. The addition of mineralized microspheres facilitates a more homogenous distribution of osteoconductive material within the hydrogel compared to pure ceramics that partition rapidly due to differences in density. Biomineralized microspheres were previously added to fibrin hydrogels to enhance osteoconductivity, evidenced by significant increases in both calcium and phosphate over 3 weeks when entrapped with human MSCs.[14] In this study, the incorporation of RGD-hyaluronate into the composite hydrogel significantly increased early and late markers of osteogenic differentiation by MSCs *in vitro* compared to RGD-alginate/hyaluronate or RGD-

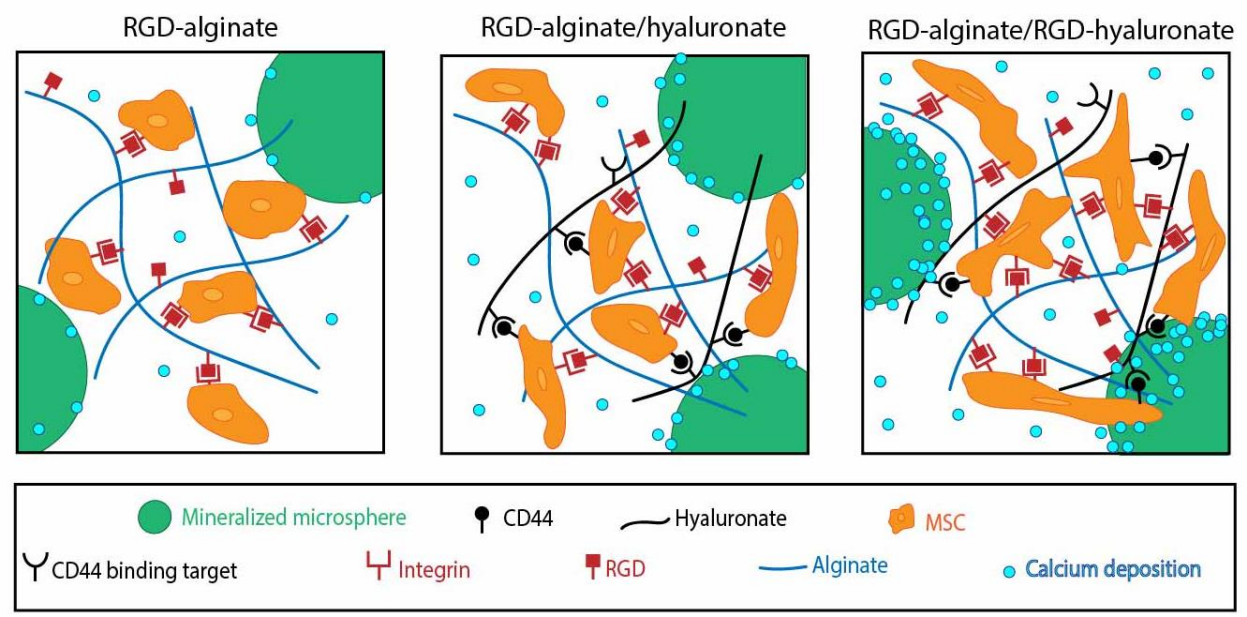

Figure 6.6. Proposed interaction of MSCs with RGD-alginate/RGD-hyaluronate composite hydrogels. MSCs engage the RGD adhesive motif on both polymers using various integrins, while also binding to hyaluronate using CD44. MSCs secrete calcium, which is nucleated by entrapped biomineralized microspheres, thereby enhancing hydrogel osteoconductivity and resultant bone formation.

alginate alone. These data are in good agreement with the response of human MSCs to fibrin gels containing biomineralized microspheres[14] and provide a more tunable platform for use in the development of injectable biomaterials for cell transplantation.

The translation of effective tissue engineering approaches for bone healing toward human patients requires their examination in large animal models.[36] In this study, we selected an ovine model of bone healing due to its specific advantages over other large animal models such as the iliac bone dimensions, ease of handling, and calm nature. The site of the bone defect in the iliac crest is effectively non-load bearing, potentially limiting the characterization of bone healing in this model. Bone defects treated with acellular or MSC-laden composite gels were filled with densely packed, cellular and mineralized tissue. We previously studied the capacity of acellular osteoconductive fibrin gels, formed by the incorporation of biomineralized microspheres, to promote healing of a rat critical-sized calvarial bone defect.[14] Acellular biomineralized microsphere-loaded fibrin gels did not increase bone formation compared to fibrin gels without microspheres, demonstrating that biomineralized microspheres are ineffective without the co-transplantation of MSCs. Compared to acellular composite gels in this iliac crest bone defect, we observed significantly greater bone volume in defects treated with MSC-laden composite gels. The treatment of bone defects with acellular composite gels did not yield significant increases in bone volume compared to untreated defects. We are unable to discern whether transplanted autologous MSCs differentiated to osteoblasts to contribute directly to bone formation, or if they induced the migration and differentiation of host progenitor cells and osteoblasts to repair the defect through the MSC secretome. Importantly, none of the animals exhibited a sustained inflammatory response to the material, demonstrating its safety for use in this model. However, bridging was incomplete at 12 weeks, suggesting that additional time is necessary to fully heal this defect.

The formation of a functional vasculature plays a pivotal role in skeletal development and bone repair, and inadequate vascularization delays bone graft regeneration.[37] Implantation of

MSCs for bone formation exhibited increased vascularization compared to acellular implants or sham-treated animals[38–40], confirming the proangiogenic potential of MSCs. Although we did not explicitly characterize the secretome of ovine MSCs, numerous studies have reported increased vascularization of defect sites treated with MSCs from various species, and the paracrine effects of MSCs are an important contribution of these cells in tissue regeneration. Defects treated with acellular hydrogels had similar vascular densities as untreated defects, suggesting that the hydrogel alone possesses little proangiogenic potential. Osteoid was evident in defects treated with both acellular or MSC-containing hydrogels, further demonstrating the osteoconductive nature of these composite hydrogels. Defects treated with MSC-laden hydrogels contained substantially more osteoid than acellular hydrogels or untreated defects. We observed considerably more collagen present in defects treated with MSCs in composite hydrogels versus acellular gels or untreated defects. The collective assessments of radiography, microCT, and histology confirm that MSC-laden composite hydrogels containing biomineralized microspheres accelerate bone formation in this ovine iliac bone defect.

6.5 CONCLUSION

The results of this study demonstrate, for the first time, that injectable composite hydrogels formed of two natural peptide-modified polymers and containing biomineralized microspheres, possess enhanced osteoconductivity, osteogenic potential, and can speed bone formation in a large preclinical animal model. When used to transplant autologous MSCs, this composite hydrogel significantly enhanced neovascularization and bone formation compared to acellular gels, demonstrating its utility as an injectable cell delivery vehicle. These data also reveal that, despite modest adhesivity of MSCs imparted by hyaluronate in this composite gel, osteogenic differentiation was enhanced by coupling the adhesive RGD tripeptide to its backbone. In light of these findings and its contribution to connective tissue homeostasis, the incorporation of

hyaluronate into this osteoconductive hydrogel provides advantages for consideration of future platforms designed to promote bone healing.

6.6 REFERENCES

[1] J. Ma, S.K. Both, F. Yang, F.Z. Cui, J. Pan, G.J. Meijer, J.A. Jansen, J.J. van den Beucken, Concise review: cell-based strategies in bone tissue engineering and regenerative medicine, Stem Cells Transl Med. 3 (2014) 98–107.

[2] J.K. Leach, J. Whitehead, Materials-directed differentiation of mesenchymal stem cells for tissue engineering and regeneration, ACS Biomater Sci Eng. 4 (2018) 1115–1127.

[3] D.A. Foyt, M.D.A. Norman, T.T.L. Yu, E. Gentleman, Exploiting advanced hydrogel technologies to address key challenges in regenerative medicine, Adv Healthc Mater. 7 (2018) e1700939.

[4] Y.S. Zhang, A. Khademhosseini, Advances in engineering hydrogels, Science (80). 356 (2017) eaaf3627.

[5] L.M. Marquardt, S.C. Heilshorn, Design of injectable materials to improve stem cell transplantation, Curr Stem Cell Rep. 2 (2016) 207–220.

[6] U. Hersel, C. Dahmen, H. Kessler, RGD modified polymers: biomaterials for stimulated cell adhesion and beyond, Biomaterials. 24 (2003) 4385–4415.

[7] C.B. Highley, G.D. Prestwich, J.A. Burdick, Recent advances in hyaluronic acid hydrogels for biomedical applications, Curr Opin Biotechnol. 40 (2016) 35–40.

[8] E.A. Makris, A.H. Gomoll, K.N. Malizos, J.C. Hu, K.A. Athanasiou, Repair and tissue engineering techniques for articular cartilage, Nat Rev Rheumatol. 11 (2015) 21–34.

[9] H. Park, K.Y. Lee, Facile control of RGD-alginate/hyaluronate hydrogel formation for cartilage regeneration, Carbohydr Polym. 86 (2011) 1107–1112.

[10] H. Park, H.J. Lee, H. An, K.Y. Lee, Alginate hydrogels modified with low molecular weight hyaluronate for cartilage regeneration, Carbohydr Polym. 162 (2017) 100–107.

[11] L. Jongpoiboonkit, T. Franklin-Ford, W.L. Murphy, Mineral-coated polymer microspheres for controlled protein binding and release, Adv Mater. 21 (2009) 1960–1963.

[12] S.W. Kang, H.S. Yang, S.W. Seo, D.K. Han, B.S. Kim, Apatite-coated poly(lactic-co-glycolic acid) microspheres as an injectable scaffold for bone tissue engineering, J Biomed Mater Res Part A. 85a (2008) 747–756.

[13] E. Saito, D. Suarez-Gonzalez, W.L. Murphy, S.J. Hollister, Biomineral coating increases bone formation by ex vivo BMP-7 gene therapy in rapid prototyped poly(L-lactic acid) (PLLA) and poly(epsilon-caprolactone) (PCL) porous scaffolds, Adv Healthc Mater. 4 (2015) 621–632.

[14] H.E. Davis, B.Y. Binder, P. Schaecher, D.D. Yakoobinsky, A. Bhat, J.K. Leach, Enhancing osteoconductivity of fibrin gels with apatite-coated polymer microspheres, Tissue Eng Part A. 19 (2013) 1773–1782.

[15] M. Dominici, K. Le Blanc, I. Mueller, I. Slaper-Cortenbach, F. Marini, D. Krause, R. Deans, A. Keating, D. Prockop, E. Horwitz, Minimal criteria for defining multipotent mesenchymal stromal cells. The International Society for Cellular Therapy position

statement, Cytotherapy. 8 (2006) 315–317.

[16] M.F. Pittenger, A.M. Mackay, S.C. Beck, R.K. Jaiswal, R. Douglas, J.D. Mosca, M.A. Moorman, D.W. Simonetti, S. Craig, D.R. Marshak, Multilineage potential of adult human mesenchymal stem cells, Science (80). 284 (1999) 143–147.

[17] H.E. Davis, R.R. Rao, J. He, J.K. Leach, Biomimetic scaffolds fabricated from apatite-coated polymer microspheres, J Biomed Mater Res A. 90 (2009) 1021–1031.

[18] S. Cohen, T. Yoshioka, M. Lucarelli, L.H. Hwang, R. Langer, Controlled delivery systems for proteins based on poly(lactic/glycolic acid) microspheres, Pharm Res. 8 (1991) 713–720.

[19] T. Boontheekul, H.J. Kong, D.J. Mooney, Controlling alginate gel degradation utilizing partial oxidation and bimodal molecular weight distribution, Biomaterials. 26 (2005) 2455–2465.

[20] S.S. Ho, A.T. Keown, B. Addison, J.K. Leach, Cell migration and bone formation from mesenchymal stem cell spheroids in alginate hydrogels are regulated by adhesive ligand density, Biomacromolecules. 18 (2017) 4331–4340.

[21] H.E. Davis, S.L. Miller, E.M. Case, J.K. Leach, Supplementation of fibrin gels with sodium chloride enhances physical properties and ensuing osteogenic response, Acta Biomater. 7 (2011) 691–699.

[22] J.L. Lansdowne, D. Devine, U. Eberli, P. Emans, T.J.M. Welting, J.C.E. Odekerken, D. Schiuma, M. Thalhauser, L. Bouré, S. Zeiter, Characterization of an ovine bilateral critical sized bone defect iliac wing model to examine treatment modalities based on bone tissue engineering, Biomed Res. Int. (2014).

[23] A. Leu, S.M. Stieger, P. Dayton, K.W. Ferrara, J.K. Leach, Angiogenic response to bioactive glass promotes bone healing in an irradiated calvarial defect, Tissue Eng Part A. 15 (2009) 877–885.

[24] K.C. Murphy, M.L. Hughbanks, B.Y.K. Binder, C.B. Vissers, J.K. Leach, Engineered fibrin gels for parallel stimulation of mesenchymal stem cell proangiogenic and osteogenic Potential, Ann Biomed Eng. 43 (2015).

[25] A. Cipitria, K. Boettcher, S. Schoenhals, D.S. Garske, K. Schmidt-Bleek, A. Ellinghaus, A. Dienelt, A. Peters, M. Mehta, C.M. Madl, N. Huebsch, D.J. Mooney, G.N. Duda, In-situ tissue regeneration through SDF-1α driven cell recruitment and stiffness-mediated bone regeneration in a critical-sized segmental femoral defect, Acta Biomater. 60 (2017) 50–63.

[26] E. Ruoslahti, RGD and other recognition sequences for integrins, Ann Rev Cell Dev Bi. 12 (1996) 697–715.

[27] F. Yang, C.G. Williams, D.. Wang, H. Lee, P.N. Manson, J. Elisseeff, The effect of incorporating RGD adhesive peptide in polyethylene glycol diacrylate hydrogel on osteogenesis of bone marrow stromal cells, Biomaterials. 26 (2005) 5991–5998.

[28] N. Huebsch, P.R. Arany, A.S. Mao, D. Shvartsman, O.A. Ali, S.A. Bencherif, J. Rivera-

Feliciano, D.J. Mooney, Harnessing traction-mediated manipulation of the cell/matrix interface to control stem-cell fate, Nat Mater. 9 (2010) 518–526.

[29] O. Chaudhuri, L. Gu, D. Klumpers, M. Darnell, S.A. Bencherif, J.C. Weaver, N. Huebsch, H.P. Lee, E. Lippens, G.N. Duda, D.J. Mooney, Hydrogels with tunable stress relaxation regulate stem cell fate and activity, Nat Mater. 15 (2016) 326–334.

[30] E. Alsberg, H.J. Kong, Y. Hirano, M.K. Smith, A. Albeiruti, D.J. Mooney, Regulating bone formation via controlled scaffold degradation, J Dent Res. 82 (2003) 903–908.

[31] R.J. Peach, D. Hollenbaugh, I. Stamenkovic, A. Aruffo, Identification of hyaluronic acid binding sites in the extracellular domain of CD44, J Cell Biol. 122 (1993) 257–264.

[32] W.K. Xiao, R.Y. Zhang, A. Sohrabi, A. Ehsanipour, S.P. Sun, J. Liang, C.M. Walthers, L. Ta, D.A. Nathanson, S.K. Seidlits, Brain-mimetic 3D culture platforms allow investigation of cooperative effects of extracellular matrix features on therapeutic resistance in glioblastoma, Cancer Res. 78 (2018) 1358–1370.

[33] B.D. Cosgrove, K.L. Mui, T.P. Driscoll, S.R. Caliari, K.D. Mehta, R.K. Assoian, J.A. Burdick, R.L. Mauck, N-cadherin adhesive interactions modulate matrix mechanosensing and fate commitment of mesenchymal stem cells, Nat Mater. 15 (2016) 1297–1306.

[34] R.R. Rao, J. He, J.K. Leach, Biomineralized composite substrates increase gene expression with nonviral delivery, J Biomed Mater Res A. 94 (2010). doi:10.1002/jbm.a.32690.

[35] W.L. Murphy, C.A. Simmons, D. Kaigler, D.J. Mooney, Bone regeneration via a mineral substrate and induced angiogenesis, J Dent Res. 83 (2004) 204–210.

[36] A. Berner, J.C. Reichert, M.B. Muller, J. Zellner, C. Pfeifer, T. Dienstknecht, M. Nerlich, S. Sommerville, I.C. Dickinson, M.A. Schutz, B. Fuchtmeier, Treatment of long bone defects and non-unions: from research to clinical practice, Cell Tissue Res. 347 (2012) 501–519.

[37] S. Stegen, N. van Gastel, G. Carmeliet, Bringing new life to damaged bone: the importance of angiogenesis in bone repair and regeneration, Bone. 70 (2015) 19–27.

[38] K.C. Murphy, M.L. Hughbanks, B.Y. Binder, C.B. Vissers, J.K. Leach, Engineered fibrin gels for parallel stimulation of mesenchymal stem cell proangiogenic and osteogenic potential, Ann Biomed Eng. 43 (2015) 2010–2021.

[39] D. Mitra, J. Whitehead, O.W. Yasui, J.K. Leach, Bioreactor culture duration of engineered constructs influences bone formation by mesenchymal stem cells, Biomaterials. 146 (2017) 29–39.

[40] L. Wang, H. Fan, Z.Y. Zhang, A.J. Lou, G.X. Pei, S. Jiang, T.W. Mu, J.J. Qin, S.Y. Chen, D. Jin, Osteogenesis and angiogenesis of tissue-engineered bone constructed by prevascularized β-tricalcium phosphate scaffold and mesenchymal stem cells, Biomaterials. 31 (2010) 9452–9461.

6.7 SUPPLEMENTARY FIGURES

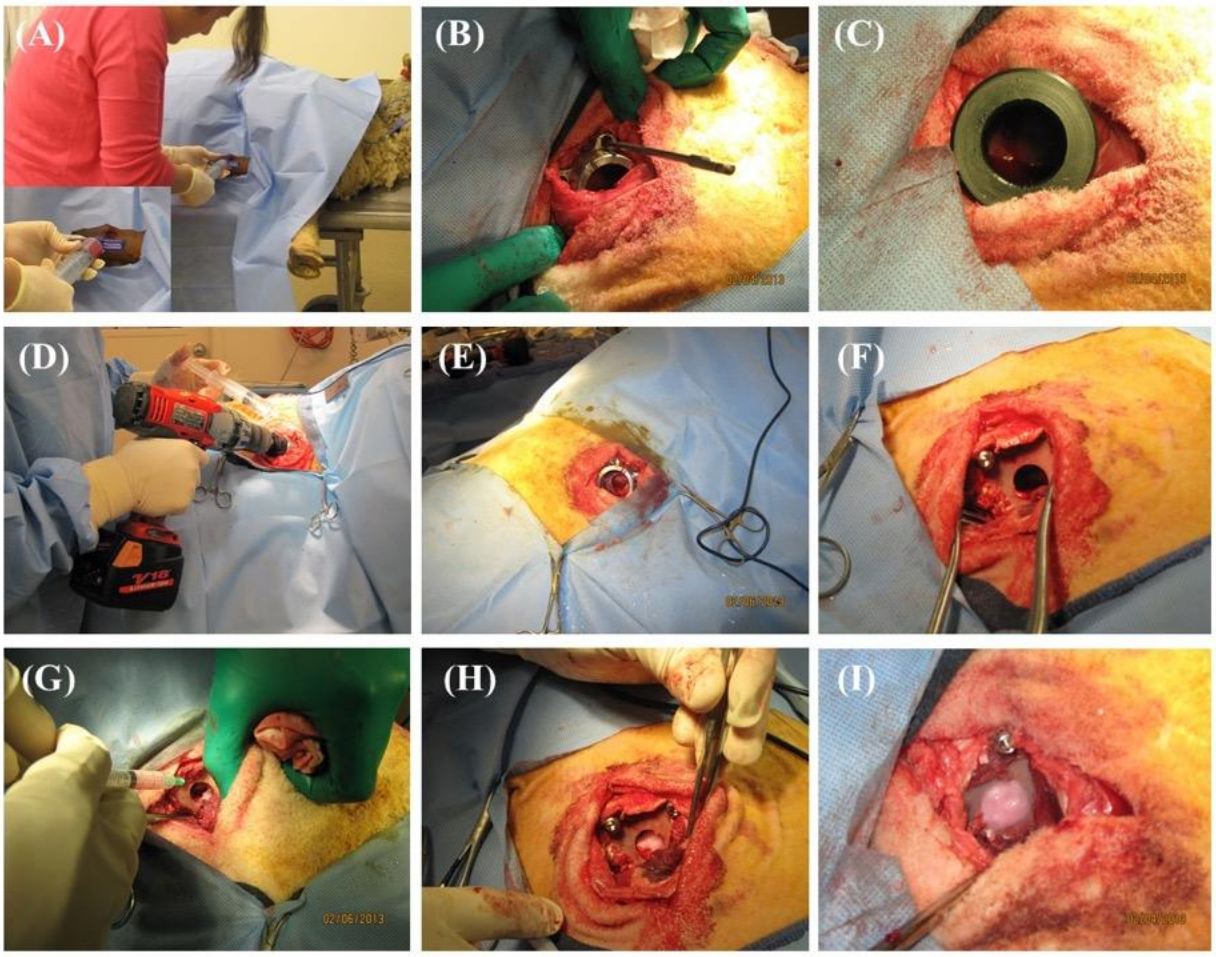

Supplementary Figure 6.1. (A) Bone marrow aspiration (60 mL) from the sternum was performed under general anesthesia. **(B-E)** Circular bone defects were created with a custom-made fixed jig and using the locating screws to ensure the correct location. A positioning jig was secured to each wing with 3 cortical bone screws, and bone defects were created using a 15 mm diameter coring device attached to a cordless drill. Sham-treated bone defects were left empty **(F)**, while other defects were immediately injected with acellular composite hydrogels or autologous MSCs in composite hydrogels **(G-I)**.

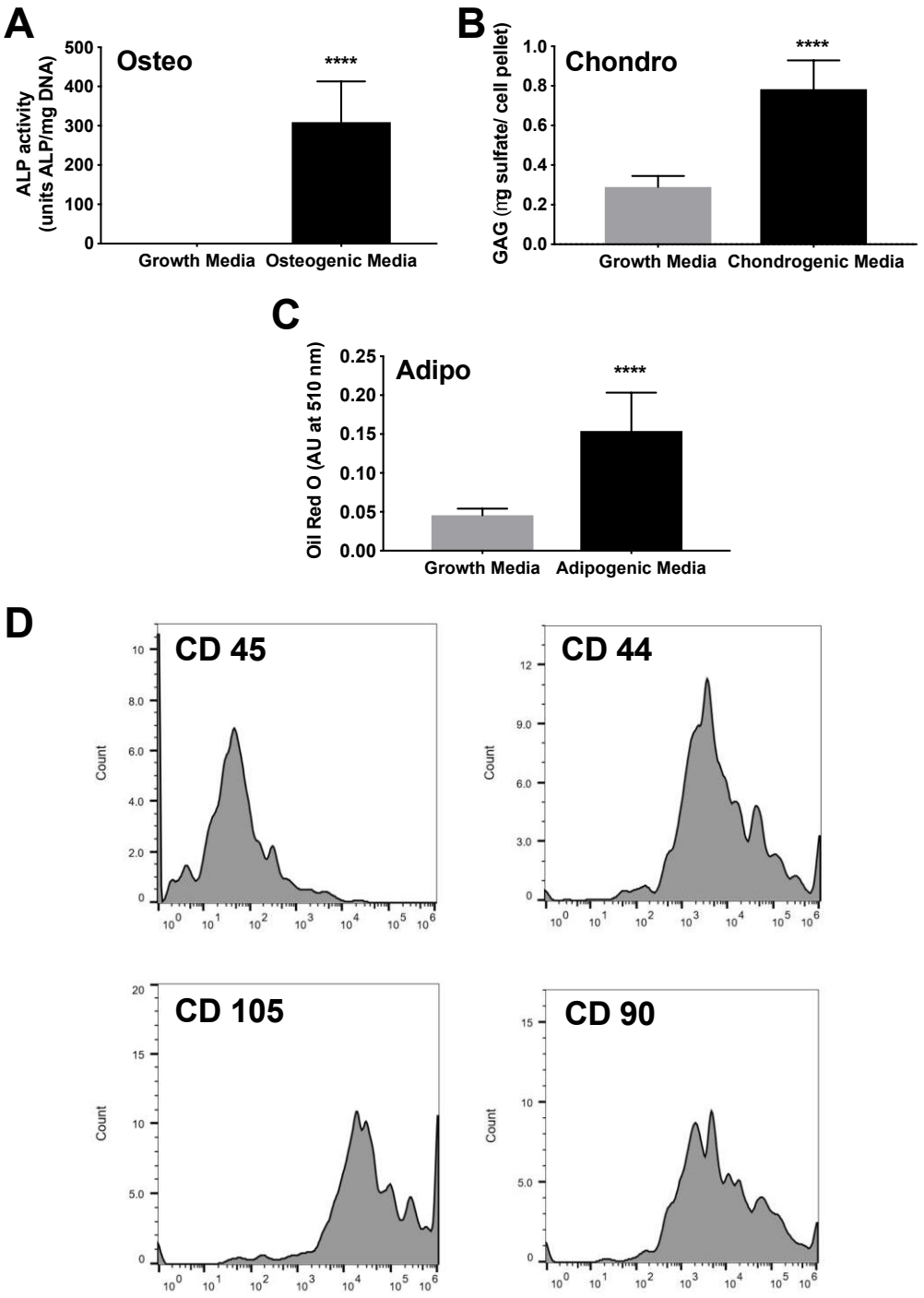

Supplementary Figure 6.2. Characterization of ovine MSCs. (A-C) Ovine MSCs exhibit expression of ALP activity (osteogenesis), sulfated glycosaminoglycan (chondrogenesis), and oil red O (adipogenesis) when maintained in lineage specific media for 3 weeks; ****p<0.0001. **(D)** The expression of cell surface markers on ovine MSCs was determined by flow cytometry.

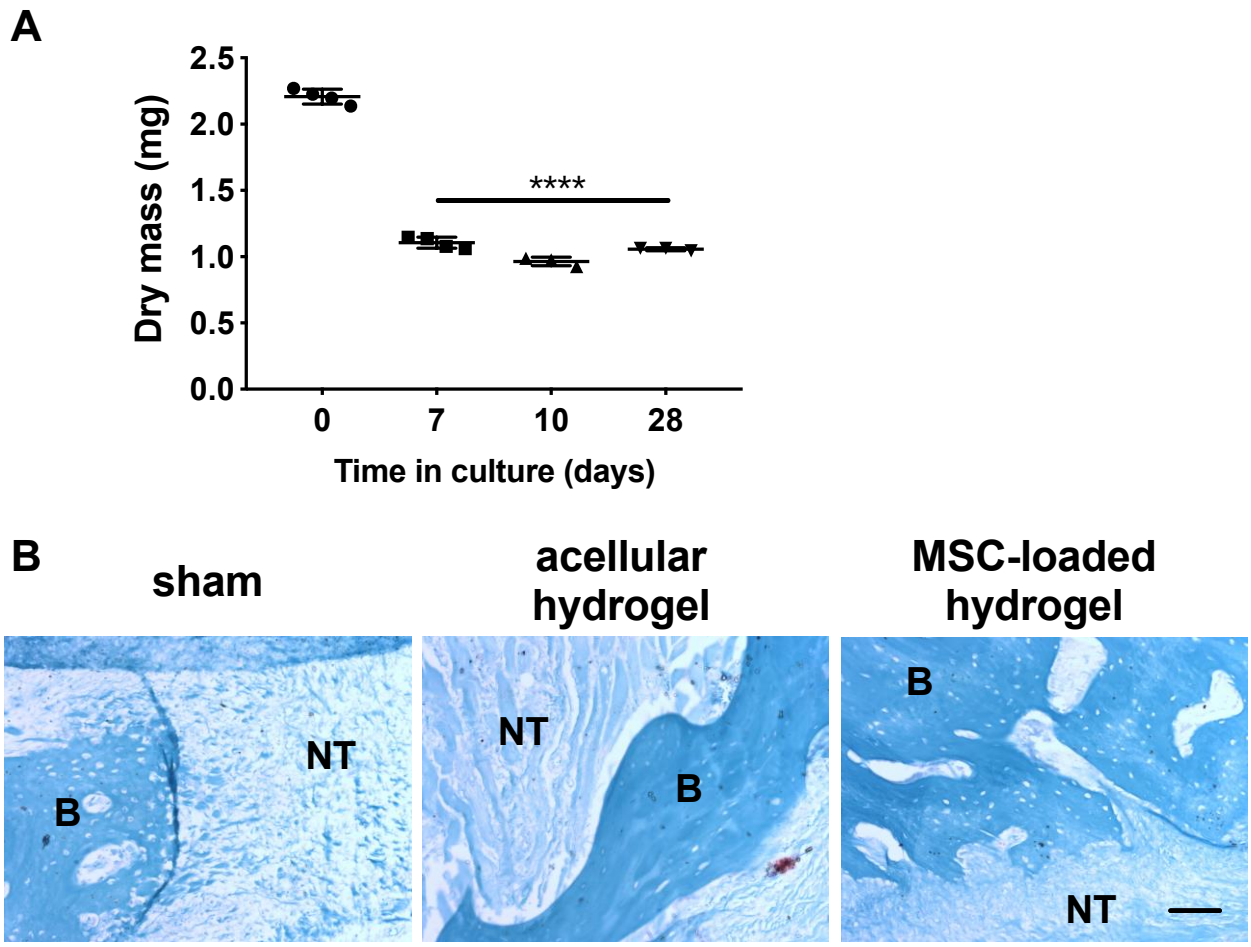

Supplementary Figure 6.3. Hydrogel degradation *in vitro* and *in vivo*. (A) Dry mass of MSC-loaded RGD-alginate/RGD-hyaluronate hydrogel over 28 days *in vitro*. ****p<0.0001, n=3-4. **(B)** Representative Safranin O/Fast green staining of tissue sections reveals no evidence of residual hydrogel at margins of implantation site after 12 weeks. B = bone, NT = new tissue. Scale bar = 100 µm.

CHAPTER 7: CONCLUSIONS AND FUTURE DIRECTIONS

7.1 A BRIEF HISTORY AND CURRENT STATE OF THE TISSUE ENGINEERING FIELD

Although a healthy human body possess the capacity to heal itself in many instances of injury, this is not always the case in large and complex wounds. This has been well understood early in human history and has motivated the formation of the tissue regeneration field. The first autologous skin grafts completed in 2500BC India are the earliest known evidence of tissue engineering within human history.[1] Modern tissue engineering approaches employing biomaterials began with the use of the first synthetic skin graft reported in 1962 from Chardack et al.[2] The field further matured with the implementation of the first cell-based tissue engineering approach described by Howard Green in 1981 utilizing expanded patient-derived keratinocytes for engraftment onto burn wounds.[3] Green's approach advanced the field on two significant fronts: 1) large-scale expansion of human cells in tissue culture, and 2) subsequent transplantation of these cells back to the patient. Although the tissue engineering field has expanded exponentially since these initial studies, it still leverages many similar tools and strategies for modern treatments. These are often referred to as the tissue engineering triad, which consists of biomaterials, cells, and either a mechanical, chemical, or biological signal to direct cell function towards regeneration (**Figure 7.1**).

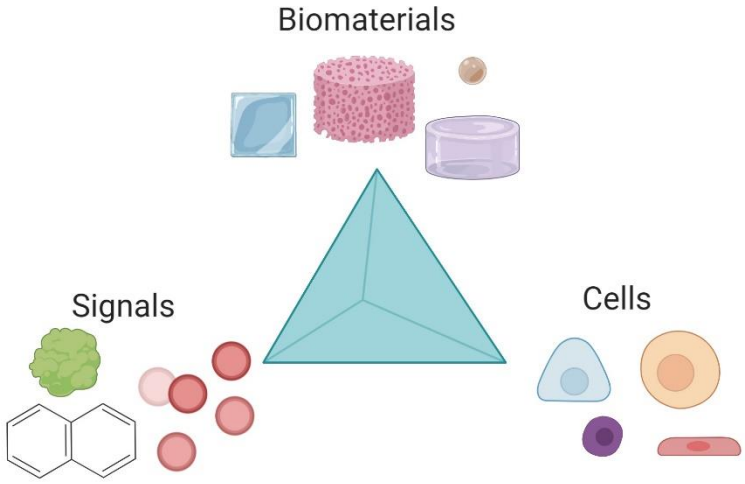

Figure 7.1: The tissue engineering Triad. The main tools of tissue engineering include cells, biomaterials, and signals.

The use of biomaterials within the field was initially motivated by instances in which autologous or cadaveric tissue was unavailable. The goal of the biomaterial was to serve as a structural support that would eventually be invaded and replaced by healthy tissue. Therefore, material biocompatibility became an important priority in biomaterial design to reduce immune or fibrotic response. This motivated Chardack to use sheets of polyvinyl alcohol (PVA) for synthetic skin grafts, as PVA has a fast degradation rate and supports limited cell and protein adhesion.[4] In more recent years there has been a pivot from the desire to have a completely bioinert material to investigation into bioactive materials that can direct cellular function. In many ways, biomaterials attempt to replicate the function of the extracellular matrix (ECM), a natural cell secreted substrate that promotes cell viability and function. ECM has been utilized as a biomaterial in the form of decellularized extracellular matrix (dECM), and has shown increasing promise within the tissue engineering field due to its ability to have an active influence on the regeneration process, promoting cell adhesion, proliferation, and differentiation.[5, 6] However, there are many obstacles to overcome before dECM could be applied as a prevalent and sucessful tissue regeneration strategies in the clinic. These include the labor-intensive process of producing dECM, the inconsistencies in production of ECM due to cell environment and decellularization method, as well as a vast gap in knowledge within the field of the interactions that occur between ECM, cells, and the *in vivo* microenvironment.[7] Currently, a small intestinal submucosa (SIS) dECM product is available for use in the clinic that has shown some success. However, studies have shown that it causes a substantial inflammation response, its remodeling within the body is variable and poorly understood, and the reoperation rate is 10% or higher.[8]

Alternatively, engineered ECM mimetics are a more readily available option that can replicate specific characteristics of ECM while limiting the complexity and inconsistency. Numerous materials have been utilized as ECM mimetics, including the isolated use of specific ECM polymers, such as collagen, hyaluronan, and fibrin; or a blank slate polymer that can be modified with a biologically relevant peptide or functional group, for example polyethylene glycol, poly (l-

lactic acid), and alginate. Within this thesis, we explore the use of alginate as an ECM mimetic. We can modify a vast array of different biological characteristics onto alginate, making it a highly tunable and valuable platform. Within this work, we conjugated alginate with an arginylglycylaspartic acid (RGD) peptide, that replicates the cell adhesion site on the ECM molecule fibronectin. Alginate was oxidized to make the polymer hydrolytically labile and allow the material to degrade within the body over time, similar to how biological components of the ECM are broken down by proteases. Alginate was further modified with sulfate groups to mimic the glycosaminoglycan component of the ECM and enable the sequestration of cell secreted growth factors. Within these studies, we have shown that alginate can be reproducibly modified with these biological attributes, resulting in enhanced cellular function towards tissue regeneration *in vitro* and *in vivo*.

Numerous cell types are under investigation for their therapeutic potential for tissue engineering applications. The strategy first employed by Green in 1981 – taking a patient's own cells, expanding them in culture, then implanting them at the wound site – continues to be a relevant approach. This method can circumvent possible immunogenic complications that can occur with non-autologous cell types. Stem cells are often the target cell types for tissue engineering strategies as they can be used to differentiate into the desired cell type and display several therapeutic qualities. However, adult stem cells are available in very small quantities within the human body, and this number further decreases in older and diseased patients. Expanding harvested cells *in vitro* can address this problem. However, *in vitro* cell culture can alter cell function, decreasing cell stemness and limiting therapeutic potential.

Mesenchymal stromal cells (MSCs) can be found any many tissues of the post-natal organism and show significant promise for tissue engineering applications. Bone marrow derived MSCs, a therapeutically potent MSC source for musculoskeletal applications, are found at very low concentrations within many tissue compartments including bone marrow, fat, and teeth. MSC culture is well established throughout the field, and MSCs retain their differentiation capacity and

therapeutic potential after several passages. Therefore, the translational potential of MSCs for tissue engineering applications is extremely high, as the cells can be harvested from a patient, expanded, and re-implanted at the wound site. Although MSCs can differentiate down osteogenic, adipogenic or chondrogenic lineages, there is little evidence to suggest direct differentiation and integration into the tissue is their main regenerative mechanism when applied in tissue engineering approaches. Alternatively, the MSC secretome, or the growth factors, cytokines and exosomes secreted by MSCs, have been identified as the main contributors to positive tissue regeneration outcomes.

Cellular therapies need to overcome the hurdle of retaining high viability of implanted cells. Several different methods have been investigated to prolong cell viability *in vivo*, including entrapment in a biomaterial, cellular aggregation, and preconditioning. Within this dissertation, we investigated the efficacy of these methods for enhancing MSC therapies for tissue regeneration. As previously stated, we entrapped MSCs within alginate biomaterials that are engineered to display mechanical and biochemical characteristics to enhance cell viability and function. To improve viability further we aggregated MSCs into spheroids. Spheroid formation increases cell to cell connections, promoting cell viability and secretome production. We further investigated preconditioning cells in hypoxic culture conditions or simulating hypoxia *via* $CoCl_2$. Hypoxia initiates the HIF1α pathway, leading to increased cell survival, proangiogenic capacity and further increases the potency of the MSC secretome.[9, 10]

Accurately replicating the proper signals to direct cell function is another important consideration for cellular therapies. These signals can be mechanical, chemical, or biological and can significantly enhance the tissue regeneration cascade. Growth factors are common signals applied in tissue engineering that have significant biological effects. For example, bone morphogenetic protein 2 (BMP-2) is a potent stimulator of bone formation, vascular endothelial growth factor (VEGF) promotes blood vessel formation, and platelet-derived growth factor (PDGF) can attract immune and vascular cells vital for wound regeneration. Although growth factors

exhibit high potential for tissue regeneration applications, there are still several drawbacks to pursuing growth factor therapies. Purified and functional growth factors are costly to produce, additionally supraphysiological concentrations of growth factors are required to see a biological response. Growth factors at these concentrations can cause off-target effects that can range from ectopic tissue formation, to promoting cancer growth. For this reason, use of recombinant growth factors as a cell signal is not an ideal solution.

As an alternative to recombinant growth factor approaches, cell-secreted growth factors exist at much safer concentrations. They can retain their high therapeutic potency due to the complexity of their secretome that is near impossible to replicate through the use of recombinant growth factors. As previously stated, the MSC secretome possesses high therapeutic potential as a tissue engineering cell signal. Additionally, tuning different environment cues around the MSC spheroid, such as oxygen concentration and substrate composition, can influence the growth factors secreted for different applications. For these reasons within this dissertation, we utilized the MSC spheroid secretome as the main source of our signal component. We hypothesized that sulfate modified alginate would mimic the ECM component of heparan sulfate, enabling us to sequester key growth factors from the secretome to enhance tissue regeneration.

7.2 RESULTS AND IMPLICATIONS

In chapter 3 of this dissertation, we investigated the potency of the MSC/myoblast secretome for bone regeneration. We found that the composition and biological response of the MSC spheroid secretome was enhanced when it was serially exposed to myoblasts. This conditioned media significantly enhanced the differentiation of MC3T3 pre-osteoblasts *in vitro*. The secretome was then lyophilized and implanted within an alginate hydrogel for delivery into a rat femoral defect. The hydrogels implanted with conditioned media and monodispersed MSCs achieved the highest regeneration, with full bridging of the critically sized bone defect within 12 weeks. This study highlighted the translational potential of the MSC/myoblast secretome for bone

regeneration. The secretome alone was able to spur osteogenesis and promote bone formation, and this ability was amplified when delivered with MSCs. Lyophilized media exhibits high stability for long periods of time at room temperature, allowing for an effective off-the-shelf therapeutic in the clinic when delivered with autologous MSCs.

To further amplify the secretome's abilities, in chapter 4 we engineered an alginate hydrogel to retain heparin binding growth factors through the addition of sulfate groups. We determined that the sulfate groups were functional and could sequester heparin-binding growth factors such as hepatocyte growth factor (HGF). We further proved that sulfation, initial moduli, and degradation rate were all properties of the hydrogel we could independently regulate. We next investigated the biological properties of the sulfated alginate in conjunction with MSC spheroids and found sulfation significantly increased myoblast engagement and penetration within the hydrogel. We identified that components of the MSC spheroid secretome were being retained by the sulfated alginate, confirming our hypothesized mechanism of action. These results indicate that sulfated alginate is a promising platform for MCS spheroid delivery, as it can actively sequester secreted growth factors and enhance biological function. This chapter lays the ground for an exciting tunable platform that has high relevance for numerous applications. Independent regulation of growth factor sequestering, peptide presentation and other mechanical and material properties offers a unique model to investigate cellular response *in vitro*. Additionally, the tunability of this platform makes it ideal to utilize for tissue engineering applications, as we have full control over many mechanical and chemical properties to leverage cellular function towards regeneration.

Chapter 5 evaluates the *in vivo* capability of the proposed technology of chapter 4 by investigating its regenerative potential in a rat soleus crush injury. Through this study, we found that sulfated hydrogels in combination with MSC spheroids, exhibited lower levels of total collagen and densely crosslinked collagen compared to spheroids entrapped in unmodified alginate. This data seems to indicate that sulfated spheroid hydrogels exhibited a lower immunogenic and fibrotic response. We further found that neuromuscular junction regeneration increased at two

weeks for the sulfated spheroid group compared to the others. We believe these data reflect the fact that the sulfated alginate is able to sequester immunomodulatory and nerve regenerative growth factors from the MSC spheroids. The hydrogel group composed of the MSC secretome entrapped in sulfated alginate exhibited some of these same trends, thought to a lesser degree, further supporting out conclusions. These data support the hypothesis that sulfated alginate can sequester MSC spheroid growth factors, resulting in enhanced regeneration *in vivo*.

7.3 CHALLENGES AND LIMITATIONS

Although the field of tissue engineering has progressed exceedingly far in the last 60 years, few cellular therapies have become common place in the clinic. Current tissue engineering studies are plagued by several limitations that need to be addressed before being translated into patients, and this dissertation is no exception.

In chapter 3, we show promising data indicating the utilization of MSC spheroid/myoblast conditioned media and MSCs, however we did little to explore the mechanism of action. Although we identified a vast array of growth factors within the conditioned media, we did not identify or interrogate the influence of exosomes, microvesicles, or miRNA. These are known secretions of MSCs that can significantly influence cellular function. It is important to identify the influence of these components in relationship to the growth factors. This is especially relevant in this dissertation which hypothesizes the growth factors are the work horses of the secretome and prioritizes their retention.

An additional limitation within this dissertation is that we did not investigate how the physical and chemical properties of our materials can be leveraged to dictate spheroid secretion. Previous studies within our group have highlighted how changing material properties can regulate the MSC spheroid secretome.[11] In chapter 4 of this dissertation, our engineered material clearly exhibited tunable properties, hypothetically allowing us to influence MSC spheroid secretome to prioritize

specific cellular actions. However, we did not investigate secretome differences due to changes in material properties.

A major limitation of our approach to retain cell secreted growth factors through sulfate groups is that we have no control over what growth factors are binding. Several therapeutic growth factors and cytokines have very low or no heparan binding ability, including prostaglandin E2 (PGE_2), Epidermal Growth Factor (EGF), and Insulin-like Growth Factor 1 (IGF-1). Therefore, even if we did leverage the material properties of our alginate to encourage secretion of certain factors to promote a specific cell response, there is in guarantee those factors will be retained. Not only do we likely lose many important factors, but it is likely pro-inflammatory and anti-regenerative growth factors are being retained within the wound site as well. Although we saw no significantly worse regeneration with sulfated alginate, indicating this likely is not occurring to a large extent, it is a concern for elder and diseased patients whose wound sites may be upregulated with such factors.

When translating our sulfated alginate platform into an animal model, we chose to sustain a crush injury to the soleus muscle. We selected a crush injury because mechanical injuries are more physiologically relevant compared to other common muscle injury models, such as those that use freeze injuries, myotoxins, or chemical injuries. Specifically, we focused on the soleus as it is a well characterized crush injury model and does not significantly inhibit rat movement.[12] However, it should be noted that this specific injury is not clinically relevant, as the soleus is located under several other muscles which would likely also be crushed and damaged in any real-life injury. As we explored in chapter 3, the myoblast secretome contains many regenerative growth factors. Therefore, the fact that the injured soleus is surrounded by healthy muscle presents an unrealistic advantage in our specific model. Additionally, injury of the soleus does not significantly inhibit limb function on a rat, and we did not impede rat locomotion during their 6-week recovery, therefore the muscle is likely being exposed to mechanical forces that a human patient would likely not experience. Mechanical stimulation has been shown to enhance muscle

regeneration, which is a factor we did not control for.[13] Future studies could investigate the effect sulfated alginate spheroid treatment has on larger crush or volumetric muscle loss injuries that are likely to show significantly improved healing when treated with a growth factor rich therapy.

7.3 FUTURE DIRECTIONS

An important next step for this project is to identify the therapeutic components of the MSC spheroid secretome more precisely and leverage different chemistries to retain them. Growth factors make up only 2% of the MSC secretome, highlighting the need to better understand and characterize all other biological components to fully harness its potential.[14] For example, MSC derived exosomes have shown increasing promise for a range of treatments including treatment for COVID-19 patients, neurological diseases, and arthritis.[15-17] A good first experiment to pursue in this direction would be to isolate several fractions of the MSC spheroid secretome, separating growth factors, exosomes, and other bioactive factors, and interrogate the influence of these factors individually on cell function *in vitro*. Through these experiments, we will hopefully be able to evaluate the influence non-growth factor components have on cellular function and determine if they potentiate the growth factors' effect. If they show increased performance, it would be advantageous to further investigate their therapeutic potential and engineer an effective delivery method.

We can also further leverage alginate's material properties to enhance growth factor secretion and retention. As previously mentioned, substrate composition can influence the MSC spheroid secretome, and this is something that was not optimized in our experiments. Through manipulation of RGD and other peptide presentation, moduli, sulfation, and degradation, we can investigate which material properties result in the highest secretion and retention of desired growth factors. Additionally, within this work, we focused mostly on alginate reacted with 2% HSO_3Cl combined in a 1:8 ratio with unmodified alginate. However, alginate can be reacted with

higher concentrations of HSO_3Cl to increase sulfation or be utilized at a higher ratio. We did not explore higher sulfation, but this would be an important investigation to determine if increased retention is necessary to see increased therapeutic return, especially since the sulfation of our alginate is still significantly lower than heparan sulfate proteoglycans within the endogenous extracellular matrix. This would be an important next step to ensure we are fully taking advantage of our tunable material platform.

It would also be beneficial to investigate other sulfate reaction chemistries that allow us more control over where the sulfate groups are attached to the alginate. The reaction we investigated with HSO_3Cl allows us very limited control over where the sulfate groups attach, and this method can result in breakdown of the alginate polymers themselves due to the strong acid involved. Other methods for sulfation can circumvent the use of acid, but still result in random attachment of sulfate groups that are less heterogeneous compared to native heparan sulfate.[18] Determining a method to allow for specific sulfation patterns would be an exciting strategy to employ, as sulfate patterning on octasaccharides can result in different affinities for specific growth factors.[19] Therefore, engineering a sulfated alginate polymer with affinity for specific growth factors for a particular *in vivo* application is a promising avenue of research to explore. A more simplified approach would be to conjugate octasaccharides on to the alginate itself, allowing us to bypass the need to invent a new sulfate chemistry mechanism. Conjugating different peptides and functional groups to retain other bioactive components of the secretome would also be an interesting route to pursue.

Regarding the tissue engineering field itself, I believe the strategies most promising for clinical translation are those that utilize simplified acellular approaches with biomaterials that mimic known bioactive elements. Currently, the FDA has not approved any cellular therapy involving significant cell manipulation, including preconditioning and expansion.[20] Considering the evidence that the main therapeutic mechanism of MSCs for tissue engineering applications continues to point to the secretome, it should be possible to leverage acellular aspects of this

secretome to replicate a similar response to cellular therapies. Indeed, within this thesis, we have shown that acellular CM groups show promising regeneration responses *in vivo*, in some cases surpassing groups that contain cells. Before this can occur, however, considerable characterization of the biological mechanisms behind cell secreted products, such as the ECM and secretome, must occur. Implementing a therapy into the clinic that is not completely understood biologically and mechanistically can have severe unintended consequences. An example of this is the widespread use of stem cell therapies for hematologic cancers, such as leukemia and lymphoma. Although there exists extensive research on hematopoietic stem cells, and this procedure can be successful, respiratory complications occur in two thirds of stem cell recipients and 2-10% of patients can experience graft failure.[21, 22] Additionally, since cell conditions have significant influences on their secretome, several checkpoints would be required to ensure consistency and quality, as batch-to-batch variation of conditioned media would introduce inevitably variable responses.

Alternatively, if specific therapeutic components of the secretome can be identified, investigation into how to replicate these aspects through synthetic chemistries would be ideal. For example, identifying important bioactive receptors of such molecules and replicating them as truncated peptides would allow us to conjugate them onto a polymer at any desired concentration or ratio. This more targeted approach would allow for the synthesis of a replicable bioactive material with a known biological mechanism, making it more likely to be FDA approved than a cellular product. However, this requires robust experimentation to imitate key biological characteristics of the secretome with no guarantee that the therapeutic potential of a synthetic polymer would reach the level of a biological product.

Overall, the tissue engineering field still has far to go before being able to translate a successful technology into the clinic. However, biomaterials that can dictate and leverage cellular function are of increasing importance to the field. Better understanding of the therapeutic

mechanism underlying cellular bioproducts will allow for increased replicability within the field and accelerate the time it takes for products to enter the clinic.

7.4 CONCLUSION

Through this thesis, we have explored several methods to employ MSC spheroids to take advantage of their naturally produced, therapeutically potent secretome. We investigated methods to deliver the secretome itself in a femoral bone defect, we then engineered an alginate biomaterial to better retain this secretome and interrogated its efficacy in a soleus crush injury model. These studies show that engineering the proper biomaterial platform for a cellular, or secretome therapy is necessary to fully attain their therapeutic benefit.

7.5 REFERENCES

[1] F. Berthiaume, T.J. Maguire, M.L. Yarmush, Tissue engineering and regenerative medicine: history, progress, and challenges, Annu Rev Chem Biomol Eng 2 (2011) 403-30.

[2] W.M. Chardack, D.A. Brueske, A.P. Santomauro, G. Fazekas, Experimental studies on synthetic substitutes for skin and their use in the treatment of burns, Ann Surg 155 (1962) 127-39.

[3] J.B.M. Nicholas E. O'Connor, Susan Banks-Schlegel, Olaniyi Kehinde, Howard Green,, Grafting of burns with cultured epithelium prepared from autologous epidermal cells, Lancet 1(8211) (1981) 75-8.

[4] M.R. Havstad, Chapter 5 - Biodegradable plastics, in: T.M. Letcher (Ed.), Plastic Waste and Recycling, Academic Press2020, pp. 97-129.

[5] B.B. Rothrauff, G. Yang, R.S. Tuan, Tissue-specific bioactivity of soluble tendon-derived and cartilage-derived extracellular matrices on adult mesenchymal stem cells, Stem Cell Research & Therapy 8(1) (2017) 133.

[6] F. Paduano, M. Marrelli, L.J. White, K.M. Shakesheff, M. Tatullo, Odontogenic Differentiation of Human Dental Pulp Stem Cells on Hydrogel Scaffolds Derived from Decellularized Bone Extracellular Matrix and Collagen Type I, PLoS One 11(2) (2016) e0148225.

[7] A. Ebrahimi Sadrabadi, P. Baei, S. Hosseini, M. Baghaban Eslaminejad, Decellularized Extracellular Matrix as a Potent Natural Biomaterial for Regenerative Medicine, Adv Exp Med Biol (2020).

[8] Z. Mosala Nezhad, A. Poncelet, L. de Kerchove, P. Gianello, C. Fervaille, G. El Khoury, Small intestinal submucosa extracellular matrix (CorMatrix®) in cardiovascular surgery: a systematic review, Interact Cardiovasc Thorac Surg 22(6) (2016) 839-50.

[9] D. Hao, C. He, B. Ma, L. Lankford, L. Reynaga, D.L. Farmer, F. Guo, A. Wang, Hypoxic Preconditioning Enhances Survival and Proangiogenic Capacity of Human First Trimester Chorionic Villus-Derived Mesenchymal Stem Cells for Fetal Tissue Engineering, Stem Cells Int 2019 (2019) 9695239.

[10] S.S. Ho, B.P. Hung, N. Heyrani, M.A. Lee, J.K. Leach, Hypoxic preconditioning of mesenchymal stem cells with subsequent spheroid formation accelerates repair of segmental bone defects, Stem Cells 36(9) (2018) 1393-1403.

[11] K.C. Murphy, J. Whitehead, P.C. Falahee, D. Zhou, S.I. Simon, J.K. Leach, Multifactorial experimental design to optimize the anti-inflammatory and proangiogenic potential of mesenchymal stem cell spheroids, Stem Cells 35(6) (2017) 1493-1504.

[12] G. Matziolis, T. Winkler, K. Schaser, M. Wiemann, D. Krocker, J. Tuischer, C. Perka, G.N. Duda, Autologous Bone Marrow-Derived Cells Enhance Muscle Strength Following Skeletal Muscle Crush Injury in Rats, Tissue Eng 12(2) (2006) 361-7.

[13] C.A. Powell, B.L. Smiley, J. Mills, H.H. Vandenburgh, Mechanical stimulation improves tissue-engineered human skeletal muscle, Am J Physiol Cell Physiol 283(5) (2002) C1557-65.

[14] D. Kehl, M. Generali, A. Mallone, M. Heller, A.C. Uldry, P. Cheng, B. Gantenbein, S.P. Hoerstrup, B. Weber, Proteomic analysis of human mesenchymal stromal cell secretomes: a systematic comparison of the angiogenic potential, NPJ Regen Med 4 (2019) 8.

[15] L. Rezakhani, A.F. Kelishadrokhi, A. Soleimanizadeh, S. Rahmati, Mesenchymal stem cell (MSC)-derived exosomes as a cell-free therapy for patients Infected with COVID-19: Real opportunities and range of promises, Chem Phys Lipids 234 (2021) 105009.

[16] M.A. Lopez-Verrilli, A. Caviedes, A. Cabrera, S. Sandoval, U. Wyneken, M. Khoury, Mesenchymal stem cell-derived exosomes from different sources selectively promote neuritic outgrowth, Neuroscience 320 (2016) 129-39.

[17] M. Maumus, C. Jorgensen, D. Noël, Mesenchymal stem cells in regenerative medicine applied to rheumatic diseases: role of secretome and exosomes, Biochimie 95(12) (2013) 2229-34.

[18] Ø. Arlov, F.L. Aachmann, A. Sundan, T. Espevik, G. Skjåk-Bræk, Heparin-Like properties of sulfated alginates with defined sequences and sulfation degrees, Biomacromolecules 15(7) (2014) 2744-2750.

[19] S. Ashikari-Hada, H. Habuchi, Y. Kariya, N. Itoh, A.H. Reddi, K. Kimata, Characterization of growth factor-binding structures in heparin/heparan sulfate using an octasaccharide library, J Biol Chem 279(13) (2004) 12346-54.

[20] K. Yano, N. Watanabe, K. Tsuyuki, T. Ikawa, H. Kasanuki, M. Yamato, Regulatory approval for autologous human cells and tissue products in the United States, the European Union, and Japan, Regen Ther 1 (2015) 45-56.

[21] P.M. Wieruszewski, S. Herasevich, O. Gajic, H. Yadav, Respiratory failure in the hematopoietic stem cell transplant recipient, World J Crit Care Med 7(5) (2018) 62-72.

[22] P. Woodard, X. Tong, S. Richardson, D.K. Srivastava, E.M. Horwitz, E. Benaim, T. Geiger, G. Hale, W. Leung, V. Turner, U. Yusuf, J. Cunningham, R. Handgretinger, Etiology and outcome of graft failure in pediatric hematopoietic stem cell transplant recipients, J Pediatr Hematol Oncol 25(12) (2003) 955-9.